SYSTEM-LEVEL TRANSIENT FIRE RESPONSE OF DOUBLE ANGLE CONNECTIONS IN STEEL FRAMED STRUCTURES

By

Purushotham Pakala

A DISSERTATION

Submitted to
Michigan State University
in partial fulfillment of the requirements
for the degree of

Civil Engineering – Doctor of Philosophy

2014

ABSTRACT

SYSTEM-LEVEL TRANSIENT FIRE RESPONSE OF DOUBLE ANGLE CONNECTIONS IN STEEL FRAMED STRUCTURES

By

Purushotham Pakala

Steel framed structural systems are frequently used in high-rise buildings due to high structural performance steel provides as compared to other construction materials. In these steel framed structures, connections play a significant role in transferring forces from one member to another member and influence the overall stability of the structural system at ambient and fire conditions. Among different connection configurations available, double angle connections possess superior tying resistance and rotational capacity as compared to other relatively brittle connection types. Performance of connections under fire conditions is much more crucial to the stability of structural system as they experience rapid degradation in load carrying capacity and stiffness, due to deterioration of strength and elastic modulus of steel with temperature.

The current approaches for evaluating fire resistance of connections have many limitations and do not take into consideration critical factors governing fire response. For example, connections experience significant fire induced axial restraint forces when exposed to fire and these forces are influenced by factors such as decay phase of fire, restraint to free thermal expansion imposed by the unheated structural elements adjacent to the connection. However, current design provisions do not consider the effect of fire induced restraint forces. Further, current provisions are based on results from scaled/isolated connection tests. However, the response of double angle connection at system-level is completely different from that of scaled/isolated connection behavior.

The system-level fire response of double angle connections is simulated by developing finite element models using ANSYS. The finite element models account for material and geometrical nonlinearities, degradation of constitutive material properties with temperature and complex non-linear contact interactions, that have significant influence on the fire response of double angle connections. The validated models are used to carry out parametric studies to quantify the influence of critical parameters. Results from the parametric study show that fire performance of double angle connections is affected by increased load level and fire characteristics, while fire resistance gets enhanced when the presence of concrete slab in the structural frame is taken into account.

To study the influence of system level interactions on the behavior of double angle connections and to validate the finite element models, fire resistances tests on two double angle connection assemblies were conducted. The test variables included load level, presence of slab, structural continuity and fire scenario. Results from fire tests show that double angle connections are highly ductile and have inherent rigidity to carry higher fire induced axial forces for which they are not typically designed for.

Results from the fire tests, data from parametric studies were utilized to develop a rational methodology for evaluating the fire resistance of connections. The proposed methodology, developed based on equilibrium principles, uses temperature dependent moment-curvature-axial force (M-κ-P) relationships to trace the response of double angle connection assemblies. The proposed methodology accounts for critical factors such as fire induced axial forces, design fire scenarios, material and geometric nonlinearities.

Dedicated to
my family and friends
who have always been with me
during various phases of my life.

ACKNOWLEDGMENTS

I would like to thank a number of people who have contributed to the successful completion of this thesis. Many thanks to Prof. Venkatesh Kodur for giving me the opportunity of doing dissertation under his guidance. I would like to specially thank distinguished faculty members Professors Alejandro Diaz, Rigoberto Burgueño and Dr. Nizar Lajnef for serving on my committee. Thanks to all my committee members for their support, encouragement, useful suggestions and guidance.

I am highly grateful to Dr. Mahmoud Dwaikat for his help and constant guidance with finite element modeling without which this dissertation would not have been completed. Thanks to Dr. Syed Haider for his advice and support during difficult times.

The success of this study was due to the support and help of faculty, staff, and personnel in the Department of Civil and Environmental Engineering at Michigan State University. Special thanks to the manager of Civil Infrastructure Laboratory, Mr. Siavosh Ravanbaksh for his help, advice and fun attitude which made experiments an enjoyable experience.

Thanks to Laura Taylor, Margaret Conner and Mary Mroz for all the help they provided. Sincere and warm thanks to my co-students who supported me during the course of my research and the rest of my friends and colleagues in the department.

I would like to thank my wife Indumathy Jayamani who was supportive of me throughout the course of the study.

TABLE OF CONTENTS

LIST OF TABLES

LIST OF FIGURES

KEY TO ABBREVIATIONS

[Q]	tangent stiffness matrix
{f}	generalized stress vector
{X}	generalized strain vector
a,n	regression coefficients for fitting the growth phase of fire scenarios
a_1,a_2,a_3,a_4	non-dimensional regression coefficients dependent on steel material model
A_s	cross sectional area of the steel section
c	specific heat
C_e^t	specific heat matrix
c_s,c_p	specific heat of steel and insulation, respectively
dA	area of element
E,E_s	elastic modulus of steel at ambient temperature
E_t	tangent modulus of steel at ambient temperature
E_t	temperature dependent elastic modulus
F_e^n	applied nodal forces
F_e^{th}	element thermal load vector
F_p	heated perimeter of the cross-section
F_u,F_y	ultimate and yield tensile strength of steel at ambient temperature, respectively
h	thickness of insulation
h_{con} , h_{rad}	convective and radiative heat flux, respectively
h_f,h_o	heat transfer coefficient on fire side and cold side, respectively
I	second moment of area of steel section
k	bending curvature
k	axial restraint stiffness

k, k_p	thermal conductivity of steel and insulation, respectively
K_a, K_r	axial and rotational restraint stiffness, respectively
K_e	element stiffness matrix
K_e^t	thermal stiffness matrix
L	total length of the beam
LR	non-dimensional load ratio at room temperature
M_{max}	maximum bending moment in the beam
M_o	maximum bending moment in the beam due to gravity load only
M_u	unfactored ultimate bending capacity of the section at ambient temperature
M_x	bending moment
M_y	unfactored yield bending capacity of the section at ambient temperature
n_y, n_z	components of vector normal to the boundary in the plane of cross-section
P	fire-induced axial force
$P_{c,max}$	maximum fire-induced compressive force
$P_{ten,max}$	maximum catenary tensile force
q_b	total heat flux on the boundary
Q_e	applied nodal thermal load
s	coefficient used for computing steel temperature
s,t,r	isoparametric locus of a element
S_x	elastic section modulus
t	time
T, T_s	temperature of steel
T_c	temperature in steel at which fire-induced axial force P=0
T_e	nodal temperatures
T_f	temperature of fire

T_{lim}	limiting temperature of steel
T_o	temperature of cold side
t_p	insulation thickness
$T_{ten,max}$	temperature in steel at maximum catenary axial force
T_y	yield temperature of steel section
u	vertical displacement of the beam at loading point
U	strain energy
u,v,w	nodal translations in x,y,z directions, respectively
u_e	nodal displacements
V	external work
W/D	ratio of weight to heated perimeter of steel section
X_A,X_R	axial and rotational restraint factor
Z_x	plastic section modulus
α	coefficient of thermal expansion
Δt	time increment
ΔT	thermal gradient (or) change in temperature in beam cross-section
ΔT_s	temperature rise in steel
ε	strain in an element
ε_{nom},ε_{true}	nominal and true strain, respectively
ε_o	axial strain
ε_r	residual strain in an element
ε_{th},ε_{me}	thermal and mechanical strain, respectively
ε_y,ε_u	yield and ultimate strain of steel, respectively
θ	rotation at connection
μ	co-efficient of friction

ρ	density
ρ_s,ρ_p	density of steel and insulation, respectively
σ	stress in an element
σ_{nom},σ_{true}	nominal and true stress, respectively
σ_y,σ_u	yield and ultimate strength of steel at ambient temperature

CHAPTER 1

1. INTRODUCTION

1.1 General

Steel is one of the widely used construction material in high-rise buildings due to numerous advantages such as high strength, stiffness, ductility characteristics and the reduced construction time, it offers over other materials. However, steel has high thermal conductivity and loses its strength and stiffness rapidly when subjected to high-temperatures such as those encountered in building fires. Therefore steel structural members have to be designed for appropriate fire safety measures when used in buildings. This is because fire represents one of the most severe hazards to which buildings may be subjected to during their life span.

In a steel framed structure, various members are connected together by structural connections to facilitate load transfer between them. A wide range of connection configurations such as all bolted, all welded and welded-bolted are commonly used to provide connections. Different types of bolted connections such as flexible end plate, flush end plate, shear tab (fin plate) and double angle connections are available for facilitating connections in steel framed structures. Previous observations show that end-plate and shear tab connections undergo brittle failure and can sustain rotations upto 3.5° (60 milli-rad) only. On the other hand bolted double angle connections possess higher ductility, tying capacity, superior rotational characteristics (Liu et al., 2002; Pakala et al., 2012a; Wang et al., 2011; Yu et al., 2009b, c) and are economical, easy and fast to erect. The higher ductility possessed by the double angle connections produces ductile failure and they can undergo rotations up to 18° (≈ 315 milli-rad) before failure. For these advantages, bolted double angle connections are often preferred over welded or other type of bolted connections.

Failure of connections can lead to failure of connected structural members which in turn can trigger progressive failure of the entire structure. Fig.1.1 illustrates the response of lower three storeys of a multi-storey building. When fire occurs in a compartment, the temperatures increase steadily in the structural members and the connection starts to lose its capacity and eventually the connection fails. As a consequence of losing lateral members (beams), the unsupported length of the column increases to twice the length of original column which in turn decreases the critical buckling load by four times thus making the column more susceptible to early failure. Once the column fails, the remaining connected beams and column might fail and might lead to the progressive collapse of the entire structural system. Observations in previous fire induced collapse of steel structures indicated that the failure most often gets initiated at the connections. Since connections play a crucial role in maintaining integrity and stability of the entire structural framing system, design of these connections to withstand loads under fire conditions is vital to improving global performance of the structure.

It is well established from previous fire investigations and standard fire tests that unprotected steel structural members can fail within 20-30 minutes of fire exposure. However, building codes specify that structural members should be capable of maintaining structural integrity and load bearing capability for duration of 30 minutes to 3 hours, during the fire event. This requirement, known as fire resistance rating is a measure of quantifying the fire safety aspect of structural members. Fire resistance is defined as the duration during which a structural member exhibits adequate resistance with respect to structural integrity, stability and temperature transmission under standard fire exposure.

In current practice fire resistance of connections is often evaluated through fire tests or numerical models on connection assemblies. In this approach, the connection assemblies are assumed to be isolated connections without considering them to be part of the structural framing system and are subjected to uniform heating (steady-state temperature regime) or standard fire conditions. Further, in most of the fire tests the connections are scaled down in size (due to size limitations imposed by the testing furnace). However, in typical building fire scenarios, connections are integral part of the structural framing system and experiences transient temperature conditions. Therefore, the current approach of evaluating fire performance of connections do not accurately capture the realistic behavior as they asses the behavior based on isolated connections subjected to uniform temperature conditions. An alternative to this is to adopt a system-level approach. In this approach the true transient connection behavior can be traced by considering the connections to be an integral part of the entire structural framing system. Connections are then designed based on the performance of the structural framing system as a whole rather than the results generated based on isolated connections. Hence, there is a critical need to understand the realistic fire behavior of connections and thus arrive at design guidelines and code provisions which can account for all the significant factors affecting the connection fire performance and provide realistic connection design strategies.

1.2 Effect of Temperature on Connection Behavior

At ambient temperature, bolted connections generally experience shear force and flexural tension or compression force depending upon the configuration of the connection. These forces are generated in the connection through force transfer that occurs from connected members (beams, columns etc.). However, when these connections are subjected to fire conditions, connections not only lose their strength and stiffness resulting from increasing temperature, but also experience additional forces due to the expansion and contraction of connected steel members, as illustrated in Fig. 1.2.

When fire occurs in a steel framed building (see Fig. 1.2(a)-(b)), all components of the frame (beams, columns, connections) experience temperature rise (Fig. 1.2(c)). During initial stages of fire, temperatures in beam increases (Fig. 1.2(c)) and this leads to expansion of the beam due to significant thermal expansion of steel. The adjoining (cold) structural members, in the frame, restrain the free thermal expansion of beam which leads to the development of axial compressive forces as shown in Fig. 1.2(d). The axial force increases with time until the beam undergoes initial yielding after which the restraint compressive force decreases in magnitude and finally transforms to tensile force. This transformation in axial force can be attributed to deteriorating strength and stiffness of beam with increasing temperatures which results in permanent deformation of beam. At this stage, the beam is able to carry very little load through flexural mechanism and is held in place by connections like a cable where load transfer happens through catenary action. Finally, during the cooling phase the beam regains part of its initial strength and undergoes thermal shrinkage leading to continuous increases in the tensile force until connection fails.

In summary, the fire behavior of connections is different from that at ambient temperature on two fronts namely, (a) the connection experience additional axial force from beams due to the restraint imposed by the adjacent (cold) structural members on thermal expansion of heated members, and (b) the nature and magnitude of the axial force can change with fire exposure time (Bailey et al., 1996; Liu et al., 2002).

Further, the type of fire scenario significantly influences the fire induced axial forces in connections. The fire exposure typically experienced in buildings comprises of a growth phase that is followed by a decay phase. Fig. 1.3 illustrates different time-temperature curves representing standard fire and realistic (design) fire scenarios. It can be seen from the figure that in the case of design fire, temperature in building increases initially after which the compartment enters cooling phase once the total available fuel is consumed and/or due to limited oxygen supply. However the temperatures in a standard fire, typically used in standard fire resistance tests, increases continuously with time without any decay phase. As mentioned earlier the presence of decay phase and specifically the rate of decay significantly influence the rate at which the beam recovers its strength and stiffness which in turn governs the magnitude and transformation time of fire-induced axial forces from compression to tension. Hence, the presence of decay phase plays a critical role in determining the failure time of connections as well as the entire structural framing system. Therefore, the type of fire exposure (design vs. standard) and the rate of decay have significant influence on the fire response of connections and should be properly accounted for in modeling the connections.

The unique and superior performance characteristics of bolted double angle connections can be better illustrated by comparing its rotation characteristics to that of other connection types, as illustrated in Fig. 1.4. The details of two types of connections namely flush end-plate and double angle connection along with their moment-rotation (M-ϕ) curves are shown in Fig. 1.4. A quick glance of the ambient temperature M-ϕ response of flush end-plate connection indicates that the response is characterized by three regions (Al-Jabri et al., 2005). Initially there is an approximately linear response with increasing rotation, until the onset of yielding in one or more of the connection components (such as bolts or angles). This is followed by curvilinear response indicating the yielding of the connection. Finally, as the connection failure becomes impending, the rate of rotation increases rapidly causing an almost flat plateau in the connection response.

However, the room temperature M-ϕ response of double angle connection consists of two stages, before and after the beam bottom flange comes into contact with the column flange. The first stage is again characterized by linear and bilinear response similar to that of flush end-plate connections. During the second stage, when beam bottom flange makes contact with the column flange, an increase in moment is accompanied by a smaller increase in rotation due to the resistance offered by the column flange to free rotation of the beam flange. Finally, an increase in moment is accompanied by increased rotation until the connection fails.

When connections are exposed to fire, they lose their strength and stiffness with increasing temperature. Therefore, as the temperature increases, there is degradation of M-ϕ response (see Fig. 1.4(c)-(d)) as the moment-carrying capacity of connection decreases and the resistance to connection rotation decreases. Previous studies indicate that double angle connections can undergo rotations up to 18° (≈ 315 milli-rad) before failure while other connection configurations can sustain only 3.5° (60 milli-rad rotations) (Yu et al., 2009c). The higher ductility possessed by the double angle connections produces ductile failure, rather than brittle failure as experienced in other connection types, which enhances connection failure time.

1.3 Research Objectives

The above illustrations clearly indicate that temperature has a significant effect on the behavior of double angle connections that are an integral part of structural frame. There is considerable lack of understanding on the transient response of double angle connections under realistic fire, loading and restraint conditions. Furthermore, the system-level response of double angle connections is completely different from that of isolated connection behavior. To address some of these knowledge gaps, it is proposed to undertake a comprehensive study on the transient structural response of double angle connections under fire conditions with the ultimate objective of developing a rational methodology for fire design of connections. The specific objectives of this research are:

- Carry out a detailed state-of-the-art review on the fire behavior of different connections and identify knowledge gaps. The comprehensive review will cover both experimental and numerical studies as well as current provisions in codes and standards.
- Model the system level transient thermal and structural response of double angle connections under realistic fire, loading and boundary conditions using the commercially available finite element programs. The models for thermal and structural analysis will account for high temperature properties of materials, geometric and material nonlinearities as well as nonlinear contact interactions.
- Carryout fire resistance experiments on assemblies with double angle connections to develop needed data for validating numerical models.
- Validate the computational models by comparing response predictions from the model with test data obtained from fire resistance experiments on double angle connections.

- Carry out parametric studies to quantify the effect of various factors on the performance of double angle connections under realistic fire, loading and restraint conditions.
- Utilize data from fire tests and parametric studies to develop a simplified design approach for fire design of double angle connections.

1.4 Scope

The research presented as part of this dissertation is arranged in seven chapters. Chapter 1 outlines general background to fire response of double angle connections and presents key objectives. Chapter 2 provides a detailed state-of-the-art review on the behavior of double angle connections subjected to fire conditions. The review includes summary of experimental and analytical studies, as well as fire design provisions in current codes and standards.

Chapter 3 deals with fire resistance experiments conducted on two full-scale double angle connection assemblies under realistic fire, loading and restraint conditions. Results from fire tests are used to discuss the response of double angle connections under realistic conditions. Chapter 4 presents details about the finite element model developed for tracing transient fire response of steel double angle connections. The validation of the finite element models (thermal and structural) is also presented in Chapter 4, where response parameters from the model are compared with test data.

Results from parametric studies are presented in Chapter 5. Different parameters governing the transient fire response of double angle connections are described along with a discussion of the results from the parametric studies. Guidelines for the fire design of steel double angle connections are presented in Chapter 6. Results from the parametric studies are applied to verify the proposed approach for evaluating the fire resistance of double angle connections. Finally, Chapter 7 summarizes the main findings arising from the current study and recommendations for further research.

CHAPTER 2

2. STATE OF THE ART REVIEW

2.1 General

Bolted double angle connections are often used in steel-framed buildings due to their higher tying resistance and rotational capacity. These connections play a crucial role in transferring forces between members (beam to beam, girder or columns) in a structural framing system. The behavior of these connections can be much different under fire conditions due to development of large fire induced forces in structural members. Current provisions in codes and standards do not specifically account for these fire induced forces, and therefore, double angle connections are designed as simple shear connections. Further, the current approach for evaluating fire resistance of connections is based on a prescriptive methodology where fire performance is evaluated based on isolated connection response rather than considering overall response of the structural framing system with embedded connections. While most of these studies aimed at developing the moment-rotation characteristics of end plate connections, very limited studies focused on performance of double angle connections under fire conditions. This section provides a state-of-the-art review on experimental and numerical studies related to fire performance of connections. Also, a review of fire resistance provisions in various codes and standards are provided.

2.2 Experimental Studies

The common approach for evaluating fire resistance of RC columns is through fire tests under standard fire conditions. A number of fire resistance tests were conducted in the last two decades to study the fire behavior of connections. The objectives, test methods, features and major conclusions reached in some of the notable studies are summarized below.

The main objectives of most of the fire resistance experiments included:

- Observing and monitoring the connection behavior under a standard fire exposure
- Generating fire resistance ratings of connections with specific configuration and load intensity
- Generating data over a range of variables for verification of computer based models, and
- Generating analytical, component based models and developing moment-rotation relationships

Lawson (Lawson, 1990) conducted tests on different types of beam-to-column connection, by subjecting them to ISO834 standard temperature-time curve, to quantify the moment capacity of the connections at elevated temperature. A total of eight tests were conducted that included five non-composite beams, two composite beams and one on a shelf angle floor beam. Three different connection types namely extended endplate; flush endplate and double angle (web cleat) were used. Beams and columns in four tests were fire protected for 1 hour by spraying with 20 mm vermiculite-cement spray. A summary of the experimental program is presented in Table. 2.1. Results from these tests indicated that the steel connections possessed significant strength at elevated temperatures and were able to sustain large moments (two-thirds of ambient temperature moment capacity) in fire. Lawson concluded that (a) the temperatures experienced by bolts were always less than that in connecting beam indicating that bolt failure is unlikely to happen before beam fails (b) bolt temperatures were significantly lower than the beam lower flange, thus enhancing the performance of connections (c) mesh reinforcement present in composite beams contributed to increasing moment capacity of the connections (d) moment transferred through the connections helped in reducing the effective load ratio of simply-supported beams and thus increasing the limiting temperature of beams.

Liu et al. (Liu et al., 2002) experimentally studied the fire behavior of two types of beam-to-column connections namely, double angle (double web-cleats) and flush end-plate. The connections were part of a sub-frame assembly and were fire-protected using 50 mm thick ceramic fiber blanket. A schematic of the tested sub-frame assembly is shown in Fig. 2.1. The authors conducted 20 fire tests, with two types of connections, by exposing the sub-frame assembly to ISO834 standard fire temperature curves and varying load levels on the beam (a load ratio of 0.3, 0.5 and 0.7). The behavior of the connection was assessed by measuring the moment and force resisted and transmitted by the connection as well as the rotation of connections. The authors observed that (a) the double angle connection resisted a minimum amount of moment (15% of the beam moment capacity) despite being regarded as a pinned joint (b) the critical temperatures of the beam with double angle connections were 20°C lower than those with end-plate connections (c) the bolt holes in the beam web were elongated due to large bearing forces resisted by double angle connections. The authors concluded that connections can improve the fire resistance of beam by reducing the mid-span moment, during the heating phase of the fire. In comparison to double angle connection, end-plate connections have larger moment transfer capacity and higher catenary action which reduces the beam deflection.

Leston-Jones et al. (Leston-Jones et al., 1997) tested flush-end plate joints at elevated temperatures in order to develop moment-rotation relationships. Results from the tests showed that the strength and moment capacity of the connections decrease with increasing temperature with a significant capacity reduction in 500-600°C temperature range. Al-Jabri et al.(Al-Jabri et al., 1998) conducted experimental studies to investigate the degradation of steel and composite connection characteristics at elevated temperature. As part of the experimental study, tests were conducted on full end-plate, flexible end-plate bare steel connections and flexible end-plate composite connections. The authors inferred that the failure modes of the connections at elevated temperatures are similar to those at ambient temperature. Based on the tests, the authors concluded that the presence of concrete slab in composite connections enhanced the connection performance at elevated temperature by acting as a heat sink to the top of the beam. Using the data generated in the elevated temperature tests conducted at constant load level, the authors interpolated moment-rotation-temperature curves for different connection types (Al-Jabri et al., 2005).

Wald et al. (Wald et al., 2006) undertook an experimental program to study the global structural response of a fire exposed compartment in 8-storey steel-concrete composite frame building at BRE's Cardington test facility. The experimental program aimed at examining temperature distribution within structural elements, distribution of internal forces, behavior of slab, beam, columns and connections. . The structure was of 33 m height with five bays wide and three bays deep. The steel frame consisted of two types of connections with M20 Grade 8.8 bolts namely, flexible end plates for beam-to-column connection and fin plates for beam-to-beam connection. Both the connections were fire protected with 15 mm of Cafco300 vermiculite-cement spray. A total of seven tests were conducted and details about the natural fire used, thermal, structural behavior of the steel frame is provided by the authors. The authors observed fracture in the end-plate connections (along the welds) and attributed this to the large rotations, tensile forces developed in the beam while it was cooling. No fracture was observed in the shear tab (fin plate) connections though the bolt holes in the beam web underwent significant elongation and this was due to the fact that the shear tab (10 mm) was thicker than the beam web (6 mm). Based on these observations, the authors concluded that the elongation of the holes in the beam web leads to increased connection flexibility thus allowing larger deformations without fracture.

Wang et al. (Wang et al., 2007) studied the capacity, failure characteristics and failure modes of extended end-plate connections under fire exposure. In addition, the effect of rib stiffeners and depth of end-plates on fire-resistance capacity was studied by comparing the connection capacity with and without rib stiffeners. The authors developed a spring-component model and established its validity by comparing the results obtained from the model with the experimental results. Based on the test results, it was concluded that the extended end-plate joint has higher rotation capacity at elevated temperatures. The rib stiffener and the thickness of end-plate have significant and moderate influence, respectively, on the critical temperature of the extended end-plate joints.

Yu et al.(Yu et al., 2009a) undertook experimental studies to characterize the behavior of fin plate, flush endplates, flexible end plate, and web cleats (angle) connections in fire. The aim of the study was to investigate the capacity and ductility of steel connections at elevated temperatures, especially when the beams are in catenary phase. The shear tab connections were made of different rows (1 row of 3 bolts, 2 rows of 3 bolts each), grade (8.8, 10.9) and diameter (M20, M24) of bolts. The authors conducted 14 tests at four different temperatures (20°C, 450°C, 550°C, 650°C) and two loading angles (35°, 55°). A summary of the test program is presented in Table 2.2. All the tests were steady-state tests in which the specimen was heated to a target temperature and then the load applied until the specimens fractured. Experimental data indicated that the resistance of fin plate connections are significantly affected by temperature rise and bolt shear fracture tends to govern the failure of fin plate connections at elevated temperatures. For the web cleat (angle) connections, the authors observed that these connections have excellent rotational ductility, and resistance of these connections decrease rapidly with increasing temperature.

Yu et al.(Yu et al., 2009b) also studied the high temperature rotational capacity, tying resistance of double angle (web cleat) connections by subjecting them to a combination of shear and tying forces. A schematic of the connection configuration is shown in Fig. 2.2. The connections were heated to a uniform target temperature and then the beam was loaded (at different angles) away from the connection region until the connection failed. A total of 14 steady-state temperature tests were conducted with one and two rows of three bolts each, different loading angles and temperatures. A summary of the test program along with the peak force and rotations experienced by the connection assemblies are presented in Table 2.3. Based on these tests, the authors concluded that for double angle connections the (a) tying capacities decreased rapidly with temperature, with the connection having little resistance after reaching 650°C; (b) failure mode is dependent mainly on temperature but not on the applied load combinations (shear and tying forces); (c) fracture of double angle close to its heel and double shear bolts through beam web are the two critical failure modes at elevated temperatures; and (d) rotational capacity that develop in double angle connections is very high as compared to other connection types.

Daryan and Yahyai (Daryan and Yahyai, 2009) studied the response of bolted top-seat angle beam-to-column connections by conducting 12 full-scale fire tests with two different connection configurations (with and without web angle). The connection details of the specimens are illustrated in Fig. 2.3. These experiments were aimed at studying the effects of temperature, failure mode, bolt grade, angle thickness, web angle and load level on the fire behavior of connections. Details of the specimens along with the applied load are shown in Table 2.4. In all the tests, the specimens were subjected to a predetermined load level and then exposed to ISO 834 or ASTM E119 standard fire temperature. The applied loading (moment in this case) on the connections was selected in such a way that the premature failure of connection would not occur and the connections can sustain the effect of elevated temperatures. As the objective of the study was to evaluate the behavior of connections, the column and beam of all the specimens were wrapped with a 2.5 cm thick ceramic fiber blanket. The authors concluded that (a) increasing the stiffness of connection does not improve temperature resistance (i.e., the temperature at which failure happens) because the premature tension failure of bolts prevents the utilization of full capacity of connection and web angle (b) the premature tension failure of bolts can be prevented by using nuts of a higher strength (grade) or by using two or three nuts of less strength (c) the onset of connection plastic behavior occurs between 500 and 650°C which is within the limiting temperature for steel beams (d) high temperature strength of connections can be improved by using temperature-resistant bolts, increasing the thickness of angles and decreasing the applied moment on connections (e) bolts play a crucial role in determining the connection capacity at elevated temperature and improper bolt behavior hinders the utilization of the full capacity of other components. Based on the limited study, the authors concluded that the connections failed at the same temperature at which beams are assumed to fail and hence the connections are not a weak link in a braced frame.

Wang et al. (Wang et al., 2011) carried out an experimental study to evaluate the robustness of different types of connection in restrained steel frames. The study was aimed at evaluating the effect of varying axial restraint (provided by columns) on the connected beam and the connection types on the overall response of the steel frame. The authors conducted fire tests with two column sections and five connection types namely fin plate (shear tab), web cleat (double angle), flush endplate, flexible endplate and extended endplate. Details of tests, beam, column and connection dimensions are reproduced in Table 2.5. Due to the limitations of the furnace, the sub-frame assembly did not have a concrete slab but the top flange of the beam was wrapped with 15 mm thick ceramic fiber blanket to simulate the heat sink effect of the slab. During the test, two point loads each of 40 kN (corresponding to a load ratio of 0.5) was applied on the beam at a distance of 600 mm from the ends and then it was exposed to ISO 834 standard fire. The columns were restrained at the ends and were free to move in longitudinal direction only thereby enabling to study the effects of axial restraint on the beam and the connection. The behavior of the connections was evaluated by beam mid-span deflection, failure modes and axial forces in the connection. Based on the observations the authors inferred that the connections experience different failure modes and the failure in connections happens only when the beam enters the catenary action phase. The primary conclusion from this study is that the double angle connection exhibited the highest performance, as compared to other types of connections, in allowing the connected beam to develop catenary action without connection failure.

Al-Jabri et al. (Al-Jabri et al., 2005) carried out an experimental study to develop moment-rotation-temperature curves for semi-rigid connections containing flexible and flush end-plate. A total of twenty tests were conducted with five different connection details that included composite and bare steel connections. Details about the beams, columns, connections used in the tests are summarized in Table 2.6. All the connections were subjected to linearly increasing temperature with a maximum temperature of 900°C achieved in 90 minutes. The applied loading on the beam was varied between 20-80% of the moment capacity of the connection. The thermal response was measured using thermocouples while the connection rotation was measured by clinometers and displacement transducers. The authors observed uniform temperature distribution across the depth in all the bare-steel connections. The presence of concrete slab in composite connections created a non-uniform temperature profile with 19-30% reduction in the average temperatures, compared to bare-steel connections. The author used the experimentally observed connection rotation and derived empirical equations (by curve fitting method) for predicting the moment-rotation of connections at different temperatures.

Yang et al. (Yang et al., 2009) conducted an experimental study to evaluate the fire performance of welded flange-bolted web type moment connections. The program aimed at studying the effect of fire-proofing, testing conditions and loading on the behavior of connections. A summary of the test specimen dimensions and test parameters are presented in Table 2.7. The authors concluded that, for welded flange-bolted web type moment connections under elevated temperature (a) the connections exhibited ductile behavior, with necking and tearing at top flange and local buckling at bottom flange (b) for temperatures beyond 500°C, deterioration of stiffness is more significant than that of strength (c) by proper design of fire-proofing material, stability of the connection can be maintained without loss of strength and stiffness.

Al-Jabri et al.(Al-Jabri et al., 1998) conducted experimental studies to investigate the degradation of steel and composite connection characteristics at elevated temperature. A total of five tests were conducted with two full end-plate, one flexible end-plate bare steel connections and two flexible end-plate composite connections. Using the results obtained from the elevated temperature tests conducted at constant load level, the authors interpolated moment-rotation-temperature curves for different connection types (Al-Jabri et al., 2005). The authors observed that the failure modes of the connections at elevated temperatures are similar to those at ambient temperature. Also, the authors concluded that the presence of concrete slab in composite connections enhanced the connection performance at elevated temperature by acting as a heat sink to the top of the beam.

The above review illustrates that there have been a number of experimental studies to characterize the fire behavior of connections. In these fire tests, the effect of structural continuity, fire protection, composite action, member characteristics and the connection configuration, on the fire response of steel connections were studied. However, most of the tests were limited to isolated and scaled connection specimens subjected to standard fire exposure and uniform temperature (steady-state) field. Further these tests focused on end-plate connections and developed moment-rotation relationships. Very few experimental studies focused on shear tab (Yu et al., 2009a) and double angle connections (Yu et al., 2009b) or on the system-level response (Wald et al., 2006) of the overall structural system. Thus, there is limited information on the behavior of double angle connections under realistic fire, loading and restraint conditions.

2.3 Numerical Studies

A review of literature indicates that a large number of numerical studies have been carried out on the fire behavior of connections. Initial modeling studies on the fire behavior of connections were carried out by Liu (Liu, 1996) who developed a three dimensional model to simulate the response of steel framed structures in fire. The model is based on tangential stiffness approach and incorporated the material plasticity, non-uniform thermal expansion, large deformation and degradation of the material properties at elevated temperatures. The model uses isoparametric shell elements and carries out the analysis in different time steps using an iterative procedure. Each iteration of the analysis starts by increasing the temperature which is followed by computing the relevant stress-strain relationship and subsequently the stiffness matrix and the thermal load vector. For a given load, using the updated stiffness and thermal load vector the increment in the displacement at each time step is iteratively computed until the displacement norm is within the allowable tolerance limit. Details about the derivation of the force-displacement equations, stress-strain curves and the nonlinear iterative procedure are described by the author. Using the validated numerical model, Liu analyzed beams and beam-to-column connection with different loading and structural continuity conditions. Based on the results, Liu concluded that the fire resistance of the beams can be substantially enhanced by accounting for continuity of the structural frame. In addition, the top tension bolts in connections were less affected by loading and structural continuity and thus they enhance connection's fire resistance.

Liu (Liu, 1998) conducted a study to evaluate the effect of connection flexibility on fire resistance of steel beams. The study was aimed to quantify the beneficial effects of the endplate type connections in terms of the reduction of effective load ratio in the beam. Liu analyzed different types of connections, isolated beams with and without moment continuity, isolated connection behavior and beams with endplate type connections. Based on the analyses, Liu inferred that the connection details such as bolt size, endplate thickness does not substantially affect the overall performance of the beam in fire.

Mao et al.(Mao et al., 2009) studied the fire response of steel semi-rigid beam-column moment connections using ANSYS. The geometry of the specimen was discretized using 8 noded Solid70 and Solid185 elements for thermal and structural analysis, respectively. The authors performed a sequentially coupled thermal-structural analysis of the connection. The FE model did not consider the effects of residual stress in the material, welding and bolting material on structure while the elevated temperature nonlinear material behavior is assumed to follow Eurocode 3 provisions. The numerical model was validated by comparing the results obtained from the numerical model with those measured during full-scale fire tests reported by Ho et al.(Ho et al., 2007). The validated model was applied to study the influence of different parameters. Results obtained from these studies showed that the applied moment level have significant effect on the stiffness of steel moment connection while the axial load of column, shear and axial force of beam have less effect.

El-Rimawi et. al. (El-Rimawi et al., 1997) carried out an analytical study to examine the influence of connection stiffness on the behavior of steel beams in fire. The authors proposed a method for extending the ambient temperature connection characteristics to higher temperatures. The analytical procedure is based on a secant stiffness approach in which each element of the structure is divided into a number of line elements with three degrees of freedom at each node. The authors validated the analytical model and conducted a parametric study to characterize the influence of connection temperature, beam span and depth on the beam behavior. Based on the results, the authors observed that the exact representation of the connection and its temperature relative to the beam are not critical in determining failure and the proportions of beam span and cross-section do not appear to have significant influence.

Liu (Liu, 1998) used a finite element model to study the effect of simple bolted connection flexibility on the fire resistance of steel beams. The aim of the study was to quantify the beneficial effect of the end plate type connections. The author presented a series of analyses on isolated beams with or without moment continuity, isolated connection behavior and beams with end plate type connections. The FE model, previously validated by the authors (Liu, 1996), considered the effect of nonlinear geometric properties and stress-strain-temperature relationships. Based on the analyses, the authors observed that the connection details such as bolt size, endplate thickness does not substantially affect the overall performance of the beam in fire. However, the authors expressed a word of caution when using the conclusions as the current study ignored the axial restrains due to the column.

Pakala et al. (Pakala et al., 2012a) studied the fire performance of bolted double angle connections using ANSYS. The model accounted for material and geometric nonlinearities, high temperature properties of steel and nonlinear contact interactions. The double angle connections were exposed to uniform temperature and then loaded until the failure. The steady-state high-temperature stress-strain relations used in the model are shown in Fig. 2.4. The FE model was validated by comparing the predicting from the model with published test data. The failure mode obtained from the numerical model and that observed in fire tests is shown in Fig. 2.5. The validated model was used to study the influence of critical factors on the fire performance of bolted double angle connections. Based on the results from parametric studies, the authors concluded that bolt-hole size, edge-distance, thermal gradient and the slenderness of beam web significantly influence the fire behavior of double angle connections.

Yang et. al. (Yang et al., 2009) conducted a finite element analysis to evaluate the performance of welded flange-bolted web type moment connections under fire load. The authors modeled four full-size steel beam-to-column specimens, with and without fire-proofing materials. The FE model accounted for the material and geometric nonlinearities, degradation of material properties with temperature and examined the load-displacement behavior. The FE model was validated by comparing the results from the model with those obtained by the experiments conducted by Yang et. al (Yang et al., 2009) and found a good correlation. The authors used the validated FE model to conducted parametric studies to examine the strength reduction characteristics of unprotected steel at elevated temperature. Based on FE analysis results, the authors observed that beam-to-column connections were able to retain their design strength up to 650 °C while the stiffness dropped to 25% of the ambient temperature value. The authors also observed ductile behavior in connections, with necking and tearing at top flange and local buckling at bottom flange. The study concluded that the integrity and stability of the steel connections can be ensured by providing proper fire-proofing materials.

Liu (Liu, 1999) used FE program FEAST to study the fire behavior of unprotected steel beams and columns connected through bolted end-plate (extended and flush) connections. The author examined the effect of bolt size, number of bolts and end-plate thickness on the behavior of end-plate type connections. Based on the results obtained from FE simulations, the author concluded that for a similar load ratio, beams with flush end-plate connections had similar fire resistance to that of the simply-supported. On the other hand, beams with extended end-plate connections had higher fire resistance than that of simply-supported beams. Also, the authors observed that only a maximum of two-thirds of the ambient temperature moment capacity can help in increasing the load capacity of the beam under fire conditions.

Garlock and Selamet (Garlock and Selamet, 2010) developed an ABAQUS FE model, of beam-to-girder floor subassembly containing shear tab (single plate) connection, based on the full-scale test performed at Cardington in 2003 (Wald et al., 2006). The effect of slab is represented with linear springs using connector elements, which have temperature dependent stiffness. The authors conducted an uncoupled thermo-mechanical analysis. The authors analyzed the floor subassembly with zero, constant, temperature dependent spring stiffness's and showed the effect of varying composite action on the structural response. The validated FE model was used to study the effects of fire characteristics such as the fast and slow fire growth curves, rate of heating and cooling on the connections. Based on the FE results, the authors observed that the beam web and flange buckled in the heating phase due to the development of large compressive forces. Also, slow heating rate produces higher axial compressive forces in the connections due to thermal elongation induced by more uniform temperatures in the section. The authors concluded that the heating and cooling rates affect the beam stress distribution, maximum temperatures and displacements but not the maximum beam axial force. Further, large tensile forces develop in the connections during the cooling phase of fire.

Selamet and Garlock (Selamet and Garlock, 2010b) extended previously validated model (Garlock and Selamet, 2010) of the floor subassembly to study the effect of modifying connection details for improved fire performance of shear tab (single plate) connections. In the study, the authors considered the effect of varying bolt grade, bolt hole type, doubler plate of the beam, thickness of connection plate, bolt pretensioning, gap distance between beam and support, bolt hole edge distance. Based on results from analysis, the authors concluded that the behavior of single plate connections can be improved by (a) adding a doubler plate to the beam web, (b) using a larger distance from the bolt-hole centerline to the beam end (c) increasing the gap distance between the end of the beam to the connection member. In addition, the authors found that larger bolt holes can improve the fire performance by imposing less axial restraint and allowing the beam to move freely under fire-imposed thermal loads.

Pakala et al. (Pakala and Kodur, 2013) developed a three-dimensional finite element model using ANSYS to assess the system-level transient fire response of double angle connections. The geometry of the connection assembly along with the connection details are shown in Fig. 2.6 while the stresses in the bolts predicted by the model are illustrated in Fig. 2.7. The authors analyzed the behavior of double angle connections under two different scenarios namely (a) the connection assembly is assumed to be part of a structural framing system and is subjected to uniform temperature (transient vs. steady-state heating) (b) the connection assembly is assumed to be isolated and is subject to a design fire scenario (system-level vs. isolated behavior) as illustrated in Fig 2.8. They observed that the behavior of double angle connections as part of a structural system is completely different from that of an isolated connection. The authors used the validated model to study the effect of system-level interactions, load level, non-standard fire scenarios and high-temperature properties of bolts on the fire performance of double angle connections. Based on the results from numerical simulation, the authors concluded that the mechanical properties of high-strength bolts have a significant effect on the fire-induced axial forces in connections as shown in Fig 2.9. Also, the magnitude of fire-induced compressive axial force in connections depends on the fire scenario only and is independent of the loading level on the connected beams.

Dai et al. (Dai et al., 2010) used general purpose finite element program ABAQUS to model the fire behavior of ten restrained steel beam-column assemblies with five different connections namely: fin plate (shear tab), flexible end plate, flush endplate, web cleat (double angle) and extended endplate. Beam, column details along with connection dimensions are presented in Table 2.5. The authors used true stress-strain relationships in conjunction with Eurocode 3 strength reduction factors to account for elevated temperature effects. The authors used artificial viscous damping, which is defined using dissipated energy fraction, to counter the effects of temporary structural instabilities caused by localized buckling and very large deformations. The FE model of the connections was validated by comparing the predicted beam deflection, axial forces, connection failure modes with those obtained from the tests and found a good correlation between the two. The authors concluded that the FE model was able to predict the fire response of all the five connection types with reasonable accuracy and can be used to conduct parametric studies.

The above review illustrates that there have been a number of numerical studies on the fire behavior of connections. These studies developed connection models, using finite element computer programs such as ANSYS or ABAQUS, and studied the effect of connection flexibility, moment rotation stiffness, moment continuity, catenary tension forces and fire protection on the fire behavior of connections. These finite element models accounted for material nonlinearity, friction and high temperature stress-strain relations. Most of these studies focused on end-plate connections while only limited studies focused on bolted angle and simple shear tab connections. Studies on double angle connections concluded that double angle connections have higher tying resistance, rotational capacity and superior ductility in comparison to other connection configurations.

2.4 High Temperature Bolt Properties

The fire performance of double angle connection depends on the type of material properties used. The type of material properties is directly affected by the type of steel used to manufacture connection components such as bolts. The types of steel used in construction can be broadly classified as normal strength (mild steel) and high strength steel. These two types of steel have different properties because of the differences in carbon content, presence of alloying elements and type of alloying elements (Kodur et al., 2012). In addition, the type of heat treatment process has significant influence on the strength properties. For example, normal strength steels are produced by annealing and normalizing while high-strength steels are produced by quenching and tempering process (Kodur et al., 2012).

Bolts are an integral part of a connection system and knowledge of high-temperature thermal and mechanical properties of bolts is critical for evaluating fire resistance using numerical models. In addition, high strength bolts are commonly used in construction to improve the overall connection efficiency. However, due to lack of experimental data, high-temperature constitutive material modes developed for mild steel are used by researchers in modeling the high-temperature behavior of bolts made with high-strength bolt steel. A review of carbon steel properties can be found elsewhere (Kodur et al., 2010) . This section provides a review of the studies involved in evaluating high temperature bolts properties.

Kirby (Kirby, 1995) studied the tension, double shear and residual strength behavior of high-strength Grade 8.8 M20 bolts in the temperature range of 20-800°C. Kirby used three sets of bolts and two sets of nut with different lengths (overall, thread length) and manufactured through different heat treatment processes. In all the tests, the bolts were heated to the desired temperature at a specific rate and then allowed to stabilize before the loading was applied. Two different heating rates of 5-10°C/min and 2-2.5°C/min and stabilization periods (15 min and 60 min) were used to assess the effect of heating rate on the strength reduction. All the tests were displacement controlled with a nominal strain rate of 0.001-0.003/min in the elastic and plastic regions. The residual strength of the bolts was evaluated by determining the hardness of a section of bolt shank after the bolts were heated to elevated temperature. The author observed that for bolts in tension and double shear (a) the ultimate capacity reduced drastically between 300-700°C (b) the slow heating rate and increased stabilization period had little influence on ultimate capacity (c) beyond 300°C, different processing conditions used in bolt manufacturing had little influence on their ultimate capacity (d) premature failure of bolts in tension by thread stripping depends on the interaction of threads between bolt and nut (e) the residual strength test data indicates that further softening of bolts occur when the fire temperature exceeds the tempering temperature used in its manufacturing process. Based on the test results and observations, the author proposed strength reduction factors that can be used to predict the variation of ultimate capacity of bolts (in shear and tension) with increasing temperature.

Yu (Yu, 2006; Yu and Frank, 2009) undertook an experimental program to evaluate the strength and stiffness reduction of A325 and A490 bolts at elevated temperatures (20°C – 800°C). All the tests were done by subjecting the bolts to a uniform constant temperature and then loading them until failure occurred. Based on the test results, Yu observed that both A325 and A490 bolts experience marginal strength and stiffness loss up to 300°C. However, the loss increases significantly in the temperature range of 300-800°C. At 800°C, A325 bolts retained only 8% of their initial capacity while A490 bolts retained 10% of their initial capacity. The authors also conducted residual (post-fire) strength tests on both the bolt types and observed that both A325 and A490 bolts lose strength when heated above tempering temperature used in the heat treatment of bolts. Residual strength tests conducted after exposing both bolt type to 800°C indicated that A325 bolts experienced a maximum residual strength loss of 45% compared to 40% experienced by A490 bolts. In addition, test results indicated that the duration of exposure has negligible effect while the cooling rate has no effect on the residual strength of A325 bolts. Based on the test data, authors proposed high temperature shear strength reduction factors for A325 and A490 bolts as illustrated in Fig. 2.10.

Lange et al. (Lange and Gonzalez, 2012) conducted experiments to study the elevated temperature tension behavior of Grade 10.9 bolts in the temperature range of 20°C-700°C. Tensile test specimens (coupons) were made from high strength grade 10.9 bolts with a diameter of 16 mm and had a gauge length of 30 mm. The specimens were tested under a strain rate of

0.001/min till the strain in specimen was 2% (in order to compute proof stress) and then the strain rate was increased to 0.025/min and maintained until failure. Based on the test results the authors observed that the strength reduction of Grade 10.9 bolts was negligible till 300°C and they undergo a drastic strength reduction between 300-700°C.

Kodur et al.(Kodur et al., 2012) carried out an experimental program aimed at evaluating the high-temperature thermal and mechanical properties of Grade A325 and A490 bolts. Thermal conductivity and specific heat of A325 and A490 bolts were measured in the temperature range of 20-735°C while the thermal expansion was measured in the range of 20-1000°C in both heating and cooling phases of fire. Single shear and tension tests were carried out under steady-state conditions in the temperature range of 20-800°C. The authors observed that (a) temperature has significant influence on the thermal and mechanical properties of high-strength bolt steel (b) the amount of carbon content influence the thermal properties of bolt steel (c) strength properties of A325 and A490 bolt steel degrades faster than those of conventional steel (d) A490 bolt steel exhibits slightly higher strength and stiffness properties than A325 steel in the temperature range of 20-800°C. Based on the test results, the authors proposed high-temperature property relationships for modeling thermo mechanical properties of bolt steel in numerical models. A comparison of the proposed high-temperature bolt strength reduction properties along with conventional steel strength reduction factors is shown in Fig. 2.11.

2.5 Codes of Practice

In most countries, specifications for fire resistant design of connections are included in steel design standards. The current fire design provisions in most codes and standards are derived from limited number of standard fire tests conducted on scaled and isolated connection specimens.

In the US, specifications for the structural design of angle connections (simple shear connections) under ambient conditions are given in the AISC steel construction manual (AISC, 2011). According to the manual, under ambient temperature conditions, simple connections should be designed as flexible and are permitted to be proportioned for the reaction shear only. The effect of temperature on the performance of connections is accounted indirectly through strength reduction factors. The Appendix provides reduction factors for strength and modulus of structural steel at high temperature. However, no specific procedures are specified for fire design of connections.

Similarly, Eurocode 3: Part 1-8 (Eurocode3, 2005a) states that the bolted shear connections loaded in shear should be designed as either bearing type or slip-critical connections. To account for the effect of fire induced strength degradation, Eurocode 3: Part 1-2 (Eurocode3, 2005b), specify the use of strength reduction factors to steel. However, Eurocode 3 does not provide specific procedures for fire design of double angle connections. In addition, there are no special design provisions to account for the effect of fire induced forces on the response of connections.

2.6 Summary

The state-of-the art review clearly indicates that there are limited studies on the system-level fire performance of double angle connections. These studies observed that the bolted double angle connections have good tying resistance and rotational capacity in comparison to other connections. However, there is a lack of knowledge with respect to a number of key areas that are critical for developing design strategies for fire safety design of double angle connections. Based on the above review, the following conclusion can be drawn:

- There have been limited studies on the fire performance of connections and most of them focused on developing moment-rotation characteristics. Most of the experimental studies tested isolated connections under standard fire or uniform temperature conditions. The effect of realistic fire, loading and structural continuity on the behavior of connections as part of structural framing system needs to be studied.

- Numerical models for predicting the fire performance of connections are available in literature. Almost all the models accounted for geometric, material nonlinearities as well as the nonlinear contact interactions between connection components. However, most models are validated for isolated connection configurations under standard fire or uniform temperatures.
- The ultimate capacity of bolts in tension and double shear reduces drastically between 300-700°C and softening of bolts occur when the fire temperature exceeds the tempering temperature used in the bolt manufacturing process.
- Connections can help in improving the fire resistance of beam by reducing the mid-span moment during the heating phase of the fire. Different failure modes in connections were observed when the beam entered catenary action phase.
- Modeling of connections poses a significant challenge because of the presence of large number of interacting contact surfaces and the need to select and define realistic contact behavior, contact model parameters. An improper selection of contact surface behavior or contact parameters can create solution convergence issues.
- There is a need for the development of numerical models which are capable of accounting realistic fire, loading and interactions between connected members (ex: beam, column, slab) on the fire performance of connections. These models can be used to carry out parametric studies and the results can be used to develop design guidelines for enhancing the fire resistance of connections.

- The chemical composition and the heat treatment processes that high strength bolts undergo are different from those encountered by typical carbon steel. Therefore the high-temperature properties of bolt steel are completely different from that of carbon steel and have significant influence on the connection response and these should be properly account for in numerical models.
- No fire resistance experiments have been conducted on double angle connections that are considered to be part of structural framing system. Restraining effects arising from structural continuity can have a significant influence on the fire performance of double angle connections. Data from the fire tests are needed to validate finite element models.
- The effect of fire scenario on the fire response of double angle connection was not considered in previous studies. Fire scenario can vary from a standard fire curve with no decay phase to a design fire curve with decay phase (Refer to Figure 1.3). The decay phase can result in cooling of steel members and thus generate tensile forces due to the thermal shrinkage of steel. The development of these tensile forces was not considered in previous studies and needs further research.
- There is a need to quantify and consider fire induced forces in modeling the fire performance of double angle connections. The fire induced axial force can have a significant influence on the performance of double angle connections. For example, double angle connections (shear connections in general) are not designed to resist tensile forces that develop due to fire induced catenary action or due to shrinkage of steel members in cooling phase of a design fire. Generally, these fire induced forces are not accounted for in fire safety design due to lack of tools for evaluating them.

CHAPTER 3

3. EXPERIMENTAL STUDIES

3.1 General

The state-of-the-art review indicated that there is lack of test data on the overall fire behavior of double angle connections as part of a structural framing system. Though large number of experimental studies were conducted on connections in recent years, almost all of them were on isolated end-plate connections under uniform temperature conditions. To develop specific test data on double angle connections forming part of structural framing system, two sub-frame assemblies with double angle connections, were tested under fire conditions. The main objective of these tests is to generate test data for validation of finite element models. Full details of the fire resistance tests, specimen details, instrumentation, test procedure and measured parameters are presented in this chapter.

3.2 Test Specimens

The experimental program consisted of fire resistance tests on two sub frame assemblies, comprising of a network of beams connected through double angle shear connections. Two sets of tests were carried out on sub frame assemblies S1 and S2. Assembly S1 did not have a slab and had a lower fire decay rate and lower level of gravity loading than assembly S2, which had a slab.

Both the test assemblies had W12x30 secondary beams (3505 mm long), W14x132 perimeter beams (4216 mm long) and W14x74 primary beams (4293 mm long), as shown in Fig. 3.1. The secondary beams were connected to perimeter beams which in turn were connected to primary beams using two different double angle connection configurations. Connection details were designed as per AISC specifications (AISC, 2005) and are shown in Fig. 3.2. All the beams and angles used in the test assembly were made with ASTM A992 Grade 50 steel, while the bolts were 22 mm (7/8 in.) in diameter and made of ASTM A490 Grade steel. The ambient temperature mechanical properties of steel measured as per ASTM A370 (ASTM, 2011b) specifications are presented in Table 3.1 while the cross-sectional dimensions of the beams and angles are shown in Table 3.2.

Initially, each connection assembly was insulated with 12.7 mm (½ in.) spray-on fire resistive material (SFRM) on all three sides of the secondary beam along the majority of its length. During the application of fire insulation, the thickness was measured at several locations to assure a uniform thickness along the length of the beam. The insulation was then allowed to adequately dry for three weeks prior to fire testing. The insulation material that was used is CAFCO 300 with a specified thermal conductivity of 0.078 W/m-K and a density of 240 kg/m^3 at room temperature.

In assembly S1 the secondary beams were welded to the steel deck so as to provide rigidity against buckling of the beam. After the steel beams were assembled, a corrugated steel deck, of 2286 mm long and 3048 mm wide, was spot welded to the top of the secondary beams at six random locations. The deck was arranged such that the ribs are oriented perpendicular to the secondary beams and primary to the perimeter beams. No concrete slab was casted on assembly S1.

For assembly S2 a concrete deck was cast on steel frame to provide rigidity against lateral torsional buckling. A steel deck of 3454 mm by 3658 mm was attached to the secondary beams through shear studs spaced at 152 mm along the length of the secondary beam. The shear studs were of 19 mm diameter and 99 mm long and were spaced at 152.4 mm along the length of the secondary beam. The concrete slab of 114 mm was cast on 6x6-W1.4xW1.4 welded wire fabric shrinkage reinforcement. The slab was cast with light weight concrete supplied from a local concrete batch mix plant. Cross-sectional details of the beam and slab used in test assembly S2 is shown in Fig. 3.3(d). The design compressive strength was 28 MPa with an actual strength 41 MPa on the day of testing of the slab. The batch proportions of concrete are shown in Table 3.3. After placing the concrete, the concrete slab was covered with a vapor proof barrier and the slab was allowed to cure at ambient conditions. The relative humidity of concrete was measured on the day of testing at four different locations on top of the slab and the average relative humidity was 88%.

3.3 Instrumentation

The sub frame assemblies were instrumented with thermocouples, strain gauges, and displacement transducers to monitor thermal and structural response during the fire test. Temperatures in steel beams were measured using Type-K Chromel-alumel thermocouples, 0.91

mm thick, installed on the lower and upper flanges as well as on the web of each secondary beam at quarter and mid-span of the beam. Thermocouple layout in beam and concrete section, cross-sectional details of the beam and slab in assembly S2 are shown in Figs. 3.3(a)-(d), respectively.

Vertically and horizontally oriented linear variable displacement transducers (LVDT's) were attached at six distinct locations on secondary beams and perimeters beams in order to calculate axial and lateral beam displacements. The pressure in the vertical actuators was also recorded as a measure of applied axial load. Ten high-temperature strain gages were attached closer to the ends of secondary beams and at the mid-span of primary beams to directly measure the total strains. Location of the LVDT's and strain gauges in assemblies S1 and S2 are shown in Fig. 3.3(a).

Data from the above instrumentation network was recorded at five second intervals via a central data acquisition system. Also, the furnace temperature was measured using six thermocouples distributed spatially inside the furnace in accordance with the ASTM E119 test procedure. The pressure in the vertical actuators of the furnace was also recorded as a measure of applied load. Additionally, visual observations were made to record any important events (beam buckling, insulation fall off) or at five minute intervals throughout the duration of the test.

3.4 Test Apparatus

The fire resistance tests on double angle connection assemblies were carried out using structural fire testing facility at Michigan State University. The furnace has been specially designed to produce varying conditions of temperature, loading and heat transfer, to which a structural member might be exposed during a fire. The test furnace, shown in Fig. 3.4, has the capacity to simultaneously apply both thermal and structural loading to the test specimen, to simulate conditions experienced in a real structure. The furnace consists of a steel framework supported by four steel columns, with the furnace chamber inside the framework. The furnace heating chamber is 2.44 m (8 feet) wide, 3.05m (10 feet) long, and 1.78 m (5.8 feet) high. The maximum heat power the furnace can produce is 2.5 MW. Six gas burners located within the furnace provide the thermal energy, while six type-K Chromel-alumel thermocouples, distributed throughout the test chamber, monitor the furnace temperature during a fire test as per ASTM E119 standard. During the course of fire test, the gas supply is manually adjusted such that the furnace temperatures follow a pre-determined standard or realistic fire curves. In this way, the furnace temperature can be maintained along a designed curve.

Loading on the test specimen is applied through a furnace loading frame which consists of a network of two large and four small vertical pressure actuators located above the furnace. The large actuators (having an individual capacity of 2750 kN each) are primarily used for testing columns while the small actuators (with an individual capacity of 240 kN each) are used for testing beams and beam-slab assemblies. Each of the actuator is connected to a loading jack which sits on the surface of test specimen (beam, column etc) and transfers load from actuator to the test specimen. For testing current sub frame assemblies, four vertical pressure actuators were used to apply load on the sub frame assembly. To facilitate the visual observation of the fire exposed specimen during the fire test, two small view ports are provided on either side of the furnace wall.

3.5 Test Conditions and Procedure

The test specimen was placed in the furnace such that only the secondary beams were inside the furnace. The perimeter and primary beams were fully outside the heating chamber of the furnace with perimeter beams resting on the cantilever supports, while the primary beams were unsupported as shown in Fig. 3.2. The connections on the secondary beam are 152 mm to 178 mm outside of the furnace walls and are exposed to some heating indirectly through conduction from secondary beams and also from some level of radiation from the furnace walls. The connections were placed outside the heating chamber in order to measure the magnitude and nature of forces experienced by the connections due to heating of the secondary beams. In order to prevent the rotation of the assembly, pieces of wood were inserted between the perimeter beam of S2 and the furnace external frame.

The secondary beams in the sub frame assemblies S1 and S2 were exposed to two design fires DF1 and DF2 respectively, from three sides. Design fire, DF1, comprised of a growth phase for the first 75 minutes as per ASTM E119 fire (ASTM, 2011a) and then a decay phase with a cooling rate of 8°C/min (see Fig. 3.5). The decay rate was computed based on the Eurocode parametric fire curve equation (Eurocode1, 2002), using the input parameters listed in Table 3.4. Detailed calculations showing the computation of decay rate for design fire DF1 are presented in Appendix A. This design fire scenario was arrived at based on the typical dimensions, construction materials and fire loads encountered in a typical office building.

Similarly DF2 included a growth phase simulating the ASTM E119 standard fire for the first 90 minutes and then followed by a decay phase with a cooling rate of 15°C/min (see Fig. 3.5). The higher cooling rate was chosen for assembly S2 to study the response of the assembly under different cooling scenario and to quantify the effect of the cooling rate. The predicted and the measured time-temperature relationship of DF1, DF2 are illustrated in Fig. 3.5. A summary of test parameters considered in this experimental study are shown in Table 3.5.

Loading on both assemblies comprised of four point loads, applied at two points along each secondary beam, as shown in Figs. 3.4(a)-(b). Assemblies S1 and S2 were subjected to an initial load of 74.7 kN and 92.2 kN at each actuator loading point, respectively. These load values correspond to a load ratio (level) of 40% and 50% of the secondary beam ultimate moment capacity. Load ratio is defined as the ratio of applied loading under fire conditions to the ambient temperature capacity of the beam. The loading was applied 30 minutes prior to the start of the test to ensure that the deflections reached a steady state before the start of the fire. During the test, the connection assemblies were exposed to heat controlled in such a way that the average temperature in the furnace followed, as closely as possible, the targeted time temperature curve. The load was kept constant throughout the test. The connection assemblies were considered to have failed and the tests were terminated when the secondary beams suffered local and lateral torsional buckling and could no longer carry the applied load.

3.6 Results and Discussion

Data generated from the fire tests were used to evaluate the thermal response, structural response and failure patterns of double angle connections under fire conditions. The naming convention used for various beams in each sub frame assembly (S1 and S2) is illustrated in Fig. 3.1.

3.6.1 Thermal Response

The progression of temperatures (at quarter and mid-span) in the secondary beams (Beam I and Beam II) of assemblies S1 and S2 is plotted as a function of time in Fig. 3.6 and 3.7 respectively. The temperatures at both mid-span and quarter span of both secondary beams follow closely with fire temperature in the growth phase of fire. The temperatures at the bottom flange are higher than that of the top flange and this is attributed to the closer vicinity of bottom flange to fire exposure. In addition the bottom flange was exposed to fire from top and bottom surfaces as opposed to bottom surface of top flange only.

The temperatures in the top flange of the secondary beams at mid-span are significantly lower compared to that at the quarter span. This discrepancy in temperatures can be attributed to non-uniform gas temperature distribution in the furnace. Specifically, the quarter span location is closer to the furnace walls, and experiences heating (radiation effect) from two furnace walls as opposed to mid-span receiving radiation from one furnace wall.

The maximum average temperatures measured in secondary beams, shown in Fig. 3.8, for assemblies S1 and S2 are 700°C and 645°C respectively and this occurred at 90 minutes into fire exposure. It can be seen from the figure that the general trend in temperature variation is similar in both beams. However the maximum average temperatures reached in assembly S2 is lower compared to S1 and this can be attributed to the shielding effect provided by the concrete slab to the top flange of the beams.

Connections in the sub frame assemblies S1 and S2 experienced heating indirectly via conduction from the secondary beam and radiation from the furnace wall. In addition, due to the availability of limited number of thermocouple channels, all the thermocouple channels were used to monitor the temperature progression in the secondary beams as well as the furnace chamber. Therefore, no temperature measurements were made directly at the connections. However, an indication of the maximum temperatures experienced by the connections could be gauged (indirectly) through the high-temperature strain gauges placed on the connections. In both tests, these strain gauges provided reliable readings throughout the duration of test without any fluctuations (abrupt variations). Based on a series of fire tests (on different structural assemblies) it has been established that these high-temperature strain gauges give reliable readings when the temperatures are below 200°C (Dwaikat et al., 2011). This led us to conclude that the temperatures in connections remained below 200°C. Thus, the connections retained most of their ambient temperature strength in both the tested assemblies.

3.6.2 Structural Response

The structural response of double angle connections can be assessed by examining the progression of rotation-time history, which in turn is related to the fire induced forces development and strain levels attained in the connections.

Connection Rotations

The progression of rotation in the connections at the ends of secondary beams is shown in Fig. 3.9. The values of rotation (θ) are evaluated using vertical deflection (u) of the secondary beams (measured by the LVDT's at the loading points) and the distance from the connection to the loading point (L), as illustrated in Fig. 3.10. Once, the vertical deflection and length to loading point is known, the rotation at connection is evaluated using the following equation:

$$\theta = tan^{-1}({}^{u}/_{L}) \qquad [3.1]$$

The north and south legends used in these figures indicate the direction with respect to the secondary beams orientation where the measurements are made (Refer to Fig. 3.4(a) for the location of LVDT).

It can be seen from Fig. 3.9(a) that the rotation at connections in assembly S1, gradually increased with time during the early stages of fire. This increase in rotations is due to deteriorating strength and modulus properties of steel, as well as increased thermal expansion of the steel with temperature. However, the connection at one end of the secondary beams (Beam II – North) underwent a sudden increase in rotations at 65 minutes into the fire test. This is because the secondary beams (Beam II) at the location of the load actuator (North) experienced sudden increase in vertical deflection due to local buckling of the top flange and web at the location of the loading point, as shown in Fig. 3.11(a). In addition to local buckling, the secondary beam (Beam II) at the location of the loading actuator (North) rotated and experienced global lateral torsional buckling, as can be seen from Fig. 3.11(b). This led to sudden increase in rotations at the connections. However due to safety concerns (to mitigate collapse of the test assembly in to the furnace), the applied loading on the beam was removed and the test was continued to trace the thermal response under cooling phase of fire. At 180 minutes, the metal deck, present on top of the secondary beams, underwent significant warping (as shown in Fig. 3.12) which distorted the entire assembly causing the connections to undergo rapid rotation.

The rotation at connections in assembly S2 progressed similar to that of S1, but the connections underwent much higher (almost double) rotations without any local and global instabilities. This can be attributed to the higher rigidity provided by the concrete slab and this enhanced the overall strength of the beams and in turn the connections. After reaching a maximum rotation at 110 minutes (slightly after the start of cooling phase of fire) the rate of rotation at connections decreased steadily. This is on expected lines since the beams regained some of their initial strength and stiffness after the start of the decay phase of fire and thus the rotations started to decrease.

Forces in Connections

The fire induced forces developed in the double angle connections were monitored by strain measurements and these strains are plotted as a function of time in Fig. 3.13. Few of the strain gauges were damaged (which is common in fire tests) so only the measurements obtained from functional strain gauges are shown in Fig. 3.13. For assembly S1, strain gauges attached to top flange of secondary beam (Beam II) and primary beams (Beam III) were damaged. Similarly in assembly S2, strain gauges attached to top flange of secondary beam (Beam I) were damaged.

As can be seen from Figs. 3.13(a)-(b), strains in the connection gradually increase with fire exposure time and are compressive in nature during the initial stages. This is on expected lines because as the secondary beams are heated they undergo a significant thermal expansion which results in the development of large compressive forces in the connection. However as the fire enters the decay phase, the compressive strains decrease and finally transform to tensile strains. This transformation in the direction of strains can be attributed to the deteriorating strength and stiffness of beam with increasing temperature which results in permanent deformation of beam. At this point the beam is no longer able to carry any load and it is held in place (like a cable) by the connections alone through catenary action(Liu et al., 2002). Thus the connections experience a shift in the nature of forces from compression to tension. The sudden increase in the compressive force in S1 is due to global buckling (of Beam I). Nonetheless, the general nature of forces experienced by the connection in two assemblies is similar except for the instabilities (caused by local and global buckling) that occurred in the secondary beam of assembly S1.

The strain readings indicate that the top and bottom flanges of the beam did not carry significant compressive (axial) forces in comparison to the beam web. This can be attributed to the fact that the web of beam was connected directly to the perimeter beams through double angles. The transfer of forces (during expansion or contraction of secondary beam) between secondary beam and perimeter beam happened only through the beam web via double angle. Hence the web experienced higher compressive (axial) force in comparison to the flanges.

Figs. 3.13(c)-(d) show the variation of strain in the primary beam (Beam III) as a function of fire exposure time. It can be seen in the figure that the strains in the beam change from positive to negative indicating that the connection between perimeter and primary beams experienced tensile force in the initial phase and compressive force during the later stages of fire exposure**.** This can be attributed to the fact that as the temperature of secondary beam increases (in initial phase) it undergoes thermal expansion which tends to push the perimeter beams. Relatively cooler perimeter beams resist the thermal expansion of secondary beam by pulling the primary beams. This results in the development of tensile forces in connection at the location of perimeter and primary beams. Similarly, the tensile forces transform to compressive forces when the secondary beams starts to cool and subsequently begin to undergo thermal contraction. It is interesting to note that the primary beams experienced a non-uniform strain indicating that the primary beams are subjected to thermally induced moments despite the connections between the beams (secondary-perimeter and perimeter-primary beams) being simple shear connections. This shows that the double angle connections exhibit some rigidity and are capable of transferring moments between the connected members under fire conditions. This is in contrast to simple shear connections wherein the connection is designed to transfer shear forces only.

It can also be seen from Fig. 3.13(c) that the global buckling experienced by Beam II in assembly S1 had an impact (caused sudden change in strain at 68 minutes) on the connection between perimeter and primary beams. Strain readings for the primary beam (Beam IV) in S1 could not be recorded since these strain gauges were damaged early into fire test.

Forces in Beams

The progression of axial forces in secondary, primary beams and concrete deck are shown in Fig. 3.14 as a function of fire exposure time for sub frame assembly S2. A positive value indicates tensile force in the beam while a negative value indicates compression in the beam. The axial force in each beam is calculated using the degrading elastic modulus (E) and the measured strain values. The axial resistance provided by the concrete deck is estimated by taking the difference between the forces carried by perimeter and primary beams.

It can be seen from the figure that during early stages of heating (till 45 minutes), secondary beam experienced compression while the concrete deck unloads (because of thermal bowing of the deck, beam) through the development of composite action facilitated by the shear studs. As the thermal gradient between the concrete deck and the bottom flange of secondary beam increases (between 45-90 minutes into fire) the top flange of the beam goes into significant tension, which brings the average secondary beam axial force into tension. This observation is also confirmed by large tensile strains observed in the top flange of secondary beam (see Fig. 3.13(b)). The increase in tensile force continues till 90 minutes after which the secondary beam stiffness gets significantly lower and the tensile force in the beam decreases. After 120 minutes, the thermal contraction of secondary beam causes it to enter into tension phase again.

3.6.3 Failure Patterns

Visual observations were continuously made during the course of each fire test and also after fire tests to trace the response of the double angle connections. Fig. 3.15 shows the local and lateral torsional buckling experienced by the secondary beam in assembly S1. It can be seen from the figure (Fig. 3.15(a)) that significant amount of insulation has fallen off from the web and top flange of secondary beam. This abrupt loss of insulation led to rapid increase in the temperatures in the web and top flange thereby decreasing the load carrying capacity of the beam. As a result, the top flange and the web of the beam in assembly S1 buckled (Fig. 3.15(b)) leading to sudden increase in deflections and subsequently increase in rotations at connections. This increase in deflections together with local buckling, caused the beam to rotate at the ends through lateral torsional buckling phenomenon, as illustrated in Figs. 3.15(c)-(d).

For test assembly S2, insulation fell-off (from the deck) and initial cracks began to form in the concrete slab at around 30 minutes into the fire test. The number of cracks, as well as the progress of these cracks in the slab gradually increased with steam and water vapor emitting out of these cracks. At about 50 minutes in to fire exposure, a large crack formed in the middle of the slab and small concrete fragments started to fly-off. By the end of the test, the deck had lost almost all of the insulation and had undergone significant warping, as illustrated in Fig. 3.16.

Observations of the double angle connections after fire tests indicated that the connections underwent permanent deformation in both assemblies and the extent of deformation in assembly S2 was lower in comparison to that of assembly S1. It was also observed that the top flange of the secondary beam in assembly S2 was intact with the concrete slab and it was free of local and global instabilities as opposed to assembly S1. These observations indicate that the presence of concrete slab stabilized secondary beam in assembly S2 throughout the fire test, which allowed the double angle connections to develop significant (more than double) rotations, without failure, in comparison to double angle connections in assembly S1.

3.7 Summary

Fire tests were conducted to evaluate the behavior of double angle connections as part of structural framing system. The influence of concrete slab on the fire behavior of connections was evaluated by comparing the thermal and structural response obtained from tested assemblies with and without the slab. Double angle connections in both the assemblies did not experience failure though they experienced permanent deformations demonstrating the inherent rigidity and the robustness of these connections. The strain profile in primary beams was non-uniform which indicates that double angle connections are capable of transferring fire induced moments between connected members despite being designed as simple shear connections. Results of these tests show that cooling rate of decay phase, load level, presence of slab and structural continuity of the framing system has significant influence on the fire response of double angle connection assemblies.

CHAPTER 4

4. NUMERICAL MODELS

4.1 General

Undertaking experiments to trace the fire behavior of connections is quite expensive, time consuming and requires sophisticated test facilities. In fire tests, only limited number of parameters can be monitored and interdependency of parameters cannot be traced. Further, for undertaking such fire tests there are lack of reliable high temperature instrumentation (such as strain gauges), that can monitor response parameters at elevated temperature. Therefore there is limited experimental data in literature on connection behavior at elevated temperature.

At present there are limited specifications for fire design of connections in design standards such as Eurocode 3. However, these design provisions are derived from limited number of standard fire tests conducted on scaled and isolated connection specimens. These design provisions do not specifically account for the effect of fire induced forces in evaluating rotation in connections. As shown in Chapters 1, 2 and 5, connections, experience significant fire induced axial forces that arise from the effect of structural continuity in a framing system. Hence, current design provisions which are developed based on isolated connection response cannot be applied to trace the system-level transient response of connections.

An alternative to overcome many of the shortcomings in fire tests is through applying numerical models to trace the fire response of connections. In recent years, commercial finite element (FE) programs became widely available thus making them an efficient alternative to model the behavior of connections. The relatively inexpensive finite element method(s) provides effective strategy to analyze fire response of connections.

This chapter presents the development of two finite element models (FEM1 and FEM2) to simulate fire response of three steel framed assemblies with double angle connections. Both the models employed system-level analysis (described later) to simulate the fire response of connections. The first finite element model (FEM1) is developed to simulate fire response of two sub-frame assemblies one with slab and the other without slab. The second finite element model (FEM2) is developed to simulate the fire response of restrained steel frame with a different double angle connection configuration compared to FEM1. Both the finite element models are validated by comparing the thermal and structural responses obtained from the model with those measured during fire tests. More details about the finite element models along with the validation are presented in the following sections.

4.2 Selection of Finite Element Program

The general-purpose finite element program ANSYS was chosen to carry out the numerical studies because of its diverse capabilities. ANSYS has the ability to efficiently model highly sophisticated material and geometrical nonlinearities. ANSYS enables the user to specify temperature-dependent thermal and mechanical properties of different material types such as steel, concrete and fire insulation.

Since forces from different structural components are transferred through connections, there will be contact interactions at the interface of each pair of these components (such as beam, column, bolts and angles). These interactions at the interface play a major role on the way forces are transferred and the development of failure modes in connection assemblies. Therefore, these interactions are to be accounted for and properly simulated in the analysis. ANSYS provides a wide range of contact interaction models and contact parameters to simulate contact interactions in addition to allowing user-defined contact parameters. This enables the user to model any specific type of contact interaction problem at hand.

In addition, ANSYS provides flexibility for creating geometry of the model using ANSYS script language (APDL-ANSYS Parametric Design Language) in which different geometric configurations and material models can be defined as parameters. Thus, APDL can be used as an effective tool for creating new models and automating parametric studies. Further, ANSYS contains a rich library of diverse categories of elements that are well suited for different purposes of analysis.

The double angle connection assembly analysis was carried out by incorporating all significant parameters that influence the response of connections, including material and geometric nonlinearities, high temperature properties of steel, concrete and insulation, and nonlinear contact interactions. Details of the finite element analysis are provided in the following sections.

4.3 Finite Element Modeling

4.3.1 General Approach

In finite element approach, fire resistance analysis of connection assemblies is generally carried out through two stages of analysis, namely, thermal and structural analysis. The thermal analysis provides temperature distribution in the connection assembly subjected to a given fire scenario. The output of the thermal analysis, nodal temperatures, is then applied as an input thermal-body-load in the structural analysis and a transient stress analysis is carried out. For practical cases of analysis, the following assumptions are adopted in undertaking fire resistance analysis:

- Fire temperature is independent of connection assembly response: As explained below, fire temperature is dependent on geometry, fuel and ventilation characteristics of the compartment only and is independent of the response of connection (and structural) assembly.
- Thermal analysis is independent of the structural analysis: The evolution of temperature profile in the connection and structural members depends only on density, thermal conductivity and specific heat of steel, concrete and insulation. However, the structural response of the members depends on the mechanical properties, modulus of elasticity, stress-strain relationships of steel and concrete. Hence, the progression of temperatures in connection assembly occurs independently of the structural response.
- Temperature distribution is uniform along the beam span length: The entire length of the beam is subjected to the same fire exposure conditions and the cross-sectional geometry remains the same throughout the member. Hence, cross-sectional temperature distribution will be uniform along the beam span length.

The fire scenarios that are typically used in fire resistance analysis can be grouped under two categories. Standard fire scenario; where fire temperature continues to increase without any cooling phase (as in ASTM E119 and ISO 834 standard fire exposures), and realistic fire scenario where fire temperature increase with time in growth phase and then gradually decrease with time in the decay or cooling phase.

In case of a “realistic” fire, a decay phase follows after reaching a maximum fire temperature in growth phase. Unlike in standard fire where temperature is expressed as a function of time only, the growth and decay phases of realistic fires are dependent on the compartment geometry and fuel and ventilation characteristics. The realistic fires can be approximated/modeled using time-temperature relationships provided in codes and standards (and referred to as design fire). Examples of design fires are the Swedish fire curves and the parametric fire curves specified in the Eurocode (Eurocode3, 2005b) and SFPE handbook.

In general, the rise of fire temperature is dependent on geometry, fuel and ventilation characteristics of the compartment. Computational fluid dynamics (CFD) models are required to compute the evolution of fire in a certain enclosure. Most of the CFD models are computationally intense as they adopt iterative, finite-difference technique and are conditionally stable (i.e., the time step depends upon the smallest element in the geometry). The goal of the current study is to simulate the system-level fire response of connection assemblies accounting for computationally expensive contact interactions. Adopting CFD analysis to predict the evolution of fire temperature will add exponentially large computational time to already computationally expensive finite element model (due to contact interactions). Therefore, CFD analysis is beyond the scope of this study and the fire scenario is assumed to follow specific time-temperature relationships specified in design standards.

The fire resistance analysis, with its thermal and structural sub models, is carried out via ANSYS finite element program using the following general procedure:

- Different structural components in the connection assembly are discretized into elements and total fire exposure time is divided into a number of time steps and the fire resistance analysis is carried out at each time step. A typical connection region in a steel framed building along with different structural components present in the connection region is illustrated in Fig. 4.1(f).
- Ambient temperature structural response: Static structural analysis is performed on the double angle connection assembly to obtain the structural response (deformations and stresses) of all connected members at ambient conditions (room-temperature).
- Thermal analysis: Temperature distribution in the beam cross-section is obtained at every time step and for the entire fire exposure history. Since the beam and connections are subjected to the same fire exposure conditions, the temperature progression at the location of connection cross-section will be the same as that obtained for a beam cross-section.
- Structural analysis: During the first time step, the temperature distribution of beam cross-section obtained from thermal analysis is applied as a thermal-body-load on the ambient-temperature deformed model of the connection assembly and a stress analysis is carried out. For the subsequent time steps, the temperature distribution of beam cross-section obtained from thermal analysis is applied as a thermal-body-load on the deformed model from previous time step and a stress analysis is carried out

More details about the thermal and structural sub models are presented in the following sections.

4.3.2 Thermal Analysis

4.3.2.1 General

The cross-sections of beam, along its entire length, is subjected to the same fire exposure conditions. Hence, the temperature distribution (profile) at any beam cross-section will be same and the temperature distribution will be uniform along the beam span length. Therefore, the beam cross-sectional temperatures can be obtained by carrying out a two dimensional heat transfer analysis instead of conducting a three-dimensional heat transfer analysis. Connections are not specifically accounted for in the thermal analysis. This is due to the fact that connections in sub-assemblies S1 and S2 were placed outside the heating zone of the furnace (Refer to Chapter 3). Therefore, the connections experienced heating indirectly via conduction from the secondary beam. This conductive heating of connections through secondary beam is accounted for in the thermal analysis.

4.3.2.2 Governing Equations

The two-dimensional governing partial differential heat transfer equation with in a structure can be written as:

$$\rho c \frac{dT}{dt} = \nabla . (k \nabla T) \qquad [4.1]$$

where k = conductivity matrix, ρc = heat capacity, ρ = density, c = specific heat, T = temperature, t = time, and ∇ = is the spatial gradient operator.

At the fire-beam interface, heat transfer occurs through radiation and convection. The total heat flux on the boundary of beam due to convection and radiation is given by the following equation:

$$q_b = (h_{con} + h_{rad})(T - T_f) \qquad [4.2]$$

where h_{rad} and h_{con} are the radiative and convective heat transfer coefficients, and are defined as:

$$h_{rad} = 4\sigma\varepsilon \left(T^2 + T_f^2\right)\left(T + T_f\right) \qquad [4.3]$$

T_f = temperature of the atmosphere surrounding the boundary (i.e., fire temperature),

h_{con} = 25 W/m^2.°K as recommended in literature (Eurocode3, 2005b)

σ = Stefan-Boltzman constant = 5.67×10^{-8} (W/m^2.°K^4), and

ε = emissivity factor for steel and it is related to the "visibility" of the exposed surface of structural member to the fire.

Fire is assumed to be emanating from a point source (infinitesimal sphere) perfect black body radiating heat equally in all spatial directions. To account for heat lost to surroundings as fire travels from its source to beam; it is assumed that only 70% of the radiant heat from fire source reaches the beam surface. Therefore, a steel emissivity factor of 0.7 specified in Eurocode (Eurocode3, 2005b) is assumed in the analysis.

The heat flux and temperature gradient are related through Fourier's law of heat conduction as:

$$q = -k\nabla T \qquad [4.4]$$

According to Fourier's law, the governing heat transfer equation on any boundary of the beam cross-section can be expressed as:

$$k\left(\frac{\partial T}{\partial y}n_y + \frac{\partial T}{\partial z}n_z\right) = -q_b \qquad [4.5]$$

where n_y and n_z = components of the vector normal to the boundary in the plane of the cross-section. The right hand side of Eq. [4.5] depends on the type of imposed boundary condition. As the beam is exposed to fire from three sides, two types of boundary equations are to be considered for thermal analysis, namely:

- On fire exposed boundaries where the heat flux is governed by the following equation:

$$q_b = -h_f\left(T - T_f\right) \qquad [4.6]$$

- On unexposed boundary (top surface of the beam) where the heat flux equation is given by:

$$q_b = -h_0 \left(T - T_0\right) \qquad [4.7]$$

where:

h_f and h_0 = heat transfer coefficient on fire side and the cold side, respectively, and

T_f and T_0 = temperature at fire and cold side, respectively.

The nodal temperatures of any element are related by the appropriate shape functions matrix (N) to arrive at the temperature of the element

$$T = \{N\}^T \cdot T_e \qquad [4.8]$$

Then the heat transfer equation (Eq.[4.1]) subjected to appropriate boundary conditions (Eq.[4.5]) can be discretized as (Cook et al., 2002; Reddy, 2005):

$$C_e^t \dot{T}_e + K_e^t T_e = Q_e \qquad [4.9]$$

C_e^t is the specific heat matrix. K_e^t is the thermal "stiffness" matrix and is the sum of conductivity and convection matrices. Q_e is the applied nodal thermal load and is composed of the convective and radiative heat fluxes. T_e are the nodal temperatures.

4.3.2.3 Discretization of Beam

The thermal analysis of the beam cross-section was carried out using two types of elements, namely SOLID70 and SURF152, as shown in Fig. 4.2. SOLID70 was used as a solid element with three-dimensional thermal conduction capability. The element has eight nodes with a single degree of freedom, temperature, at each node. The element is applicable to a three-dimensional, steady-state or transient thermal analysis. The temperature within SOLID70 element is interpolated from the nodal degrees of freedom (T_e = $T_{i,j,k,l,m,n,o,p}$) using the following isoparametric function:

$$T = \frac{1}{8}\begin{bmatrix} T_i(1-s)(1-t)(1-r) + T_j(1+s)(1-t)(1-r) + T_k(1+s)(1+t)(1-r) \\ +T_l(1-s)(1+t)(1-r) + T_m(1-s)(1-t)(1+r) + T_n(1+s)(1-t)(1+r) \\ +T_o(1+s)(1+t)(1+r) + T_p(1-s)(1+t)(1+r) \end{bmatrix} \qquad [4.10]$$

where s,t and r are the isoparametric locus of a point in the element domain. In order to carry out the numerical integrations, 2x2x2 integration points are used in SOLID70 elements.

The SURF152 element is generally used for various load and surface effect applications. In the thermal analysis, SURF152 element is overlaid onto the face of SOLID70 3D thermal solid element to simulate the effect of both thermal radiation and heat convection from ambient air to the exposed boundaries of the steel section (refer to Eq.[4.2]).

Heat convection load was applied around the section, and a convection coefficient of h_{con} = 25 W/(m^2 .˚C) was assumed in the analysis. The ambient (bulk) temperature on the node M of SURF152 element was assumed to be equal to either the fire temperature (T_f) in case the boundary is exposed to fire, or to room-temperature, in case the boundary is not exposed to fire. SURF152 uses linear interpolation functions and two integration points for numerical integration.

4.3.3 Structural Analysis

The structural analysis is carried out by discretizing the geometry of connection assembly with SOLID185 elements (see Fig. 4.2), suitable for 3-D modeling of solid structures. This element has the capability of representing plasticity, stress stiffening, large deflections, large strains, material and geometrical nonlinearities (ANSYS Inc, 2009c). Material nonlinearities can be introduced through nonlinear temperature-stress-strain curves and temperature-dependent thermal strain while geometric nonlinearities are introduced through accounting for large deformations. SOLID185 (ANSYS Inc, 2009c) element has eight nodes with three degrees of freedom at each node, namely translations in the nodal x,y and z directions. In the element notation, the translations in x,y and z directions are referred to as u,v and w respectively. The translation (in any direction) within SOLID185 is interpolated from the nodal degrees of freedom ($u_e = u_{i,j,k,l,m,n,o,p}$; $v_e = v_{i,j,k,l,m,n,o,p}$ and $w_e = w_{i,j,k,l,m,n,o,p}$) using the following isoparametric function:

$$u = \frac{1}{8}\begin{bmatrix} u_i(1-s)(1-t)(1-r) + u_j(1+s)(1-t)(1-r) + u_k(1+s)(1+t)(1-r) \\ +u_l(1-s)(1+t)(1-r) + u_m(1-s)(1-t)(1+r) + u_n(1+s)(1-t)(1+r) \\ +u_o(1+s)(1+t)(1+r) + u_p(1-s)(1+t)(1+r) \end{bmatrix} \quad [4.11]$$

$$v = \frac{1}{8}\begin{bmatrix} v_i(1-s)(1-t)(1-r) + v_j(1+s)(1-t)(1-r) + v_k(1+s)(1+t)(1-r) \\ +v_l(1-s)(1+t)(1-r) + v_m(1-s)(1-t)(1+r) + v_n(1+s)(1-t)(1+r) \\ +v_o(1+s)(1+t)(1+r) + v_p(1-s)(1+t)(1+r) \end{bmatrix} \quad [4.12]$$

$$w = \frac{1}{8}\begin{bmatrix} w_i(1-s)(1-t)(1-r) + w_j(1+s)(1-t)(1-r) + w_k(1+s)(1+t)(1-r) \\ +w_l(1-s)(1+t)(1-r) + w_m(1-s)(1-t)(1+r) + w_n(1+s)(1-t)(1+r) \\ +w_o(1+s)(1+t)(1+r) + w_p(1-s)(1+t)(1+r) \end{bmatrix} \quad [4.13]$$

where s,t and r are the isoparametric locus of a point in the element domain. In order to carry out the numerical integrations, 2x2x2 integration points are used in SOLID185 elements.

The structural analysis is carried out based on the principle of virtual work. According to this principle, any virtual change in the internal strain energy must be balanced by a change in the external work due to the applied loads.

$$\delta U = \delta V \quad [4.14]$$

where U is the strain energy and V is the external work. Variation in strain energy (δU) can be evaluated as:

$$\delta U = \int_{vol} \{\delta \varepsilon\} \sigma dvol \quad [4.15]$$

For structural members subjected to fire conditions, the strain vector (ε) is the sum of thermal (ε_{th}) and mechanical strains (ε_m) in steel,i.e.:

$$\varepsilon = \varepsilon_m + \varepsilon_{th} \quad [4.16]$$

Creep strain is steel is not explicitly accounted for in the analysis. Creep strain is defined as the time-dependent plastic strain under constant stress and temperature. The effect of creep in steel becomes noticeable at temperatures above 400°C with the creep effects increasing with increasing temperature. Including high-temperature creep in the analysis generally requires the use of explicit solver which is computationally expensive. This is due to the fact that the time increment in explicit solver is dictated by the size of the smallest element in the model. Hence, accounting for creep in addition to already computationally intense contact interaction will exponentially increase the overall computational time of the model. However, high-temperature creep in steel is accounted for indirectly by using the high-temperature constitutive material properties specified in Eurocode (Eurocode3, 2005b). This is because the steel properties specified in Eurocode (Eurocode3, 2005b) , are based on transient-state tests, which accounts for part of the high-temperature creep (Buchanan, 2002; Kodur et al., 2010). In fact, Eurocode (Eurocode3, 2005b) explicitly states that the “effects of transient thermal creep need not be given explicit consideration provided that the steel stress-strain relationships given in Eurocode are used”.

Variation of external work (δV) due to the applied nodal forces (F_e^n) can be computed by assuming a variation of nodal displacement $\{\delta u\}$ as:

$$\delta V = \{\delta u\}^{\mathrm{T}} \{F_e^n\} \quad [4.17]$$

The nodal displacements (u_e) of the finite elements are related to the nodal displacement field through shape functions matrix (N)as follows:

$$u_e = \{N\}^T \cdot u \quad [4.18]$$

Then the virtual work equation (Eq. [4.14]) can be rewritten in matrix form as:

$$K_e u_e - F_e^{th} = F_e^n \qquad [4.19]$$

where K_e is the element stiffness matrix, and F_e^{th} is the element thermal load vector.

4.3.4 Modeling Contact Interactions

In the connection assembly, contact interactions exist between different components (refer to Figs. 4.1(d),(e) and (f)) such as bolt shank and bolt hole, angle and beam/column web, bolt head/nut to the angle etc. Simulating these contact interactions is quite complex due to large number of interacting surfaces (parts), highly nonlinear interaction response and numerical convergence issues to reach a solution. Additionally, selecting a surface as contact or target surface prior to analysis is often unclear in most cases and some trial runs have to be conducted.

Added to the above complexity, the behavior of interacting surfaces is highly dynamic because the surfaces can move in and out of contact regions within or between iterations(ANSYS Inc, 2009b). This dynamic movement of surfaces leads to sudden change in stiffness matrix and more equilibrium iterations (often with reduced time steps) have to be carried out to achieve convergence. Thus, the computational time for structural analysis with contact elements is generally much higher than those without contact elements. Further, the computational time increases nonlinearly with each additional pair of interacting surfaces. This is due to the fact that at any time step, if equilibrium conditions are not satisfied even for one contact pair the iterations for all the contact pairs are to be repeated with a reduced time step.

The contact interactions between different parts are defined using “contact pairs” and are modeled as “surface-to-surface” contact using contact elements CONTA174 and TARGE170(ANSYS Inc, 2009c). CONTA174 was used as a surface element and was overlaid on the underlying SOLID185 elements. This element is capable of three-dimensional structural and coupled field contact analyses. The element has eight nodes and is capable of modeling three-dimensional surface-to-surface contact interactions.

The three-dimensional contact surface elements (CONTA174) are associated with corresponding three-dimensional target segment elements (TARGE170) using a set of parameters called as real constant set. In ANSYS, contact can happen only between CONTA174 and TARG170 elements with the same set of real constants. Thus, the problem of spurious contact between non-interacting parts is taken care of.

Proper selection of contact pair parameters (contact algorithm, contact surface behavior, key options, real constant set etc.) are crucial for avoiding most numerical convergence issues (Pakala et al., 2012a) in the model. In addition, care should be taken to make sure that finite element geometry is properly constrained (by appropriate boundary conditions) and there are no rigid body modes. The presence of gap(s) between contact surfaces (ex: bolt holes are oversize compared to bolt shank) is often the root cause for developing unconstrained/under-constrained models. These gaps directly lead to rigid body modes and proper care must be taken to stabilize and fully constrain the finite element model before starting the analysis. More details on the guidelines for implementing nonlinear contact interactions in finite element programs can be found elsewhere (Bursi and Jaspart, 1997a, b, 1998; Selamet and Garlock, 2010a; Van der Vegte and Makino, 2004).

The contact between interacting surfaces is successfully incorporated using “surface-to-surface” contact with “no separation but sliding permitted” option (ANSYS Inc, 2009b). The amount of sliding depends on the frictional model, which is defined according to Coulumb’s frictional law with a constant co-efficient of friction of μ=0.3 (assuming Class A faying surfaces) throughout the analysis. To determine the optimum set of contact parameters, a sensitivity study was carried out by varying the contact stiffness from 0.01 to 1 (as suggested in the ANSYS contact technology guide) (ANSYS Inc, 2009b). The upper bound value of contact stiffness is more appropriate for bulk deformation problems while the lower bound value is appropriate for bending deformation dominated problems (similar to the current one) while ANSYS uses a default value of 1 for the contact stiffness (ANSYS Inc, 2009b). A summary of contact parameters used are presented in Table 4.1.

4.3.5 High-temperature Material Properties

To accurately model the behavior of connection assemblies, appropriate thermal and mechanical properties of the constitutive material should be specified as input in ANSYS. The thermal properties include density, thermal conductivity and specific heat while the mechanical properties include the stress-strain relationships of steel, all of which vary as a function of fire temperature. For the thermal properties, empirical relations of steel provided in Eurocode 3 (Eurocode3, 2005b) are used, while the empirical relations of concrete specified in Eurocode 2 (Eurocode2, 2004) are used. The temperature-dependent thermal property relationships of steel and concrete are presented in Appendix B. The thermal properties of insulation at elevated temperatures are assumed to be same as that at room temperature due to lack of data on the variation of insulation properties with temperature. Since the insulation material has significantly low strength and stiffness, the strength contribution from the insulation is neglected.

For steel, the mechanical properties along with constitutive relationships and strength reduction factors provided in Eurocode 3 (Eurocode3, 2005b) were used to generate nominal stress-strain-temperature relationships. The strength reduction factors for carbon steel are shown in Fig. 4.3. The constitutive relationships and the reduction factors for carbon steel are presented in Appendix B. The strength reduction factors for bolt steel are based on the values proposed in a recent study (Kodur et al., 2012) and are presented in Appendix B. The nominal stress-strain relations were then converted into true stress-strain curves using the following relations:

$$\sigma_{true} = \sigma_{nom}(1+\varepsilon_{nom}) \quad and \quad \varepsilon_{true} = \ln(1+\varepsilon_{nom}) \qquad [4.20]$$

where σ_{true},ε_{true} represent true stress and strain while σ_{nom},ε_{nom} represent nominal stress and strain respectively.

For concrete, the mechanical properties along with constitutive relationships and strength reduction factors specified in Eurocode 2 (Eurocode2, 2004) were used to generate nominal stress-strain-temperature relationships. The constitutive relationships and the reduction factors for concrete are presented in Appendix B.

All the connection components (beam, column, double angle and bolts) are assumed to follow elasto-plastic material behavior with Von-Mises plasticity yielding criterion and isotropic hardening rule.

4.3.6 Failure Criteria and Numerical Convergence

The failure criteria adopted in the analysis is the one based on attaining ultimate plastic strain in steel. This failure criterion was adopted in previous studies for modeling connection response at elevated temperature (Selamet and Garlock, 2010b). Accordingly, the “failure” of the connection (steel) is said to occur when the ultimate plastic strain of steel in any of connection component exceeds 15% in 20-800°C temperatures range. The limiting strain of steel at failure is specified as 15% in Eurocode3 (Eurocode3, 2005b) for all temperatures. When the strain in steel reaches this limiting value, the governing finite element equations do not converge leading to non-convergence of the solution.

Force (load) controlled solution technique is used in the finite element analysis as displacement controlled technique cannot be used in conjunction with contact elements (ANSYS Inc, 2009b).

Numerically, convergence in the structural model is governed by the Newton-Raphson equilibrium iterations (ANSYS Inc, 2009c). In the structural model simulations, force convergence is said to be achieved if the error between successive iterations is less than 0.5% (i.e., having an accuracy of 99.5%) (ANSYS Inc, 2009a). Similarly, in thermal analysis the temperature convergence is assumed to be reached when the temperature difference at each node between successive equilibrium iterations is less than 0.5 °C.

4.4 Connection Models

4.4.1 General

The response of connections under fire conditions can be studied at three levels, namely: component-level, member-level (isolated member) and system-level. The component-level analysis captures the response at the component (connection) level and does not capture the effect of structural interaction on the response of connection. This is typically suitable for use in design office environments and can be implemented using spreadsheet calculations. According to this approach, the failure time of connection is determined by comparing the connection capacity against the fire induced forces. Failure time of connection is defined as the time at which connection capacity falls below that of fire induced forces. Though the component-level analysis is relatively simple to use it has several drawbacks namely: (a) this analysis does not account for the forces resulting from the interaction between structural members on the response of connection; (b) the effect of local beam instabilities (such as local buckling and lateral torsional buckling) on the connection response cannot be accounted for in this analysis, and (c) the transformation of fire induced axial forces from compression phase to tension phase cannot be captured. Therefore, component-level analysis cannot be used to predict the realistic fire response of connection

The member-level analysis (or isolated member analysis) is commonly used to simulate the response of connections which are not considered to be a part of the structural framing system. As the structural members (ex: beams) are considered to be isolated implying that they are free to expand thermally. Since the free thermal expansion is not restrained by surrounding structural members no fire induced forces will be generated in the beam and subsequently in the connections. However, in reality connections are always an integral part of a structural framing system and the connected beams have restraint (from surrounding structural members) to their free thermal expansion. This restraint to free thermal expansion, resulting in the development of fire induced axial forces in beams and connections. Therefore, member-level analysis also does not capture the realistic fire response of connections.

The system-level analysis refers to comprehensive analysis using finite element models. In this approach connections are considered to be an integral part of the structural framing system. Hence the connection region along with the surrounding structural members is modeled. In this approach, the fire induced forces developed in the beam are computed through a second order nonlinear analysis based on actual temperature profiles (in beam and connection), as well as deformed geometry of beam and connection. Therefore, this type of analysis simulates realistic response of the connection assembly and can capture the influence of surrounding structural system on the fire response of connections.

Hence, system-level approach has been adopted in developing the numerical models presented in this chapter and subsequent parametric studies presented in Chapter 5.

4.4.2 Assembly Level Connection Model (FEM1)

As mentioned earlier, two finite element models (FEM1 and FEM2) simulating the fire response of three typical connection assemblies have been developed and validated. The first finite element model (FEM1) is developed to simulate two tested sub-frame assemblies, namely S1 and S2 (Refer to Chapter 3). This model, consisting of beam slab assembly with double angle connections, was developed to simulate the response of sub-frame assemblies. Both the connection assemblies, S1 and S2, had fire insulated secondary beam connected to perimeter beam using double angle connections. However, assembly S1 did not have a slab and had a smaller fire decay rate and gravity load ratio than S2, which had a slab.

As the geometry of sub-frame assemblies was symmetrical about two vertical planes, only one quarter of the geometry was modeled, as shown in Fig. 4.4. The thermal analysis is carried out using SOLID70 and SURF152 elements. The structural analysis is carried out by discretizing the beams and connections in assemblies S1 and S2 using SOLID185 elements (see Fig. 4.2).

The boundary conditions of the sub-frame assemblies S1 and S2 were chosen to simulate conditions present in the fire test (Pakala et al., 2012b). During the fire test, the stiffeners present on the perimeter beam were placed on the furnace supports. In order to prevent the rotation of the assembly, pieces of wood were inserted between the perimeter beam and the furnace external frame. To simulate these conditions in the finite element model stiffener present on the perimeter beam was fully fixed.

As mentioned in Chapter 3, concrete slab is added to test assembly S2 in order to avoid local/global instabilities of the secondary beam (as observed in S1) and not to enhance its composite action. Additionally, the concrete slab was not restrained in any direction, thus the extent of composite action developed (if any) is minimal. Therefore, shear studs are not explicitly modeled to avoid the need for defining and accounting for additional contact interactions associated with studs. However, the beam-slab composite action is accounted for indirectly by modeling surface-to-surface contact interactions between top flange and bottom most layer of concrete slab. These contact interactions will ensure shear forces (which is the primary mechanism of force transfer in composite action) are effectively transferred at the interface of beam-slab.

The contact interactions between surfaces of different structural members are defined using "contact pairs" and are modeled as "surface-to-surface" contact using contact elements CONTA174 and TARGE170(ANSYS Inc, 2009c). In this model, there are one hundred and seventeen contact pairs defined with approximately 42,113 contact elements for both assemblies S1 and S2. In the current model, the contact between interacting surfaces is successfully incorporated using "surface-to-surface" contact with "no separation but sliding permitted" option. Based on the results of the sensitivity study, optimum normal contact stiffness (FKN) value of 0.1 was assumed in the first iteration of the analysis. This value is updated in subsequent iterations based on the current mean stress of the underlying element and the allowable penetration of contact elements.

4.4.3 Validation of Assembly Level Connection Model (FEM1)

The finite element model FEM1 created in ANSYS was validated by comparing predictions from the analysis with results obtained from fire experiments on connection assemblies S1 and S2 discussed in Chapter 3 (Fig. 3.6(a), Fig. 3.7(a) and Fig. 3.9). The validation process covered both thermal and mechanical response. In order to accurately capture stress concentrations in the connection region (angles, bolts, bolt holes), a relatively finer mesh was used within the vicinity of these regions. During the fire test, static gravity loading was applied on secondary beam prior to heating the connection assembly. Loading on the assembly comprised of four point loads, applied at two points along each secondary beam. To circumvent the problems of high-stress concentrations and numerical singularities due to external loading, the base of actuator pads was modeled and the load is applied as nodal force in the vertical direction (y direction).

The properties for different steel members used in this model are based on ambient temperature tensile coupon tests reported in Table 4.2. No coupon tests were performed to evaluate the mechanical properties of bolts. Hence, the nominal yield strength, ultimate strength and modulus of elasticity (as specified in the ASTM A490 standard (ASTM, 2012)) of bolts were assumed to be 940 MPa, 1040 MPa and 210000 MPa respectively. The properties of concrete used for slab are presented in Table 4.3. The reduction factors specified in Eurocode 2 (Eurocode2, 2004) (Fig. 4.5) are used to arrive at the elevated temperature constitutive relations for concrete. Since the insulation material has significantly low strength and stiffness, the strength contribution from the insulation is neglected. However, thermal properties of insulation are accounted for in the thermal analysis. For the current analysis thermal conductivity and dry density of fire insulation are obtained from the values proposed for spray applied fire resistive material (SFRM) in a recent study (Kodur and Shakya, 2013). It should be noted that there is limited data on the variation of thermal properties with temperature of the insulation material; hence thermal properties at elevated temperatures are assumed to be same as that at room temperature. A summary of insulation properties used in the analysis is presented in Table 4.4. The following sections provide details on the validation process.

4.4.3.1 Thermal Response

Figs. 4.6 and 4.7 shows the comparison between measured steel temperature and that predicted by finite element model in fire exposed secondary beams in both connection assemblies. It can be seen that there is good agreement between predicted and measured temperatures across the depth of steel beam. In both the assemblies, temperatures at the bottom flange of the beam were higher than that of the top flange and this can be attributed to the closer vicinity of bottom flange to fire. However, the maximum temperatures reached in subassembly S2 were lower as compared to that in subassembly S1, and this can be attributed to thermal shielding effect provided by the concrete slab to the top flange of the beams.

Figs. 4.6 and 4.7 show that the predicted secondary beam temperatures in both assemblies were initially conservative because the computational thermal model does not account for the evaporation of the insulation's residual water near 100°C, which slowed the initial increase of temperature. The discrepancy in the top flange temperature during the cooling phase might be due to the movement of thermocouple when the top flange experienced local buckling. Temperature variation between the computational and experimental results throughout the time series may also have been caused by variation in the actual insulation thickness as compared to the idealized constant 12.7-mm thickness used for computational thermal analysis. In addition, the discrepancy might also have been caused due to change in thermal properties of insulation with temperature. However, due to lack of tests data, the elevated temperature properties of insulation were assumed to be same as that at room temperature in the model. Therefore, it can be concluded that the developed thermal sub model is capable of predicting steel temperatures with reasonable accuracy.

4.4.3.2 Structural Response

The structural response of double angle connections can be assessed by examining the progression of rotation at connection with fire exposure time. The values of rotation at connections are evaluated using vertical deflection (u) of the secondary beams at the loading points and the distance from the connection to the loading point (L), as illustrated in Fig. 3.10. A comparison of predicted and measured rotations in connections is plotted as a function of fire exposure time in Fig. 4.8 for both sub frame assemblies S1 and S2. It can be seen from the figure that the predicted rotations from the model follows closely with those measured during fire tests. In both assemblies, predicted rotation at connection gradually increases with time during the early stages (till 60 minutes for S1 and 90 minutes for S2) of fire. This increase in rotation is due to deteriorating strength and stiffness properties of steel, as well as increased thermal expansion of the steel with temperature. However, during the fire test, assembly S1 experienced a sudden increase in rotation at 65 minutes into the fire test. This is due to local and lateral torsional buckling of the secondary beam which led to failure of assembly S1. However due to safety concerns (to mitigate collapse of the test assembly in to the furnace), the applied loading on the beam was removed and the test was continued to trace the thermal response (65 – 180 minutes) under cooling phase of fire. The rapid change in rotation during the final stages (beyond 180 minutes), was caused by the significant warping (refer shown in Fig. 3.11) of the metal deck present on top of secondary beams.

The current model captures the sudden increase in connection rotation and predicts a failure time of around 60 minutes for S1, which is comparable to 65 minutes failure time measured during the test. As seen in Fig. 4.9, a closer examination of the deformed shape indicates that the secondary beam experienced local and lateral torsional buckling similar to that observed during the test. As the assembly S1 failed at 60 minutes, the response of assembly beyond 60 minutes cannot be simulated by the model.

The rotation response of assembly S2 progressed similar to that of S1, but the connection in this assembly experienced higher rotation without any local or global instabilities. This can be attributed to the higher rigidity provided by the concrete slab which enhanced the overall strength of the beams and in turn the connections. The rate of increase in the rotation at connection decreased steadily after reaching a maximum value. This is on expected lines because as soon as the cooling phase of fire started, the beams regained some of their initial strength and stiffness and thus the rotation at connection started to decrease.

Progression of connection axial forces, predicted from the model for both assemblies S1 and S2 is presented in Fig. 4.10. It can be seen from Fig. 4.10 that axial force in connection for both assemblies S1 and S2 is compressive in nature initially and it increase gradually. This is due to the fact that as the beam temperature increases, steel undergoes significant thermal expansion leading to expansion of the beam. The free thermal expansion of the beam is restrained by the surrounding (cold) structural members resulting in the development of compressive axial forces. In assembly S1, the fire induced axial force starts to decrease (as can be seen from change in the slope of the curve), till failure, after reaching a peak value at 52 minutes. This can be attributed to degrading strength and stiffness properties of steel with increasing steel temperature. Similarly in assembly S2, the axial force starts to decrease at about 75 minutes before continuing to decrease further during the cooling phase of fire. During the cooling phase the beam regains part of its initial strength and undergoes thermal shrinkage leading to continuous decrease in axial force. The progression of axial force is in line with the expected trends presented in Chapter 1, for the case of a typical connection assembly. A summary of predicted and measured thermal and structural response of both connection assemblies S1 and S2 is presented in Table 4.5.

A comparison of predicted and measured vertical deflections (at loading point) in the secondary beam for assemblies S1 and S2 are plotted in Fig. 4.11. It can be seen from the figure that the vertical deflection of assembly S1 increases during early stages of fire (0-60 minutes). This is due to gradual deterioration of strength and stiffness properties of steel with increasing temperature. However, the model predicts a sudden increase in vertical deflection around 60 minutes. This sudden increase is due to the fact that secondary beam experienced failure by local and lateral torsional buckling (see Fig. 4.9). The predicted failure time of around 60 minutes for S1, is comparable to 65 minutes failure time measured during the test. As the assembly S1 failed at 60 minutes, the response of assembly beyond 60 minutes cannot be simulated by the model.

Similar to S1, the vertical deflection of secondary beam in assembly S2 increases with time during the initial stage (0-90 minutes) of fire. The increase in deflection can be attributed to gradual deterioration of strength and stiffness properties of steel with increasing temperature. The vertical deflection of secondary beam starts to decrease (beyond 90 minutes) after reaching a maximum value. This is on expected lines because as soon as the cooling phase of fire starts, the secondary beam regains some of its initial strength and stiffness and thus the vertical deflection in secondary beam starts to decrease.

Based on the above comparisons, it can be concluded that the proposed finite element model is capable of simulating the response of assemblies with double angle connections to a good degree of accuracy.

4.4.4 System Level Connection Model (FEM2)

The second finite element model (FEM2), consisting of system level connection model, was developed to simulate the fire response of restrained steel frame previously tested by Wang et al. (Wang et al., 2011). The restrained steel frame has an unprotected beam (without any concrete slab) connected to column with a different double angle connection configuration compared to FEM1.

The tested steel frame assembly comprised of a column (UC 254x254x 73 section) connected to beam (UB 178x102x19 section) through 130 mm deep angles (90x150x10 mm). The geometry of the selected connection assembly along with the connection details are shown in Fig. 4.12.

Since the geometry of the connection assembly is symmetrical about the vertical plane, only one column and half of the beam are modeled. SOLID70, SURF152 elements are used for the thermal analysis while SOLID185 elements are used for structural analysis.

The boundary conditions of the connection assembly were simulated as present in the fire test (Wang et al., 2011). During the test, the bottom of the column was attached to a base plate which in turn was fixed to the ground using four bolts. The top of the column was allowed to freely expand axially (longitudinally) in the gap between the column top and the reaction frame, while it was restrained to move in the lateral direction. To simulate these conditions in the finite element model, all the nodes at the bottom of the column were completely fixed in all three directions (x,y and z) while the nodes at the top of the column were fixed in two directions (x and z) only (free to expand axially in y direction).

In the fire test, the lateral restraining effect of the concrete slab was simulated by connecting steel truss bars to the beam top flange. However, for simplicity in the current model FEM2 the truss bars were replaced by 50x8 mm plates of 750 mm long on either side of the beam top flange, as shown in Fig. 4.13. These plate dimensions were determined such that they contributed the same amount of bending capacity of the beam (Dai et al., 2010) as that of lateral restraining truss bars used in experiment. In addition, the top flange of the beam was prevented from any lateral movement by restraining the nodes in lateral (X) direction. The bolt heads and nuts were modeled as circular volumes and the root radius between the angle legs, beam/column web and flange are ignored in the model.

The contact interactions between different parts are defined using “contact pairs” and are modeled as “surface-to-surface” contact using contact elements CONTA174 and TARGE170(ANSYS Inc, 2009c). In this model, there are forty-five contact pairs with 28,171 contact elements. In the current model, the contact between interacting surfaces is successfully incorporated using "surface-to-surface" contact with "no separation but sliding permitted" option. Based on the results of the sensitivity study, optimum normal contact stiffness (FKN) value of 0.1 was assumed in the first iteration of the analysis. This value is updated in subsequent iterations based on the current mean stress of the underlying element and the allowable penetration of contact elements. In order to accurately capture thermal and structural stress concentration in the connection region (angles, bolts, bolt holes), a relatively finer mesh was used within the vicinity of these regions, as depicted in Fig. 4.14.

4.4.5 Validation of System Level Connection Model (FEM2)

The finite element model FEM2 was validated by comparing predictions from the finite element analysis with measured data on connection assembly tested by Wang et al. (Wang et al., 2011) . In the fire test, double angles connected to an unprotected beam were subjected to ISO 834 standard fire conditions. The top flange of the beam was covered with a 15 mmm layer of ceramic fiber blanket to simulate the heat-sink effect of the concrete slab. However, as the connection assembly was relatively larger as compared to the volume of the furnace and due to the unsymmetrical arrangement of the gas burners and exhaust inside the furnace, the connection assembly was not subjected to symmetrical heating conditions(Wang et al., 2011). Further, the average temperature difference inside the furnace, measured by six thermocouples, was about 200°C lower in comparison to ISO834 standard fire temperature conditions (Wang et al., 2011). Thus, to account for the unsymmetrical heating and lower temperature distribution, the connection assembly is analyzed by subjecting it to scaled time-temperature curve (shown in Fig. 4.15) from three sides. This modified fire scenario (referred to as scaled fire scenario hereafter) is computed by scaling down the standard ISO834 temperatures by 25% i.e., using a scale factor of 0.75. It can be seen from the figure that the maximum temperature difference remains around 200°C for the first 100 minutes of scaled ISO834 fire conditions.

During the fire test, static gravity load was applied on the beam before heating the connection assembly. The load was applied using two loading actuators located at a distance of 600 mm from the beam ends (refer to Fig. 4.12(a)). The magnitude of load in each actuator was 40 KN which corresponds to a load ratio of 0.5 in the beam. Load ratio (LR) is defined as the ratio of applied bending moment in the beam at the fire limit state to the ambient temperature plastic bending moment capacity of the beam. To circumvent the problems of high-stress concentrations and numerical singularities due to external loading, the base of actuator pads was modeled (refer to Fig. 4.13) and the load is applied as nodal force in vertical direction (y direction).

The mechanical properties of steel used in the model are based on the temperature tensile coupon tests reported by Wang et al. is shown in Table 4.6. These mechanical properties along with constitutive relationships and strength reduction factors provided in Eurocode 3 (Eurocode3, 2005b) were used to generate nominal stress-strain-temperature relationships. The nominal stress-strain relations were then converted into true stress-strain curves and used in the model. As the connection assembly had an unprotected beam the properties of insulation were not considered in the model.

Wang et al.(Wang et al., 2011) did not perform any tests to evaluate the mechanical properties of bolts. Hence, the nominal yield strength, ultimate strength and modulus of elasticity (as specified in the standards) of bolts were assumed to be 640 MPa, 800 MPa and 210000 MPa respectively. The strength reduction factors specified in Eurocode 3 (Eurocode3, 2005b) for carbon steel at elevated temperatures were used. The effect of high-temperature bolt properties on the system-level transient fire performance of connection assembly is discussed in Chapter 5. The following sections provide details on the validation process.

4.4.5.1 Thermal Response

The predicted beam temperatures from the model are shown in Fig. 4.16. The temperature progression in the beam from fire tests was not reported by the authors. It can be seen from the figure that the temperatures in the bottom flange and web of the beam were similar and increase more rapidly with fire exposure time. However, the top flange experienced much slower rise in temperature as compared to the web and the bottom flange. This is due to the fact that only top flange of the beam is insulated and the beam is subjected to three-side fire exposure conditions. The predicted temperatures follow expected trends within a typical unprotected steel section that is heated. When a steel section is subjected to increasing temperature, the temperature in steel section increases rapidly because of high thermal conductivity and specific heat of steel. The rate of temperature increase depends upon the thickness of steel component (web, flange) as well as the number of sides of fire exposure (3 side, 4 side exposure). For the same fire exposure conditions, temperature increase in thicker steel components (ex: flanges) will be slower compared to thin components (ex: web) because of the high thermal mass that needs to be heated up.

4.4.5.2 Structural Response

The authors reported the variation of beam mid-span deflection and the development of axial force in connection from the fire tests. A comparison of predicted and measured mid-span deflections in the beam and the axial force in the connection is plotted in Fig. 4.17(a) and (b), as a function of beam bottom flange temperature. It can be seen from Fig. 4.17(a) that the mid-span deflection increases steadily with increasing bottom flange temperature up to 680°C. This is due to gradual deterioration of strength and stiffness properties of steel with increasing temperature. However, the beam undergoes runaway deflection towards the later stages of fire exposure as steel has lost most of its strength and can no longer contribute to capacity of the beam to sustain external loading. For example, steel retains 27% of its ambient temperature capacity at 680°C and retains only 11% of its initial capacity at 800°C (Eurocode3, 2005b).

The axial forces developed in the connection, predicted from the model, are compared to the measured values from the fire test in Fig. 4.17(b). It can be seen from the figure that there is a good agreement between the trends of the predicted and measured axial forces in the entire range of fire exposure. However, some discrepancies in the values can be attributed to unsymmetrical heating experienced by the connection assembly during the fire test as reported by Wang et.al. (Wang et al., 2011). In contrast, in the finite element model, the connection assembly is analyzed with symmetrical heating conditions.

A review of predicted axial force indicates that model predictions follow expected trends. The variation of axial force in Fig. 4.17(b) can be grouped into three stages. The axial force in connection is compressive in nature initially and it increases gradually with increasing beam temperature during stage 1. After reaching a peak value, the fire induced axial force decreases with fire exposure time (stage 2) due to temperature induced degradation in strength and stiffness properties of steel. The axial force continues to decrease and finally transforms into tensile force (stage 3) when the beam load carrying mechanism changes from "flexural action" to "catenary action". During this stage, the beam is held in place (like a cable) by connections.

In addition to the axial force, rotation characteristics of the connection better reflect the connections behavior. Though no test data was reported by the authors on connection rotation, the rotation characteristics predicted from the model are illustrated for the sake of completeness.

The rotations are plotted in Fig. 4.17(c) and the response can be grouped into two stages, before and after the beam bottom flange comes into contact with the column flange. In the first stage, the rotation of the connection increases proportional to the external loading until the beam bottom flange makes contact with the column flange (1.5° rotation and 8% plastic strain in steel at 52 minutes). After making the contact, the connection exhibits stiff behavior because of the additional resistance offered by the column flange to the free rotation of the beam flange. A summary of predicted and measured thermal and structural response of restrained steel frame is presented in Table 4.7.

Therefore, based on the assumptions considered in modeling the connection assembly and response predicted from the ANSYS analysis, it can be concluded that the above developed finite element model FEM2 is capable of simulating the fire response of connection assembly with reasonable accuracy.

4.5 Summary

This chapter presents the development and validation of two numerical models for simulating the system-level transient fire response of double angle connection assemblies. Both numerical models, each comprising of thermal and structural finite element sub models, were developed using commercially available finite element software ANSYS. All the stages associated with the fire resistance analysis, namely: thermal and structural analyses, modeling contact interactions, are explained. The developed models account for high temperature thermal and mechanical properties, various fire scenarios, geometrical nonlinearities and non-linear contact interactions.

Both the finite element models used system-level approach to simulate the fire response of connection assemblies. The first finite element model (FEM1) was developed to simulate the fire response of connection assemblies with and without concrete slab. The second finite element model (FEM2) was developed to trace the fire response of restrained steel frame assembly with a different double angle connection configuration compared to FEM1.

The validity of the thermal and structural models (for FEM1 and FEM2) is established by comparing the prediction from the analysis with data generated from fire resistance tests. This validation indicates that two models, FEM1 and FEM2, developed in ANSYS are capable of simulating the fire response of double angle connection assemblies with good level of accuracy. In the next chapter, these two finite element models will be applied to carry out a set of parametric studies to quantify the effect of critical parameters influencing fire response of double angle connection assemblies.

CHAPTER 5

5. PARAMETRIC STUDIES

5.1 General

Fire response of connections in steel framed buildings is influenced by a number of factors including fire induced restraint forces, composite action arising from slab, interactions between different members in the structural frame. Although fire tests can provide better insight into the behavior of connections, it is not feasible to undertake large number of fire experiments due to high complexity, huge costs and time constraints. Further, there are limitations on the number of variables that can be varied in fire tests, reliable instrumentation for monitoring response and test facilities for undertaking tests. An alternative to fire tests is the use of numerical models for tracing the performance of double angle connection. Such numerical models can be applied to undertake large set of parametric studies and generate data to quantify the influence of various factors on fire resistance.

The validated numerical models presented in Chapter 4 are applied to quantify the effect of various parameters on the fire response of double angle connection assemblies. The varied parameters include: decay rate, loading type and load level, degree of restraint, composite action arising from the presence of slab, system-level interactions, heating profile, fire scenarios and high-temperature properties of bolts.

5.2 Characteristics of Double Angle Connections

Wide range of connection configurations such as all bolted, all welded and welded-bolted are commonly used in practice. Most common types of bolted connections include endplate, shear tab and double angle connections. However, bolted double angle connections are unique since their higher tying capacity can sustain additional axial tensile forces and this is in contrast to bolted shear connections which cannot withstand the axial forces. Also, double angle connections experience ductile failure, due to higher ductility, as compared to brittle failure experienced in other connection types. This ductile failure delays the failure time of connections.

A comparison of rotation characteristics of two types of connections, namely: flush end-plate and double angle connection along with their moment-rotation (M-ϕ) curves is illustrated in Fig. 5.1. As explained in Chapter 1 and shown in Fig. 5.1, the response of flush end-plate connections can be grouped in one stage characterized by three regions. Initially there is an approximately linear response with increasing rotation, until the onset of yielding in one or more of the connection components (such as bolts or angles). This is followed by curvilinear response indicating the yielding of the connection. Finally, as the connection failure is imminent, the rate of rotation increases rapidly causing an almost flat plateau in the connection response.

However, response of double angle connections can be grouped into two stages as can be seen in Fig. 5.1, before and after the bottom flange of beam comes into contact with the column flange.

The first stage response is again characterized by linear and bilinear response similar to that of flush end-plate connections. During the second stage, when beam bottom flange makes contact with the column flange, an increase in moment is accompanied by a smaller increase in rotation due to the resistance offered by the column flange to free rotation of the beam flange. Therefore, double angle connections can carry additional load by undergoing higher rotations before experiencing failure when compared to other connection types. For example, previous experimental studies reported that double angle connections can undergo rotations up to 18° (≈ 315 milli-rad) before failure, while other connection configurations can sustain only upto 3.5° (60 milli-rad rotations) (Yu et al., 2009c). Despite, double angle connections have superior performance characteristics compared to other connection types; very few studies (refer to Chapter 2) focused on studying the behavior or isolated double angle connection. Therefore, this chapter is focused on studying the effect of influencing parameters on the fire response of double angle connections.

5.3 Comparative Analysis

Detailed information about different levels of analysis that are adopted to predict the fire response of connection assemblies is discussed in this section. In addition, fire induced forces obtained using different approaches are compared.

5.3.1 Levels of analysis

The response of connections under fire conditions can be studied at three levels, namely: component-level, member-level (isolated member) and system-level. The component-level analysis captures the response at the isolated connection and does not capture the effect of member interactions (beams, columns) on the response of connection. This is typically used to get a crude estimate of connection performance and this analysis can be implemented using spreadsheet calculations. In this type of analysis, the fire exposure time is divided into several time steps. At a given time step, the capacity of the connection is calculated by knowing the temperature of the beam, connection and the high-temperature strength-reduction factors for steel (connection). Once the temperature in beam is known, the fire induced axial forces generated in the beam (and in turn in connections) are calculated using the following equation:

$$P(t) = E_T A \alpha \Delta T \qquad [5.1]$$

where $P(t)$ is the fire induced axial force at any time, E_T is the temperature dependent elastic modulus of beam, A is the cross-sectional area of the beam, α is the coefficient of linear thermal expansion of steel and ΔT is the change in temperature.

The capacity of the connection is calculated by knowing the temperature of the beam, connection and the high-temperature strength-reduction factors for steel (connection). Once the connection capacity and fire induced forces are computed, the failure time of connection is taken to be the time step at which the connection capacity against the fire induced forces. Failure time of connection is defined as the time at which connection capacity falls below that of fire induced forces.

Though the component-level analysis is relatively simple to use it has several drawbacks namely: (a) this analysis does not account for the fire induced axial forces resulting from the interaction between structural members on the response of connection; (b) the effect of local beam instabilities (such as local buckling and lateral torsional buckling) on the connection response cannot be accounted for in this analysis, and (c) the transformation of fire induced axial forces from compression phase to tension phase cannot be captured. Therefore, component-level analysis does not give realistic fire response of connection.

The member-level analysis (or isolated member analysis) is commonly used to simulate the response of connections which are not considered to be a part of the structural framing system. A schematic of typical isolated connection is shown in Fig. 5.2. As can be seen from the figure, as the beam end is free to expand thermally no fire induced forces will be generated in the beam and transferred to the connections. However, in reality connections are always an integral part of a structural framing system and connected beams have some level of restraint (from surrounding structural members) to free thermal expansion. This restraint to free thermal expansion, leads to development of fire induced axial forces in beams and connections. Therefore, member-level analysis also does not capture the realistic fire response of connections.

The system-level analysis refers to comprehensive analysis where in the connections are considered to be an integral part of the structural framing system. Hence the connection region, along with the surrounding structural members, is modeled as a system. In the analysis, fire induced forces developed in the beam are computed through a second order nonlinear analysis based on actual temperature profiles (in beam and connection), as well as deformed geometry of beam and connection. Therefore, this type of analysis simulates realistic response of the connection assembly and can capture the influence of surrounding structural system on the fire response of connections.

5.3.2 Analysis details

To demonstrate the varying response of connection assemblies, predicted using component-level, member-level and system-level analysis, three different connection configuration were modeled under fire exposure. The connection configurations analyzed are: a shear tab (fin plate), a single angle, and a double angle connection. All the three different connection configurations are assumed to be connected to same beam (W12x30) section, shown in Fig. 5.3. The beam is assumed to be unprotected for analysis purpose while the key mechanical properties of connections are presented in Table 5.1. The coefficient of linear thermal expansion of steel is assumed to be equal to 12×10^{-6} /°C. The bolts are of ASTM A490 grade with 19mm (3/4 inch) in diameter. The ambient temperature capacity of shear tab, single angle and double angle connection is equal to 211 kN, 211 kN and 306 kN, respectively. Detailed calculations for evaluating the capacity of three connection types are presented in Appendix C. For comparative purposes, the fire induced forces in all three connections are presented for the first 30 minutes of exposure to parametric fire curve shown in Fig. 5.4.

5.3.3 Comparative Performance

The variation of connection capacity and progression of fire induced axial force for three connection types is presented in Table 5.2. The fire induced axial forces obtained from the system-level analysis (Refer to Fig. 4.10 assembly S1 data) is also presented in the table for comparison purposes. As can be seen from Table 5.2, the fire induced axial force computed using component-level analysis increases rapidly while the member-level analysis predicts no axial force. This is on the expected lines because member-level analysis assumes that the connections are not part of the structural framing system. Therefore, as beam temperature increases the thermal expansion in the beam is not restrained by structural members resulting in no axial force. Further, the fire induced forces predicted using component-level analysis increases rapidly and this can be attributed to the fact that as beam temperature increases (ΔT increases) the fire induced force increases according to Eq.[5.1].

It can be seen from Table 5.2, the fire induced forces computed using component-level and system-level analysis increases with increasing fire temperature. However, the fire induced axial force computed using component-level analysis increases rapidly and gives unrealistic values of fire induced forces compared to axial forces obtained from system-level analysis. This can be attributed to the fact that component-level analysis does not consider the effect of stiffness of connection and surrounding structural members on the development of fire induced forces in beam. Hence, the predictions from component level analysis cannot be used for rational design of connections.

To demonstrate the difference in the double angle connection fire response obtained by adopting a system-level analysis and member-level (isolated) analysis, the connection assembly presented in the second finite element model (FEM2) is used. However, the symmetrical boundary conditions at the beam end, away from the connection region, is removed so that the beam is free to move axially. Isolated connection assembly along with the modified boundary conditions is shown in Fig. 5.2. The connection assembly is analyzed by subjecting it to the parametric fire curve shown in Fig. 5.4.

The variation of axial force and rotation in connection obtained from the analysis is shown in Fig. 5.5. It can be seen from Fig. 5.5(a) that the axial force in the connection (using system-level analysis) exposed to parametric fire curve (see Fig. 5.4) is compressive in nature in initial stages of fire exposure. After reaching a peak value, the fire induced axial force decreases with fire exposure time and finally transforms to tensile force. On the contrary when the connection is considered to be isolated (member-level) and exposed to fire it experiences no fire induced axial force. This is on the expected lines because the connected beam is no longer restrained against free thermal expansion which leads to zero fire induced axial force.

A comparison of rotation in connection (Fig. 5.5(b)) indicate that the rotation of connection assembly subjected to parametric fire increases with increasing fire exposure time and then decreases after reaching a maximum value. This is consistent with the fact that the assembly experiences increasing deflection as the temperature increases (during the growth phase of fire curve). Once the fire enters the decay phase, the beam regains part of its initial strength and stiffness which leads to reduced deflections.

However, when the connection assembly is analyzed as member-level it experienced much higher rotation as compared to that analyzed using system-level analysis. This can be attributed to the absence of the beneficial effect provided by the restraining effect. Beams analyzed at system-level experience lower deflections compared to isolated ones because the restraining force generally acts below the neutral axis of any cross-section along the span of the beam. This develops an arch action which counters the effect of the applied external loading and reduces the downward deflection of the beam. Therefore, the absence of restraining effect (due to the structural continuity or system-level) produces higher beam deflections and hence higher connection rotation.

5.3.4 Connection capacity

As can be seen from Table 5.2, a comparison of connection capacity of all three connection types and the fire induced forces (obtained from system-level analysis) indicate that the capacity of shear tab and single angle connection drops below the fire induced forces around 30 minutes. On the other hand, double angle connection has capacity which is greater than the fire induced forces. This implies that shear tab and single angle connections will experience failure by 30 minutes while double angle connections do not experience failure. Results from the system-level analysis indicate that double angle connections experience failure around 60 minutes. This indicates the robustness of double angle connections and therefore the current study focuses on tracing the fire response of double angle connections.

An illustration of the variation of connection capacity and fire induced axial force with increasing temperature is shown in Fig. 5.6. It can be seen from the figure the connection capacity decreases with increasing temperature due to degradation in strength and stiffness of steel. On the other hand the fire induced axial force increases with temperature due to the increase in thermal expansion of steel beam. The thermal expansion of beam is restrained by the adjacent structural members resulting in an increase in axial forces. Failure of connection happens when the connection capacity drops below that of the fire induced axial forces.

5.3.5 Summary

Based on the results, it can be inferred that the (a) response of connection analyzed using system-level approach is different from that obtained using member-level (or isolated, component level) analysis, (b) development and progression of fire induced axial forces cannot be captured when the connections are analyzed at member-level, (c) beneficial effect of arch action on the connection is accurately captured through system-level approach (d) beneficial effect of arch action developed due to structural interactions reduces rotation at connection (e) double angle connections due to their inherent robustness can sustain additional fire induced forces compared to shear tab and single angle connections.

Therefore, double-angle connection assemblies are considered as part of this study. Further, numerical models presented in Chapter 4 and subsequent parametric studies presented in the following sections are carried out using system-level approach.

5.4 Factors influencing fire resistance

A state-of-the-art review presented in Chapter 2 clearly indicates that several factors govern the response of double angle connections under high temperature exposure. Previous sub-frame assemblies and isolated connection tests clearly show that the main factors influencing the fire response of double angle connections are:

- Decay rate of a design fire,
- Loading type and intensity,
- Axial restraint stiffness,
- Presence of concrete slab,
- Composite action of slab,
- System-level interactions,
- Heating profile (transient vs. steady-state heating),
- Fire scenario (duration of growth phase, maximum temperature and total duration of fire),
- High-temperature properties of bolts.

In previous studies, many of the above factors were not fully incorporated in modeling the system-level behavior of connection assemblies. Two different numerical models (FEM1 and FEM2), presented in Chapter 4, are used to study the influence of each of the above factors on the fire resistance of sub-frame assemblies containing double angle connections. The first finite element model (FEM1) simulates the fire response of two sub-frame assemblies one with slab and the other without slab. The second finite element model (FEM2) simulates the fire response of restrained steel frame with a different double angle connection configuration compared to FEM1. The effect of decay rate, loading type, presence of concrete slab and axial restraint is studied using first finite element model (FEM1) while the effect of heating profile, load level, fire scenarios and high-temperature bolt properties is studied using second finite element model (FEM2). The effect of composite action arising from the presence of concrete slab is studied indirectly by comparing the response of connections in assembly S1 with that of assembly S2.

Details about the parameters and the results obtained from numerical simulations are presented in the following sections.

5.5 Parametric Studies

In this section, the parameters influencing transient fire response of double angle connections are introduced and defined. Range of these parameters analyzed is also discussed. For the first finite element model (FEM1), parametric studies were conducted by exposing the sub-frame assemblies to the design fires shown in Fig. 3.5. In the case of second finite element model (FEM2), parametric studies were conducted by exposing the restrained steel frame assembly to a parametric fire curve (FS) as illustrated in Fig. 5.4. In this fire scenario there is a growth phase (increasing temperatures) for the first 90 minutes which is followed by a decay phase with a cooling rate of 3.5°C/min. This fire scenario is computed based on the parametric fire time-temperature curve proposed in Eurocode1 (Eurocode1, 2002). The fire scenario is assumed to occur in a typical compartment having dimensions of 6mx5mx3m with an opening factor (F_v) of 0.011 $m^{-1/2}$, fuel load energy density of 600 MJ/m^2 and made up of materials having a thermal inertia value of 1600 $Ws^{0.5}/m^2K$.

This fire scenario is selected such that the maximum temperature does not exceed 700°C due to the fact that (a) the emphasis of this study is on the failure of the connections and any premature failure of the beam should be avoided, and (b) the steel beam analyzed is an unprotected beam. Beams with external fire protection can sustain fires with much higher temperatures, while unprotected beams can fail when the fire temperatures exceed 700°C and steel temperatures exceed 650°C.

5.5.1 Selection of Connection Assemblies

To study the effect of influencing parameters on fire response of double angle connections, three connection assemblies presented in Chapter 4 are selected. This includes connection assemblies S1 and S2 sub-frame assemblies with and without slab, as shown in Fig. 4.5, and a restrained steel-frame assembly modeled as shown in Fig. 4.11(a). Detailed description of all three connection assemblies is presented in Chapter 4.

5.5.2 Analysis Details

The effect of influencing parameters (discussed in Section 5.4) on the fire behavior of double angle connections is analyzed using the two validated finite element models (i.e., FEM1 and FEM2) presented in Chapter 4. The influence of parameters on the fire performance of all three (S1,S2 and restrained steel frame) connection assemblies is analyzed at system-level by subjecting them to transient temperature conditions (except for the case of steady-state conditions mentioned in Section 5.6.5). Details about the high-temperature constitutive material properties and failure criteria used in the finite element models are discussed in Chapter 4. In all the parametric studies, the connection assemblies are analyzed either for the total duration of fire exposure time or till the connection assembly experienced failure, whichever occurs earlier. If the assembly experiences failure before the end of fire duration, the failure time is mentioned in the relevant sections.

5.5.3 Range of Variables

A list of parameters varied, together with the range of these parameters, used in the parametric studies are summarized in Table 5.3. The range for these parameters is selected to reflect the typical values encountered in steel framing systems. In practical situations, beams are subjected to a load ratio in the range of 30% to 70%, under fire conditions, where load ratio (LR) is defined as the ratio of applied bending moment in the beam at the fire limit state to the ambient temperature plastic bending moment capacity of the beam. Depending upon the size of the connected members and end boundary conditions, beams in connection assemblies can experience axial restraint ranging from nil to full (100%) restraint. The decay rate of the design fire depends upon the fuel load, ventilation characteristics, firefighting activities and can vary from rapid cooling to a slow cooling. Therefore, the decay rates are selected to represent a slow cooling fire (decay rate of 2°C/min) to rapid cooling fire (decay rate of 22.5°C/min).

Typical fire exposure experienced in buildings consists of a growth phase during which fire temperature increases and this is followed by a decay phase where the fire cools down. The presence of cooling phase of fire influences the performance of connections due to the fact that structural members regain part of their strength and stiffness after undergoing large deformations. Hence, the effect of cooling phase is studies by subjecting the connection assembly to design fire scenarios.

High strength bolts of Grade ASTM A325 and A490 are commonly used in construction to improve the overall connection efficiency. The chemical composition and the heat treatment processes that the high strength bolts undergo are different from those encountered by conventional bolts made of carbon (mild) steel Hence, high-temperature properties and the performance of bolts can be different from that of conventional steels (A36, A992) used for structural members such as columns and beams. To assess the effect of bolt properties on the transient fire performance of double angle connections, an analysis was carried out by incorporating the high-temperature properties of steel specific to two types of bolt grades, namely ASTM A325 and A490.

5.6 Results and Discussion

Details about the results obtained from the parametric studies are presented in the following section. The effect of each of the parameters on the fire response is discussed below.

5.6.1 Effect of Composite Action

The effect of composite action, arising from the presence of slab, on connection response can be studies by comparing the rotation response of connection assemblies S1 and S2, as shown in Fig. 5.7. It can be seen from the figure that the rotation in both assemblies increases with fire exposure time during the early stages. This increase in rotation is due to deteriorating strength and stiffness properties of steel as well as increased thermal expansion of the steel with temperature. However, assembly S1 experiences sudden increase in rotation and fails around 60 minutes. This sudden increase in rotation is due to local and lateral torsional buckling of the secondary beam which led to failure of assembly S1 (refer to Fig. 4.9).

On the other hand, rotation at connection in assembly S2 continued to increase and assembly S2 experienced higher rotation without any local or global instabilities. The rate of increase in rotation at connection decreased steadily after reaching a maximum value. The increase in rotation can be attributed to the composite action of slab which enhanced the strength retention of the secondary beam and this in turn the connections. In addition, higher rigidity of concrete slab stabilized the secondary beam from onset of instabilities such as local and lateral torsional buckling. The higher rigidity and lateral stability enhanced beam strength enabled connections in assembly S2 to sustain 40% higher rotation compared to assembly S1. During the final stages of fire, the decrease in rotation at connection is due to the fact that as soon as the cooling phase of fire started, the beams regained some of their initial strength and stiffness and thus the rotation at connection started to decrease.

5.6.2 Effect of Decay Rate

It is well established that accounting for decay phase in a fire significantly influences the connection behavior (Garlock and Selamet, 2010; Lennon and Moore, 2003; Wald et al., 2006). This is due to the fact that the temperature level attained in the beam directly dictates the rate of recovery of beam's capacity, stiffness, thermal shrinkage and also the extent of tensile forces developed in the connection region. To study the effect of decay rate, assembly S1 was subjected to modified design fire DF1 (see Fig. 5.8(a)) which had a growth phase duration of 45 minutes instead of 75 minutes used during the fire test (Refer to Fig. 3.5). Similarly, connection assembly S2 was subjected to modified design fire DF2 (see Fig. 5.8(b)) which had a growth phase duration of 120 minutes instead of 90 minutes used during the fire test (Refer to Fig. 3.5). Then, the connection assemblies were analyzed by varying the decay rate of both design fires from 25% to 150% of the initial decay rates (8°C/min for DF1 and 15°C/min for DF2) i.e., the decay rate of design fire DF1 was varied from 2°C/min to 12°C/min while that of DF2 from 3.75°C/min to 22.5°C/min.

Fig. 5.9 shows the predicted rotation in connections of both assemblies for varying decay rate scenarios. For assembly S1, it can be seen from the figure that with changing decay rate the connection response is similar in the initial stages of fire exposure. In all cases, except for 10°C/min, connections experienced failure due to instability in beam (local and lateral torsional buckling) immediately after the start of decay phase of fire. Therefore, no specific conclusions can be drawn for assembly S1.

For all decay rates, rotation in connection of assembly S2 progressed similar to that of S1, but the connection experienced much higher rotation without any instabilities in the beam. This can be attributed to higher rigidity provided by the composite action of slab which enhanced the overall strength of the beam and in turn the connection. However, the failure time of the assembly decreased with increasing decay rate. This can be attributed to the fact that at higher decay rates, the beam experiences large thermal gradients which in turn leads to the development of higher thermal shrinkage forces in connections. Therefore, the connections are not able to carry forces for a longer duration under higher decay rates as compared to the cases of lower decay rates of fire.

Based on these observations, it can be inferred that a lower rate of decay (slow cooling rate of a fire) improves the fire performance of the connection by decreasing the extent of thermal shrinkage (restraint) forces in connections. The rigidity provided through the composite action of slab increases the strength of beams and double angle connections which enables connections to sustain higher rotation.

5.6.3 Effect of Loading Type

The type of loading on the beam can influence the performance of connection, especially under fire conditions. This is due to effect of loading on resulting bending moment and deflection in the connected beam and rotation in the connection. Further, the progression of contact forces between bolt shanks and bolt holes, stress concentrations in the beam and in the connection region are governed by loading on the beam.

During the fire test, the connection assemblies were tested by applying two point loads (see Fig. 3.4(b)) along each secondary beam. In the analysis, the assemblies are analyzed by applying two loading types namely, mid-point load and uniformly distributed load along each secondary beam. A schematic of two loading types, along with the corresponding bending moment diagram is illustrated in Fig. 5.10. The magnitudes of concentrated loading at mid-span and distributed loading are selected such that same level of mid-span bending moment is produced in the secondary beam. The magnitude of concentrated load for the case of mid-point loading was

111.2 kN and 138.9 kN, while that for uniformly distributed loading was 63.5 kN/m and 79.3 kN/m for connection assemblies S1 and S2, respectively.

The effect of loading type on the fire response of connection can be illustrated by reviewing the results presented in Fig. 5.11. It can be seen from Fig. 5.11(a) that the connections in assembly S1, with two point and mid point loading experienced gradual increase in rotation during the early stages of fire till experiencing sudden failure. This increase in rotation is due to deteriorating strength and stiffness properties of steel in connection and beam as well as increased thermal expansion of steel with temperature. However, when the assembly was analyzed with distributed loading it experienced failure with a sudden increase in rotation at the start (less than a minute) of the analysis itself. As can be seen from Fig. 5.12(b) a review of the deformed shape indicated that the secondary beam rotated and experienced lateral torsional buckling which led to the failure of the assembly.

Compared to S1, rotation in connection for assembly S2 (Fig. 5.11(b)) increased with time during the early stages (growth phase) of fire followed by a decrease during the later stages (decay phase) of fire. The increase in rotation during early stages is due to the decreasing strength and stiffness of the beam with increasing temperatures in steel. The decrease in connection rotation during later stages can be attributed to the fact that beam regains part of its initial strength due to decreasing steel temperatures during the decay phase of fire. The regaining strength in beam results in lower deflections in beam and which in turn leads to lower rotation in connection.

It can also be seen from the Fig. 5.11(b) that the connections analyzed with distributed loading were able to sustain higher rotations. The connections analyzed with distributed loading experienced and sustained 50% more rotation compared to two point loading and 80% more rotation compared to mid point loading. This can be attributed to the fact that the distributed loading produced a quadratic increase in moment (Fig. 5.10(c)) as compared to linear variation in the moment produced by two point and mid point loading. The quadratic moment leads to the development of higher stresses and deflection in the beam which results in higher rotation in connection.

The progression of axial force in connections for both assemblies S1 and S2 obtained from the analysis are shown in Fig. 5.13. It can be seen from the Fig. 5.13(a) that the fire induced forces in assembly S1 (with mid point and two point loading) is compressive in nature and increases gradually till failure. This increase in axial force can be attributed to the fact that as the beam temperature increases, steel undergoes thermal expansion resulting in expansion of the beam. The thermal expansion of beam is restrained by surrounding structural members leading to the development of compressive axial forces. However, when assembly S1 was analyzed with distributed loading it experienced failure less than a minute into the analysis (by lateral torsional buckling) at early stage of fire exposure.

On the contrary, the type of loading had marginal influence on the progression of fire induced axial forces in assembly S2 (Fig. 5.13(b)). The fire induced axial forces in assembly S2 increased with time during the early stages (growth phase) of fire followed by a reduction during later stages (decay phase) of fire exposure. The increase in axial force is attributed to thermal expansion of the steel beam (during growth phase of fire) while the decrease in axial force can be attributed to recovery of strength and stiffness of beams (during decay phase of fire). Additionally, fire induces forces are compressive in nature for the entire duration of fire exposure time. The compressive nature of axial forces indicates that the primary load carrying mechanism in beam is through “flexural action” for the entire duration and the load carrying mechanism did not change to “catenary action”. This can be attributed to the fact that the presence of slab increased the strength of the beam (via composite action) and stabilized the beam from local instabilities (such as lateral torsional buckling experienced by assembly S1). The increased strength of beam and enhanced stability of beam enabled assembly S2 to sustain the applied loading through flexural action.

Based on the progression of rotation in connection, it can be inferred that (a) distributed loading represent the extreme loading case scenario for both connection assemblies, (b) for connection assemblies without slab (or laterally unsupported), distributed loading creates instability in the beam leading to early failure of the assembly, (c) composite action arising from the presence of slab stabilizes and enhances the load carrying capacity of connection assembly, enabling the connection assembly to sustaining higher rotations generated by distributed loading.

5.6.4 Effect of Axial Restraint

In a typical building, double angle connections form an integral part of structural framing system and this fire performance of connections is highly influenced by the effect of adjacent structural members. This is due to the fact that the adjoining structural members directly influence the extent of thermal expansion of the heated beam, stresses generated in the beam and connection region as well as the extent of restraint force applied on the connection. To study this effect, the connection assemblies were analyzed by assuming the beam to be under four cases of axial restraint stiffness, namely 25%, 50%, 75% and 100% of the secondary beam stiffness. The axial restraint considered in this study is the one created by the flexural rigidity of the secondary beam (Refer to Fig. 4.4) and is assumed to be arising from the presence of secondary beam in the adjacent sub frame. The value of axial restraint (stiffness) of the beam can be computed as:

$$k = \frac{EA}{L} \qquad [5.2]$$

where k is the value of axial restraint, E,A and L are the room-temperature elastic modulus of steel, cross-sectional area and length of the secondary beam, respectively.

In the finite element model, the presence of axial restraint is simulated through spar element (LINK180), available in ANSYS. Nodes at one end of the spar elements were connected to the perimeter beam while the nodes at the other end were completely fixed in all three directions (x,y and z), as shown in Fig. 5.14.

Fig. 5.15 shows the progression of rotation in connection as a function of fire exposure time for different values of axial restraint stiffness. It can be seen from Fig. 5.15(a) that the presence of axial restraint significantly affects the fire response in assembly S1 and the failure time decreases with increasing axial stiffness. This can be attributed to the fact that higher axial stiffness (restraint) limits the extent of free thermal expansion that beam can undergo. The higher the value of axial restraint, the lower will be free thermal movement in the beam. This restrained movement in the beam results in the development of higher stresses and local instabilities (local buckling and lateral torsional buckling) in the beam which ultimately lead to the failure in the connection. Failure modes in assembly S1 for different values of axial restraint stiffness, obtained from the analysis, are shown in Fig. 5.16. As can be seen from the figure, increasing axial restraint from 25% to 100% increases the instability in beam from local buckling to flange and web crippling (see Fig. 5.16(d)) of the entire beam.

A comparison of rotation in connection, presented in Fig. 5.15(b), indicates that the axial restraint stiffness has marginal influence on the fire response of assembly S2. This is on expected lines because assembly S2 had concrete slab which increased the rigidity and enhanced the strength retention in the secondary beams and thus in turn enhanced the connection response.

Further, in S2 the presence of slab stabilized secondary beam and prevented it from any local instabilities compared to assembly S1.

5.6.5 Effect of Steady-state and Transient Heating

The type of heating conditions, steady-state or transient state heating, can influence the response of connection. In most previous studies a steady-state heating that generates a uniform temperature across the member and connection was adopted (refer to Chapter 2). To illustrate the effect of heating conditions on the connection behavior the restrained steel frame assembly is analyzed by subjecting it to a uniform temperature of 550°C (representing a steady-state heating) and to a parametric fire (representing a transient heating). All other parameters remained invariant in the analysis.

The variation of axial force and rotation, in connection, obtained from the analysis under steady-state and transient heating conditions are shown in Fig. 5.17. It can be seen from Fig. 5.17(a) that the axial force developed in the connection exposed to transient heating conditions under parametric fire (see Fig. 5.4) is compressive initially. After reaching a peak value, the fire induced axial force decreases with fire exposure time and finally transforms to tensile force. However, the connection assembly exposed to a uniform temperature (steady-state) experiences a constant axial (compressive) force that is higher than that in transient heating conditions. This change can be attributed to the fact that the connection assembly is subjected to constant temperature rather than gradual temperature increase as encountered in the case of transient heating under parametric fire. This higher initial temperature in steady-state heating produce higher thermal expansion in the beam and this inturn generates higher axial forces in the connection.

A comparison of rotation in connection shown in Fig. 5.17(b) indicate that the rotation of connection assembly subjected to transient heating under parametric fire increases with increasing fire exposure time and then decreases after reaching a maximum value. This is consistent with the fact that the assembly experiences increase in deflection as the temperature increases (during the growth phase of fire curve). Once the fire enters the decay phase, the beam regains part of its initial strength and stiffness which leads to reduced deflections. In comparison, the connection assembly subjected to uniform temperature (steady-state heating) experienced lower rotation due to the fact that the beam it is subjected to a lower temperature (550°C) as compared to the maximum temperature in parametric fire (≈700°C). The lower temperature (heating) produces smaller deflection in the beam and this intun leads to lower rotation in the connection. As can be seen from Fig. 5.17(b), connection subjected to steady-state heating had a constant rotation of 0.57° at 60 minutes and 120 minutes into the fire exposure time. On the contrary, connection subjected to transient heating experienced a rotation of 0.83° and 1.13° at 60 and 120 minutes, respectively.

5.6.6 Effect of Load Level

The level of loading on structural members can significantly influence the performance of adjoining connection, especially under fire conditions, due to its influence on resulting deflection in the beam, rotation in connection, contact forces between bolt shanks and bolt holes and the stress concentration in the connection region. To quantify this effect a parametric study was carried out by subjecting the beam to four load ratios. In the analysis, the beam was subjected to an increasing loading corresponding to a load ratio (LR) of 30%, 40%, 60% and 70%, and was exposed to parametric fire (see Fig. 5.4). Load ratio (LR) defined earlier is the ratio of applied bending moment in the beam at the fire limit state to the ambient temperature plastic bending moment capacity of the beam. In the fire tests the connection assembly, analyzed here, is tested by applying a load of 40 kN on the beam and this corresponds to a load ratio of 50%.

The progression of rotation and fire induced axial force in connection is plotted, in Fig. 5.18, as a function of fire exposure time for varying load levels. It can be seen from Fig. 5.18(a) that the connections experienced same level of fire induced compressive force, generated due to the thermal expansion of steel beam, regardless of the applied load ratio. This can be attributed to the fact that the compressive force is primarily governed by the thermal expansion of the steel beam which is solely dependent on the temperature and is independent of the applied load ratio. However, when connection assembly is subjected to increasing load levels (above 50%), the axial compressive force transformed into tensile force at an earlier times (i.e., the curve shifts left). This can be attributed to the fact that increasing load level produces larger deflections and higher stresses in beam. The higher deflections, stresses in beam along with the degraded capacity of beam (steel) not only results in higher fire-induced (tensile) axial force but also forces the beam to go into “catenary action” from “flexural action” at earlier stages resulting in the early development of tensile axial force in connection.

A comparison of rotation in connection, shown in Fig. 5.18(b), indicates that the maximum rotation experienced by the connection increases with increasing load intensity. Connections analyzed with a load ratio of 40% experienced marginal increase in rotation as compared to the connections analyzed with 30% load ratio. However, connections analyzed with load ratios of 50%, 60% and 70% experienced 27%, 61% and 67% higher rotations, respectively, compared to connections analyzed with a load ratio of 30%. This is on expected lines because an increase in load produces higher deflections, higher stresses and rapid run-away deflections in the beam, which inturn generates higher restraint forces, especially in connections.

5.6.7 Effect of Fire Scenarios

The fire exposure typically experienced in buildings consists of a growth phase during which the fire temperature increases with time followed by a decay phase when the compartment cools down due to limited fuel and/or oxygen supply. Further, it is well established that accounting for cooling phase of a fire can influence fire performance of connections due to the fact that members and connection (beam, angle, bolts etc.) regain part of their initial strength and stiffness after undergoing large deformations (during the growth phase). In order to study the effect of fire exposure, specifically duration of growth phase, maximum temperature and total duration of fire, the restrained steel framed connection assembly (in FEM2) was analyzed by subjecting it to three different design fire scenarios (DF1-DF3), as illustrated in Fig. 5.19.

The parametric fire time-temperature curve proposed in Eurocode1 (Eurocode1, 2002) and the recent modifications suggested by Feasey and Buchanan (Feasey and Buchanan, 2002) are implemented to arrive at varying design fire scenarios. These design fires (DF1, DF2 and DF3) are assumed to occur in a room of dimension 6x4x3 m^3. Different compartment characteristics utilized to establish the design fire scenarios are presented in Table 5.4.

Fig. 5.20 shows progression of fire induced axial force and rotation in connections exposed to different design fire scenarios (see Fig. 5.19). It can be seen from Fig. 5.20 that the axial force in is compressive in nature initially and it increases gradually due to increasing beam temperature and restraint to free thermal expansion of beam. After reaching a peak value, the fire induced axial force decreases with fire exposure time due to temperature induced degradation in strength and stiffness properties of steel. The axial force continues to decrease and finally transforms into tensile force when the beam load carrying mechanism changes from “flexural action” to “catenary action”.

As can be seen in Fig. 5.20(a), the maximum axial compressive force experienced by the connection changes marginally and is directly proportional to maximum temperature attained in the growth phase of design fire (due to marginal difference in thermal expansion of steel). However, the time to reach the maximum compressive force increases with increasing duration of growth phase. This reinforces the earlier conclusion that the compressive forces (that develop during the early stages of fire) resulting from the thermal expansion of steel beam solely depends on the maximum temperature (fire scenario) attained in a steel beam. A summary of the maximum fire induced forces and rotation experienced by connection for different design fire scenarios is presented in Table 5.5.

During later stages of fire exposure the axial force in the connection transforms from compression to tension and increase in magnitude throughout the decay phase. This is due to the fact that large deflections in the beam (during the growth phase of fire) transform the load carrying mechanism in the beam from “flexural action” to “catenary action”. In addition, steel beam regains part of its initial strength and stiffness with decreasing temperatures and thus exerts more axial force on the connections

Further, the time at which the axial force changes from compression to tension depends only on the duration of growth phase. The shorter the growth phase duration, the earlier the transformation time and this is due to the fact that beam loses its strength at a faster rate and enters the “catenary action” phase earlier when subjected to higher temperatures within a short period of time.

A comparison of rotations in Fig. 5.20(b) indicates that the maximum rotation (refer to Table 5.5) experienced by the connection is influenced by the duration of the growth phase i.e., the longer the growth phase duration the higher is the maximum connection rotation. This can be attributed to the fact that an increase in fire temperature decreases the capacity of the beam leading to higher deflection in the beam and subsequently higher rotation in connection. These results clearly indicate that the response of the connection and subsequently the entire structural system is significantly influenced by fire characteristics.

5.6.8 Effect of High-temperature Bolt Properties

Bolts are an integral part of a connection system and thermal and mechanical properties of steel, which the bolt is made of, plays a crucial role on the response of connections during fire exposure. In recent years high strength bolts of Grade ASTM A325 and A490 are commonly used in construction, in place of conventional ASTM A307 bolts, to improve the overall connection efficiency. The chemical composition and the heat treatment processes that the high strength bolts undergo are completely different from those encountered by conventional bolts (A307) made of carbon (mild) steel (Kodur et al., 2011). Recent study has shown that high-temperature properties of A325 and A490 are different from that of conventional bolts made of steel (A36). Due to lack of property data specific to high strength bolts, high-temperature constitutive material models (strength degradation relations) developed for carbon steel (A36) are used in modeling the high-temperature behavior of high strength bolts. To assess the effect of bolt properties on the transient fire performance of double angle connections, an analysis was carried out by incorporating specific high-temperature properties of steel for A325 and A490 bolts (Kodur et al., 2011). Two types of bolt grades, namely ASTM A325 and A490, (similar to Grade 6.8 and Grade 10.9 in Europe practice) are considered to illustrate comparative connection performance. In addition, analysis was carried out with properties of carbon steel provided in Eurocode 3. Conclusions are drawn by comparing the axial force and connections rotation with those obtained using carbon steel (Eurocode3) and high-strength bolt steel material properties used for the connection.

The progression of axial force and rotation in connection for two types of bolts obtained from the analysis are shown in Fig. 5.21 and Fig. 5.22, respectively. It can be seen from Fig. 5.21 that the high-temperature properties of bolt steel significantly affects the axial force in connection resulting in premature failure of the connection. Both bolt types analyzed with conventional carbon steel bolt properties (those specified in Eurocode3) survived the entire duration of fire exposure time. On the contrary, A325 bolts analyzed with high-temperature properties specific to A325 bolts failed at 70 minutes while A490 bolts analyzed with high-temperature properties specific to A490 bolts failed at 90 minutes into the fire exposure. This can be attributed to the different heat treatment process that the high strength bolts undergo which significantly affects thermal conductivity (Kodur et al., 2011) (refer to Appendix B). For example, at 100°C carbon steel has approximately 8% and 14% higher thermal conductivity compared to high-strength steel used in A325 and A490 bolt steel, respectively.

Furthermore, compared to conventional steel, high strength steel (used in A325, A490 bolts) undergoes a rapid degradation in strength beyond 450°C (Kodur et al., 2011). For example, at 500°C, A325 and A490 bolt steel has approximately 55% and 42% lower residual strength, respectively, compared to carbon steel. The rapid reduction in strength for high strength bolts is attributed to its different chemical composition, manufacturing process and the microstructure (Kodur et al., 2011). Therefore, the rapid reduction in strength and thermal conductivity led to earlier failure of A325 and A490 bolts analyzed with high-temperature properties of bolt steel.

A comparison of rotation in connection (Fig. 5.22) indicates that the rotation tends to increase with increase in temperature, during the growth phase, and then decreases steadily during the decay phase of fire. However, analysis of the connection assembly using high-temperature bolt properties lead to earlier connection failure. This can be attributed to the rapid reduction in bolt strength which produces higher beam deflections and reduces the connection failure time.

Additional numerical simulations were carried out to study the effect of bolt strength (grade) on the connection performance by using bolt grades commonly used in Europe, namely Grade 6.8 and Grade 10.9. These bolt grades are equivalent to ASTM A325 and ASTM A490 bolt grades used in North America. The ambient temperature material properties of different bolt grades are presented in Table 5.6. Results from the simulations indicated that the bolt strength has negligible effect on the connections axial force and rotation. This indicated that bolts did not experience forces in excess of their load carrying capacity and failure occurred in the beam prior to that in bolts (either by tension, block-shear or bearing against beam web).

Based on the above results, it can be inferred that the response of connections made of high strength bolts can be different from that of bolts with conventional steel due to variation in properties of steel at elevated temperatures. Therefore, high-temperature steel properties, specific to the bolt grade, should be accounted for in the analysis to evaluate the true connection response.

5.7 Summary

This chapter presents results of parametric studies to illustrate the influence of various factors on the system-level transient fire performance of double angle connection assemblies. The studied parameters are: effect of decay rate, loading type, degree of axial restraint, effect of composite action arising from the presence of slab, system-level interactions, heating profile, load level, fire scenarios and high-temperature bolt properties. Data from parametric studies indicate that:

- System-level analysis treats connections to be an integral part of structural framing system and accounts for the effect of surrounding structural members in order to trace the fire response of double angle connections.
- Double angle connections are robust to a higher degree and can sustain additional fire induced axial forces compared to other connection types (such as shear tab and single angle).
- Presence of concrete slab significantly enhances the rigidity of a steel frame assembly under fire conditions through composite action and restrains the secondary beam against instabilities such as lateral torsional buckling.
- The failure time of connection assemblies without slab decreases with increasing axial stiffness because a higher value of axial restraint stiffness restricts the free thermal movement of the beam. This results in the development of higher stresses and local instabilities in the beam which ultimately leads to the failure of the connection assembly.
- The high-temperature properties of high-strength steel used in bolts are different from that of carbon steel used in beams and columns and have significant influence on the connection response. The mechanical properties of high-strength bolts (such as A325 and A490 bolts) have a significant effect on the development of axial forces and connection's rotation while the thermal properties of A490 bolts influences the connection's axial force only.

Results from the parametric studies are utilized in Chapter 6 to develop guidelines for evaluating fire resistance of double angle connections.

CHAPTER 6

6. METHODOLOGY FOR EVALUATING FIRE RESISTANCE

6.1 General

Beams under fire conditions can experience large fire induced forces. This is because of the restraint provided by surrounding (cold) structural members to the free thermal expansion of the beams. These fire induced forces gets transferred from the heated beam to the connected beam or column through connections. Further, the fire induced axial forces change from compressive forces during initial stages of fire to tensile forces in later stages of fire. These additional fire induced forces on connections are to be considered in evaluating fire resistance of connection assemblies. There are no simplified methods till date that account for fire induced forces in evaluating fire response of connections. A methodology is developed in this chapter to account for the effect of fire induced forces in evaluating fire resistance of double angle connection assemblies.

6.2 Outline of Proposed Methodology

The proposed rational approach for evaluating the fire resistance of connection assemblies comprises of two steps, namely: developing a methodology to predict the response of connection. The validity of the proposed methodology is established by comparing the fire resistance predictions from the methodology with values obtained from numerical studies for double angle and shear tab connection assemblies. Predictions from the proposed empirical equation are compared with fire resistance obtained from finite element models. Also the applicability of the proposed approach to design situations is illustrated through numerical example.

The proposed methodology uses moment-curvature-axial force (M-κ-P) relationships to trace the response of double angle connection assemblies in fire over the entire rage of loading up to collapse. The connected beam is divided into a number of segments along its length. The axial and rotational stiffness provided by the connections is approximated by using axial and rotational springs. The mid-section of each segment is assumed to represent the behavior of the whole segment. The fire resistance analysis is carried out by incrementing time in steps. At each time interval, the analysis is performed through two main stages, namely:

- Pre strength analysis of connection assemblies, which includes:
  - Establishing the fire temperature for a given fire exposure condition (ex: ISO834 or ASTM E119),
  - Computing temperatures in the cross-section of beam segment,
  - Computing fire-induced axial force developed in the beam,
- Perform a strength and rotation analysis on connected beam and connection, through five sub-steps, namely:

- Generate moment-curvature-axial force relationships (using the cross-sectional temperature and axial force computed above) for each beam segment,
- Develop moment profile (bending moment diagram) of the beam using external loading,
- Determine the curvature profile at each segment of the beam based on the pre-established moment profile,
- Integrate the curvatures across the span of the beam to evaluate rotation in connections, and
- Compute the failure time (fire resistance) of connection by checking connection and beam limit states.

The above steps are illustrated through a flow chart as shown in Fig. 6.1. The first step of the analysis is to establish fire temperatures, cross-sectional temperatures and fire-induced axial forces that develop in the beam. Empirical equations developed by previous researchers are utilized to evaluate temperatures in the beam.

Once the temperature distribution and fire induced axial force are computed, the next step is to generate time dependent moment-curvature-axial force (M-κ-P) relationships in various beam segments. These relationships are generated using an iterative approach, by increasing moment so as to satisfy equilibrium and compatibility criteria for each segment along the span of the beam.

The moment profile along the span of the beam can be computed knowing external loading. Using the M-κ-P relationships and pre-established moment profile, curvature distribution is established in each segment along the length of the beam. Once the curvature profile is established, rotation at connection is calculated by integrating curvatures along the span of the beam. Knowing all the response parameters, failure state of beam and connection at each time step is checked by comparing the fire induced axial force in the beam and rotation in connection against pre-determined failure criteria. The failure criteria include performance-based strength criteria (for connection) and deflection (in the beam) considerations. Details of the analysis procedure are presented in the following sub-sections.

6.3 Computing Temperatures

The fire resistance analysis is carried out by incrementing time in steps. At each time step, fire temperatures are established based on standard or design fire relations given in standards such as ASTM E119, ISO 834 or Eurocode. Next, for standard fire exposure conditions, the temperature in beam (steel) cross-section and fire-induced axial forces are evaluated based on the empirical equations previously developed by Dwaikat and Kodur (Dwaikat and Kodur, 2011, 2013). This equation for computing steel temperatures is used because of its simplicity to use as well as the fact that steel temperatures can be computed for any given time without employing an iterative approach. For design fire exposure conditions, the temperature in beam (steel) cross-section is computed using a lumped heat capacity approach. As explained below, the empirical equation provided by Dwaikat and Kodur cannot be applied for design fire conditions.

6.3.1 Standard Fire Exposure

The fire temperatures are calculated by assuming three sides of a beam is exposed to a fire, whose temperatures follow that of a standard fire exposure ISO834 (ISO, 1975) or ASTM E119 (ASTM, 2011a) fire exposure conditions. The ISO 834 standard fire is similar to ASTM E119 standard fire, as shown in Fig. 6.2. Time-temperature relationship of ISO 834 standard fire is given by the following equation:

$$T_f = 20 + 345 * \log(8t + 1) \tag{6.1a}$$

where T_f is fire temperature (in °C) as a function of time t (in minutes).

Similarly, the time-temperature relationship of ASTM E119 standard fire is given by the following equation:

$$T_f = 750 * \left(1 - e^{-3.79553\sqrt{t}}\right) + 170.41\sqrt{t} + 20 \tag{6.1b}$$

where T_f is fire temperature (in °C) as a function of time t (in hours).

The fire time-temperature curve can be approximated by a power function as following (Dwaikat and Kodur, 2013):

$$T_f = at^n \tag{6.2}$$

where a and n are regression coefficients. For ISO 834 standard fire a = 469.9 and n = 0.1677. Similarly, for ASTM E119 standard fire a = 496.5 and n = 0.1478.

Based on the standard fire temperatures (Eq. [6.2]), the temperatures in the steel (T_s) beam cross-section can be established by the following empirical relationship (Dwaikat and Kodur, 2013):

$$T_s(t) = T_f(1 - e^{-st}) \tag{6.3}$$

where T_s is the steel temperature (in °C) as a function of time t (min), s is a correlation coefficient which is defined for protected steel sections as:

$$s = \frac{\left({}^{F_p}\!/_{A_s}\right)}{c_s\rho_s(1/h + t_p/k_p)\Big(1 + (c_p\rho_p/c_s\rho_s)(F_p/A_s)(t_p/m)\Big)(n+1)} \tag{6.4a}$$

where the terms are defined as below

F_p : heated perimeter of the cross section (or steel plate),

A_s : cross sectional area of the section (or the steel plate),

c_s,c_p : specific heat of steel and insulation, respectively,

ρ_s,ρ_p : density of steel and insulation, respectively,

h : convective heat flux coefficient,

t_p : thickness of insulation,

k_p : thermal conductivity of insulation, and

m : constant used for averaging temperature of insulation layer around steel section.

For unprotected steel sections, the value of s can be calculated by using a value of zero for the insulation thickness (i.e., t_p=0) in Eq. [6.4a]) resulting in the following equation:

$$s = \frac{\left({F_p}/{A_s} \right)}{c_s \rho_s (1/h)(n+1)} \qquad [6.4b]$$

Therefore, the above equation can be used to evaluate the temperature of protected and unprotected steel section. In addition, the above equation can evaluate the temperature of the entire cross section or for individual parts of the section such as top flange, web and bottom flange using appropriate parameters (F_p, A_s etc) in Eq. [6.3] and Eq. [6.4].

6.3.2 Comparison to Other Methods

To demonstrate the accuracy of Dwaikat and Kodur relationship (Eq. [6.3]) in predicting steel temperatures, temperatures obtained using Dwaikat and Kodur relationship are compared to temperatures calculated using two other widely used methods namely: best-fit method and step-by-step (lumped heat capacity) method.

The best-fit method for computing steel temperatures includes two equations that are derived from statistical regression analysis of one-dimensional finite difference solutions of heat transfer equation. According to this method, the temperature in a contour-insulated steel section can be computed as follows (Buchanan, 2002):

$$t = \frac{40(T_{lim} - 140)}{\left((F_p/A_s)/(t_p/k_p)\right)^{0.77}} \quad \text{,or} \qquad [6.5a]$$

$$T_{lim} = 140 + \frac{t}{40}\left(\frac{F_p/A_s}{t_p/k_p}\right)^{0.77} \qquad [6.5b]$$

Similarly, the temperature in unprotected steel section can be computed as follows:

$$t = \frac{0.54(T_{lim} - 50)}{(F_p/A_s)^{0.6}} \quad \text{,or} \qquad [6.5c]$$

$$T_{lim} = 50 + \frac{t}{0.54}(F_p/A_s)^{0.6} \qquad [6.5d]$$

where t is time in minutes, T_{lim} is the required or given limiting temperature of steel in °C, F_p/A_s is the section factor in m^{-1}, t_p is insulation thickness in m and k_p is the thermal conductivity of insulation material in W/m°K.

Similarly, the step-by-step method or lumped heat capacity method provides an equation for predicting temperatures in a contour-insulated steel section. This method assumes that a steel member is at a uniform temperature and adopts a quasi-steady-state lumped heat capacity approach (Buchanan, 2002). According to this approach the increment in temperature of a protected steel member can be computed as follows:

$$\Delta T_s = \frac{k_p}{c_s h W/D}(T_f - T_s)\Delta t \qquad [6.6a]$$

where ΔT_s is the temperature rise in steel in °C, k_p is the thermal conductivity of insulation material in W/m°K, c_s is the specific heat of steel in J/kg °K, h is the thickness of the insulation in m,W is the weight of steel per unit length in kg/m, D is the heated perimeter in m, T_f is the fire temperature in °C, T_s is the steel temperature in °C and Δt is the time increment in seconds.

The increment in steel temperature for an unprotected steel member can be computed using the following equation:

$$\Delta T_s = \frac{\alpha}{c_s(W/D)}(T_f - T_s)\Delta t \quad [6.6b]$$

$$\alpha = \alpha_r + \alpha_c \text{ , and} \quad [6.6c]$$

$$\alpha_r = \frac{\sigma\varepsilon}{(T_f - T_s)}(T_f^4 - T_s^4) \quad [6.6d]$$

where ΔT_s is the temperature rise in steel in °C, α is the heat transfer coefficient (W/m^2 K), c_s is the specific heat of steel in J/kg °K, W is the weight of steel per unit length in kg/m, D is the heated perimeter in m, T_f is the fire temperature in °C, T_s is the steel temperature in °C and Δt is the time increment in seconds, α_r is the radiative heat transfer coefficient (W/m^2 K), α_c is the convective heat transfer coefficient (W/m^2 K), σ is the Stefan-Boltzmann coefficient ($5.67*10^{-8}$ W/m^2 K^4) and ε is the effective emissivity.

Temperatures in two representative steel sections, W12x30 and W24x76, are computed using the best-fit method, step-by-step method and the Dwaikat and Kodur relationship (Eq. [6.3]). Geometric details of both steel sections are presented in Table 6.1. The schematic of beam section used in computing temperatures for protected and unprotected steel sections is illustrated in Fig. 6.3 and Fig. 6.5, respectively. The temperatures of steel sections with fire protection are presented in Fig. 6.4 while Fig. 6.6 shows the temperatures for unprotected steel sections. For the case of insulated scenario, both the steel sections are assumed to be protected with 15mm thick insulation having a thermal conductivity of 0.12 W/m°K.

As can be seen from Fig. 6.4 and Fig. 6.6, temperatures predicted by best-fit method are accurate in a narrow range of temperatures (400-700°C). This can be attributed to the fact that the best-fit method is based on statistical regression and is derived for calculating average steel temperatures in the vicinity of the critical temperature of steel which is 538°C (Buchanan, 2002; Dwaikat and

Kodur, 2013). Critical temperature of steel is defined as the temperature at which steel loses about 50% of its strength.

On the other hand, temperatures predicted by Dwaikat and Kodur relationship and step-by-step method are similar and there are marginal differences between the two for the entire range of fire exposure time. Step-by-step (lumped heat capacity) method is based on one-dimensional finite difference technique and computes steel temperatures incrementally (Buchanan, 2002). Hence, the accuracy of this approach depends on the time increment used. The smaller the time increment the better the accuracy of the method, however as the time increment decreases the computational time increases. Therefore, this method can be used with smaller time steps where higher accuracy in predicting the steel temperatures is required and for comparison/calibration purposes. Further, as this method uses incremental approach to compute steel temperatures, in order to predict the steel temperature at any particular time (say 30 minutes) steel temperatures should be computed incrementally up to this time. To achieve a high level of accuracy, an incremental time increment of 10 seconds was used in computing the steel temperatures presented in Fig. 6.4 and Fig. 6.6.

Temperatures predicted by Dwaikat and Kodur relationship are in good agreement with those predicted using step-by-step method for the entire duration. The temperatures predicted by Dwaikat and Kodur relationship are slightly lower compared to step-by-step method. This can be attributed to the fact that Dwaikat and Kodur relationship approximates radiative heat transfer as an equivalent convective heat transfer. However, it is important to note that the Dwaikat and Kodur relationship can be used to predict steel temperature at any given time step, without the need for incrementing time steps. Eq. [6.3] can be used to compute steel temperatures in one step (no time-steps) and this is the advantage of using Eq. [6.3] compared to other incremental approaches (such as step-by-step method). The simplicity of use and accuracy in predicting steel temperatures makes the Dwaikat and Kodur relationship (Eq. [6.3]) a better approach to compute steel temperatures. Hence, Dwaikat and Kodur relationship is adopted in the proposed approach to compute steel temperatures.

6.3.3 Design Fire Exposure

Unlike standard fire, compartment temperatures in a design fire increases initially during growth phase and then decrease once the total available fuel is consumed and/or oxygen supply gets restricted. Dwaikat and Kodur relationship (Eq. [6.3]) cannot capture the temperatures in steel when exposed to design fire scenario. This is due to the fact that the exponential term in Eq.[6.3] increases asymptotically with time which will yield a continuous increase in steel temperature during the growth phase of fire. During the decay phase of fire, according to Eq. [6.3] when the time is large the temperature in steel tends to approximate fire temperature (i.e., as $t \rightarrow \infty$, $e^{-st} \rightarrow 0$ and $T_s \rightarrow T_f$). However, in reality the temperature in steel increases and decreases slowly compared to fire temperatures because of the lag effect of steel. Hence, the temperatures in steel will be higher than fire temperatures during the decay phase of fire. But Eq. [6.3] will predict steel temperatures equal to that of fire temperatures thereby underestimating the temperatures in steel. In lieu of using Eq. [6.3] to predict temperatures in steel, the lumped heat capacity method described earlier is used to predict temperatures in steel sections subjected to design fire exposure.

To verify the applicability of lumped heat capacity approach temperatures in two representative steel sections, W12x30 and W24x76 subjected to design fire scenarios are computed using the step-by-step method. Geometric details of both steel sections are presented in Table 6.1. The schematic of beam section used in computing temperatures for protected and unprotected steel sections is illustrated in Fig. 6.3 and Fig. 6.5, respectively. The representative design fire selected for the analysis is design fire DF1 described in Chapter 3. Design fire, DF1, comprised of a growth phase for the first 75 minutes as per ASTM E119 fire (ASTM, 2011a) and then a decay phase with a cooling rate of 8°C/min (see Fig. 3.5). The input parameters used in arriving at this design fire scenario are listed in Table 3.4.

Both the sections are analyzed with and without fire insulation protection on steel. For the case of insulated scenario, both the steel sections are assumed to be protected with 15mm thick insulation having a thermal conductivity of 0.12 W/m°K. The progression of temperatures in steel sections with and without fire protection is presented in Fig. 6.7. It can be seen from the figure that the temperature in protected and unprotected steel sections increase during the growth phase of fire and decrease during the decay phase of fire. However, the temperatures in protected steel increases slowly compared to rapid rise in unprotected steel temperatures. In addition, temperatures in unprotected steel sections are significantly higher compared to that of protected steel sections. These observations are on the expected lines because the presence of fire insulation decreases the amount of heat transmission to steel thereby limiting the temperature rise in steel.

Next, temperatures in protected and unprotected steel increases slowly compared to fire temperature during the growth phase of fire. Similarly, during the decay phase of fire steel temperatures decrease slowly compared to fire temperature. Further, the steel temperatures are always higher than that of the fire temperatures for the entire duration of decay phase of fire. As described earlier, this can be attributed to the lag effect of steel which will delay the increase and decrease of steel temperatures compared to fire temperature.

Based on these observations, it can be concluded that the step-by-step method is capable of predicting temperatures in steel with reasonable accuracy. Hence, step-by-step method is adopted in the proposed approach to compute the temperatures in steel sections exposed to design fire scenarios.

6.4 Computing Fire Induced Axial Force

Once temperatures in the beam cross-section are established, the fire-induced axial force (P) generated in the beam can be computed using the relationships developed by Dwaikat and Kodur (Dwaikat and Kodur, 2011). As shown in Fig. 6.8, this fire induced force acting on the connection is compressive in nature during the initial stages of fire. The axial force increases with time (stage 1) and the combined effect of restraining axial force and bending moment results in initial yielding of the beam. After yielding of steel, the compressive force decreases in magnitude (stage 2) and finally transforms into tensile force (stage 3). During the final stages of fire exposure, the beam regains part of its initial strength and undergoes thermal shrinkage leading to continuous increase in the tensile force until connection fails. During this stage, the beam is held in place (like a cable) by the connections through catenary action.

The fire-induced axial force (P) can be calculated using the following equations developed by Dwaikat and Kodur (Dwaikat and Kodur, 2011):

Stage 1: When steel temperature (T_s) is less than steel yield temperature (T_y) (i.e., $T_s < T_y$),

$$P = (T_s - 20)X_A F_y A_s \qquad [6.7]$$

where P is the fire induced axial force (in kN), F_y is the yield strength (in MPa) and X_A is the axial restraint factor defined as:

$$X_A = \frac{\alpha E_s}{F_y}\left(\frac{a_1 K_a L/(E_s A_s)}{2a_1 + K_a L/(E_s A_s)}\right) \qquad [6.8]$$

where

α : coefficient of thermal expansion,

E_s : elastic modulus of steel at ambient temperature,

F_y : yield strength of steel at ambient temperature,

A_s : cross-sectional area of steel section,

K_a : axial restraint stiffness of the connection,

L : total length of the beam, and

a_1 : non-dimensional (constant) temperature-dependent reduction of steel elastic modulus.

- For steel properties as specified in Eurocode 3: $a_1 = 0.6$.
- For steel properties as specified in ASCE manual: $a_1 = 0.6829$.

The temperature (T_y) at which steel yeilds is given by:

$$T_y = \frac{1 - M_0/M_y - 0.5 X_R \Delta T}{X_A + a_2}, \qquad T_y < 600°C \qquad [6.9]$$

where

M_0 : maximum bending moment in the beam due to gravity load,

M_y : unfactored yield bending capcity of the section at ambient temperature,

ΔT : thermal gradient in the beam cross-section (difference in temperature of bottom flange and top flange of beam),

a_2 : factor (constant) that accounts for temperature-dependent reduction in steel yield strength,

- In case of Eurocode 3 steel properties: $a_2 = 0.0013$.
- In case of steel properties specified in ASCE manual: $a_2 = 0.0008$.

X_R : rotational restraint stiffness factor of the connection which is computed as

$$X_R = \frac{\alpha E_s}{F_y}\left(\frac{a_1 K_r L/(E_s I)}{2a_1 + K_r L/(E_s I)}\right) \qquad [6.10]$$

K_r : rotational restraint stiffness due to the connection, and

I : second moment of area of the section in the direction of the thermal gradient.

The maximum value of fire-induced compressive axial force ($P_{c,max}$) in the connection can be computed by substituting yield temperature (T_y) into Eq. [6.7]:

$$P_{c,max} = (T_y - 20)X_A F_y A_s \qquad [6.11]$$

Stage 2: When steel temperature (T_s) is greater than steel yield temperature (T_y) but less than steel catenary temperature (T_c) (i.e., $T_y < T_s < T_c$),

After reaching a maximum value (stage 2) (refer to Fig. 6.8), the axial compressive force decreases in magnitude until it reaches zero (P=0) at catenary temperature (T_c), which is defined as:

$$T_c = \frac{1}{a_2}\left(1 - \frac{M_o}{M_u} - \frac{M_y}{M_u}\frac{X_R \Delta T}{2}\right) \qquad [6.12]$$

where M_u is the unfactored ultimate bending capacity of the section at ambient temperature.

At any temperature between the yield temperatures (T_y) and the catenary temperature (T_c) (i.e., stage 2), the fire induced force is computed by linear interpolation between the point of maximum compressive force (T_y, $P_{c,max}$) and the point of catenary (T_c, $P=0$), as can be seen in Fig. 6.8.

Stage 3: When steel temperature (T_s) is greater than steel catenary temperature (T_c) but less than maximum tensile catenary force temperature ($T_{ten,max}$) (i.e., $T_c < T_s < T_{ten,max}$),

Beyond catenary temperature (stage 3), the axial force transforms to tensile force and continues to increase till it reaches a maximum value, as can be seen in Fig. 6.8. The maximum tensile catenary force ($P_{ten,max}$) is computed using the following equations:

$$P_{ten,max} = \left(a_3 - a_4 T_{ten,max}\right)F_y A_s, \quad 500°C \le T_{ten,max} \le 900°C \qquad [6.13]$$

and

$$T_{ten,max} = \frac{T_c T_y F_A + a_1 a_3 (T_c - T_y)}{T_y F_A + a_1 a_4 (T_c - T_y)} \qquad [6.14]$$

where

$T_{ten,max}$: temperature at the maximum tensile catenary force,

a_3, a_4: regression coefficients (constants) that are dependent on steel properties,

- In case of Eurocode 3 steel properties: $a_3 = 1.139$, $a_4 = 0.0013$.
- In case of steel properties specified in ASCE manual: $a_3 = 1.329$, $a_4 = 0.0014$.

The fire induced axial force in the temperature range between the catenary temperature (T_c) and the maximum tensile catenary force temperature ($T_{ten,max}$) (i.e., stage 3), is computed by linear interpolation between the point of catenary (T_c, $P=0$) and the point of maximum tensile catenary force ($T_{ten,max}$, $P_{ten,max}$).

Therefore, through this approach the fire induced forces generated in the beam and that gets applied on the connection can be evaluated.

6.5 Strength Analysis

6.5.1. General Analysis Procedure

The next step in the methodology is the strength analysis at the mid-section of each segment of the beam. The cross-sectional steel temperatures, as generated in the previous section, are used as input to the strength analysis. For strength analysis, the following assumptions are made:

- Plane sections before bending remain plane after bending,
- The beam is subjected to uniform fire exposure throughout the span length,
- At a given time step, fire induced axial force is constant along the span of the beam,
- The connected beam is assumed to be free of instabilities such as local buckling and lateral torsional buckling, till failure through loss of capacity in connection or excessive beam deflections.

At each time step, the strength analysis is performed in five sub-steps, namely, (1) generate moment-curvature-axial force relationships in each beam segment, (2) evaluate moment profile along the length of the beam using external loading and beam length, (3) compute curvature profile at each segment along the length of the beam using the generated moment-curvature-axial force relationships and pre-established moment profile, (4) evaluate the rotation in connection by integrating the curvatures along the span length of the beam, and (e) estimate the failure time (fie resistance) of connection by applying failure limit states for connection and beam.

The M-κ-P relationships, at various time steps, are generated using the calculated axial force and constitutive relationships for steel (refer to Appendix B). The interaction between fire induced axial force and bending moment capacity is automatically accounted for in generating M-κ-P relationships. In the nonlinear strength analysis, rotation of connection at each time step can be calculated through an iterative approach that utilizes generated M-κ-P relationships to compute curvature in each beam segment.

6.5.2 Generation of M-κ-P relationships

The M-κ-P relationships generation, at elevated temperatures, is carried out by dividing the beam in different segments as described above. An illustration of the beam elevation and cross-section along with the longitudinal segments and discretized cross-section is shown in Fig. 6.9.

Once the fire induced axial force is computed, the M-κ-P relationships are generated through a tangential stiffness method proposed by Santathadaporn et al. (Santathadaporn and Chen, 1972). The generalized stresses and strains in a beam cross-section are shown in Fig. 6.10. In addition, Fig. 6.10 also shows the sign convention used in this approach for positive values of generalized stresses and strains. As per this approach and illustrated in Fig. 6.10, if a steel section is subjected simultaneously to generalized stresses (f) such as bending moment (M_x) and axial force

(P) then the corresponding set of generalized strains (X) are bending curvature (κ) and axial strain (ε_o). The generalized stresses and strains can be written in vector form as follows:

$$\{f\} = \begin{Bmatrix} -M_x \\ -P \end{Bmatrix} \qquad [6.15a]$$

$$\{X\} = \begin{Bmatrix} \kappa \\ \varepsilon_o \end{Bmatrix} \qquad [6.15b]$$

This approach is based on sectional analysis and the steel cross-section is discretized into a number of elements as shown in Fig. 6.9(d). Equilibrium state of the section is satisfied when the applied external forces (generalized stresses) are equal to the generated internal forces i.e.,

$$- Mx = -\int \sigma . y . dA \qquad [6.16a]$$

$$- P = -\int \sigma . dA \qquad [6.16b]$$

where σ is the stress in an element of area dA. The sign for stress σ is assumed to be positive when it produces tensile stress.

The stress in each element is computed using the constitutive stress-strain relationships of the material (steel). For example, the ambient temperature stress-strain relationship for a strain-hardening steel is given by

$$\sigma = \begin{cases} E\varepsilon, & |\varepsilon| < \varepsilon_y \\ \sigma_y + E_t(\varepsilon - \varepsilon_y), & \varepsilon_y \le |\varepsilon| \ge \varepsilon_u \\ \sigma_u, & |\varepsilon| \ge \varepsilon_u \end{cases} \qquad [6.17]$$

where E is the modulus of elasticity, E_t is the tangent modulus of elasticity, ε is the strain in the element, ε_y is the yield strain of the material, ε_u is the ultimate strain of the material, σ_y is the yield strength of the material and σ_u is the ultimate strength of the material.

If it is assumed that the plane section remains plane before and after deformation, the strain at any point in the cross-section can be evaluated as (refer to Fig. 6.11):

$$\varepsilon = -y\kappa + \varepsilon_o + \varepsilon_r \qquad [6.18]$$

where y is the distance from centroid to the center of the elemental area dA, ε_r is the residual strain in an element and ε_o is the axial strain in an element. Since the plastic behavior of material (steel) is load path dependent, rate equations of equilibrium needs to be used to capture the effect of history of loading on the material behavior. Therefore, once the existing state of stress and strain for each element is known, the rate equations of equilibrium (derivate of equilibrium equations i.e., Eq. [6.16]) for generalized stress and generalized strains can be evaluated as follows:

$$-\dot{M}_x = -\int \dot{\sigma}\, y\, dA \qquad [6.19a]$$

$$-\dot{P} = -\int \dot{\sigma}\, dA \qquad [6.19b]$$

Then, the rate of change of stress (derivative of Eq. [6.17]) is given by

$$\dot{\sigma} = \begin{cases} E\dot{\varepsilon}, & |\varepsilon| < \varepsilon_y \\ E_t\dot{\varepsilon}, & \varepsilon_y \leq |\varepsilon| \geq \varepsilon_u \\ 0, & |\varepsilon| \geq \varepsilon_u \end{cases} \qquad [6.20]$$

The strain rate equation (derivative of Eq. [6.18]) becomes

$$\dot{\varepsilon} = -y\dot{\kappa} + \dot{\varepsilon_o} \qquad [6.21]$$

Note that the residual strain (ε_r) is independent of time.

Equations [6.19], [6.20] and [6.21] can be combined so that they give a set of simultaneous linear equations which can be written in the following matrix form:

$$\begin{Bmatrix} -\dot{M}_x \\ -\dot{P} \end{Bmatrix} = \begin{bmatrix} Q_{11} & Q_{12} \\ Q_{21} & Q_{22} \end{bmatrix} \begin{Bmatrix} \dot{\kappa} \\ \dot{\varepsilon_o} \end{Bmatrix} \qquad [6.22]$$

where Q_{ij} is defined as

$$Q_{11} = \int E\, y^2\, dA \qquad [6.23a]$$

$$Q_{22} = \int E\, dA \qquad [6.23b]$$

$$Q_{12} = Q_{21} = -\int E\, y\, dA \qquad [6.23c]$$

Equation [6.22] can be rewritten as

$$\{\dot{f}\} = [Q]\{\dot{X}\} \quad [6.24]$$

Matrix $[Q]$ is known as tangent stiffness matrix as it represents the tangent of force-deformation curve as well as the stiffness of the cross-section. The above equation represents a general form of linear force-deformation relationship which can be incorporated into a numerical program and solved using an iterative technique(s). It should be noted that Equations [6.23] are applicable for the elastic regime of the material only. For strain-hardening region, the value of E should be replaced by the tangent modulus E_t.

In this approach, the value of fire induced axial force (P) and the tangent stiffness matrix are known at the beginning of each time step. Then the applied moment (M_x) is incremented and Eq.[6.24] is solved to compute the value of curvature and axial strain. Once these values are known, the internal forces are computed using Eqs. [6.19]-[6.21]. The curvature is iterated until equilibrium of forces is satisfied i.e., internal force (Eq. [6.19]) must be equal to the external applied forces. Once equilibrium is satisfied, the value of curvature corresponding to the applied moment is calculated. Thus, the values of moment and curvature are stored to represent a point on the moment-curvature curve for a given value of fire induced force. A flow chart illustrating the steps involved in generating moment-curvature-axial force relationships is shown in Fig. 6.12.

The value of applied moment is incremented to generate subsequent points on the moment curvature curve. This procedure is repeated at each preselected time step of fire exposure. The generated M-κ-P relationships are used to trace the performance of connections through nonlinear structural analysis. The generation of M-κ-P relationships is an important part of the proposed methodology since these relationships form the basis for the fire resistance analysis of connection.

6.5.3 Iterative solution

Equation [6.24] represents a general form of force-deformation relationship and can be solved using an iterative technique. A graphical illustration of representative force-deformation curve is shown in Fig. 6.13. The curve OABC represents the true force-deformation curve. Region OA represents the linear portion of the force-deformation relationship. $\{f_A\}$ and $\{X_A\}$ be the force and deformation vectors (Eq. [6.15]), at point A along the curve, which satisfy equilibrium conditions. The next step is to compute the deformation at point B when the prescribed force is $\{f_B\}$. The incremental value of force from point A to point B is

$$\{\dot{f}_A\} = \{f_B\} - \{f_A\} \qquad [6.25]$$

Till point A, the response is linear and thus the tangent stiffness matrix at point A $[Q_A]$ (Eq. [6.23]) is known and it represents the slope at point A on the curve. With the applied force increment (Eq. [6.25]), the increment in deformation is obtained from

$$\{\dot{X}_A\} = [Q_A]^{-1}\{\dot{f}_A\} \qquad [6.26]$$

where $[Q_A]^{-1}$ is the inverse of matrix $[Q_A]$.

The above equation is an approximation (predictor) to the solution as the tangent stiffness matrix is computed before the force increment occurs. The accuracy of deformation, approximated by the above equation, can be increased by applying a small increment in the external force.

The first estimated deformation value can be computed by adding $\{X_A\}$ and the incremental deformation predicted by Eq. [6.26]

$$\{X_1\} = \{X_A\} + \{\dot{X}_A\} \qquad [6.27]$$

This deformation $\{X_1\}$ develops an internal force $\{f_1\}$ that is not in equilibrium with the external force $\{f_B\}$. Therefore, the first unbalanced (residual) force can be computed as:

$$\{\dot{f}_1\} = \{f_B\} - \{f_1\} \qquad [6.28]$$

Next, the unbalanced force is applied and the correction in displacement vector (corrector vector) $\{\dot{X}_1\}$ is computed to eliminate unbalanced forces. Then, the corrector vector is added to the first estimated deformation values $\{X_1\}$ to compute the subsequent estimation of deformation vector.

$$\{\dot{X}_1\} = [Q_1]^{-1}\{\dot{f}_1\} \quad [6.29]$$

where $[Q_1]^{-1}$ is the inverse of new tangent stiffness matrix $[Q_1]$ which corresponds to the state $\{f_1\}$and $\{X_1\}$.

This process of computing residual (unbalanced) force vector and the corresponding correction in displacement vector is repeated until the unbalanced force becomes zero or is within the predetermined tolerance limit, which is taken to be 0.1% (i.e., having an accuracy of 99.9%) in the analysis.

The accuracy and convergence of this method can be improved by applying small increment of force. If the force increment is small, the first estimate of the displacement vector will be accurate and subsequent corrections will not be necessary.

6.6 Computer Implementation

6.6.1 Computer Program

The above outlined procedure requires a large amount of computational effort since it involves use of an iterative approach. To facilitate numerical calculations the above procedure was incorporated into a custom-built computer program written in MATLAB. Empirical relationships for computing fire temperature, temperature in beam cross-section along with the fire-induced axial forces are incorporated into the MATLAB program. The iterative scheme for generating moment-curvature-axial force relationships, illustrated in Fig. 6.12 and Fig. 6.13, is implemented in the program as well. Fig. 6.14 shows the flowchart of the numerical procedure associated with the computer program. The MATLAB code is included in Appendix D.

6.6.2 Material properties

Steel properties suggested by Eurocode 3 (Eurocode3, 2005b), and presented in Appendix B, were incorporated in the MATLAB program. Relevant thermal and constitutive material properties (stress-strain relationships) of steel along with the high-temperature strength reduction factors are built into the code. Since the insulation material has significantly low strength and stiffness, the strength, stiffness contribution from the insulation is neglected. However, thermal properties of fire insulation are accounted when computing the temperature of beam (steel). For the current analysis thermal conductivity and dry density of fire insulation are obtained from the values proposed by recent study (Kodur and Shakya, 2013). It should be noted that there is limited data on the variation of thermal properties with temperature of the insulation material; hence thermal properties at room temperature are used in the analysis.

6.6.3 Beam, Connection Idealization

The steel beam is idealized as a set of longitudinal beam segment and cross-section of each beam segment is further discretized into a number of elements as shown in Fig. 6.9. The number of longitudinal segments and the number of element divisions in each direction must be specified as input to the program. Based on the number of elements, the program determines the element size. Uniform and non-uniform element sizes can be input into the program. The connections (double angle or any other connection configuration) at the beam ends are idealized as springs having axial restraint stiffness (K_a) and rotational restraint stiffness (K_r) and these stiffness values need to be specified as an input.

6.6.4 Input data

The input to the program consists of beam length, cross-sectional properties, number of divisions in each direction of the cross-section, steel and insulation properties, type of fire exposure

(ISO834 or ASTME119) as well as the analysis time and tolerance limits for convergence. The failure limit states are automatically computed based on the input data for beam and connection. Thermal and mechanical properties of steel and insulation are built into the program. In addition, the program also provides the flexibility to allow users to incorporate any general stress strain relationships as a function of temperature.

6.6.5 Output data

At each time step, the output from the program includes temperatures distribution in the beam cross-section, fire induced axial force (P), M-κ-P relationships. In addition, the program checks for failure of connection against pre-defined failure criteria and outputs the failure time (fire resistance) of the connection.

6.6.6 Analysis of typical beams

The above proposed approach, implemented in MATLAB, is used to generate moment-curvature-axial force relationships for steel beams. This is illustrated for two representative steel sections, namely W12x30 and W24x76, with 15mm thick fire insulation having a thermal conductivity of 0.12 W/m° K and specific heat of 900 J/kg K. Geometric details of both steel sections are presented in Table 6.1. Both these steel sections are assumed to be exposed to ISO834 standard fire and the generated moment-curvature relationships (which inherently accounted for axial forces) are shown in Fig. 6.15, as a function of fire exposure time. The fire induced axial forces corresponding to the moment-curvature relationships (in Fig. 6.15) are also shown in the same figure. The computed temperatures in both steel sections are presented in Fig. 6.4 and Fig. 6.6.

It can be seen from Fig. 6.15, that there is only a marginal decrease in moment capacity of W12x30 and W24x76 upto 45 minutes and 60 minutes of fire exposure time, respectively. This is due to the fact that at these times the temperature in W12x30 and W24x76 beams does not exceed 400°C (Refer to Fig. 6.4 and Fig. 6.6). As can be seen in Appendix B, steel retains almost all of its strength when exposed to temperatures below 400°C which resulted in marginal change of moment capacity in both the beams. After 45 and 60 minutes, the moment capacity of beam decreases with increasing time of fire exposure (increasing time steps) in beam W12x30 and W24x76, respectively. This can be attributed to the fact that the strength and stiffness of steel deteriorates as a result of increasing temperatures, beyond 400°C.

6.7 Rotation Analysis

The M-κ-P relationships and the fire induced axial force generated for different segments are used to trace the rotation of the connections exposed to fire. At each time step, moment profile along the length of the beam is evaluated using externally applied load and beam length. Using the moment profile and the M-κ-P relationships the curvature profile along the length of the beam is established. The curvatures are then integrated about the beam end to compute the rotation of the connection.

Thus, at any given time step, the temperatures, fire induced axial force, M-κ-P relationships and connection rotation are known for a given fire exposure condition. These output parameters are used to evaluate the failure of the connection by checking against connections bearing strength, block shear strength, bolts shear strength, tension strength of beam, tension strength of connection. Additionally, deflection limit of beam (beam span/20) is used to compute the rotation at connection. The connection is assumed to be failed if the rotation at connection (evaluated through integrating curvatures) exceeds the rotation limit obtained through beam deflection limit state.

6.8 Verification of the proposed methodology

6.8.1 Double Angle Connection

The proposed methodology is verified by comparing is predicted response parameters from the Matlab analysis with the results of the finite element model presented in Chapter 4. The secondary beam and double angle connection in the connection assembly S2 is selected for the validation of the methodology. The secondary beam is made up of W12x30 section and 3505 mm long. The beam is insulated with 12.7 mm (½ in.) spray-on fire resistive material (SFRM) on all three sides. Geometric details of the beam are shown in Table 6.1 while a summary of insulation properties used in the analysis is presented in Table 6.2. The beam is analyzed by exposing it to ASTM E119 (ASTM, 2011a) standard fire time-temperature curve and subjecting to an uniformly distributed load of 63.5 kN/m. This loading corresponds to a load ratio of 40% of the secondary beam ultimate moment capacity. Load ratio (LR) is defined as the ratio of applied bending moment in the beam under fire conditions to the ambient temperature plastic bending moment capacity of the beam. In the MATLAB program, axial restraint stiffness (K_a) and rotational restraint stiffness (K_r) were assumed to be equal to 0.1 and 2 times that of the secondary beam axial and rotational stiffness, respectively. These values are commonly used in the literature to approximate the axial, rotational stiffness of the connections (Dwaikat and Kodur, 2011; Eurocode3, 2005a). In addition, the secondary beam is divided into 100 longitudinal segments for the analysis.

The progression of temperature, moment-curvature-axial force relationships in the beam as well as the rotation at connection predicted from the proposed methodology is presented in Fig. 6.16.

Results from the proposed methodology predicted a failure time (fire resistance) of the connection as 89 minutes while the finite element indicated that the connection failed in 78 minutes. The higher fire resistance predicted in the simplified methodology might have been caused by the underlying assumptions made in predicting the steel temperatures as well as the fire induced axial forces. In addition, in simplified Matlab analysis the beam is assumed to be free of instabilities (such as local and lateral torsional buckling), while the finite element analysis accounts for beam instabilities. Indeed, results from the finite element analysis show that the beam web experienced local bucking which led to the failure of connection assembly. In order to indirectly account for the beam instabilities, the failure time of connection is corrected by assuming a 10% error margin and thereby reducing the failure time by 10%. Therefore, the corrected failure time of connection assembly will be 80 minutes which is in close agreement to that predicted by the finite element model. Hence, it can be concluded that the proposed methodology is capable of predicting the fire resistance of double angle connection assemblies with good accuracy.

6.8.2 Shear Tab Connection

To verify the robustness of proposed methodology in predicting fire response of other connection types, a shear tab connection is also analyzed. The shear tab connection is a part of floor system from a full-scale building tested as part of 2003 full-scale fire tests performed in Cardington (Garlock and Selamet, 2010; Lennon and Moore, 2003; Selamet and Garlock, 2010b; Wald et al., 2006). A plan of the tested compartment and the corresponding beam sizes and connection details are shown in Fig. 6.17. The shear tab connection used as part of this verification is the one connecting beam at gridline 1/2 to the girder at gridline D.

The tested assembly had UB365x171x51 girder (6000 mm long) connected to UB305x165x40 beam (9000 mm long), as shown in Fig. 6.17. The girder was connected to the beam using 10mm thick shear tab (fin plate) connection containing four Grade 8.8 M20 bolts. Both the girder and the beam do not have any external fire protection. The ambient temperature mechanical properties of different components of the subassembly are presented in Table 6.3.

The sub frame assembly was tested by exposing it a design fire scenario, comprised of a growth phase for the first 52 minutes and then a decay phase with an approximate cooling rate of 10°C/min. The measured gas temperatures during the test are shown in Fig. 6.18. The shear tab connection assembly beam was tested by applying a uniformly distributed load of 13.5 kN/m. This load value corresponds to a load ratio (level) of 56% of beam ultimate moment capacity.

As the proposed methodology needs an equation for fire temperature as an input, a nonlinear regression analysis using least sum of square of errors analysis is carried out to obtain a best fit for the fire temperatures measured during the fire test. Accordingly, the growth phase is approximated using a power function (i.e., $T_f = 47.3*t^{0.76}$) with a regression (R^2) coefficient of 0.95 while the decay phase is approximated using an exponential function ((i.e., $T_f = 2393.5*e^{-0.018*t}$) with a regression ($R^2$) coefficient of 0.98. A comparison of measured and approximated fire temperatures are shown in Fig. 6.19.

The Cardington experimental data by Wald et al.(Wald et al., 2006) does not have any information about the rotation at connections, and it only provides deflection data in the beam However, a finite element model was developed by Selamet et al.(Selamet and Garlock, 2010b) to simulate the response of the same tested shear tab connection assembly. The authors applied a reduced fire load (with 10% reduced temperature) on the beam and analyzed the shear tab connection assembly. The concrete slab was not explicitly modeled by the authors. However, the effect of concrete slab was considered indirectly using vertical springs, whose stiffness is calculated by conducting a calibration study on the results of Cardington fire test. The response of the connection assembly predicted from the finite element model was slightly different from that measured during the fire test. This can be attributed to the use of reduced fire load and the approximation of concrete slab using linear springs. In addition, detailed finite element modeling has limitations due to uncertainties in modeling highly non-linear contact interactions. Nonetheless, the finite element model captured the trends in the behavior of shear tab connection assembly. The authors provided data about the connection rotation at a distance of 100mm from the connection location and this data is used for comparison purposed as described below. More details about the finite element model can be found elsewhere (Garlock and Selamet, 2010) (Selamet and Garlock, 2010b).

A comparison of the observed and predicted rotation of shear tab connection is shown in Fig. 6.20. The shear tab connection did not experience failure during the fire test, while the proposed methodology predicts a failure time of 44 minutes. However, as can be seen from Fig. 6.20, a review of the predicted connection rotation indicates that predictions from the proposed methodology follow expected trends. The rotation in connection gradually increases with increasing steel temperature and this is due to degrading strength and stiffness properties of steel with increasing temperature. The connection experiences a sudden increase in rotation at 48 minutes indicating the failure of connection.

The discrepancy between experimental and predicted data can be attributed to (a) the fact that the concrete slab is approximated as linear springs which might provide vertical restraint to the beam but the highly non-linear interaction between concrete slab and beam cannot be captured using linear springs, (b) the authors analyzed the connection assembly with a reduced fire load (with 10% reduced temperature), (c) the shear tab connection had a concrete slab during the fire test while the shear tab connection analyzed did not have a concrete slab (d) the presence of concrete slab provides a shielding effect to the beam top flange thereby reducing the beam top flange temperatures. This shielding effect results in higher residual strength of the beam compared to the beam without concrete slab even for the same fire exposure time, (e) the underlying assumptions made in predicting the steel temperatures as well as the fire induced axial forces, and (f) the higher temperatures predicted by the Dwaikat and Kodur relationship (Eq. [6.3]) results in the development of higher fire induced axial forces resulting in early failure time of connections.

Therefore, based on the underlying assumptions considered in developing the methodology, it can be concluded that the proposed methodology is capable of predicting fire resistance of shear tab connections with a reasonable level of accuracy.

6.9 Limitations

The proposed equation expresses fire resistance as a function of structural parameters, and thus it offer a convenient way to evaluate fire resistance. As the proposed equation is based on the results from numerical studies, it is necessary to set limits of the applicability on the parameters such that they are within the range of values used for developing the equation. The proposed equation is valid for the following range of parameters:

- Type of fire exposure: ASTM E119 standard fire, ISO 834 standard fire, or its equivalent.
- Fire insulation thickness: 10 – 50 mm.
- Load level on beam: 0.2 – 0.6.
- Span of beam: 2.8 – 4.2 mm.

6.10 Design Applicability

To demonstrate the applicability of the proposed methodology in design situations, a numerical example analyzing a typical double angle connection in presented in Appendix E.

6.11 Summary

The development of a methodology for evaluating the fire resistance of connection assemblies is presented in this chapter. The approach is derived based on basic principles and is supported by detailed parametric studies presented in this chapter. The proposed methodology uses temperature dependent moment-curvature-axial force (M-κ-P) relationships to trace the response of double angle connection assemblies in fire over the entire rage of loading up to collapse. To proposed methodology is incorporated into a custom-built computer program written in MATLAB. Empirical relationships for computing fire temperature, temperature in beam cross-section along with the fire-induced axial forces, constitutive material properties are incorporated into the MATLAB program.

The methodology is validated by comparing the predicted response of double angle, shear tab connections with those measured during fire test. The validation indicates that the methodology is capable of tracing the fire response of connections with a reasonable level of accuracy.

CHAPTER 7

7. CONCLUSIONS AND RECOMMENDATIONS

7.1 General

The fire response of double angle connections was investigated in this study taking into consideration of transient heating conditions and system-level interactions. In order to generate experimental data on the behavior of double angle connections under realistic fire conditions, fire resistance tests were carried out on two sub frame assemblies. The parameters that were varied in the fire tests included load ratio, decay rate and the presence of concrete slab. Results from these fire resistance tests, were used to validate finite element models. The finite element models, developed in ANSYS, accounts for critical factors namely: material and geometrical nonlinearities, fire induced material property degradation and non-linear contact interactions that influence the fire response of double angle connections. The finite element models were validated by comparing the prediction from the model with those measured during fire tests. It is shown through the comparisons that the models can simulate the behavior, as well as the failure modes, in double angle connection with good accuracy. The validated finite element models were applied to conduct parametric studies to quantify the influence of various factors on the fire response of double angle connections. Results from parametric studies and data from the fire tests were utilized to develop a rational methodology for evaluating the fire resistance of connections based on engineering principles.

The proposed methodology uses temperature dependent moment-curvature-axial force (M-κ-P) relationships to trace the fire response of double angle connection at various time steps till failure. At each time step, the fire induced forces generated from the beams on double angle connection is taken into consideration in the analysis. The failure of connection is evaluated at each time step by comparing fire induced axial force in the beam and rotation in connection against connection capacity. This simplified approach for evaluating fire performance of connections is implemented in a custom-built MATLAB code and the analysis can be carried out without the need for complex finite element models. The validity of the proposed methodology is established by comparing the fire resistance predictions from the methodology with values obtained from numerical studies for double angle and shear tab connections.

7.2 Key Findings

Based on the information generated in this study, the following key conclusions can be drawn:

1. There have been only few studies on fire performance of double angle connections, especially under realistic fire, restraint and loading scenarios. The current fire resistance provisions, developed based on isolated connections under standard fire or uniform temperature conditions, are prescriptive and do not yield reliable fire resistance. Also, to date, no simplified rational methodologies for evaluating fire resistance of double angle connections, based on system-level response, have been developed.

2. Double angle connections exhibit higher ductility, better tying capacity, superior rotational characteristics, and are easy to erect. The higher ductility of the double angle connections leads to attaining higher rotation prior to failure (about 18° (≈ 315 milli-rad)) rotation prior to failure as compared to conventional shear tab connections where failure typically occurs at about 3.5° (60 milli-rad).
3. Fire resistance tests on double angle connection sub frame assemblies under realistic fire, loading and restraint conditions indicate:
    - Double angle connections, under fire conditions, can undergo significant rotations prior to failure despite the connections undergoing permanent residual deformations.
    - Double angle connections are capable of transferring fire induced forces (especially moments) between connected members despite being designed as simple shear connections.
    - Presence of concrete slab significantly enhances the rigidity of a steel frame assembly under fire conditions and restrains the secondary beam against instabilities such as local buckling and lateral torsional buckling.
4. The proposed finite element models takes into consideration transient heating conditions and system-level response in modeling the response of double angle connections under realistic fire and loading conditions. The models accounts for material and geometrical nonlinearities, temperature induced degradation of material properties and highly complex non-linear contact interactions. Results from finite element studies infer:

- The response of connections can be significantly different when modeled using system-level approach as compared to that under isolated, component level analysis.
- The development and progression of fire induced axial forces cannot be fully captured when the connections are analyzed at member-level.
- The beneficial effect of arch action (developed due to structural interactions) on the response of connection is accurately captured through system-level approach. The effect of such arch action reduces rotations in a connection.
- Composite action arising from the presence of slab enhances the overall strength of the connection in addition to eliminating instabilities (local and lateral torsional buckling) in the connected beam.

5. Data from numerical studies infer that the main factors influencing the fire response of double angle connections are decay rate of design fire, loading type, axial restraint stiffness, system-level interactions, load level, fire scenarios and high-temperature properties of bolts. Specifically:
    - Connections analyzed at system-level experience significant fire-induced axial forces while member-level analysis predicts no axial force in connection.
    - Lower rate of decay in a design fire improves the fire performance of connections by decreasing the amount of thermal shrinkage forces developed in the beam. Lower shrinkage forces in beam leads to lower fire induced axial forces on connections.
    - Distributed loading on a beam represents the extreme loading case scenario by producing higher stresses and deflection compared to two-point and four-point

loading scenarios. These higher stresses and deflections result in higher rotation in connection.

- Higher value of axial restraint stiffness decreases the failure time of double angle connections without concrete slab by generating instabilities (local buckling, lateral torsional buckling, web and flange crippling) in the connected beam.
- System-level interactions generate lower beam deflections due to the beneficial effect of the arch action (developed by the restraining effect arising from surrounding (cold) structural members). The arch action creates a counter moment that reduces the beam deflections.
- Steady-state heating conditions produce higher axial forces compared to transient heating conditions due to higher temperature change in steady-state heating compared to gradual temperature increase in transient heating.
- The longer the duration of growth phase of fire, the higher is the maximum rotation developed in the connection because of degradation in capacity of the connection.
- Use of high-temperature properties specific to high-strength bolts lead to higher axial forces and connection's rotation as compared to general properties of conventional (A36 or A992) steel.

6. The proposed simplified methodology for evaluating fire response of double angle connections accounts for critical parameters influencing the fire response of connections. Thus this methodology is capable of predicting the response of connections under realistic fire, loading and support conditions.

7.3 Recommendations for Future Research

This study has advanced the state-of-the-art with respect to fire response of double angle connections (a) by generating unique test data on the fire performance of full-scale double angle connections, (b) implementing system-level approach to simulate the transient fire response of double angle connections, and (c) developing a design methodology to evaluate the fire resistance of connections. These experimental, numerical and analytical studies are a major step forward in understanding the realistic (system-level) performance of double angle connections in steel framed buildings. However, further research is required to fully characterize the complex behavior of connections especially at system-level. The following are some of the key recommendations for further research in this area:

- The fire resistance test data generated as part of this study is the only test data available on the system-level response of double angle connections exposed to fire. Restraining effects arising from structural continuity have a significant influence on the fire performance of connections. The fire induced restraining forces on connections arising from multiple-bay or multiple-stories in steel framed building needs to be studied. Future research can be directed towards generating such test data which is very valuable for validating numerical models.
- The proposed simplified methodology, developed herein, cannot account for the composite action between concrete slab and the beam. However, the methodology can be extended to include the effect of composite action arising from the presence of concrete slab on top of the beam. This can be done by revising the equations to include the effect of concrete slab and generating moment-curvature-axial force relationships.

- The proposed methodology can be extended to include the effect of high-temperature bolt properties in predicting the fire resistance of double angle connections. Improvements in such constitutive models will help to enhance the accuracy of the model predictions.

7.4 Research Impact

Connections form critical part of a steel framed structure and the behavior of these connections are governed by their interaction with surrounding structural members. The research undertaken as a part of this study was aimed at evaluating fire behavior of double angle connections by considering transient heating conditions and system-level interactions.

The current fire design provisions in most codes and standards are derived from limited number of standard fire tests conducted on scaled and isolated connection specimens. These provisions do not consider system-level interactions and thus have a number of drawbacks. Thus, the current design approaches are not applicable for undertaking performance-based design which provides rational and cost-effective fire safety solutions. Hence, numerical models are developed to simulate the realistic fire performance of connections under realistic fire, loading and restraint conditions. For validating the models, fire resistance tests on double angle connections are undertaken as part of this study to generate unique test data. The validated models are applied to study the influence of various factors on the fire response of double angle connections.

Results from the fire tests and parametric studies are utilized to develop a rational methodology for evaluating the fire resistance of connections. The proposed methodology uses temperature dependent moment-curvature-axial force (M-κ-P) relationships to trace the response of double angle connections in fire over the entire rage of loading up to collapse.

In summary, the use of the proposed methodology can facilitate a rational fire resistance design under a performance-based code environment. Such a rational design approach will contribute to reduced loss of life and property damage in fire incidents.

APPENDICES

APPENDIX A

The rate of decay for design fire DF1 is computed using the following equation:

$$\frac{dT}{dt} = \left(\frac{dT}{dt}\right)_{ref} \frac{\sqrt{F_v/0.04}}{\sqrt{b/1900}} \qquad \text{[A3.1]}$$

where

$\frac{dT}{dt}$: decay rate (°C/hr)

$\left(\frac{dT}{dt}\right)_{ref}$: reference decay rate (°C/hr)

= 625°C/hr for fire with a growth period less than half an hour

= 250°C/hr for fire with a growth period greater than 2 hours

= for fires having growth phase duration between 0.5 to 2 hrs, the reference decay rate can be evaluated by linearly interpolating the above two extreme case reference values

F_v : ventilation factor ($m^{-0.5}$)

b : thermal inertia ($Ws^{0.5}/m^2K$)

= $\sqrt{k\rho c_p}$

k: thermal conductivity (W/mK)

ρ: density (kg/m^3)

c_p: specific heat (J/kg K)

The duration of growth phase for design fire DF1 is 75 min (1.25 hrs). Therefore, the reference decay rate is equal to 437.5°C/hr. Using the compartment parameters presented in Table 3.4, the rate of decay can be computed as:

$$\frac{dT}{dt} = 437.5 * \frac{\sqrt{0.0372/0.04}}{\sqrt{1900/1900}} = 422°\,\mathrm{C/hr} \cong 8°\mathrm{C/min}.$$

APPENDIX B

Table B.1 – Constitutive relationships for high temperature properties of carbon steel (Eurocode3, 2005b)

Stress-strain relationships	$\sigma_s = \left\{ \begin{array}{ll} \varepsilon_s E_{s,T} & \varepsilon_s \leq \varepsilon_{sp,T} \\ f_{sp,T} - c + (b/a)\left(a^2 - (\varepsilon_{sy,T} - \varepsilon_s)^2\right)^{0.5} & \varepsilon_{sp,T} < \varepsilon_s \leq \varepsilon_{sy,T} \\ f_{sy,T} & \varepsilon_{sy,T} < \varepsilon_s \leq \varepsilon_{st,T} \\ f_{sy,T}\left(1 - \dfrac{\varepsilon_s - \varepsilon_{st,T}}{\varepsilon_{su,T} - \varepsilon_{st,T}}\right) & \varepsilon_{st,T} < \varepsilon_s \leq \varepsilon_{su,T} \\ 0 & \varepsilon_s > \varepsilon_{su,T} \end{array} \right\}$ Parameters $\varepsilon_{sp,T} = \dfrac{f_{sp,T}}{E_{s,T}}$ $\varepsilon_{sy,T} = 0.02$ $\varepsilon_{st,T} = 0.15$ $\varepsilon_{su,T} = 0.2$ Functions $a^2 = (\varepsilon_{sy,T} - \varepsilon_{sp,T})\left(\varepsilon_{sy,T} - \varepsilon_{sp,T} + \dfrac{c}{E_{s,T}}\right)$ $b^2 = c(\varepsilon_{sy,T} - \varepsilon_{sp,T})E_{s,T} + c^2$ $c = \dfrac{(f_{sy,T} - f_{sp,T})^2}{(\varepsilon_{sy,T} - \varepsilon_{sp,T})E_{s,T} - (f_{sy,T} - f_{sp,T})}$ Values of $f_{sp,T}$, $f_{sy,T}$ and $E_{s,T}$ can be obtained from Table B.2

Table B.1 (cont'd)

Stress-strain relationships (Strain-hardening region)	For temperatures below 400°C $$\sigma_s = \begin{cases} 50\left(f_{su,T} - f_{sy,T}\right)\varepsilon_s + 2f_{y,T} - f_{su,T} & 0.02 < \varepsilon_s \le 0.04 \\ f_{su,T} & 0.04 \le \varepsilon_s \le 0.15 \\ f_{su,T}\left[1 - 20(\varepsilon_s - 0.15)\right] & 0.15 < \varepsilon_s < 0.2 \\ 0 & \varepsilon_s \ge 0.2 \end{cases}$$ $$f_{u,T} = \begin{cases} 1.25 f_{sy,T} & T < 300°C \\ f_{sy,T}(2 - 0.0025T) & 300°C \le T < 400°C \\ f_{sy,T} & T \ge 400°C \end{cases}$$
Thermal strain	$$\varepsilon_{ths} = \begin{cases} 1.2\times10^{-5}T + 0.4\times10^{-8}T^2 - 2.416\times10^{-4} & 20^oC \le T \le 750^oC \\ 1.1\times10^{-2} & 750^oC < T \le 860^oC \\ 2\times10^{-5}T - 6.2\times10^{-3} & 860^oC < T \le 1200^oC \end{cases}$$
Specific heat (J/kg K)	$$c_s = \begin{cases} 425 + 7.73\times10^{-1}T - 1.69\times10^{-3}T^2 + 2.22\times10^{-6}T^3 & 20^oC \le T < 600^oC \\ 666 + \dfrac{13002}{738 - T} & 600^oC \le T < 735^oC \\ 545 + \dfrac{17820}{T - 731} & 735^oC \le T < 900^oC \\ 650 & 900^oC \le T \le 1200^oC \end{cases}$$
Thermal conductivity (W/m K)	$$k_s = \begin{cases} 54 - 3.33\times10^{-2}T & 20^oC \le T < 800^oC \\ 27.3 & 800^oC \le T \le 1200^oC \end{cases}$$

Table B.2 – Values for the main parameters of the stress-strain relationships of carbon steel at elevated temperatures (Eurocode3, 2005b)

Steel temperature T(°C)	$\frac{f_{yT}}{f_y}$	$\frac{f_{sp}}{f_y}$ *	$\frac{E_{sT}}{E_s}$ *
20	1	1	1
100	1	1	1
200	1	0.807	0.9
300	1	0.613	0.8
400	1	0.42	0.7
500	0.78	0.36	0.6
600	0.47	0.18	0.31
700	0.23	0.075	0.13
800	0.11	0.05	0.09
900	0.06	0.0375	0.0675
1000	0.04	0.025	0.045
1100	0.02	0.0125	0.0225
1200	0	0	0

* f_y and E_s are yield strength and modulus of elasticity at room temperature

Table B.3 – Constitutive relationships for high temperature properties of concrete(Eurocode2, 2004)

Stress-strain relationships	$$\sigma_c = \frac{3\varepsilon\ f'_{c,T}}{\varepsilon_{c1,T}\left(2+\left(\frac{\varepsilon}{\varepsilon_{c1,T}}\right)^3\right)} \quad , \varepsilon \le \varepsilon_{cu1,T}$$ For $\varepsilon_{c1(T)} < \varepsilon \le \varepsilon_{cu1(T)}$, the Eurocode permits the use of linear as well as nonlinear descending branch in the numerical analysis. For the parameters in this equation refer to Table A.2
Thermal capacity	*Specific heat (J/kg C)* *c= 900, for 20°C ≤ T ≤ 100°C* *c = 900 + (T - 100), for 100°C < T ≤ 200°C* *c = 1000 + (T - 200)/2, for 200°C < T ≤ 400°C* *c = 1100, for 400°C < T ≤ 1200°C* *Density change (kg/m³)* *ρ = ρ(20°C) = Reference density* *for 20°C ≤ T ≤ 115°C* *ρ = ρ(20°C) (1 – 0.02(T - 115)/85)* *for 115°C < T ≤ 200°C* *ρ= ρ(20°C) (0.98 – 0.03(T - 200)/200)* *for 200°C < T ≤ 400°C* *ρ= ρ(20°C) (0.95 – 0.07(T - 400)/800)* *for 400°C < T ≤ 1200°C* *Thermal Capacity = ρ × c*

Table B.3 (cont'd)

Thermal conductivity (W/m K)	All types : Upper limit: $k_c = 2 - 0.2451\ (T / 100) + 0.0107\ (T / 100)^2$ *for* $20°C \leq T \leq 1200°C$ Lower limit: $k_c = 1.36 - 0.136\ (T / 100) + 0.0057\ (T / 100)^2$ *for* $20°C \leq T \leq 1200°C$
Thermal strain	*Siliceous aggregates:* $\varepsilon_{th} = -1.8\times10^{-4}+9\times10^{-6}T+2.3\times10^{-11}T^3$ *for* $20°C \leq T \leq 700°C$ $\varepsilon_{th} = 14\times10^{-3}$ *for* $700°C < T \leq 1200°C$ *Calcareous aggregates:* $\varepsilon_{th} = -1.2\times10^{-4}+6\times10^{-6}T+1.4\times10^{-11}T^3$ *for* $20°C \leq T \leq 805°C$ $\varepsilon_{th} = 12\times10^{-3}$ *for* $805°C < T \leq 1200°C$

Table B.4 – Values for the main parameters of the stress-strain relationships of normal strength concrete at elevated temperatures (Eurocode2, 2004)

Temp. (˚C)	Normal Strength Concrete					
	Siliceous Aggregate			Calcareous Aggregate		
	$\frac{f'_{c,T}}{f'_c(20^\circ C)}$	$\varepsilon_{c1,T}$	$\varepsilon_{cu1,T}$	$\frac{f'_{c,T}}{f'_c(20^\circ C)}$	$\varepsilon_{c1,T}$	$\varepsilon_{cu1,T}$
20	1	0.0025	0.02	1	0.0025	0.02
100	1	0.004	0.0225	1	0.004	0.023
200	0.95	0.0055	0.025	0.97	0.0055	0.025
300	0.85	0.007	0.0275	0.91	0.007	0.028
400	0.75	0.01	0.03	0.85	0.01	0.03
500	0.6	0.015	0.0325	0.74	0.015	0.033
600	0.45	0.025	0.035	0.6	0.025	0.035
700	0.3	0.025	0.0375	0.43	0.025	0.038
800	0.15	0.025	0.04	0.27	0.025	0.04
900	0.08	0.025	0.0425	0.15	0.025	0.043
1000	0.04	0.025	0.045	0.06	0.025	0.045
1100	0.01	0.025	0.0475	0.02	0.025	0.048
1200	0	-	-	0	-	-

Table B.5 – Constitutive relationships for high temperature properties of bolt steel (Kodur et al., 2012)

Strength reduction factors (Yield and ultimate strength)	A325	$\beta_{y,T} = \beta_{u,T} = \begin{cases} 1 & 20°C \le T \le 350°C \\ 0.00001T^2 - 0.0137T + 4.7 & 350°C < T \le 800°C \end{cases}$
	A490	$\beta_{y,T} = \beta_{u,T} = \begin{cases} 1 & 20°C \le T \le 350°C \\ 0.000006T^2 - 0.0094T + 3.65 & 350°C < T \le 700°C \\ 0.000006T^2 - 0.0094T + 3.72 & 700°C < T \le 800°C \end{cases}$
Thermal expansion (%)	A325	$\varepsilon_{th} = 0.0017T - 0.1 \quad 20^o C \le T \le 1000^o C$
	A490	$\varepsilon_{th} = 0.0015T - 0.1 \quad 20^o C \le T \le 1000^o C$
Specific heat (MJ/m^3 °C)	A325	$c_p = \begin{cases} 490 - 0.19T + 0.0014T^2 & 20^o C \le T < 600^o C \\ 20.79T - 0.0118T^2 - 7350 & 600^o C \le T < 735^o C \end{cases}$
	A490	$c_p = \begin{cases} 490 - 0.39T + 0.001T^2 & 20^o C \le T < 600^o C \\ 15.274T - 9438.8 & 600^o C \le T < 735^o C \end{cases}$
Thermal conductivity (W/m °C)	A325	$k_t = 50 - 0.027T \quad 20^o C \le T \le 735^o C$
	A490	$k_t = 47 - 0.023T \quad 20^o C \le T \le 735^o C$

APPENDIX C

C1. Double angle connection strength calculations

1. Bearing strength of beam web

Bolt diameter (d) = 19.05 mm

Bolt hole diameter (h) = 20.63 mm

Edge distance (L_e) = 57.15 mm

Thickness of web (t) = 6.6 mm

Ultimate strength of beam steel (F_u) = 451 MPa

Clear distance (L_c)= L_e –h/2 = 57.15 – 20.63/2 = 46.835 mm

Bearing strength per bolt R_{ni} = 1.2*L_c*t*F_u

= 1.2*46.835*6.6*451

= 167.27 kN

Upper limit R_{ni} = 2.4*d*t*F_u

= 2.4*19.05*6.6*451

= 136.1 kN

Design bearing strength for 3 bolts = $\emptyset \sum_{i=1}^{3} R_{ni}$

=0.75*3*136.1

= 306.23 kN (**Controls**)

2. Bearing strength of double angle

Bolt diameter (d) = 19.05 mm

Bolt hole diameter (h) = 20.63 mm

Edge distance (L_e) = 31.75 mm

Thickness of angle (t) = 7.94 mm

Ultimate strength of angle steel (F_u) = 459 MPa

Clear distance (L_c)= L_e –h/2 = 31.75 – 20.63/2 = 21.435 mm

Bearing strength per bolt R_{ni} = 1.2*L_c*t*F_u

= 1.2*21.435*7.94*459

= 93.73 kN

Upper limit R_{ni} = 2.4*d*t*F_u

= 2.4*19.05*7.94*459

= 166.62 kN

Hence, bearing strength per bolt = 97.73 kN

Design bearing strength (per angle) for 3 bolts = $\emptyset \sum_{i=1}^{3} R_{ni}$

= 0.75*3*93.73

= 210. 88 kN

Therefore, design bearing strength for double angle = 2*210.88 = 421.76 kN.

3. Block shear strength of beam web

Gross area in shear (A_{gv}) = 754.38 mm^2

Net area in shear (A_{nv}) = 607.7 mm^2

Net area in tension (A_{nt}) = 712.47 mm^2

Yield strength of beam steel (F_y) = 375 MPa

Ultimate strength of beam steel (F_u) = 451 MPa

Block shear strength (R_n) = 0.6*F_u*A_{nv} + F_u*A_{nt}

= 0.6*451*607.7+451*712.47

= 485.77 kN

Upper limit (R_n) = 0.6*F_y*A_{gv} + F_u*A_{nt}

= 0.6*375*754.38 + 451*712.47

= 491 kN

Hence, block shear strength of beam web = 485.77 kN

Design block shear strength of beam web = $\emptyset R_n$

= 0.75*485.77

= 364.33 kN (**Controls**)

<u>4. Block shear strength of double angle</u>

Gross area in shear (A_{gv}) = 504.19 mm^2

Net area in shear (A_{nv}) = 327.72 mm^2

Net area in tension (A_{nt}) = 857.12 mm^2

Yield strength of angle steel (F_y) = 308 MPa

Ultimate strength of angle steel (F_u) = 459 MPa

Block shear strength (R_n) = $0.6*F_u*A_{nv} + F_u*A_{nt}$

= 0.6*459*327.72 + 459*857.12

= 483.67 kN

Upper limit (R_n) = $0.6*F_y*A_{gv} + F_u*A_{nt}$

= 0.6*308*504.19 + 459*857.12

= 486.59 kN

Hence, block shear strength of single angle = 483.67 kN

Block shear strength for double angle = 2*483.67 = 967.34 kN

Design block shear strength of double angle = $\emptyset R_n$

= 0.75*967.34

= 725.5 kN

<u>5. Shear strength of bolts</u>

Bolt diameter (d) = 19.05 mm

Area of bolt (A_b) = $\frac{\pi}{4} d^2$ = 285 mm^2

Shear strength of bolt (single shear plane) = F_{nv}*A_b

= 0.5*1210*285

= 172.43 kN

Shear strength of bolt for double shear = 2*172.43

= 344.85 kN

Hence, the shear strength for 3 bolts (R_n) = 3*344.85

= 1034.55 kN

Design shear strength of bolts = $\emptyset R_n$

= 0.75*1034.55

= 775.92 kN

6. Tensile strength of beam web

Yield strength of beam steel (F_y) = 375 MPa

Ultimate strength of beam steel (F_u) = 451 MPa

Gross area (A_g) = 5670.96 mm^2

Area of holes (A_{holes}) = 440.06 mm^2

Net area (A_n) = A_g – A_{holes}

= 5670.96 – 440.06

= 5230.9 mm^2

Gross section tensile strength = F_y*A_g

= 375*5670.96

= 2126.61 kN

Net section tensile strength = F_u*A_n

= 451*5230.9

= 2359.14 kN

Design tensile strength of beam ($\emptyset R_n$) = min [0.9* F_y*A_g, 0.75* F_u*A_n]

= min [0.9*2126.61, 0.75*2359.14]

= 1769.35 kN

7. Tensile strength of double angle

Yield strength of angle steel (F_y) = 308 MPa

Ultimate strength of angle steel (F_u) = 459 MPa

Gross area (A_g) per angle = 1714.25 mm^2

Area of holes (A_{holes}) per angle = 529.25 mm^2

Net area (A_n) per angle = A_g – A_{holes}

= 1714.25 – 529.25

= 1185 mm^2

Gross section tensile strength per angle = F_y*A_g

= 308*1714.25

= 528 kN

Net section tensile strength per angle = F_u*A_n

= 459*1185

= 544 kN

Design tensile strength of single angle ($\emptyset R_n$) = min [0.9* F_y*A_g, 0.75* F_u*A_n]

= min [0.9*528, 0.75*544]

= 408 kN

Design tensile strength of double angle ($\emptyset R_n$) = 2*408

= 816 kN (**Controls**)

Table C.1: Summary of double angle connection strength computed based on different limit states

Limit state	**Component**	**Value (kN)**
Bearing strength	Beam web	**306.23**
	Double angle	421.76
Block shear strength	Beam web	364.33
	Double angle	725.5
Shear strength	Bolts	775.92
Tensile strength	Beam web	1769.35
	Double angle	816
Connection Capacity		**306.23**

C2. Single angle connection strength calculations

1. Bearing strength of beam web

Bolt diameter (d) = 19.05 mm

Bolt hole diameter (h) = 20.63 mm

Edge distance (L_e) = 57.15 mm

Thickness of web (t) = 6.6 mm

Ultimate strength of beam steel (F_u) = 451 MPa

Clear distance (L_c)= L_e –h/2 = 57.15 – 20.63/2 = 46.835 mm

Bearing strength per bolt R_{ni} = 1.2*L_c*t*F_u

= 1.2*46.835*6.6*451

= 167.27 kN

Upper limit R_{ni} = 2.4*d*t*F_u

= 2.4*19.05*6.6*451

= 136.1 kN

Design bearing strength for 3 bolts = $\emptyset \sum_{i=1}^{3} R_{ni}$

=0.75*3*136.1

= 306.23 kN

2. Bearing strength of single angle

Bolt diameter (d) = 19.05 mm

Bolt hole diameter (h) = 20.63 mm

Edge distance (L_e) = 31.75 mm

Thickness of angle (t) = 7.94 mm

Ultimate strength of angle steel (F_u) = 459 MPa

Clear distance (L_c)= L_e –h/2 = 31.75 – 20.63/2 = 21.435 mm

Bearing strength per bolt R_{ni} = 1.2*L_c*t*F_u

= 1.2*21.435*7.94*459

= 93.73 kN

Upper limit R_{ni} = 2.4*d*t*F_u

= 2.4*19.05*7.94*459

= 166.62 kN

Hence, bearing strength per bolt = 97.73 kN

Design bearing strength (per angle) for 3 bolts = $\emptyset \sum_{i=1}^{3} R_{ni}$

= 0.75*3*93.73

= 210. 88 kN (**Controls**)

<u>3. Block shear strength of beam web</u>

Gross area in shear (A_{gv}) = 754.38 mm^2

Net area in shear (A_{nv}) = 607.7 mm^2

Net area in tension (A_{nt}) = 712.47 mm^2

Yield strength of beam steel (F_y) = 375 MPa

Ultimate strength of beam steel (F_u) = 451 MPa

Block shear strength (R_n) = 0.6*F_u*A_{nv} + F_u*A_{nt}

= 0.6*451*607.7+451*712.47

= 485.77 kN

Upper limit (R_n) = 0.6*F_y*A_{gv} + F_u*A_{nt}

= 0.6*375*754.38 + 451*712.47

= 491 kN

Hence, block shear strength of beam web = 485.77 kN

Design block shear strength of beam web = $\emptyset R_n$

= 0.75*485.77

= 364.33 kN

4. Block shear strength of single angle

Gross area in shear (A_{gv}) = 504.19 mm^2

Net area in shear (A_{nv}) = 327.72 mm^2

Net area in tension (A_{nt}) = 857.12 mm^2

Yield strength of angle steel (F_y) = 308 MPa

Ultimate strength of angle steel (F_u) = 459 MPa

Block shear strength (R_n) = $0.6*F_u*A_{nv} + F_u*A_{nt}$

= 0.6*459*327.72 + 459*857.12

= 483.67 kN

Upper limit (R_n) = $0.6*F_y*A_{gv} + F_u*A_{nt}$

= 0.6*308*504.19 + 459*857.12

= 486.59 kN

Hence, block shear strength of single angle = 483.67 kN

Design block shear strength of single angle = $\emptyset R_n$

= 0.75*483.67

= 362.75 kN (**Controls**)

5. Shear strength of bolts

Bolt diameter (d) = 19.05 mm

Area of bolt (A_b) = $\frac{\pi}{4}d^2$ = 285 mm^2

Shear strength of bolt (single shear plane) = $F_{nv}*A_b$

= 0.5*1210*285

= 172.43 kN

Shear strength of bolt for double shear = 2*172.43

= 344.85 kN

Hence, the shear strength for 3 bolts (R_n) = 3*344.85

= 1034.55 kN

Design shear strength of bolts = $\emptyset R_n$

= 0.75*1034.55

= 775.92 kN

6. Tensile strength of beam web

Yield strength of beam steel (F_y) = 375 MPa

Ultimate strength of beam steel (F_u) = 451 MPa

Gross area (A_g) = 5670.96 mm^2

Area of holes (A_{holes}) = 440.06 mm^2

Net area (A_n) = A_g – A_{holes}

= 5670.96 – 440.06

= 5230.9 mm^2

Gross section tensile strength = F_y*A_g

= 375*5670.96

= 2126.61 kN

Net section tensile strength = F_u*A_n

= 451*5230.9

= 2359.14 kN

Design tensile strength of beam ($\emptyset R_n$) = min [0.9* F_y*A_g, 0.75* F_u*A_n]

= min [0.9*2126.61, 0.75*2359.14]

= 1769.35 kN

7. Tensile strength of single angle

Yield strength of angle steel (F_y) = 308 MPa

Ultimate strength of angle steel (F_u) = 459 MPa

Gross area (A_g) per angle = 1714.25 mm^2

Area of holes (A_{holes}) per angle = 529.25 mm^2

Net area (A_n) per angle = A_g – A_{holes}

= 1714.25 – 529.25

= 1185 mm^2

Gross section tensile strength per angle = F_y*A_g

= 308*1714.25

= 528 kN

Net section tensile strength per angle = F_u*A_n

= 459*1185

= 544 kN

Design tensile strength of single angle ($\emptyset R_n$) = min [0.9* F_y*A_g, 0.75* F_u*A_n]

= min [0.9*528, 0.75*544]

= 408 kN (**Controls**)

Table C.2: Summary of single angle connection strength computed based on different limit states

Limit state	Component	Value (kN)
Bearing strength	Beam web	306.23
	Single angle	**210.88**
Block shear strength	Beam web	364.33
	Single angle	362.75
Shear strength	Bolts	775.92
Tensile strength	Beam web	1769.35
	Single angle	408
Connection Capacity		**210.88**

C3. Shear tab connection strength calculations

1. Bearing strength of beam web

Bolt diameter (d) = 19.05 mm

Bolt hole diameter (h) = 20.63 mm

Edge distance (L_e) = 57.15 mm

Thickness of web (t) = 6.6 mm

Ultimate strength of beam steel (F_u) = 451 MPa

Clear distance (L_c)= L_e –h/2 = 57.15 – 20.63/2 = 46.835 mm

Bearing strength per bolt R_{ni} = 1.2*L_c*t*F_u

= 1.2*46.835*6.6*451

= 167.27 kN

Upper limit R_{ni} = 2.4*d*t*F_u

= 2.4*19.05*6.6*451

= 136.1 kN

Design bearing strength for 3 bolts = $\emptyset \sum_{i=1}^{3} R_{ni}$

=0.75*3*136.1

= 306.23 kN

2. Bearing strength of shear tab

Bolt diameter (d) = 19.05 mm

Bolt hole diameter (h) = 20.63 mm

Edge distance (L_e) = 31.75 mm

Thickness of angle (t) = 7.94 mm

Ultimate strength of shear tab (F_u) = 459 MPa

Clear distance (L_c)= L_e –h/2 = 31.75 – 20.63/2 = 21.435 mm

Bearing strength per bolt R_{ni} = 1.2*L_c*t*F_u

= 1.2*21.435*7.94*459

= 93.73 kN

Upper limit R_{ni} = 2.4*d*t*F_u

= 2.4*19.05*7.94*459

= 166.62 kN

Hence, bearing strength per bolt = 97.73 kN

Design bearing strength of shear tab for 3 bolts = $\emptyset \sum_{i=1}^{3} R_{ni}$

= 0.75*3*93.73

= 210. 88 kN (**Controls**)

<u>3. Block shear strength of beam web</u>

Gross area in shear (A_{gv}) = 754.38 mm^2

Net area in shear (A_{nv}) = 607.7 mm^2

Net area in tension (A_{nt}) = 712.47 mm^2

Yield strength of beam steel (F_y) = 375 MPa

Ultimate strength of beam steel (F_u) = 451 MPa

Block shear strength (R_n) = 0.6*F_u*A_{nv} + F_u*A_{nt}

= 0.6*451*607.7+451*712.47

= 485.77 kN

Upper limit (R_n) = 0.6*F_y*A_{gv} + F_u*A_{nt}

= 0.6*375*754.38 + 451*712.47

= 491 kN

Hence, block shear strength of beam web = 485.77 kN

Design block shear strength of beam web = $\emptyset R_n$

= 0.75*485.77

= 364.33 kN

4. Block shear strength of shear tab

Gross area in shear (A_{gv}) = 504.19 mm^2

Net area in shear (A_{nv}) = 327.72 mm^2

Net area in tension (A_{nt}) = 857.12 mm^2

Yield strength of shear tab (F_y) = 308 MPa

Ultimate strength of shear tab (F_u) = 459 MPa

Block shear strength (R_n) = $0.6*F_u*A_{nv} + F_u*A_{nt}$

= 0.6*459*327.72 + 459*857.12

= 483.67 kN

Upper limit (R_n) = $0.6*F_y*A_{gv} + F_u*A_{nt}$

= 0.6*308*504.19 + 459*857.12

= 486.59 kN

Hence, block shear strength of shear tab = 483.67 kN

Design block shear strength of shear tab = $\emptyset R_n$

= 0.75*483.67

= 362.75 kN (**Controls**)

5. Shear strength of bolts

Bolt diameter (d) = 19.05 mm

Area of bolt (A_b) = $\frac{\pi}{4}d^2$ = 285 mm^2

Shear strength of bolt (single shear plane) = $F_{nv}*A_b$

= 0.5*1210*285

= 172.43 kN

Shear strength of bolt for double shear = 2*172.43

= 344.85 kN

Hence, the shear strength for 3 bolts (R_n) = 3*344.85

= 1034.55 kN

Design shear strength of bolts = $\emptyset R_n$

= 0.75*1034.55

= 775.92 kN

<u>6. Tensile strength of beam web</u>

Yield strength of beam steel (F_y) = 375 MPa

Ultimate strength of beam steel (F_u) = 451 MPa

Gross area (A_g) = 5670.96 mm^2

Area of holes (A_{holes}) = 440.06 mm^2

Net area (A_n) = A_g – A_{holes}

= 5670.96 – 440.06

= 5230.9 mm^2

Gross section tensile strength = F_y*A_g

= 375*5670.96

= 2126.61 kN

Net section tensile strength = F_u*A_n

= 451*5230.9

= 2359.14 kN

Design tensile strength of beam ($\emptyset R_n$) = min [0.9* F_y*A_g, 0.75* F_u*A_n]

= min [0.9*2126.61, 0.75*2359.14]

= 1769.35 kN

7. Tensile strength of shear tab

Yield strength of angle steel (F_y) = 308 MPa

Ultimate strength of angle steel (F_u) = 459 MPa

Gross area (A_g) per shear tab = 1714.25 mm^2

Area of holes (A_{holes}) per shear tab = 529.25 mm^2

Net area (A_n) per shear tab = A_g – A_{holes}

= 1714.25 – 529.25

= 1185 mm^2

Gross section tensile strength shear tab = F_y*A_g

= 308*1714.25

= 528 kN

Net section tensile strength per shear tab = F_u*A_n

= 459*1185

= 544 kN

Design tensile strength of shear tab ($\emptyset R_n$) = min [0.9* F_y*A_g, 0.75* F_u*A_n]

= min [0.9*528, 0.75*544]

= 408 kN (**Controls**)

Table C.3: Summary of shear tab connection strength computed based on different limit states

Limit state	Component	Value (kN)
Bearing strength	Beam web	306.23
	Shear tab	**210.88**
Block shear strength	Beam web	364.33
	Shear tab	362.75
Shear strength	Bolts	775.92
Tensile strength	Beam web	1769.35
	Shear tab	408
Connection Capacity		**210.88**

APPENDIX D

```
clc;
clear all;


Inputdata

%% Calling the function to compute the Node/Element numbering
[a,b,poin] =
Node_Num(mem,nodes,nxtf_tot,nytf_tot,nxw_tot,nyw_tot,nxbf_tot,nybf_tot,xtf,yt
f,xw,yw,xbf,ybf);

%% Calculating the function to compute the x,y coordinate numbering
[x1,x2,x3,x4,y1,y2,y3,y4,x,y,xx,yyy] =
Coordinate_Num(mem,nxtf_tot,nytf_tot,nxw_tot,nyw_tot,nxbf_tot,nybf_tot,xtf,yt
f,xw,yw,xbf,ybf,poin);

RLS = 0.1;
column = 0;
tt = 0:1:100;
data_arr    = cell(1,2,length(tt));

%% Computing the fire,steel temperature
    for i=1:length(tt)
        time = tt(i);

        [p,tf,ts,fy,fu,es,sx,Ix,zx,xvec,Mvec] =
Axial_F(As,time,Props,w,h,T,t);

        Axl_force(i) = p;

        [Cap] = Connection_cap(t,As,ts,fy,fu);
        Cnctn_cap(i) = Cap;

        % Calling the function to compute the M-phi curves
        [mom,phi,axl,eps]  =
Moment1(p,tf,ts,fy,fu,es,a,b,x1,x2,x3,x4,y1,y2,y3,y4,x,y,mem,nxtf_tot,nytf_to
t,nxw_tot,nyw_tot,nxbf_tot,nybf_tot,sx,Ix,As,zx);
        end

        column = column+1;

        data_arr{1,1,i}     = mom/1e6;
        data_arr{1,2,i}     = phi*1e6;
    end

Moment = data_arr{1,1,1};
Curvature = data_arr{1,2,1};
grid off;
grid on;
plot(Curvature,Moment);
```

```
xlabel('Curvature (1/km)');ylabel('Moment (kN-m)');title('M-k
relationships');
    for i=1:length(tt)
        Moment = 0;
        Curvature = 0;
        Moment = data_arr{1,1,i};
        Curvature = data_arr{1,2,i};
        Curvvec(:,i) = interp1(Moment,Curvature,abs(Mvec),'spline');


    Curvvec(isnan(Curvvec))=0;              % Checking to eliminate NaN

    for i=1:length(tt)
        Curvature = Curvvec(:,i);
        Curvature = Curvature*(1e-6);
        rotation(i) = trapz(xvec,Curvature);
        rotation(i) = rotation(i)*(180/pi);
    end

    flag = 0;
    for i=1:length(tt)
            if((Cnctn_cap(i)-Axl_force(i))<=0)
                failure_time(1) = tt(i);
                flag = 1;
            end
    end


    flag = 0;
    for i=1:length(tt)
        if(abs((rotation(i)*(pi/180)))>RLS)&&(flag==0)
            failure_time(2) = tt(i);
            flag = 1;
        end
    end

data = [tt' rotation' (rotation*(pi/180))'];


function [a,b,poin] =
Node_Num(mem,nodes,nxtf_tot,nytf_tot,nxw_tot,nyw_tot,nxbf_tot,nybf_tot,xtf,yt
f,xw,yw,xbf,ybf)

%% Assigning values to temporary variables
    nxtf    = nxtf_tot;
    nytf    = nytf_tot;
    nxw     = nxw_tot;
    nyw     = nyw_tot;
    nxbf    = nxbf_tot;
    nybf    = nybf_tot;

%% Computing the node numbers and element dimensions

%$$$$$$$ TOP FLANGE  $$$$$$$$
```

```
% Loop to account for numbering in the top flange
    for i = 1:nytf
        for j = 1:nxtf
            m        = (i-1)*nxtf+j;
            a(m)     = xtf(j);
            b(m)     = ytf(i);

            poin(m,1)    = i*(nxtf+1)+j;
            poin(m,2)    = i*(nxtf+1)+j+1;
            poin(m,3)    = (i-1)*(nxtf+1)+j+1;
            poin(m,4)    = (i-1)*(nxtf+1)+j;

        end
    end

% Tracking the numbe rof members, node numbers allocated in top flange
    nm   = nxtf*nytf;
    nn   = (nytf+1)*(nxtf+1);

 % Temporary variables used to offset the node numbering
    nxtf_left    = (nxtf-nxw)/2;
    nxtf_right   = nxtf_left;

    nxbf_left    = (nxbf-nxw)/2;
    nxbf_right   = nxbf_left;

 %$$$$$$$$ WEB  $$$$$$$$
 % Loop to account for numbering in the web
    m    = nm;

    for i=1:nxw
        m        = nm+i;
        a(m)     = xw(i);
        b(m)     = yw(i);

        poin(m,1)    = nn+i;
        poin(m,2)    = nn+i+1;
        poin(m,3)    = (nxtf+1)*(nytf)+(nxtf_left+1+1)+(i-1);
        poin(m,4)    = (nxtf+1)*(nytf)+(nxtf_left+1)+(i-1);
    end

    nn   = nn+nxw+1;
    nm   = nm+nxw;

  % Assigning node number from 2nd row to last but one (n-1) row of the web
    for i=1:(nyw-2)
        for j = 1:nxw
            m        = nm+(i-1)*nxw+j;
            a(m)     = xw(j);
            b(m)     = yw(i+1);

            poin(m,1)  = ((i-1)*(nxw+1))+j+nn;
            poin(m,2)  = (i-1)*(nxw+1)+j+1+nn;
            poin(m,3)  = (i-2)*(nxw+1)+j+1+nn;
            poin(m,4)  = (i-2)*(nxw+1)+j+nn;
```

```
        end
    end

    nn   = (nyw-2)*(nxw+1)+nn;
    nm   = m;

% Assigning node number in the last row of the web

    for i=1:nxw
        m        = nm+i;
        a(m)     = xw(i);
        b(m)     = yw(nyw);

        poin(m,1)  = nn+i+nxbf_right;
        poin(m,2)  = nn+i+1+nxbf_right;
        poin(m,3)  = nn+(i-nxw);
        poin(m,4)  = nn+(i-nxw)-1;

    end

     nm = nm+nxw;
     temp_nn = nn+(nxbf+1);
     %poin

%$$$$$$$ BOTTOM FLANGE  $$$$$$$$
    for i = 1:nybf
        for j = 1:nxbf

            m = (nytf*nxtf)+(nyw*nxw)+(i-1)*(nxbf)+j;
            a(m)  = xbf(j);
            b(m)  = ybf(i);

            poin(m,1)  = temp_nn + (i-1)*(nxbf+1)+j;
            poin(m,2)  = temp_nn + (i-1)*(nxbf+1)+j+1;
            poin(m,3)  = temp_nn + (i-2)*(nxbf+1)+j+1;
            poin(m,4)  = temp_nn + (i-2)*(nxbf+1)+j;
        end
    end


function [x1,x2,x3,x4,y1,y2,y3,y4,x,y,xx,yyy] =
Coordinate_Num(mem,nxtf_tot,nytf_tot,nxw_tot,nyw_tot,nxbf_tot,nybf_tot,xtf,yt
f,xw,yw,xbf,ybf,poin)

x1=0;
x2=0;
x3=0;
x4=0;

y1=0;
y2=0;
y3=0;
y4=0;
```

```
x=0;
y=0;
xx=0;
yyy=0;

    width_tf    = 0;
    height_tf   = 0;
    width_web   = 0;
    height_web  = 0;
    width_bf    = 0;
    height_bf   = 0;

    nxtf    = nxtf_tot;
    nytf    = nytf_tot;
    nxw     = nxw_tot;
    nyw     = nyw_tot;
    nxbf    = nxbf_tot;
    nybf    = nybf_tot;

%% Calculating the dimensions of the section

% Calculating the dimensions of top flange
    for i=1:nxtf
        width_tf = width_tf+xtf(i);
    end

    for i=1:nytf
        height_tf = height_tf+ytf(i);
    end

% Calculating the dimensions of web
    for i=1:nxw
        width_web = width_web+xw(i);
    end

    for i=1:nyw
        height_web = height_web+yw(i);
    end

% Calculating the dimension of bottom flange
    for i=1:nxbf
        width_bf = width_bf+xbf(i);
    end

    for i=1:nybf
        height_bf = height_bf+ybf(i);
    end

%% Calculating the coordinates of the nodes

%$$$$$$$ TOP FLANGE  $$$$$$$$
    temp_y1 = 0;
    temp_y2 = 0;
    temp_y3 = 0;
    temp_y4 = 0;
```

```
    y_incr_tf = 0;
    x_incr_tf = 0;

    for i = 1:nytf
        if(i==1)
            temp_y3 = temp_y3;
            temp_y4 = temp_y4;
        else
            temp_y3 = temp_y3 + ytf(i-1);
            temp_y4 = temp_y4 + ytf(i-1);
        end

                temp_y1 = temp_y1 + ytf(i);
                temp_y2 = temp_y2 + ytf(i);

       temp_x1 = 0;
       temp_x2 = 0;
       temp_x3 = 0;
       temp_x4 = 0;

           for j = 1:nxtf
               m = (i-1)*nxtf+j;

               if(j==1)
                   temp_x1 = temp_x1;
                   temp_x4 = temp_x4;
               else
                   temp_x1 = temp_x1 + xtf(j-1);
                   temp_x4 = temp_x4 + xtf(j-1);
               end

                    temp_x2 = temp_x2 + xtf(j);
                    temp_x3 = temp_x3 + xtf(j);

                x1(m,1) = x_incr_tf + temp_x1;
                x2(m,1) = x_incr_tf + temp_x2;
                x3(m,1) = x_incr_tf + temp_x3;
                x4(m,1) = x_incr_tf + temp_x4;

                y1(m,1) = y_incr_tf + temp_y1;
                y2(m,1) = y_incr_tf + temp_y2;
                y3(m,1) = y_incr_tf + temp_y3;
                y4(m,1) = y_incr_tf + temp_y4;
           end
    end

%$$$$$$$ WEB  $$$$$$$$

    x_incr_web  = 0;
    y_incr_web  = 0;

    x_incr_web  = (width_bf-width_web)/2;
    y_incr_web  = height_tf;
```

```
    nm  = nxtf*nytf;     % Accounting for the member number to start in the
web

        temp_y1 = 0;
        temp_y2 = 0;
        temp_y3 = 0;
        temp_y4 = 0;

    for i = 1:nyw
        if(i==1)
            temp_y3      = temp_y3;
            temp_y4      = temp_y4;
        else
            temp_y3 = temp_y3 + yw(i-1);
            temp_y4 = temp_y4 + yw(i-1);
        end

                temp_y1 = temp_y1 + yw(i);
                temp_y2 = temp_y2 + yw(i);

       temp_x1 = 0;
       temp_x2 = 0;
       temp_x3 = 0;
       temp_x4 = 0;

            for j =1:nxw
                m = nm+(i-1)*nxw+j;

               if(j==1)
                   temp_x1 = temp_x1;
                   temp_x4 = temp_x4;
               else
                   temp_x1 = temp_x1 + xw(j-1);
                   temp_x4 = temp_x4 + xw(j-1);
               end

                    temp_x2 = temp_x2 + xw(j);
                    temp_x3 = temp_x3 + xw(j);

                x1(m,1)  = x_incr_web + temp_x1;
                x2(m,1)  = x_incr_web + temp_x2;
                x3(m,1)  = x_incr_web + temp_x3;
                x4(m,1)  = x_incr_web + temp_x4;

                y1(m,1)  = y_incr_web + temp_y1;
                y2(m,1)  = y_incr_web + temp_y2;
                y3(m,1)  = y_incr_web + temp_y3;
                y4(m,1)  = y_incr_web + temp_y4;
            end
    end

%$$$$$$$ BOTTOM FLANGE  $$$$$$$$
```

```
    x_incr_bf = 0;
    y_incr_bf = 0;

    y_incr_bf = height_tf + height_web;

    nm = nytf*nxtf + nyw*nxw;       %Accounting for the member number to
start in bottom flange

    temp_y1 = 0;
    temp_y2 = 0;
    temp_y3 = 0;
    temp_y4 = 0;

    for i =1:nybf
        if(i==1)
            temp_y3 = temp_y3;
            temp_y4 = temp_y4;
        else
            temp_y3 = temp_y3 + ybf(i-1);
            temp_y4 = temp_y4 + ybf(i-1);
        end

            temp_y1 = temp_y1 + ybf(i);
            temp_y2 = temp_y2 + ybf(i);

        temp_x1 = 0;
        temp_x2 = 0;
        temp_x3 = 0;
        temp_x4 = 0;

            for j =1:nxbf
                m = nm+(i-1)*nxbf+j;

                if(j==1)
                    temp_x1 = temp_x1;
                    temp_x4 = temp_x4;
                else
                    temp_x1 = temp_x1 + xbf(j-1);
                    temp_x4 = temp_x4 + xbf(j-1);
                end

                    temp_x2 = temp_x2 + xbf(j);
                    temp_x3 = temp_x3 + xbf(j);


                x1(m,1)  = x_incr_bf + temp_x1;
                x2(m,1)  = x_incr_bf + temp_x2;
                x3(m,1)  = x_incr_bf + temp_x3;
                x4(m,1)  = x_incr_bf + temp_x4;

                y1(m,1)  = y_incr_bf + temp_y1;
                y2(m,1)  = y_incr_bf + temp_y2;
                y3(m,1)  = y_incr_bf + temp_y3;
                y4(m,1)  = y_incr_bf + temp_y4;
```

```
            end
    end


   %% Calculating the location of the geometrical centroid
   GC_x     = width_tf/2;                                  % x coordinate of geometrical centroid
   GC_y     = (height_tf + height_web + height_bf)/2;     % y coordinate of geometrical centroid

%% Correcting the nodal coordinates to shift the origin to geomtrical centroid

    x1 = x1 - GC_x;
    x2 = x2 - GC_x;
    x3 = x3 - GC_x;
    x4 = x4 - GC_x;

    y1 = GC_y - y1;
    y2 = GC_y - y2;
    y3 = GC_y - y3;
    y4 = GC_y - y4;


%% Calculate the centroid of each element
    for i =1:mem
        x(i) = (x1(i,1)+x2(i,1))/2;
        y(i) = (y1(i,1)+y4(i,1))/2;
    end


function [P,Tf,Ts,Fy,Fu,Es,Sx,Ix,Zx,x_vec,M_vec] =
Axial_F(As,time,Props,w,h,T,t)

%% Input data and temporary variables
alpha = 14e-6;              % Coefficient of thermal expansion of steel

% Steel data
rhocs    = (7850*450);
hcon     = 25;
Sx       = 0.6325e6;
Zx       = 0.7062e6;
Ix       = 99.0630e6;
Fy       = 375;
Fu       = 451;
Es       = 187500;
L        = 3505;
UDL      = 63.5;

ka       = 0.1;
kr       = 2;
support = 0;

% Insulation data
```

```
tp      = 12.7;
kp      = 0.1;
rhocp   = (200*900);

% Fire parameters
m   = 2;
n   = 0.1677;
a   = 469.9;

%% Computing the section factors and "s" for different parts of the section
    % Units: mm
    Fp(1)    = 2*T+w-t;            % Fp for the top flange
    Fp(2)    = h-2*T;              % Fp for the web
    Fp(3)    = 2*T+w+w-t;          % Fp for the bottom flange
    Fp(4)    = w+2*h+2*(w-t);      % Fp for the total section

    % Units: mm2
    V(1)     = w*T;                % Area of the top flange
    V(2)     = (h-2*T)*t;          % Area of the web
    V(3)     = w*T;                % Area of the bottom flange
    V(4)     = As;                 % Area of the entire section

    num      = (Fp./V)*(10^3);
    den_t1   = rhocs*((1/hcon)+((tp/1000)/kp));
    den_t2   = 1+(rhocp/rhocs)*(Fp./V)*(10^3)*((tp/1000)/m);
    den      = den_t1.*den_t2*(n+1);

    s        = num./den;

        Tf = a*(time^n);
        Ts = Tf*(1-exp(-s*time*60));

        Ts(Ts<20)=20;

%% Computing the moments at mid-span and the ends of the beam
        if(support==0)
            M_mid_span  = (UDL*((L/1000)^2))/8;     %Units:kN.m
            M_end       = 0;
        else
            M_mid_span  = (UDL*((L/1000)^2))/24;
            M_end       = (UDL*((L/1000)^2))/12;
        end

        Mo   = max(M_mid_span,M_end);
        My   = (Fy*Sx)*(10^-6);
        Mu   = (Fu*Zx)*(10^-6);

%% Computing the moment distribution along the length of the beam
    x_vec = [linspace(0,0.211*L,20),linspace(0.211*L,L/2,31)];
    x_vec(21) = [];

    M_vec = (UDL/12)*((6*L.*x_vec)-(L*L)-(6.*x_vec.*x_vec));
    M_vec = M_vec*(10^-6);
```

```
%% Axial force calculation
% Factor to compute the axial restraint factor
    if (Props==1)
        a1 = 0.6;       % Eurocode 3 factor
        a2 = 0.0013;
        a3 = 1.139;
        a4 = 0.0013;
    else
        a1 = 0.6829;    % ASCE manual factor
        a2 = 0.0008;
        a3 = 1.329;
        a4 = 0.0014;
    end

Ka      = (ka*(Es*As/L));
num     = (a1*Ka*L)/(Es*As);
den     = 2*a1+ ((Ka*L)/(Es*As));
Xa  = (alpha*Es/Fy)*(num/den);

Kr      = (kr*(Es*Ix/L));
num = 0;
den = 0;
num     = (a1*Kr*L)/(Es*Ix);
den     = 2*a1+ ((Kr*L)/(Es*Ix));
Xr  = (alpha*Es/Fy)*(num/den);
deltaT = Ts(3)-Ts(1);

    Ty  = (1-(Mo/My)-(0.5*Xr*deltaT))/(Xa+a2);
    Tc  = (1/a2)*(1-(Mo/Mu)-(My/Mu)*((Xr*deltaT)/2));

    Ttenmax = (Tc*Ty*Xa+a1*a3*(Tc-Ty))/(Ty*Xa+a1*a4*(Tc-Ty));

    Pcmax = Fy*As*Xa*(Ty-20);
    Ptmax = Fy*As*(a3-a4*Ttenmax);


    if(Ts(4)<=Ty)                   % Axial force will be in N
        P   = (Ts(4)-20)*Xa*Fy*As;
    elseif(Ts(4)>Ty) && (Ts(4)<=Tc)
        P = Pcmax-Pcmax*((Ts(4)-Ty)/(Tc-Ty));
    elseif(Ts(4)>Tc) && (Ts(4)<=Ttenmax)
        P = Pcmax-Pcmax*((Ts(4)-Ty)/(Tc-Ty));
    else
        P = 0;
    end


    P   = P/1000;                       % Converting axial force into kN


function [Cap] = Connection_cap(t_beam,As,ts,Fy_beam,Fu_beam)

n_bolts  = 3;               % Number of bolts
n_angle  = 2;               % Number of angles
```

```
Bolt_dia = (3/4)*25.4;       % Diameter of bolts in mm
h_bearing = (1/16)*25.4;     % Oversize clearance for bearing computations
h_blockshear = (1/8)*25.4;   % Oversize clearance for block shear computations
Bolt_separation = 76.2;      % Clear distance between bolt centers

Fy_angle = 308;              % Yield strength of angle in MPa
Fu_angle = 459;              % Ultimate strength of angle in MPa
t_angle  = 7.94;             % Thickness of angle in mm
d_angle  = 215.9;            % Depth of the angle in mm

Fy_bolt = 940;               % Yield strength of bolt in MPa
Fu_bolt = 1210;              % Ultimate strength of bolt in MPa

[Fyt_angle,Fut_angle] = Reduced_props(Fy_angle,Fu_angle,ts(4));
[Fyt_beam,Fut_beam]   = Reduced_props(Fy_beam,Fu_beam,ts(4));
[Fyt_bolt,Fut_bolt]   = Reduced_props(Fy_bolt,Fu_bolt,ts(4));

Le = [57.15, 31.75];         % Clear length of beam, angle
Fu = [Fut_beam,Fut_angle];     % Ultimate strength of beam, angle in MPa
Fy = [Fyt_beam,Fyt_angle];     % Yield strength of beam, angle in MPa
t  = [t_beam,t_angle];       % Thickness of beam, angle in mm


%##########################################################
%   Calculating bearing strength in Beam web and angles

Lc = Le-(0.5)*(Bolt_dia+h_bearing);
Bearing_LL = 1.2.*Lc.*t.*Fu;;
Bearing_UL = 2.4.*Bolt_dia.*t.*Fu;

Bearing_str =
0.75*min(n_bolts*min(Bearing_LL(1),Bearing_UL(1)),n_angle*n_bolts*min(Bearing
_LL(2),Bearing_UL(2)));

%################################################################
%   Calculating block shear strength of beam web and angle
Agv = 2*t.*Le;       % Accounting for 2 shear planes

Lc_temp = Le-(0.5)*(Bolt_dia+h_blockshear);
Anv = 2*t.*Lc_temp; % Accounting for 2 shear planes


Lc_temp = 0;
Lc_temp = 2*(Bolt_separation-(Bolt_dia+h_blockshear));
Ant = t.*Lc_temp;

Blockshear_LL = 0.6.*Fu.*Anv+Fu.*Ant;
Blockshear_UL = 0.6.*Fy.*Agv+Fu.*Ant;

Blockshear_str =
0.75*min(min(Blockshear_LL(1),Blockshear_UL(1)),n_angle*(min(Blockshear_LL(2)
,Blockshear_UL(2))));
```

```
%##################################################################
%   Calculating the shear strength of bolts

Ab = (pi/4)*(Bolt_dia.^2);
Rn = 2*(0.5*(Fut_bolt)*Ab);      % Multiplying by 2 to account for double
shear
Shear_str = 0.75*n_bolts*Rn;

%##################################################################
%   Calculating the tensile strength of beam and angle

Ag = [As, (d_angle*t_angle)];
Aholes = n_bolts.*(Bolt_dia+h_blockshear).*t;

An = Ag-Aholes;

T_grossarea = 0.9*Fy.*Ag;
T_netarea   = 0.75*Fu.*An;

Tensile_str =
min(min(T_grossarea(1),T_netarea(1)),n_angle*min(T_grossarea(2),T_netarea(2))
);

%##################################################################
%   Computing the connection capacity
Strength = [Bearing_str,Blockshear_str,Shear_str,Tensile_str]/1000;

Cap = min(Strength);


function [mom,phi,axl,eps]  =
Moment1(p,tf,ts,fy,fu,es,a,b,x1,x2,x3,x4,y1,y2,y3,y4,x,y,mem,nxtf_tot,nytf_to
t,nxw_tot,nyw_tot,nxbf_tot,nybf_tot,sx,Ix,As,Zx)


%% Initializing temporary variables
    Fyrt  = fy;
    Furt  = fu;
    Esrt  = es;
    Sx    = sx;
    p     = p*1000;             % Converting p to N from kN

    nxtf    = nxtf_tot;
    nytf    = nytf_tot;
    nxw     = nxw_tot;
    nyw     = nyw_tot;
    nxbf    = nxbf_tot;
    nybf    = nybf_tot;

    q11     = 0;
    q13     = 0;
    q31     = 0;
    q33     = 0;
```

```
    tolerance = [1;1]*(1/100);
    error     = [1;1];
    iter      = 0;
    mx        = 0;                    % Initial value of moment
    loading   = [mx;p];               % Initial laod vector

    incr      = [(10^6);0];           % Increment in moment (Mx) Units: N.mm

    tolerance = [(10^2);0.1];             %Tolerance

    jj   = 0;
    mom  = 0;
    phi  = 0;
    axl  = 0;
    eps  = 0;

    f_app     = [0;0];            % Applied load vector
    f_int     = [0;0];            % Internal force vector
    f_res     = [1;1]*(10^50);    % Residual force vector (Initially it should
be > tolerance)

%%
%#######################################
% Calculating initial K matrix

    for i=1:mem
            % Calculations for elements in the top flange
            if (i<= nxtf*nytf)

                [mod]     = Factors_Steel(ts(1),Esrt);

                q11     = q11 + mod*(y(i)^2)*a(i)*b(i);
                q13     = q13 + mod*y(i)*a(i)*b(i);
                %q31      = q13;
                q33     = q33 + mod*a(i)*b(i);
                Ein(1)  = mod;
            % Calculations for elements in the web
            elseif ((i > nxtf*nytf)& (i <=nytf*nxtf + nyw*nxw))

                [mod]     = Factors_Steel(ts(2),Esrt);

                q11     = q11 + mod*(y(i)^2)*a(i)*b(i);
                q13     = q13 + mod*y(i)*a(i)*b(i);

                q33     = q33 + mod*a(i)*b(i);
                Ein(2)  = mod;
            % Calculations for elements in the bottom flange
            elseif ((i >nytf*nxtf + nyw*nxw) & (i<=mem))
                [mod]     = Factors_Steel(ts(3),Esrt);

                q11     = q11 + mod*(y(i)^2)*a(i)*b(i);
                q13     = q13 + mod*y(i)*a(i)*b(i);
                q33     = q33 + mod*a(i)*b(i);
                Ein(3)  = mod;
            end
```

```
    end

    K(1,1) = q11;
    K(1,2) = -q13;
    K(2,1) = -q13;
    K(2,2) = q33;

    K_ref = K(1,1);
    Mp = fu*Zx;

    % Assigning axial force value
    P = p;

    e0(1:mem) = -p/(As*es);
    e   = zeros(1,mem);

    sigma = zeros(1,mem);

% Computing the reduced strength properties
[Est,Fyt,Fut,Telem] =
Factors_Stl(Esrt,Fyrt,Furt,ts,mem,nxtf,nytf,nxw,nyw,nxbf,nybf);

% Increase Mx
Mx = 0;
dMx = 10^6;          % Increment in moment (Mx) Units: N.mm
phix = 0;
ii = 1;
momentx(1) =0;
rotationx(1) = 0;
f = [0;0];
delta = [0;0];
aaaa = 1;

while(aaaa>0.01)
    Mx = Mx+dMx;
    aaaa=K(1,1)/(K_ref);
    mmx=dMx;
    pp=P;
    Pint = 0;
    Mxint = 0;
    dif1 = 2;
    dif2 = 2;
    f(1) = mmx;
    f(2) = pp;

    while(dif1>1&&dif2>1)
        delta=inv(K)*f;
        phix = phix+delta(1);
        e0 = e0+delta(2);
        e = e0+(-1*phix*y);
        epst = e;
        q11 =0;
        q33 = 0;
        q13 = 0;
        q31 = 0;
```

```
        for i = 1:mem
            [stress,modulus] =
Stress_stl(epst(i),Est(i),Fyt(i),Fut(i),Telem(i));
            Et(i) = modulus;
            sigma(i) = stress;

            q11 = q11 + modulus*(y(i)^2)*a(i)*b(i);
            q13 = q13 + modulus*y(i)*a(i)*b(i);
            q33 = q33 + modulus*a(i)*b(i);
        end
        K(1,1) = q11;
        K(1,2) = -q13;
        K(2,1) = -q13;
        K(2,2) = q33;
        if q11==0
            break
        end
        PPP = 0;
        MMMx = 0;
        for i =1:mem
            MMMx = MMMx + (sigma(i)*y(i)*a(i)*b(i));
            PPP  = PPP  + (sigma(i)*a(i)*b(i));
        end
        Pint = PPP;
        Mxint = -MMMx;
        dif1 =abs(-Mx-Mxint);
        dif2 =abs(-P-Pint);
        if(dif1<=1 && dif2<=1)
            ii = ii+1;
            momentx(ii)=Mx;
            rotationx(ii)=phix;

            mom(ii)=Mx;
            phi(ii)=phix;
        end
        mmx = -Mx-Mxint;
        pp  = -P-Pint;
        f(1)= mmx;
        f(2)= pp;
    end
end
```

APPENDIX E

The proposed methodology can be applied in fire design of connections. A numerical example is presented here to demonstrate the applicability and rationality of the proposed methodology. Step-by-step design procedure in analyzing a typical connection under fire is presented below:

Problem:

- Evaluate the fire resistance of double angle connection in a steel framed building subjected to ASTM E119 standard fire exposure.

Building details:

- The steel framed building considered for this example is a typical 3-storey building shown in Fig. E.1(a). The fire is assumed to occur in the first level of the building subjecting the beam and the connections to elevated temperature, as shown in Fig. E.1(b).

Beam characteristics:

- Beam length and section: 6000 mm, W24x76
- Loading: Distributed dead and live service loads: W_D = 35 kN/m and W_L = 70 kN/m, respectively
- Steel properties; Grade 50 steel with F_y = 355 MPa and F_u = 445 MPa
- Beam is assumed to be protected with 15mm thick insulation. The geometric details of the beam are presented in Table 6.1 while the thermal properties of insulation are presented in Table 6.2.

Connection details:

- The double angle connection configuration connection the beam to column is illustrated in Fig. E.2.

Response parameters:

- Load combination under fire $W_f = 1.0W_D + 0.5W_L = 70$ kN/m (≈30% of beam ultimate load carrying capacity at ambient temperature).
- The computed beam temperatures along with the generated moment-curvature relationships as well as evolution of fire-induced forces in connection are presented in Fig. E.3.
- The predicted failure time (fire resistance) of the connection is 66 minutes when subjected to ASTM E119 standard fire exposure.

Summary:

To ensure that the connections will not experience premature failure when exposed to ASTM E119 fire conditions the designer has to ensure that the connection capacity is always greater than the fire-induced axial forces (from Fig. E.3(c)) experienced by the connection. Therefore, this methodology will not only provide the designer with the tool to evaluate fire-induced axial forces in connection but also enables the designer to design fail-proof connections for the particular fire exposure conditions.

APPENDIX F

Chapter 2 tables

Table 2.1: Summary of the experimental program conducted by Lawson (Lawson, 1990)

Test number	Connection type	Beam section	Column section	Bolt details	Fire protection	Applied moment
1	Extended end-plate (bare)	305x165x40 UB	203x203x52 UC	M20 Grade 8.8	No	0.4 Mp
2	Flush end-plate (bare)	305x165x40 UB	203x203x52 UC	M20 Grade 8.8	No	0.2 Mp
3	Extended end-plate (bare)	305x165x40 UB	203x203x52 UC	M20 Grade 8.8	No	0.2 Mp
4	Flush end-plate (bare)	305x165x40 UB	203x203x52 UC	M20 Grade 8.8	Yes	0.2 Mp
5	Double angle (bare)	305x165x40 UB	203x203x52 UC	M20 Grade 8.8	Yes	0.1 Mp
6	Flush end-plate (composite)	305x165x40 UB	203x203x52 UC	M20 Grade 8.8	Yes	0.4 Mp
7	Double angle (composite)	305x165x40 UB	203x203x52 UC	M20 Grade 8.8	Yes	0.2 Mp
8	Shelf-angle Flush endplate (bare)	305x165x40 UB	203x203x52 UC	M20 Grade 8.8	No	0.2 Mp
M_p is the plastic moment capacity of steel beam						

Table 2.2: Summary of test parameters used by Yu et al.(Yu et al., 2009a)

Test number	Specimen geometry	Temperature (°C)	Target load angle (°)	Observed initial angle (°)	Observed final angle (°)	Force (kN)	Rotation (°)
1	3-8.8-20	20	55	53.85	32.41	145.95	8.107
2	3-8.8-20	450	55	51.47	41.37	70.48	6.093
3	3-8.8-20	550	55	53.44	42.68	34.81	6.558
4	3-8.8-20	650	55	53.09	44.02	17.99	6.255
5	3-8.8-20	20	35	33.8	34.06	185.11	7.805
6	3-8.8-20	450	35	39.04	33.52	84.47	6.237
7	3-8.8-20	550	35	40.94	31.51	37.46	7.121
8	3-8.8-20	650	35	40.5	30.6	19.3	7.367
9	6-8.8-20	550	35	41.56	32.21	81.12	6.853
10	6-8.8-20	550	55	55.99	46.6	67.01	4.782
11	3-10.9-20	20	35	36.53	29.8	213	10.62
12	3-10.9-20	550	35	40.85	23.9	56.82	11.5
13	3-8.8-24	20	35	37.38	29.67	203.1	8.339
14	3-8.8-24	550	35	42.1	29.06	74.02	7.855

Table 2.3: Summary of experimental program conducted by Yu et al.(Yu et al., 2009b)

Test number	Specimen geometry	Temperature (°C)	Target load angle (°)	Observed initial angle (°)	Observed final angle (°)	Force (kN)	Rotation (°)
1	3-8.8-20	20	55	55	34.4	186.34	16.57
2	3-8.8-20	450	55	55.8	43.5	93.74	9.39
3	3-8.8-20	550	55	56	42.2	52.91	10.52
4	3-8.8-20	650	55	56.5	34.4	25.7	14.15
5	3-8.8-20	20	45	45.7	32	212.54	17.12
6	3-8.8-20	450	45	46.7	37.3	99.42	10.29
7	3-8.8-20	550	45	47	36.8	56.35	11.53
8	3-8.8-20	650	45	48.1	34.5	28.18	15.94
9	3-8.8-20	20	35	37.4	21.2	243.17	16.71
10	3-8.8-20	450	35	41.1	29.1	112.85	10.75
11	3-8.8-20	550	35	41.4	26.6	61.21	12.56
12	3-8.8-20	650	35	40.9	21.6	31.57	14.86
13	6-8.8-20	550	35	40.2	27.2	85.01	10.95
14	6-8.8-20	550	55	55.7	41	66.78	9.19

Table 2.4: Summary of specimen and loading details used by Daryan and Yahyai (Daryan and Yahyai, 2009)

Specimen number	**Group number***	**Angle dimensions (mm)**	**Gap (mm)†**	**Grade of bolt**	**No of nuts**	**Applied moment‡**
1	2	150x100x15	0	8.8	1	0.4 M_{cc}
2	1	150x100x15	0	8.8	1	0.6 M_{cc}
3	1	100x100x10	15	8.8	1	M_{cc}
4	1	100x100x15	15	8.8	1	0.6 M_{cc}
5	2	150x100x15	15	8.8	1	0.4 M_{cc}
6	1	100x100x15	15	10.9	1	0.6 M_{cc}
7	2	150x100x15	15	10.9	3	0.4 M_{cc}
8	1	100x100x10	15	10.9	1	0.5 M_{cc}
9	1	150x100x15	15	8.8	1	0.6 M_{cc}
10	1	100x100x15	15	10.9	3	0.6 M_{cc}
11	2	150x100x15	15	10.9	1	0.4 M_{cc}
12	2	150x100x15	15	10.9	1	0.2 M_{cc}
*1:Specimen without web angle; 2: Specimen with web angle						
† Gap: Distance between beam and column flange						
‡M_{cc} is the moment capacity of the connection						

Table 2.5: Summary of specimen dimensions used by Wang et al. (Wang et al., 2011)

Test	**Connection type**	**Connection component dimension (mm)**	**Column section**	**Beam section**
1	Shear tab (fin plate)	150x130x10	UC 254x254x73	UB 178x102x19
2	Flexible endplate	150x130x8		
3	Flush endplate	150x200x8		
4	Double angle (web cleat)	90x150x10*		
5	Extended endplate	150x250x8		
6	Shear tab (fin plate)	150x130x10	UC 152x152x23	
7	Flexible endplate	150x130x8		
8	Flush endplate	150x200x8		
9	Double angle (web cleat)	90x150x10*		
10	Extended endplate	150x250x8		
* depth = 130 mm				

Table 2.6: Summary of connection details tested by Al-Jabri (Al-Jabri et al., 2005)

Group	Connection type	Beam section	Column section	Bolt	Thickness of end-plate (mm)	Test	Moment level
1	Flush end-plate (bare)	254x102x22 UB	152x152x23 UC	M16 Grade 8.8	8	Test 1	0.2 M_{cc}
						Test 2	0.4 M_{cc}
						Test 3	0.6 M_{cc}
						Test 4	0.8 M_{cc}
2	Flush end-plate (bare)	356x171x51 UB	254x254x89 UC	M20 Grade 8.8	10	Test 1	0.2 M_{cc}
						Test 2	0.4 M_{cc}
						Test 3	0.6 M_{cc}
						Test 4	0.8 M_{cc}
3	Flexible end-plate (bare)	356x171x51 UB	254x254x89 UC	M20 Grade 8.8	8	Test 1	0.1 M_{cc}
						Test 2	0.2 M_{cc}
						Test 3	0.5 M_{cc}
4	Flexible end-plate (composite)	356x171x51 UB	254x254x89 UC	M20 Grade 8.8	8	Test 0*	1.0 M_{cc}
						Test 1	0.32 M_{cc}
						Test 2	0.46 M_{cc}
						Test 3	0.59 M_{cc}
						Test 4	0.78 M_{cc}
5	Flexible end-plate (composite)	610x229x101 UB	305x305x137 UC	M20 Grade 8.8	10	Test 0*	1.0 M_{cc}
						Test 1	0.27 M_{cc}
						Test 2	0.46 M_{cc}
						Test 3	0.77 M_{cc}
* indicates ambient temperature test; M_{cc} is the moment capacity of connection							

Table 2.7: Test parameters and specimen dimensions used by Yang et al.(Yang et al., 2009)

Test no.	**Beam section**	**Column section**	**Test method**	**Fire proofing**	**Heating condition**	**Applied loading**	
						Column†	**Beam‡**
1	H600x300x12x25	H600x600x25x36	Steady state	No	550°C	0.3 P_{nc} (5390 kN)	Loaded to failure
2			Steady state	No	650°C	0.25 P_{nc} (3920 kN)	Loaded to failure
3			Transient state	No	ISO 834	0.25 P_{nc} (3920 kN)	0.6 P_y (333 kN)
4			Transient state	Yes (3 hrs)	ISO 834	0.25 P_{nc} (3920 kN)	0.6 P_y (333 kN)
†P_{nc} = nominal axial strength of column							
‡ P_y = yield strength of beam loaded at beam tip							

Chapter 3 tables

Table 3.1: Mechanical properties of steel members used in test assemblies

Component	Beam	Angle
Elastic modulus (MPa)	187500	154000
Yield strength (MPa)	375	308
Maximum strength (MPa)	451	459
Ultimate strain (%)	16	23

Table 3.2: Dimensions of beams and angles used in the test assemblies

Section	Depth (D) (mm)	Width of the flange (bf) (mm)	Thickness of flange (tf) (mm)	Thickness of web (tw) (mm)	Length (mm)
W12x30	313.4	165.6	11.2	6.6	3505
W14x132	372.4	374.1	26.2	16.4	4216
W14x74	360.0	255.8	20.0	11.4	4293
L4x3.5x5/16	101.6*	88.9†	8‡		215.9 and 292.1

*Length of long leg, † Length of short leg, ‡ Thickness of the angle

Table 3.3: Mix-proportions of concrete used in the slab of test assembly S2

Item	Quantity
Type I Portland cement	332 kg/m^3
Fly ash	60 kg/m^3
Fine aggregate (sand)	753 kg/m^3
Lightweight aggregate	495 kg/m^3
Coarse aggregate (gravel)	89 kg/m^3
Water	161 kg/m^3
28 day compressive strength	34 MPa

Table 3.4: Input parameters used in the computation of design fire, DF1

Fire input parameters	Energy density	$q_{f,d}$	865 MJ/m^2
	Heat of combustion	H_c	17.3 MJ/kg
Concrete properties	Conductivity	λ	1.75 W/m.K
	Specific heat	C_p	960 J/kg.k
	Density	ρ	2150 kg/m^3
	Thermal inertia	$\sqrt{\lambda c_p \rho}$	1900 Ws$^{0.5}$/m^2.k
Fire protection properties	Conductivity	λ	0.12 W/m.k
	Specific heat	C_p	1200 J/kg.K
	Density	ρ	300 kg/m^3
Compartment dimensions	Length	L	10 m
	Width	W	5 m
	Height	h	3 m
	Floor area	A_f	50 m^2
	Total surface area	A_t	190 m^2
	Average window height	H_v	2 m
	Average window width	W_d	1.25 m
	Ventilation factor	F_v	0.0372 m$^{-0.5}$

Table 3.5: Variables used in fire resistance tests on steel beam assemblies

Test Specimen	**Slab presence**	**Fire Scenario**	**Composite action (via shear studs)**	**Loading (Load ratio)**
S1	No	75 min of ASTM E119 followed by a decay rate of 8°C/min	No	74.7 kN (40%)
S2	Yes	90 min of ASTM E119 followed by a decay rate of 15°C/min	Yes	92.2 kN (50%)

Chapter 4 tables

Table 4.1: Summary of contact parameters used in the finite element models

Contact parameter	Value
FKN	0.1
FTOLN	0.1
ICONT	0.1
PINB	0.2
KEYOPT(2)	0
KEYOPT(5)	1
KEYOPT(9)	1
KEYOPT(10)	2
KEYOPT(12)	2

Table 4.2: Summary of key thermal and mechanical properties of steel members used in the test assemblies (S1, S2) used in the finite element model FEM1

Component	Beam	Angle	High-temperature properties
Elastic modulus (Mpa)	146258	122216	As per Eurocode 3 provisions
Yield strength (Mpa)	367	305	
Maximum strength (Mpa)	451	459	
Ultimate strain (%)	16	23	
Thermal conductivity (W/m K)	53		
Specific heat (J/kg K)	440		
Density (kg/m^3)	7850		

Table 4.3: Summary of key thermal and mechanical properties of concrete used in the assembly S2 used in the finite element model FEM1

Property	Value	High-temperature properties
Thermal conductivity (W/m K)	1.3	As per Eurocode 2 provisions
Specific heat (J/kg K)	900	
Density (kg/m^3)	2300	
Compressive strength (Mpa)	41	

Table 4.4: Summary of thermal properties of insulation for test assemblies (S1, S2) used in the finite element model FEM1

Property	**Value**	**High-temperature properties**
Thermal conductivity (W/m.K)	0.086	Same as room temperature
Dry density (kg/m^3)	240	
Specific heat (J/kg K)	3000	

Table 4.5: Summary of thermal and structural response of assemblies S1 and S2 obtained from finite element model FEM1and measured test data

			FEM1	**Test**
Maximum beam temperature (°C)	**S1**	Bottom flange	766.73	764.39
		Web	834.23	722.00
		Top flange	660.55	617.78
	S2	Bottom flange	726.90	719.22
		Web	769.55	664.39
		Top flange	490.66	554.39
Maximum rotation (rad)	**S1**		0.1	0.12
	S2		0.03	0.03
Maximum axial force (kN) (compressive)	**S1**		233.4	NA
	S2		224	NA

Table 4.6: Ambient temperature mechanical properties of different steel members used in the finite element model FEM2

	Elastic modulus (MPa)	**Yield strength (MPa)**	**Ultimate strength (MPa)**
Beam	226580	344	514
Column	200000	390	553
Angle	228170	342	493
Bolt	210000	640	800

Table 4.7: Summary of thermal and structural response of restrained steel frame assembly obtained from finite element model FEM2 and measured test data

		FEM2	Test
Maximum beam temperature at failure (°C)	Bottom flange	738.24	NA
	Web	738.83	NA
	Top flange	217.04	NA
Maximum axial force (kN) (compressive)		78	82.9
Maximum beam deflection (mm)		229	251
Maximum rotation (°)		12.8	NA

Chapter 5 tables

Table 5.1: Summary of key mechanical properties of beam and connections used in comparative analysis

Component	Beam	Shear tab	Single angle	Double angle	Bolt (19mm dia)
Elastic modulus (Mpa)	187500	154000	154000	154000	200000
Yield strength (Mpa)	375	308	308	308	940
Ultimate strength (Mpa)	451	459	459	459	1210

Table 5.2: Variation of connection capacity and fire induced forces in three connection types with fire exposure time

		Fire induced axial force (kN) (compressive)			Connection capacity (kN)		
Time (min)	Temperature in connections (°C)	Component-level analysis (Eq. [5.1])	Member-level analysis	System-level analysis	Shear tab	Single angle	Double angle
0	20	0	0	0	211	211	306
5	58	485	0	18	196	196	292
10	128	1336	0	50	196	196	292
15	189	1963	0	70	196	196	292
20	249	2490	0	100	196	196	292
25	328	3035	0	124	185	185	275
30	399	3391	0	167	157	157	234

Table 5.3: Summary of parameters and their range used in the parametric studies

No.	**Parameter**		**Value/Description of parameter**	**Connection assembly**
1	Decay rate (°C/min)		2	S1
			4	S1
			10	S1
			12	S1
			3.75	S2
			7	S2
			18.75	S2
			22.5	S2
2	Loading type	Four point loading (kN)	46.3	S1
			57.8	S2
		Distributed loading (kN/m)	63.5	S1
			79.3	S2
3	Axial restraint (% of secondary beam stiffness)		25	S1,S2
			50	S1,S2
			75	S1,S2
			100	S1,S2
4	System-level interactions	Isolated connection (transient heating)	Parametric fire curve (FS)	Restrained steel frame
		System-level connection (uniform heating)	Uniform temperature of 550°C	
5	Load ratio		30%	Restrained steel frame
			40%	
			60%	
			70%	
6	Design fire scenarios		DF1	Restrained steel frame
			DF2	
			DF3	
7	High-temperature bolt properties	A325 bolts	Eurocode 3	Restrained steel frame
		A490 bolts	Kodur et al.	

Table 5.4: Compartment characteristics used for arriving at different design fire scenarios

Fire scenario	Fuel load (MJ/m^2 floor area)	Ventilation factor ($m^{0.5}$)	Thermal capacity ($Ws^{0.5}/m^2k$)	Maximum temperature (°C)	Duration of growth phase (min)	Total duration (min)	Decay rate (°C/min)
DF1	510	0.014	1600	706	60	192	5.4
DF2	750	0.014	1900	707	92	291	3.5
DF3	725	0.010	1600	709	120	432	2.3

Table 5.5: Maximum value of fire induced forces and rotation in connection for different fire scenarios

	Fire induced forces (kN)		
Fire scenario	**Compressive**	**Tensile**	**Rotation (°)**
DF	82	48	1.27
DF1	79	51	1.35
DF2	80	52	1.53
DF3	81	58	1.65

Table 5.6: Ambient temperature mechanical properties for different bolt grades

Bolt grade	Yield strength (MPa)	Ultimate strength (MPa)	Ultimate strain (%)	Elastic modulus (MPa)
Grade 6.8	480	600	15	200000
Grade 10.9	900	1000	15	200000
ASTM A325	660	830	15	200000
ASTM A490	940	1210	15	200000

Chapter 6 tables

Table 6.1: Geometric details of steel sections used in the analysis

	Section	
	W 12x30	**W 24x76**
Depth (mm)	313.4	607.1
Flange width (mm)	165.6	228.6
Flange thickness (mm)	11.2	17.3
Web thickness (mm)	6.6	11.2
Yield strength (MPa)	375	345
Ultimate strength (MPa)	451	448

Table 6.2: Summary of thermal properties of insulation used in the analysis

Property	Value
Thermal conductivity (W/m.K)	0.086
Dry density (kg/m^3)	240
Specific heat (J/kg K)	3000

Table 6.3: Ambient temperature mechanical properties of different components measured in Cardington tests

Component	Material grade	Yield strength (MPa)	Ultimate strength (MPa)
Beam (UB 305x165x40)	S375	303	469
Girder (UB 356x171x51)	S355	396	544
Shear tab (thickness = 10mm)	Grade 43	275	430
Bolt (M20) (diameter = 20 mm)	Grade 8.8	695	869

APPENDIX G

Chapter 1 figures

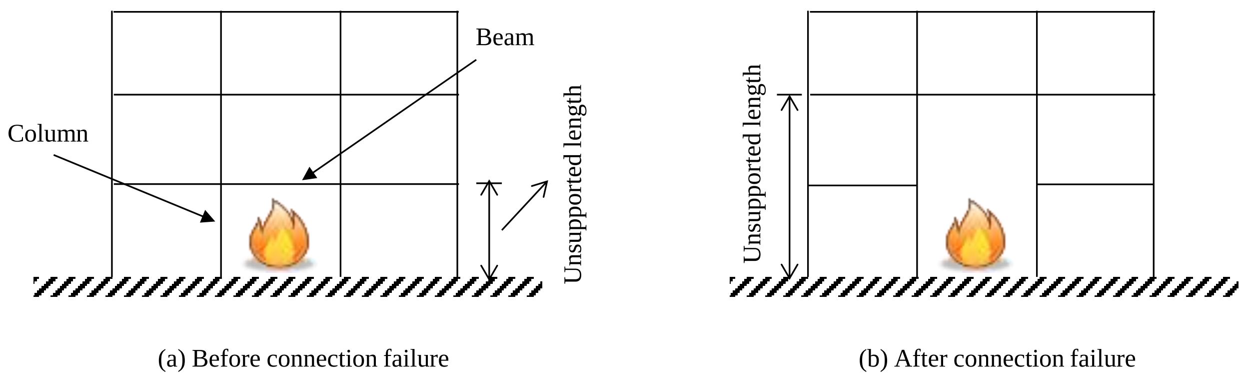

Figure 1.1: Typical steel frame in an office building (a) before and (b) after failure of beam-to-column connection

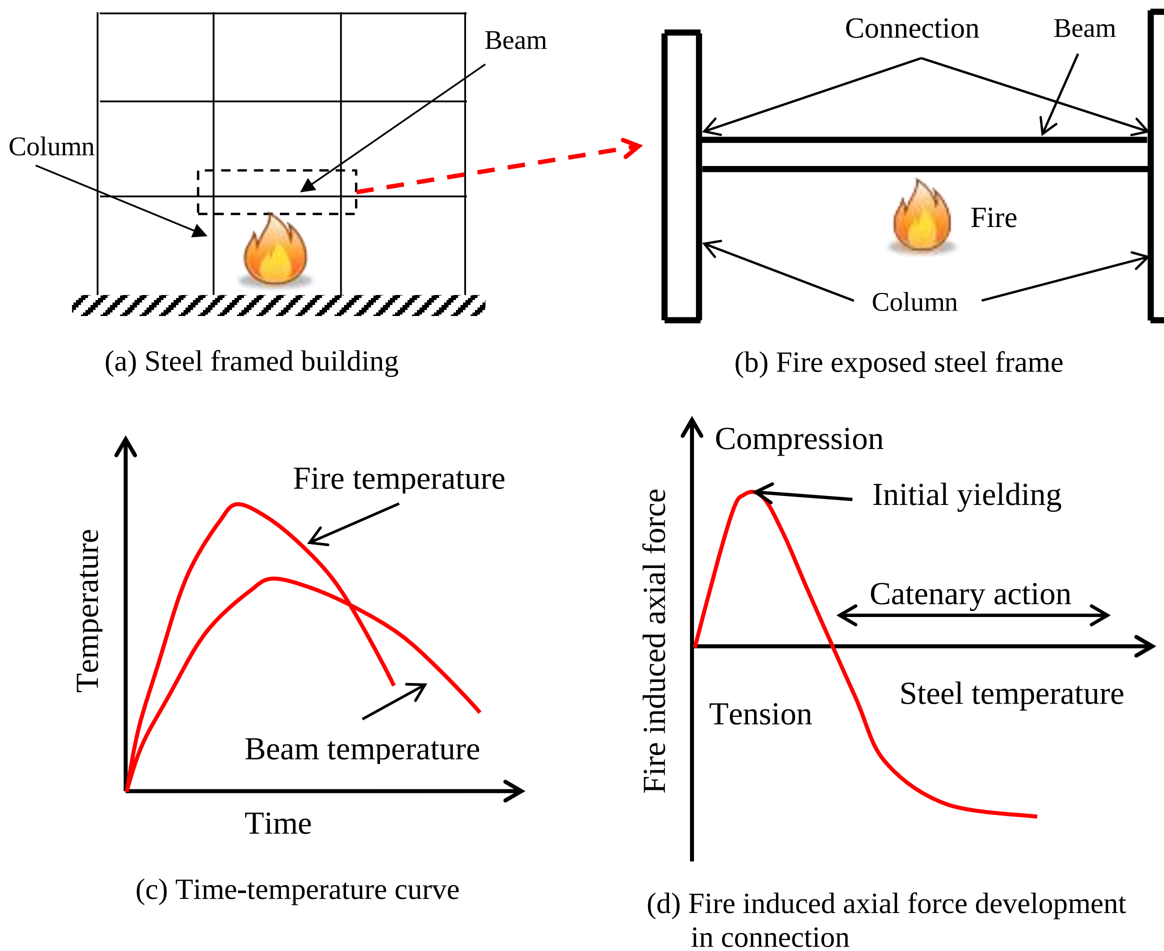

Figure 1.2: Development of axial forces in connection

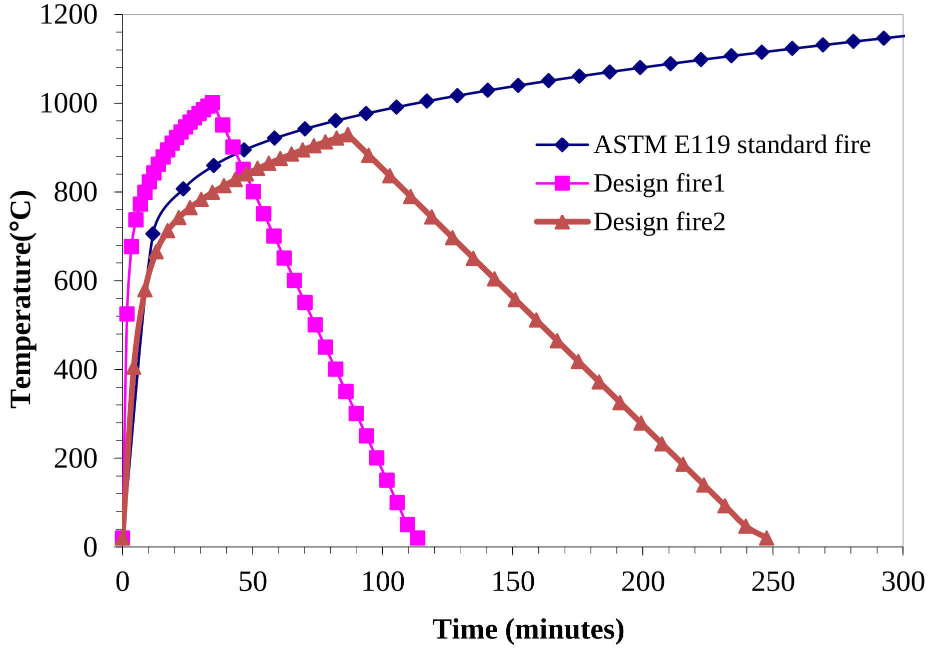

Figure 1.3: Illustration of standard and design fire scenarios in typical buildings

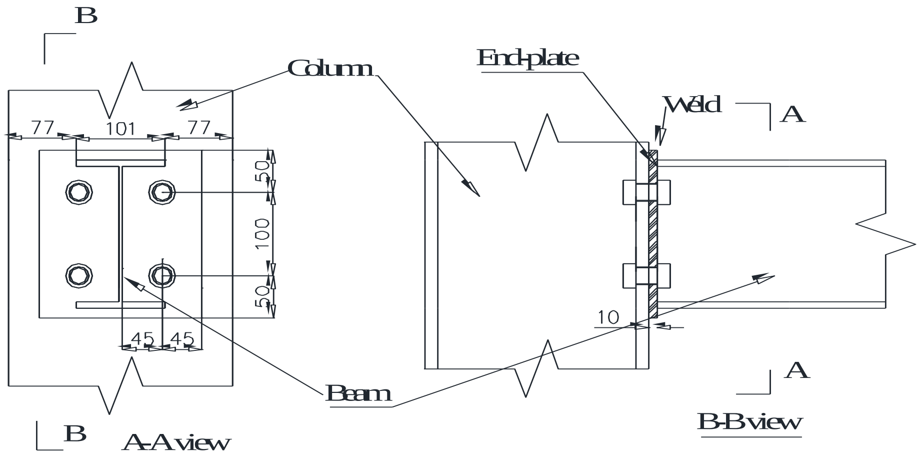

(a) Flush end-plate connection

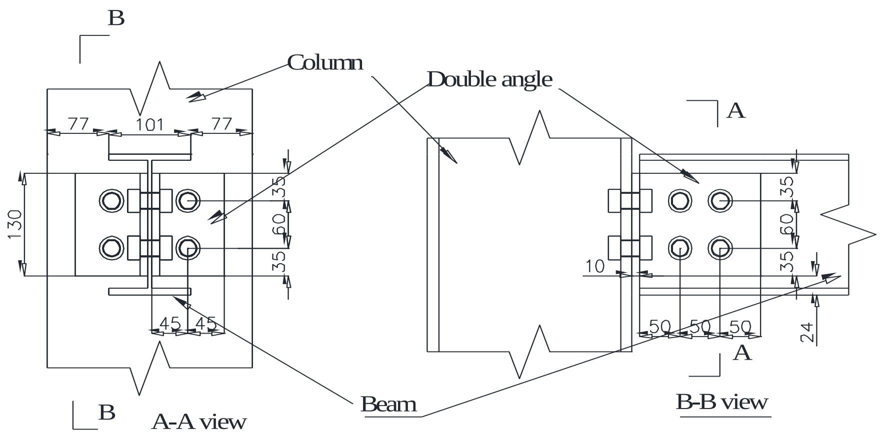

(b) Double angle connection

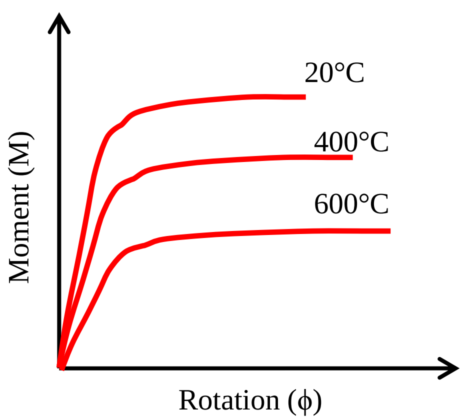

(c) Flush end-plate M-ϕ curves

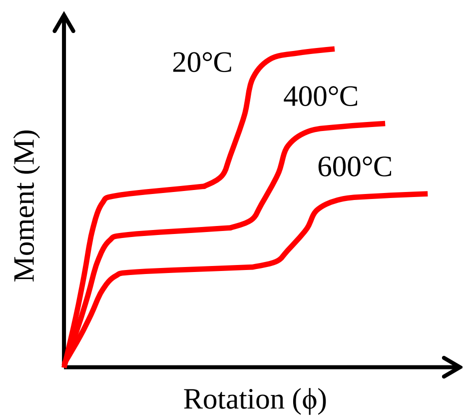

(d) Double angle M-ϕ curves

Figure 1.4: Connection details and moment-rotation curves for flush end-plate and double angle connections

Chapter 2 figures

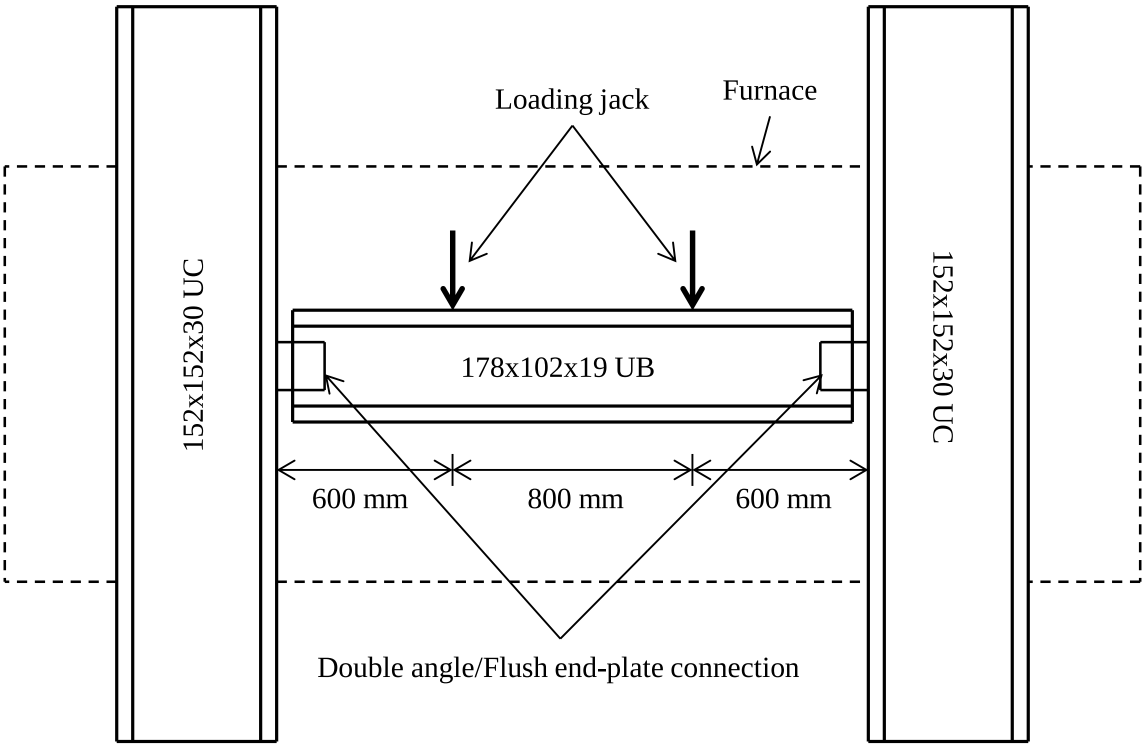

Figure 2.1: Schematic of the sub-frame assembly tested by Liu et al.(Liu et al., 2002)

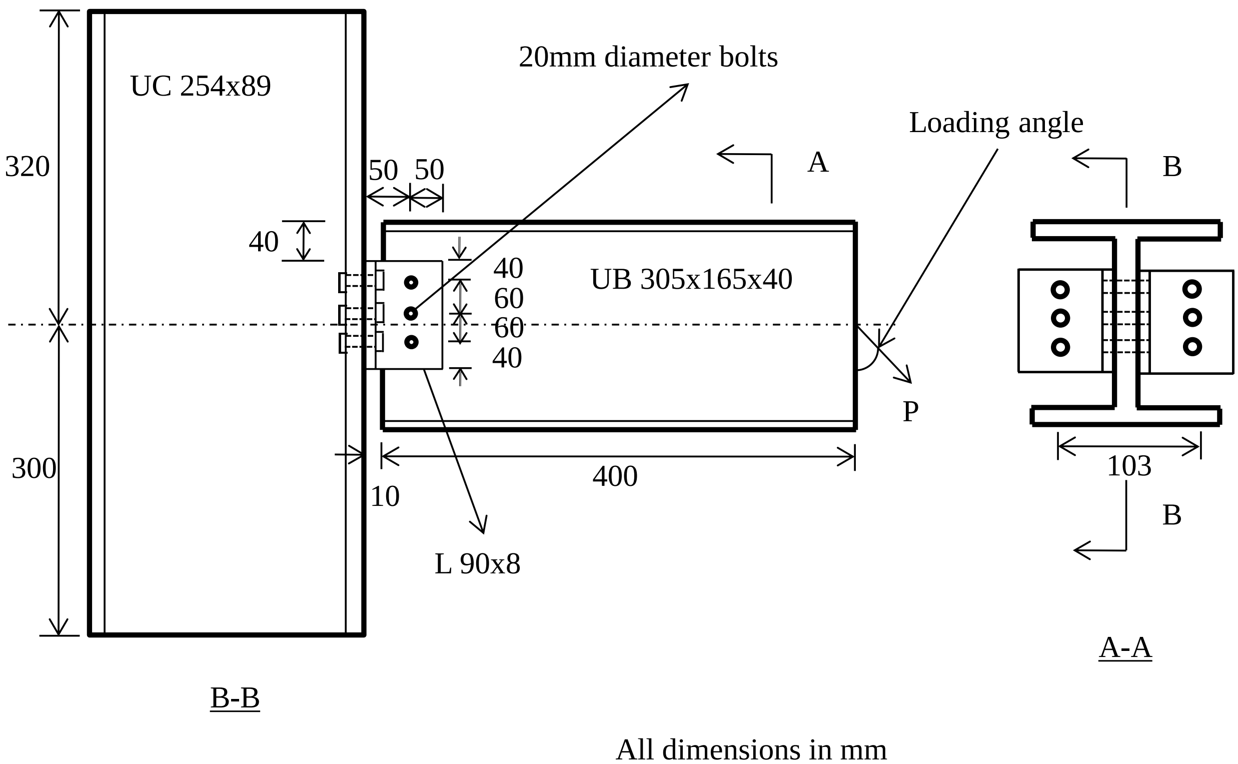

Figure 2.2: Schematic of connection configuration tested by Yu et al. (Yu et al., 2009b)

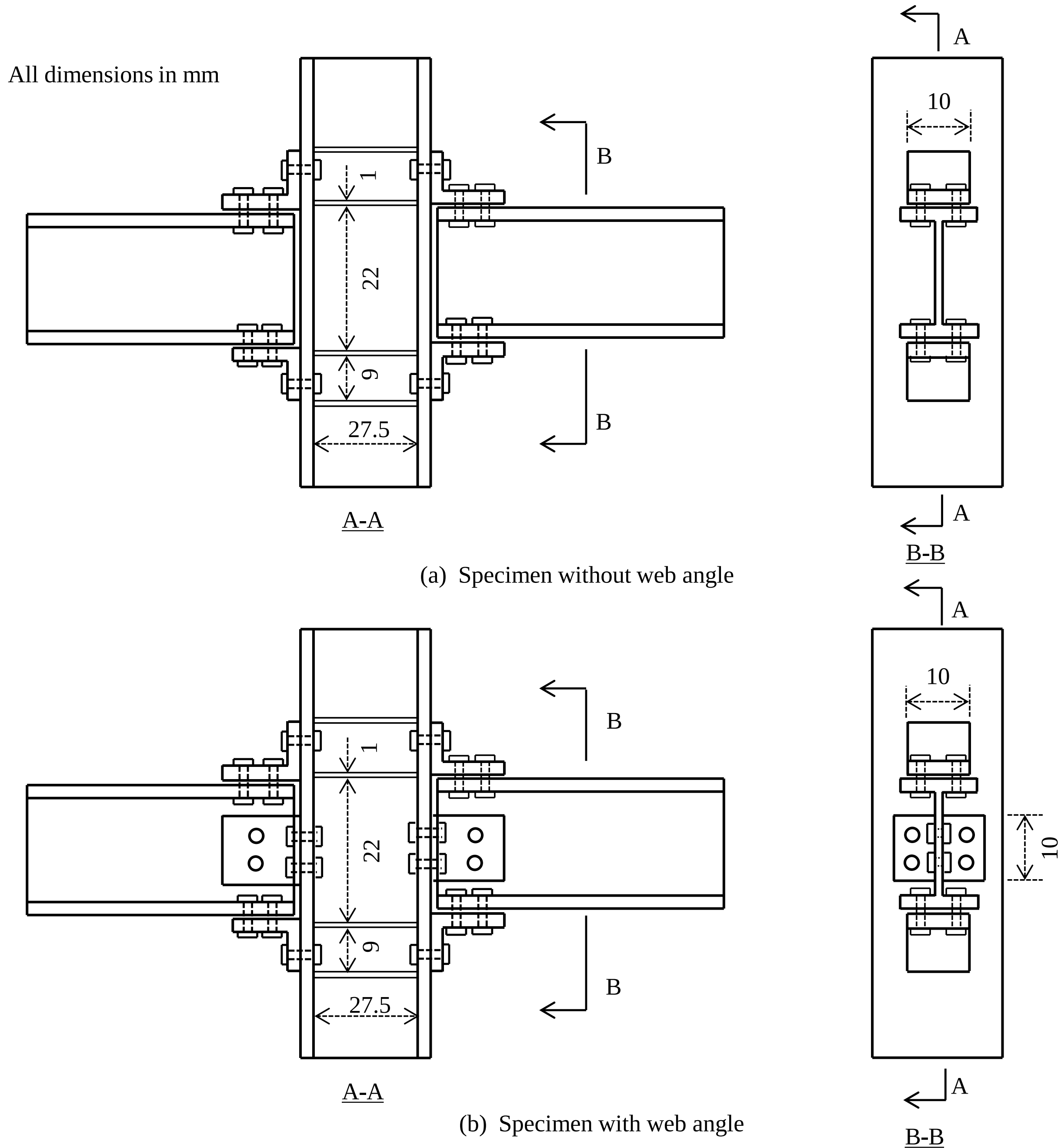

Figure 2.3: Connection details of the specimens tested by Daryan and Yahyai (Daryan and Yahyai, 2009)

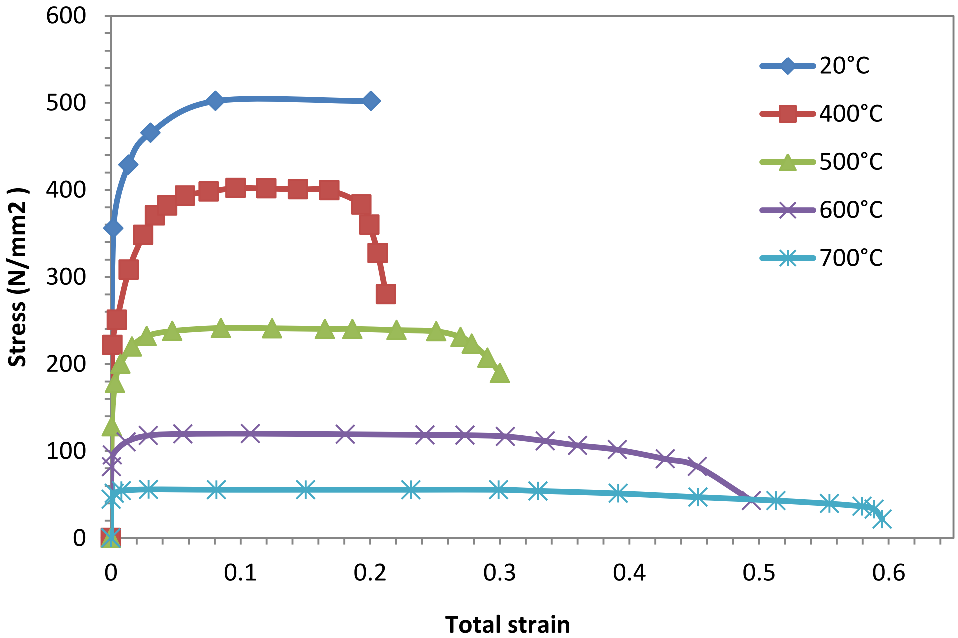

Figure 2.4: High-temperature stress-strain curves used in the FE model by Pakala et al. (Pakala et al., 2012a)

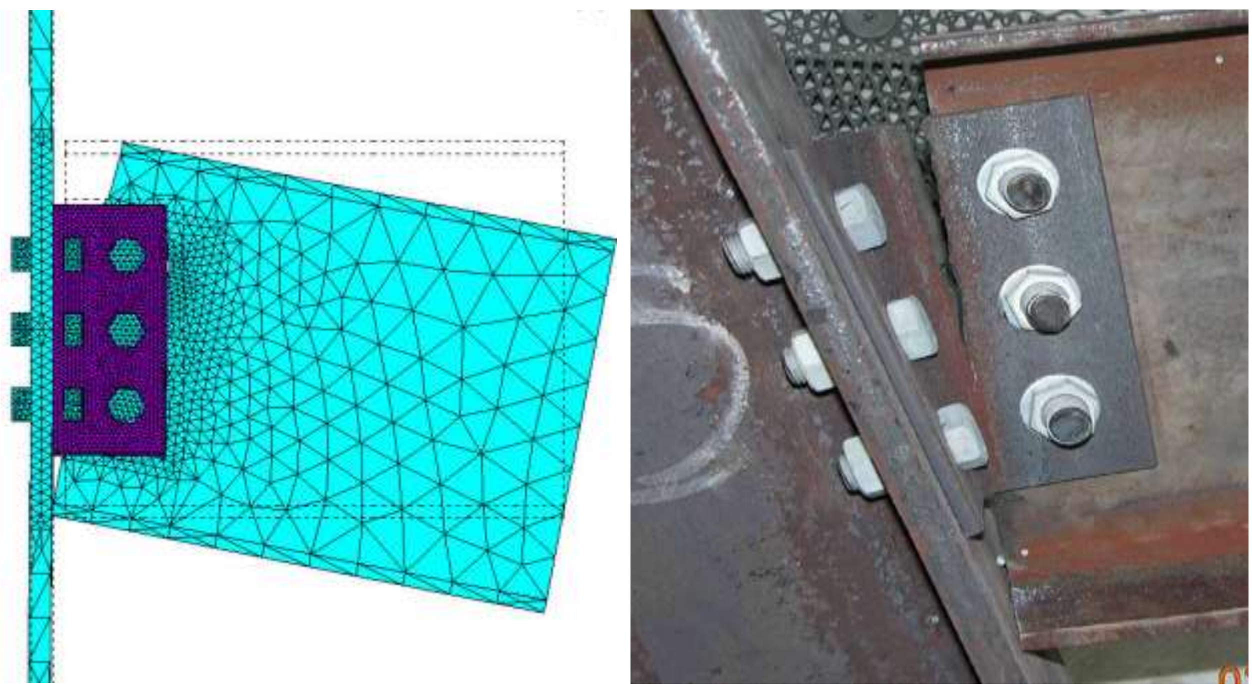

(a) FE model (b) Fire test

Figure 2.5: Comparison of predicted deformed shape of connection assembly with that observed in fire tests (Part (b) adapted from Yu et al. (Yu et al., 2009b))

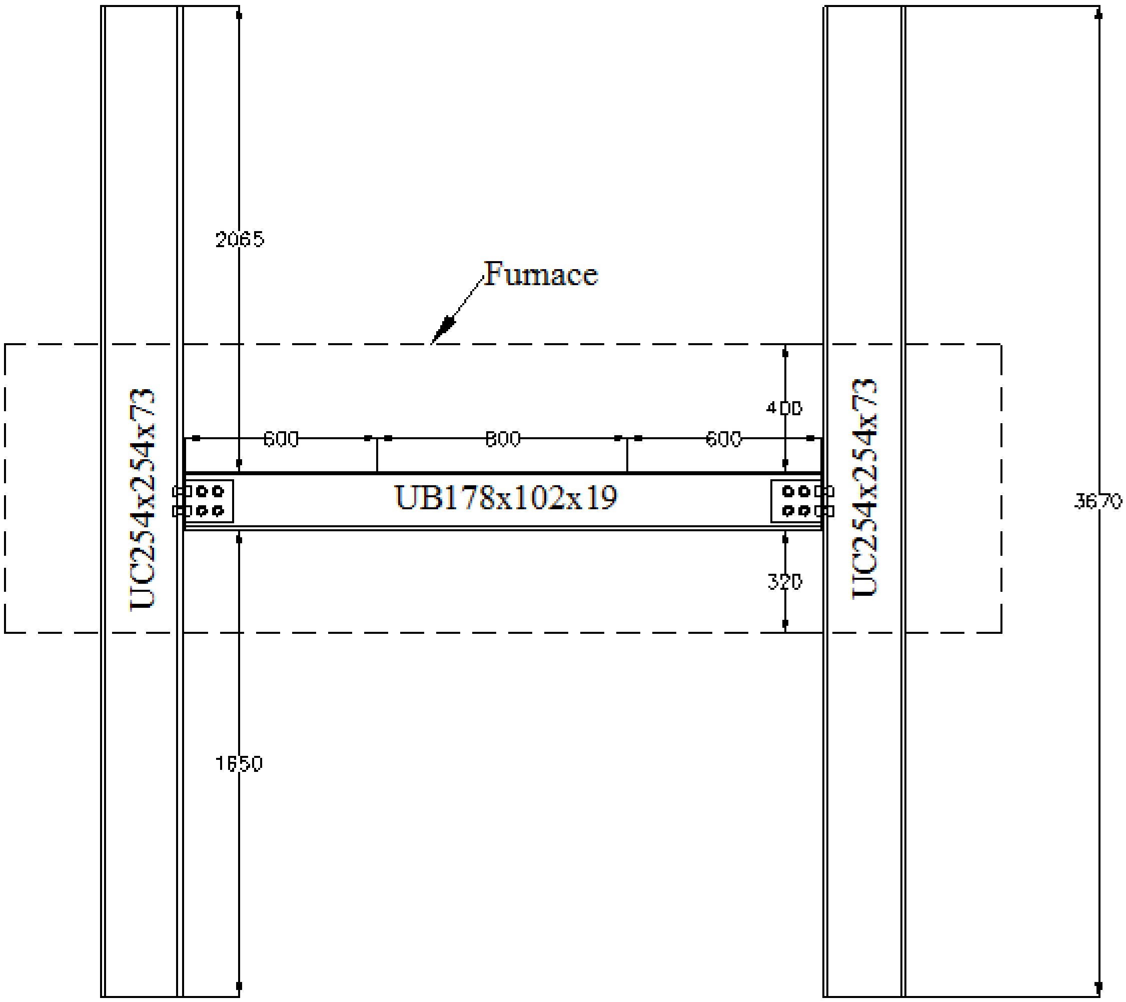

(a) Layout of the connection assembly

Figure 2.6: Geometrical details of the connection assembly used in the finite element model (all dimensions in mm)

Figure 2.6 (cont'd)

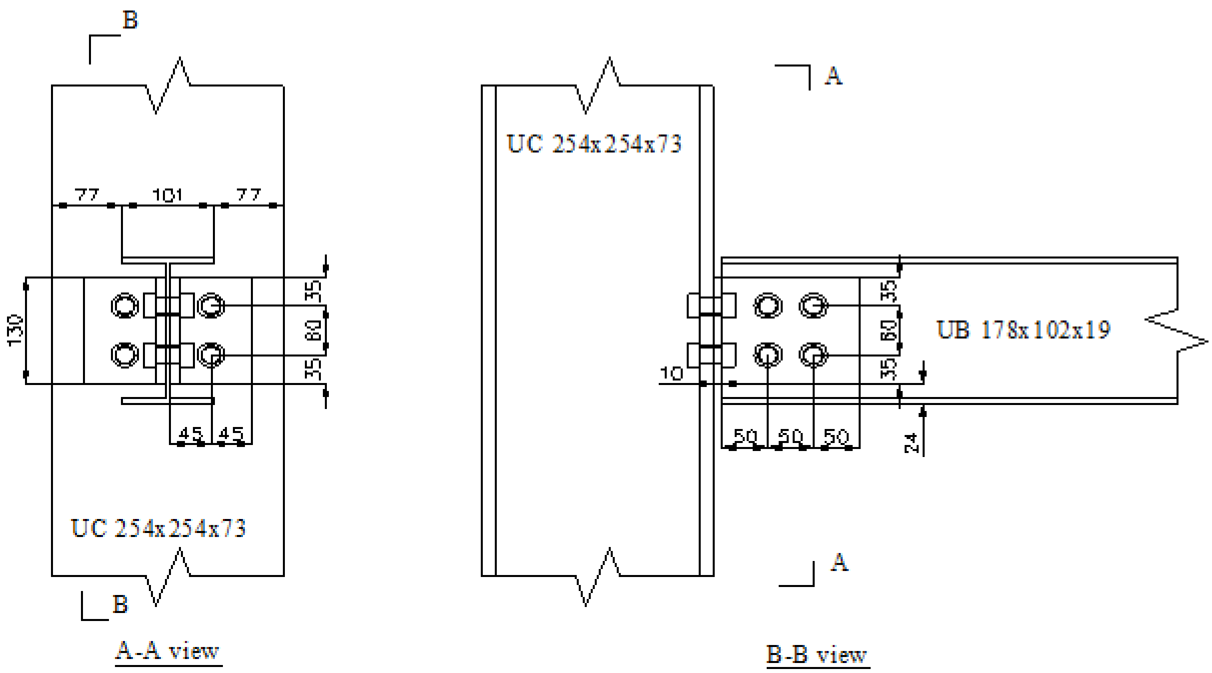

(b) Dimensions of the double angle connection

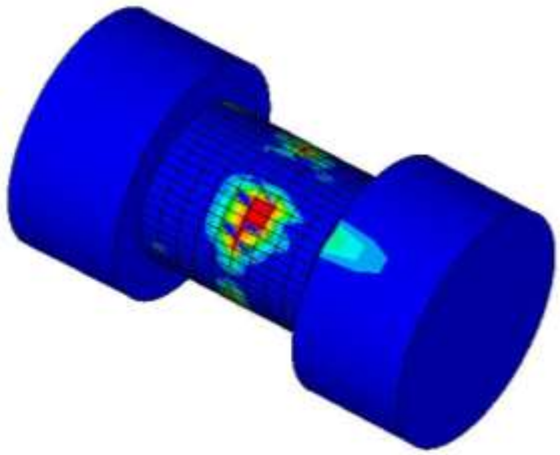

(a) Stress in the bolt shank region

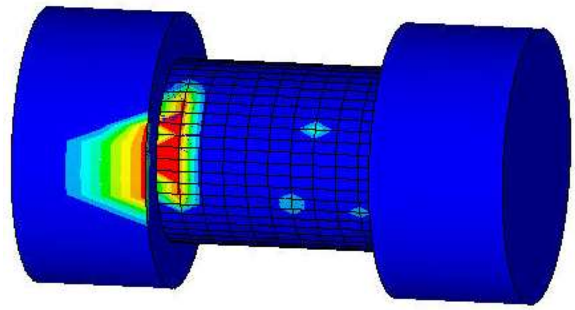

(b) Stresses in the bolt head region

Figure 2.7: Illustration of stresses in the (a) bolt shank region and (b) bolt head region at the time of beam failure predicted by the model

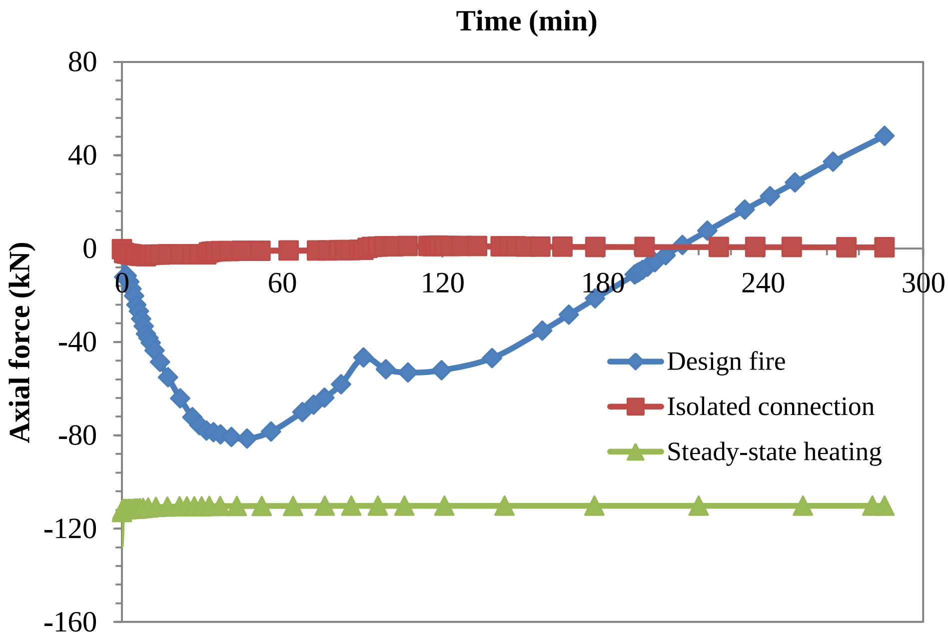

Figure 2.8: Variation of connections axial force as a function of fire exposure time for different scenarios

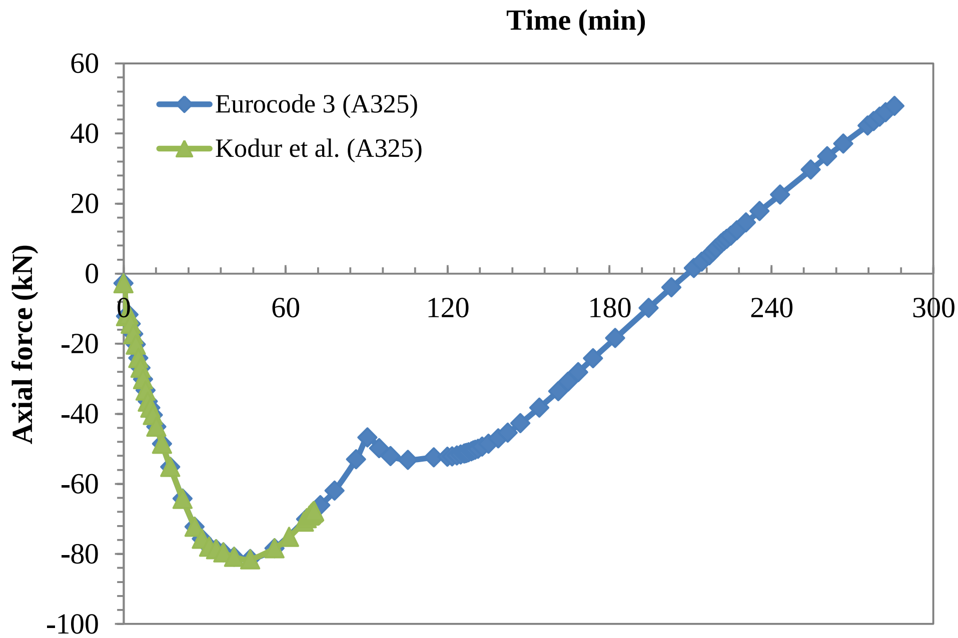

(a) A325 bolts

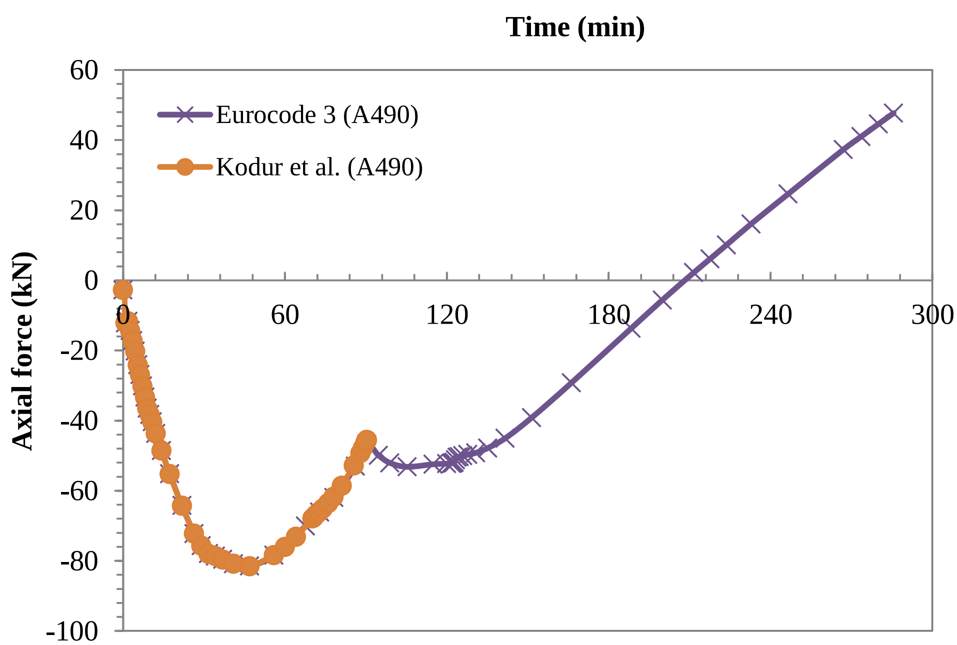

(b) A490 bolts

Figure 2.9: Progression of connection axial force as a function of fire exposure time for (a) A325 and (b) A490 bolts types with different material models

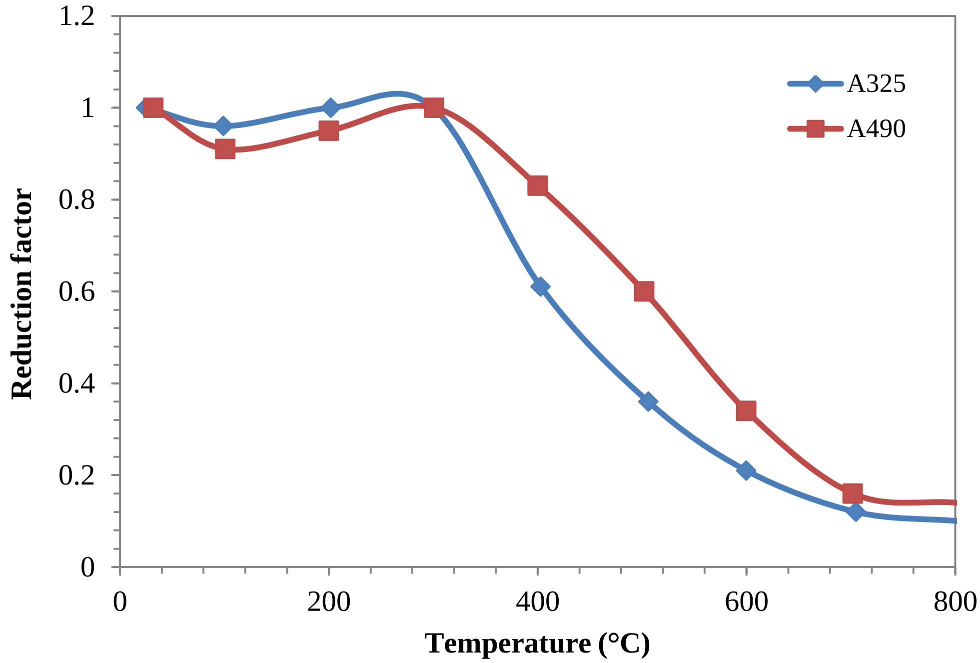

Figure 2.10: Variation in shear strength of A325 and A490 bolts with temperature

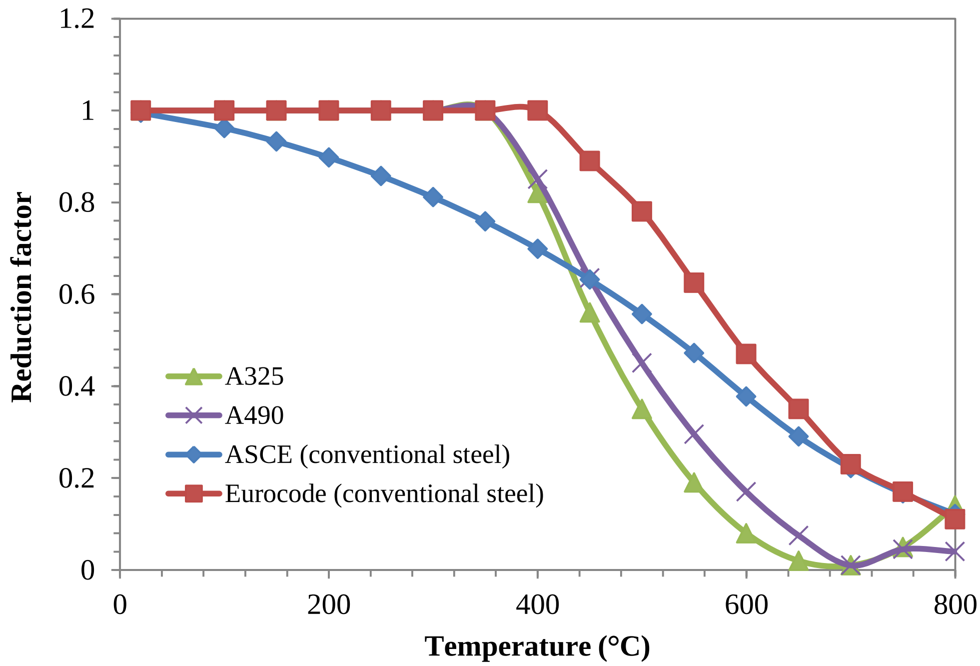

Figure 2.11: Comparison of high-temperature yield strength of A325 and A490 bolt steel with conventional steel

Chapter 3 figures

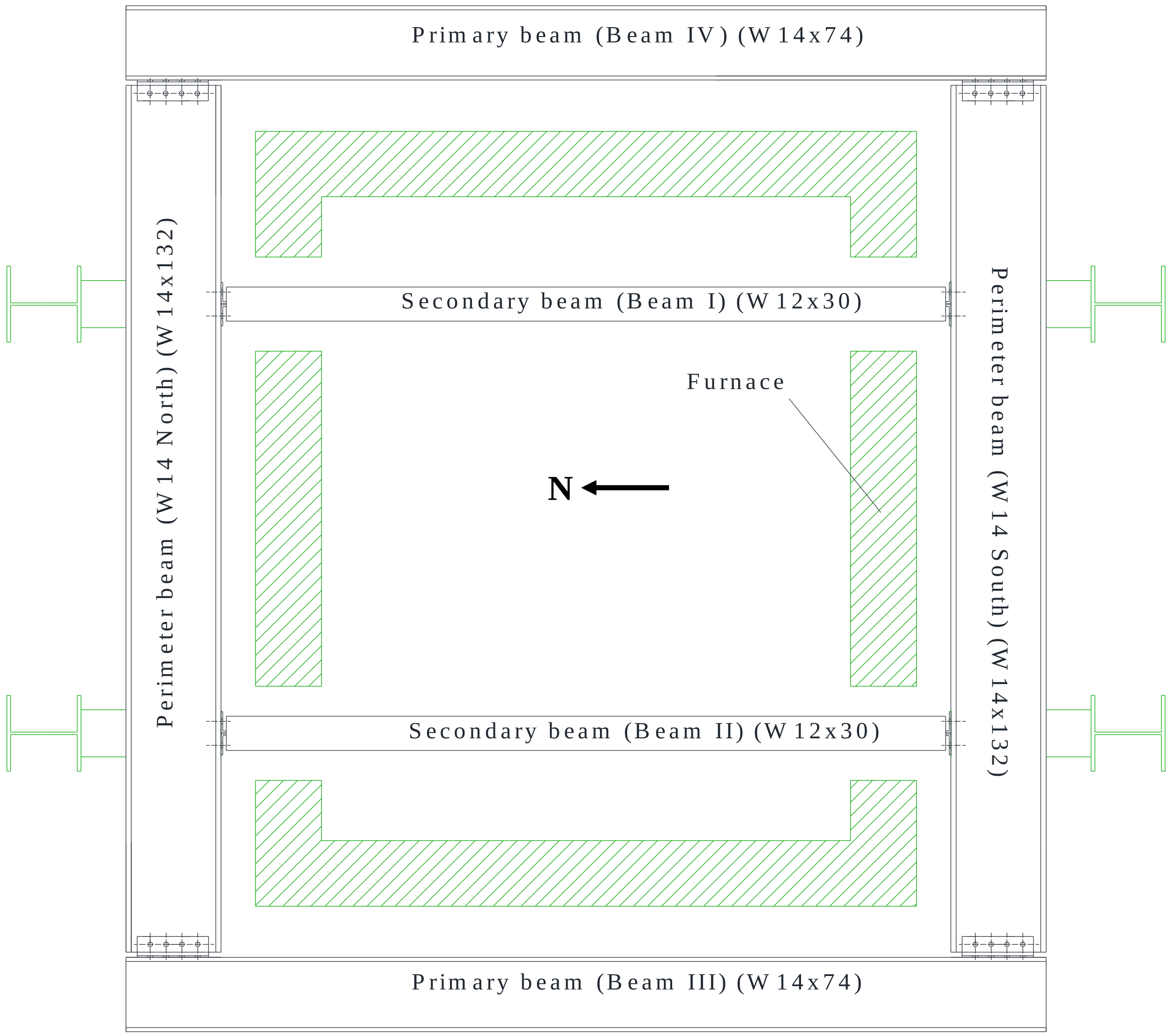

Figure 3.1: Layout of the steel beams used in test assemblies S1 and S2 (plan view)

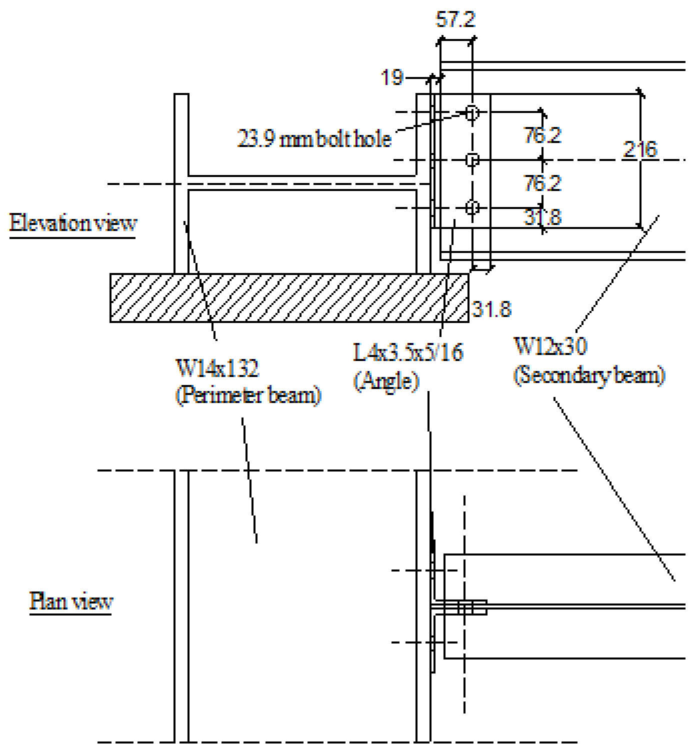

(a) Secondary and perimeter beam connection

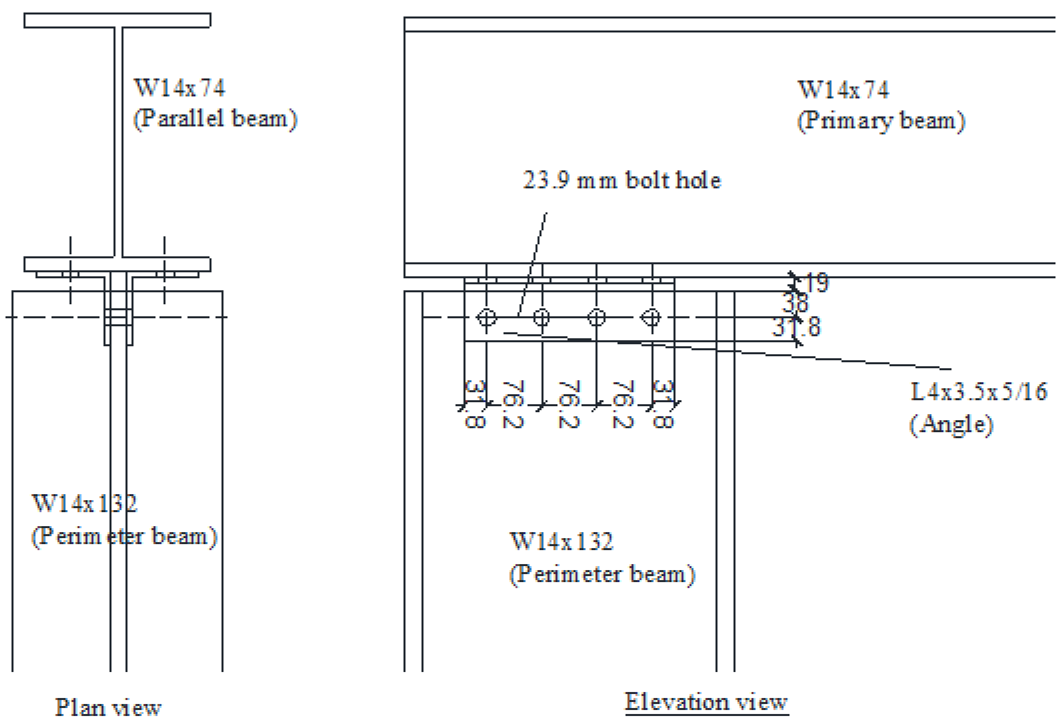

(b) Perimeter and primary beam connection

Figure 3.2: Connection details used in test assembly (all dimensions in mm)

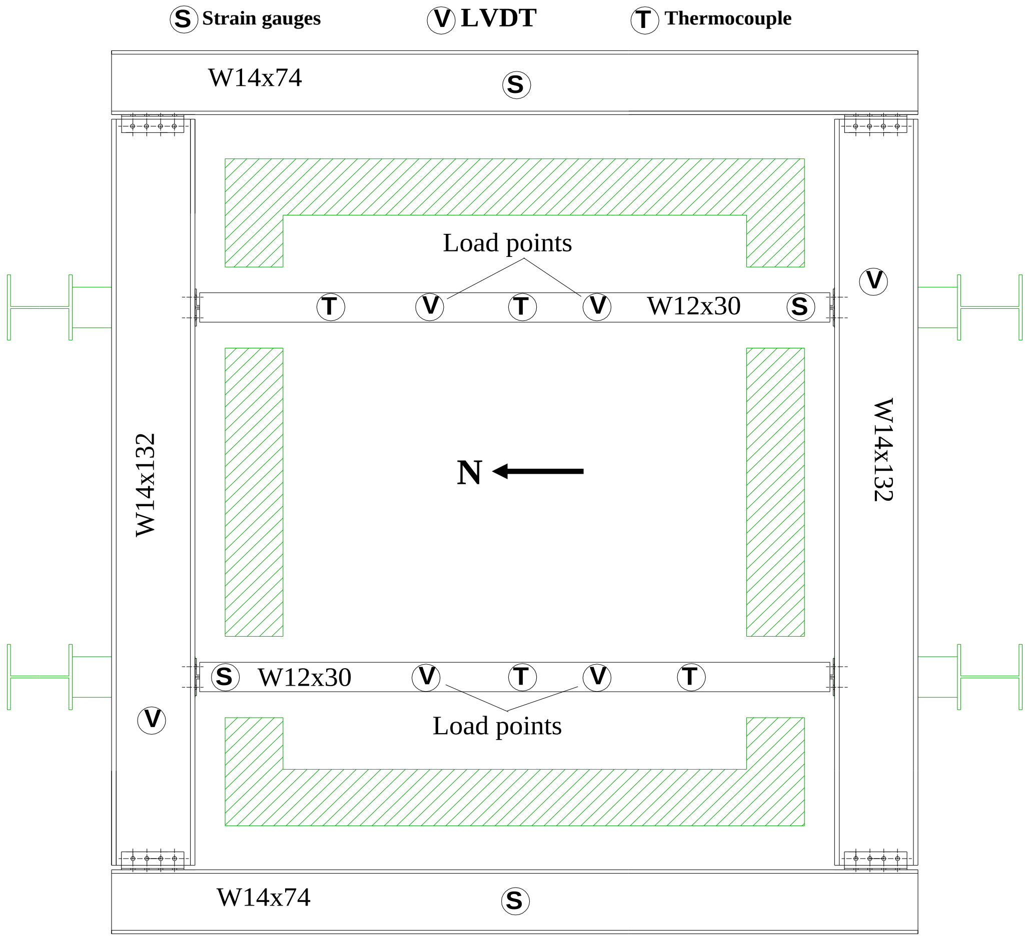

(a) Location of instrumentation, loading in the test assemblies

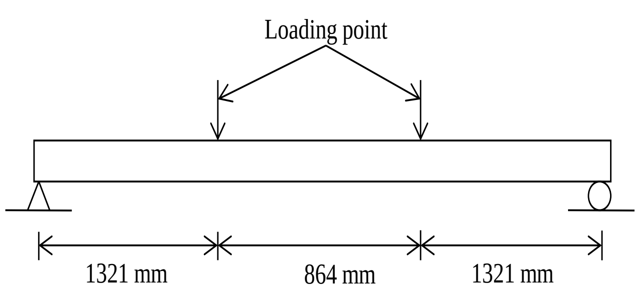

(b) Schematic of load configuration on secondary beam

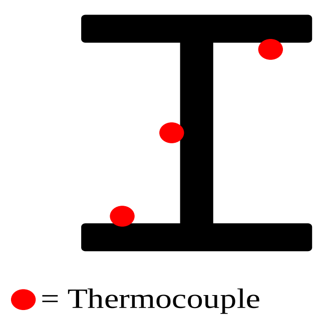

(c) Location of thermocouples along The secondary beam cross-section

Figure 3.3: Layout of the instrumentations and loading used in the steel beam assembly

Figure 3.3 (cont'd)

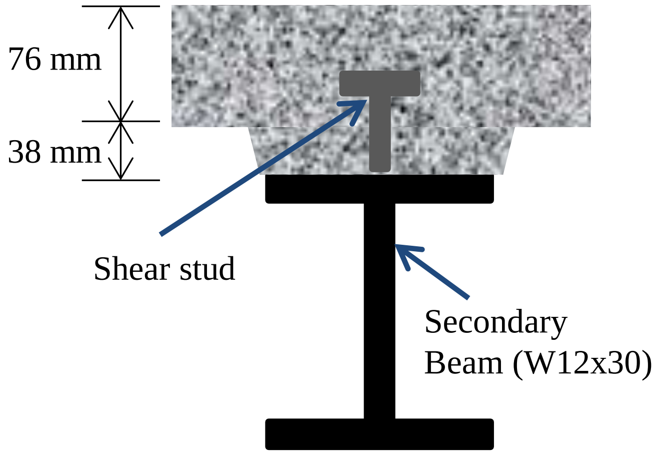

(d) Cross-sectional details of the beam and slab in assembly S2

Figure 3.4: Structural fire furnace at Michigan State University

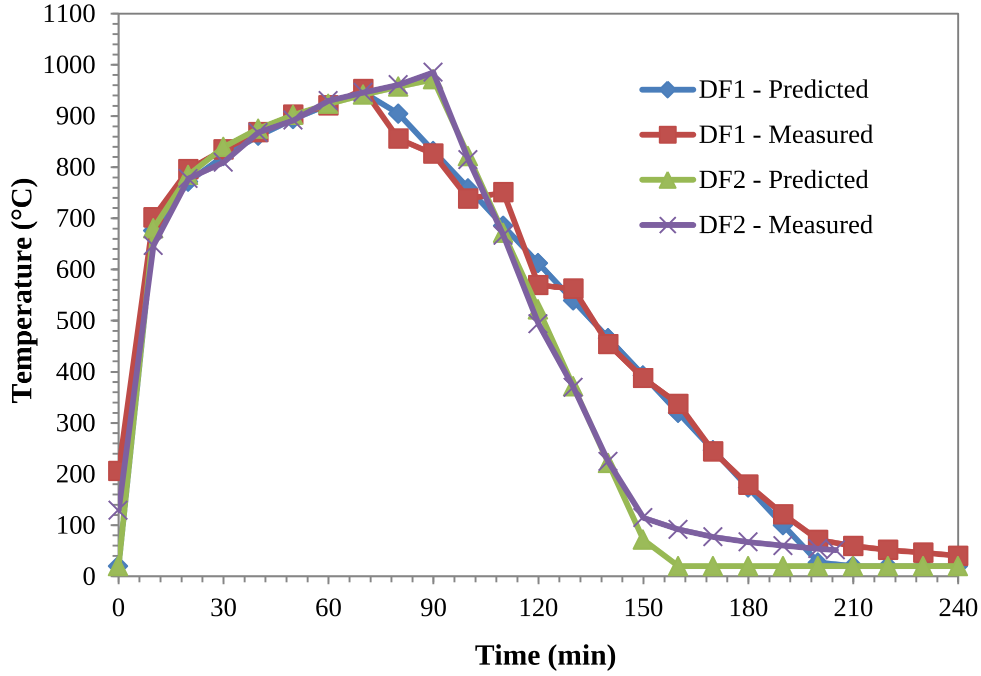

Figure 3.5: Predicted and measured time-temperature curves for design fires DF1 and DF2

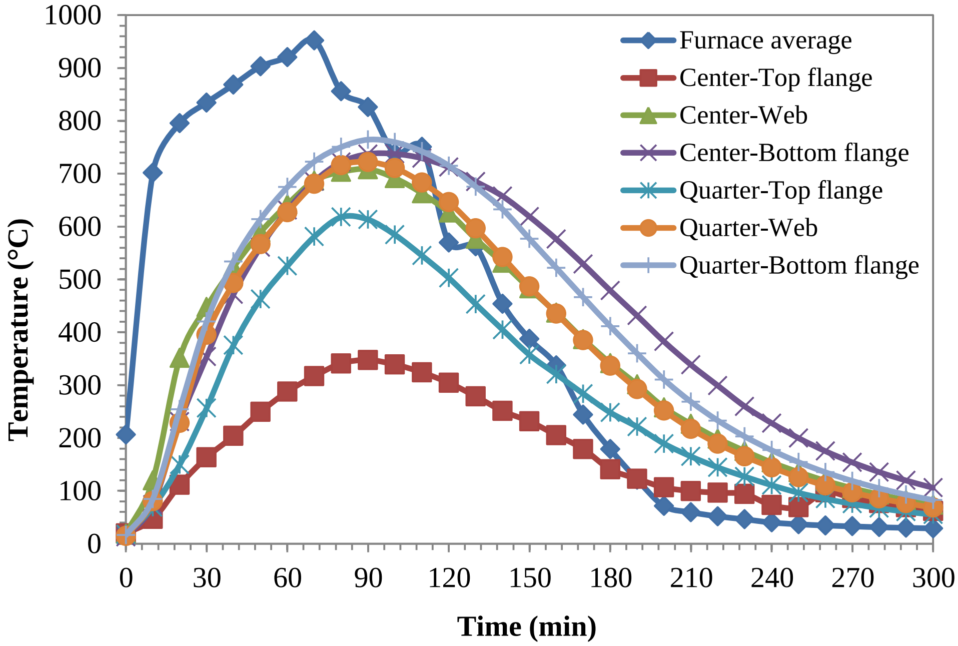

(a) S1- Beam I

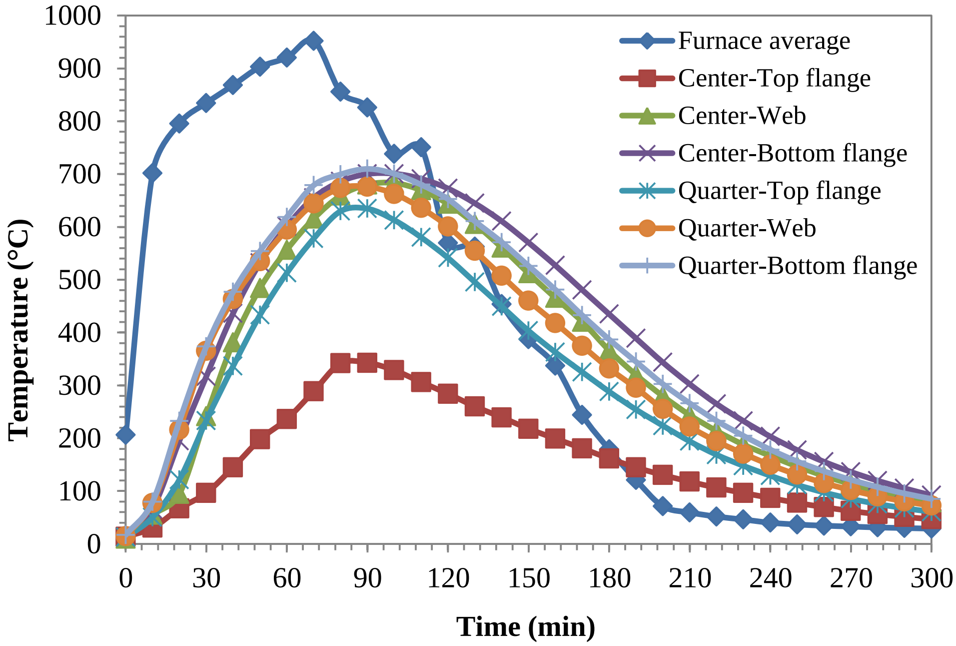

(b) S1- Beam II

Figure 3.6: Recorded temperatures at center (mid-span) and quarter span of the Beam I, Beam II of S1 as a function of fire exposure time (Refer to Fig. 3.1 for naming convention)

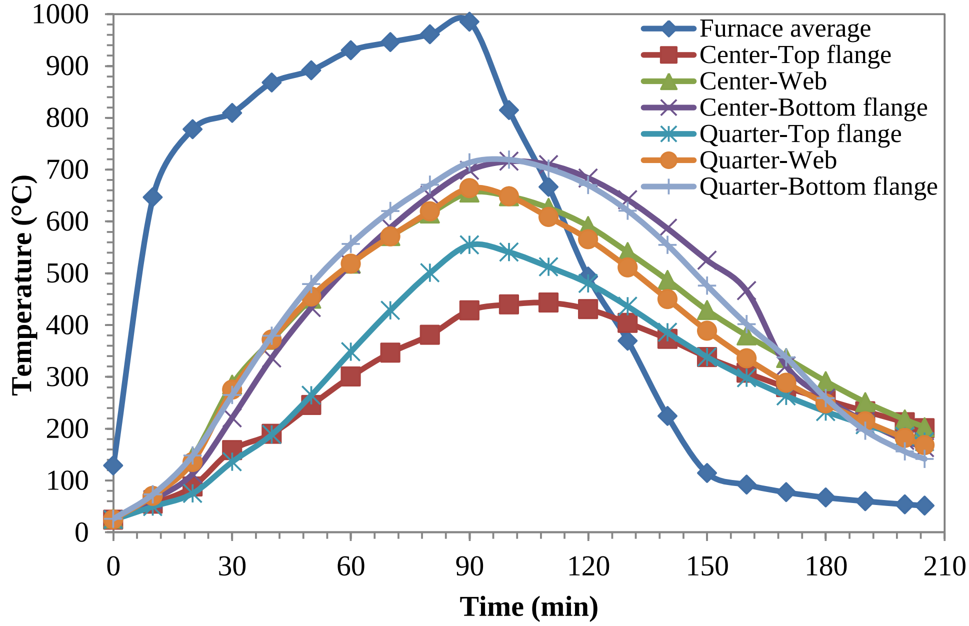

(a) S2- Beam I

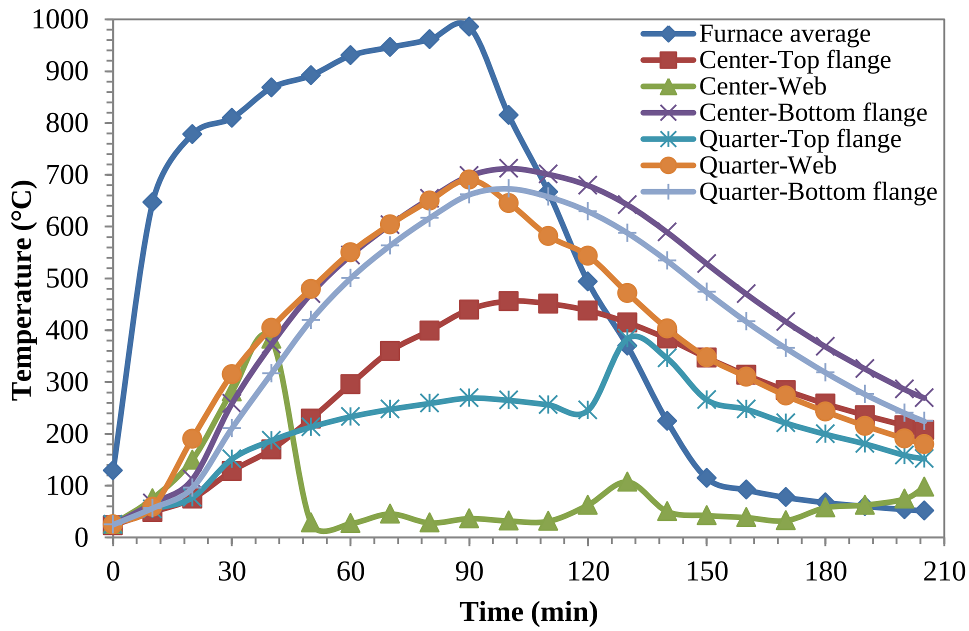

(b) S2- Beam II

Figure 3.7: Recorded temperatures at center (mid-span) and quarter span of the Beam I, Beam II of S2 as a function of fire exposure time (Refer to Fig. 3.1 for naming convention)

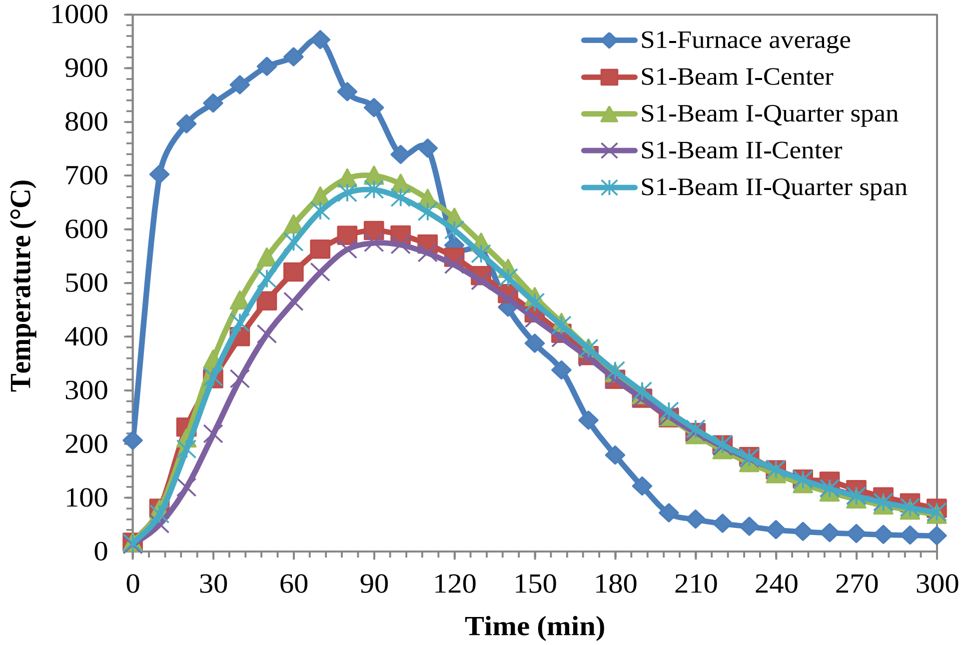

(a) S1

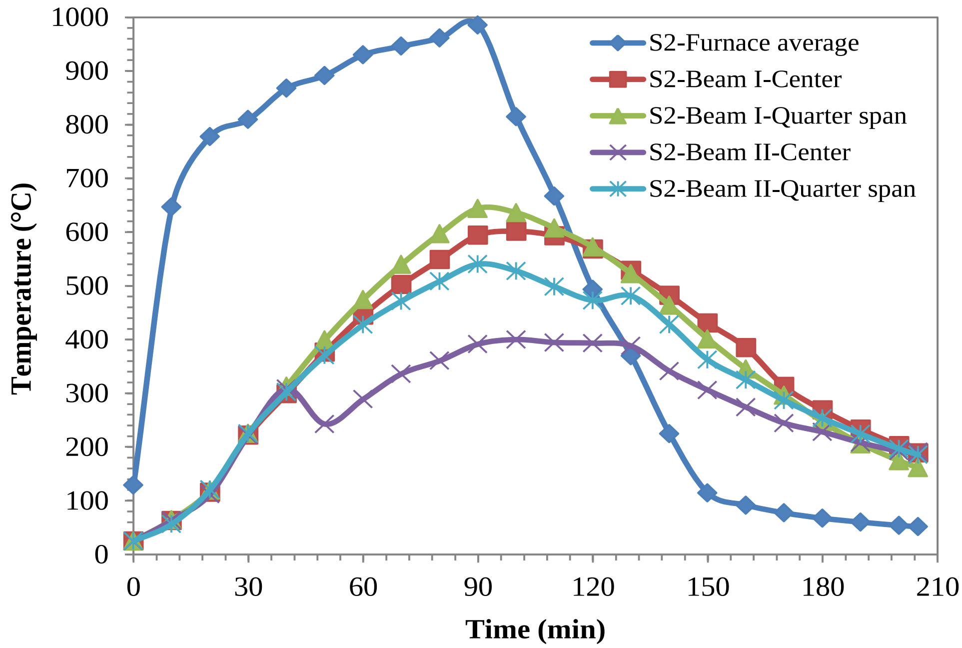

(b) S2

Figure 3.8: Recorded average temperatures at center (mid-span) and quarter span of the Beam I, Beam II of assemblies (a) S1 and (b) S2 as a function of fire exposure time (Refer to Fig. 3.1 for naming convention)

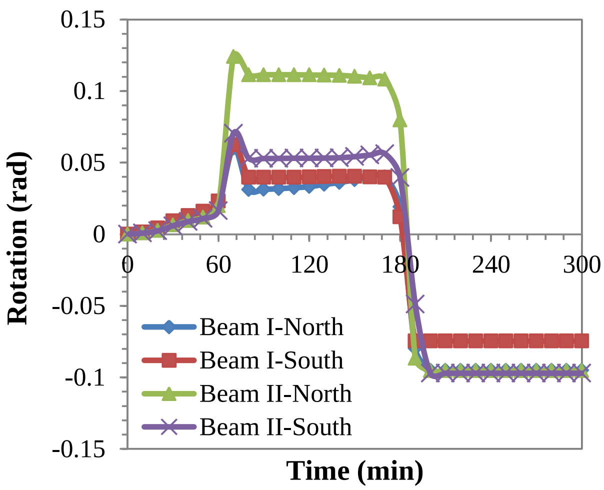

(a) S1

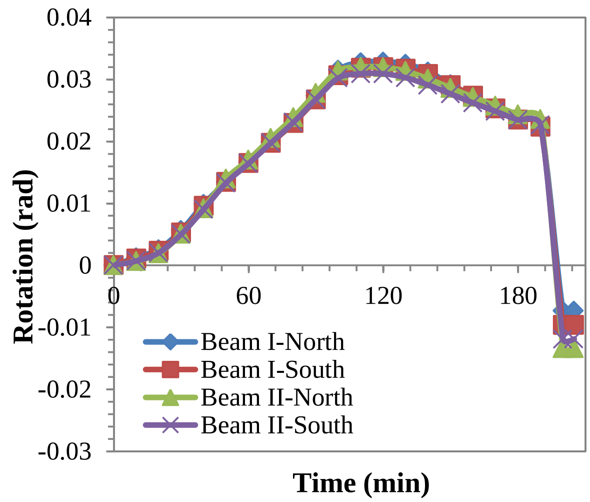

(b) S2

Figure 3.9: Connection rotation recorded as a function of fire exposure time in test assemblies (a) S1 and (b) S2

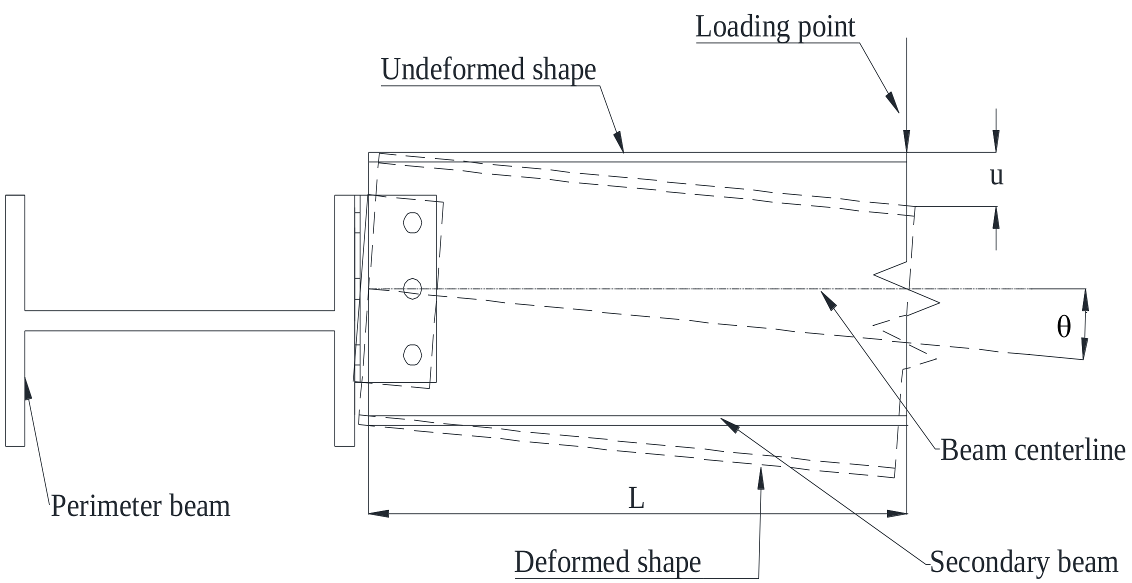

Figure 3.10: Schematic illustration of evaluating the rotation at connection

(a) Local buckling (b) Global buckling

Figure 3.11: (a) Local and (b) global buckling experienced by the secondary beam (Beam II – North) in assembly S1

(a) Top view (b) Bottom view

Figure 3.12: Warping and distortion of the metal deck in test assembly S1

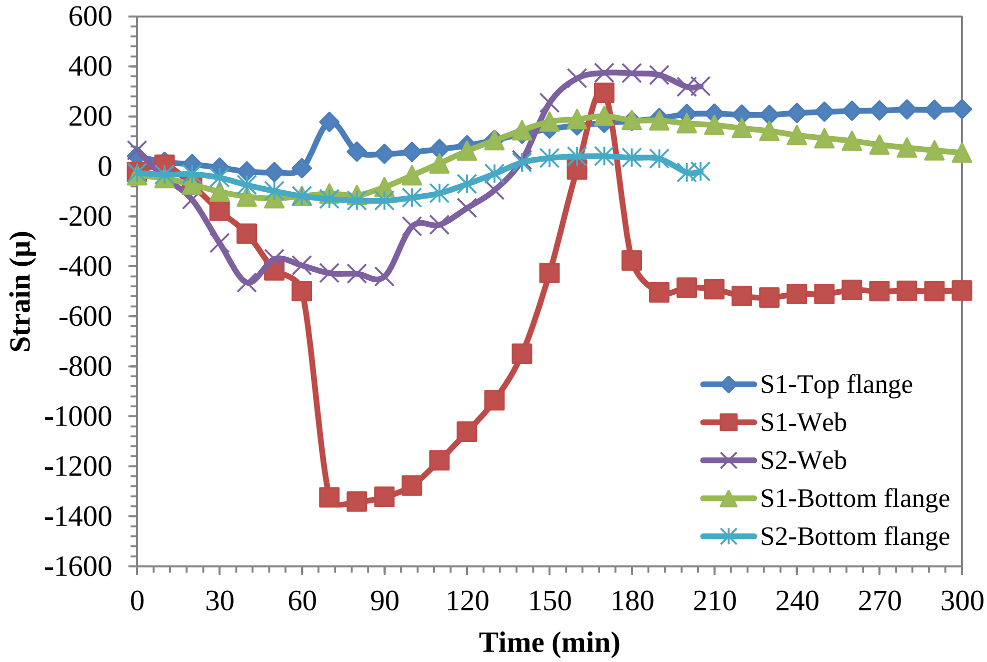

(a) Beam I (Secondary beam)

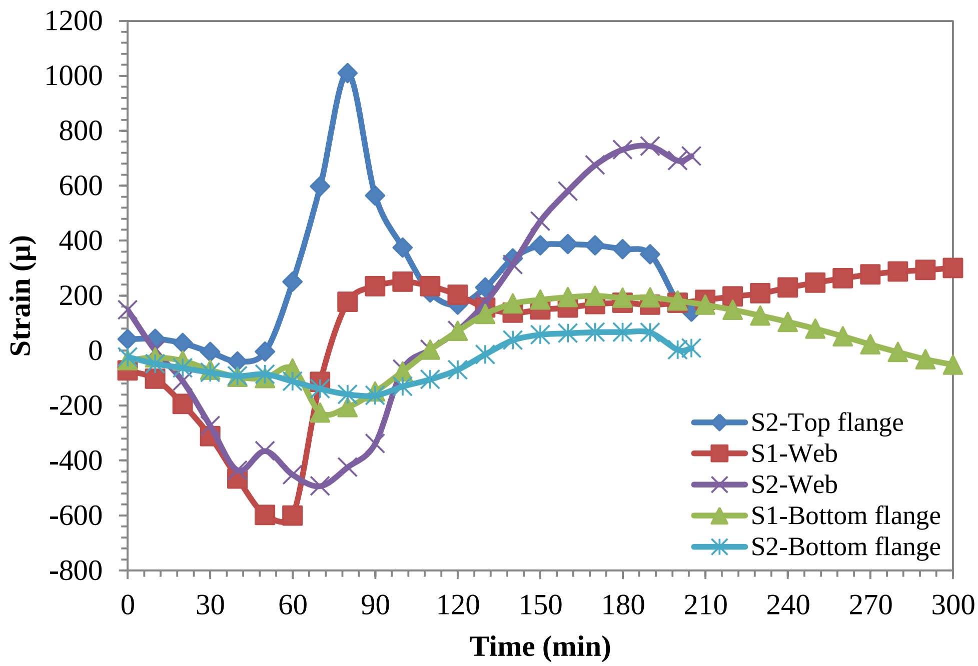

(b) Beam II (Secondary beam)

Figure 3.13: Variation of strains in secondary and primary beam as a function of fire exposure time (Refer to Fig. 3.1 for naming convention)

Figure 3.13 (cont'd)

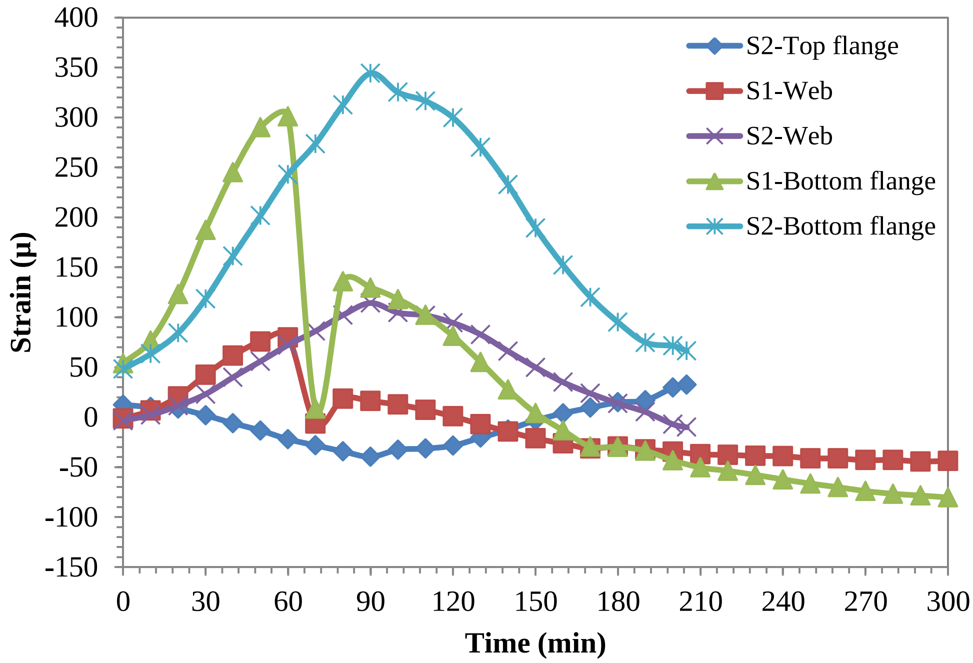

(c) Beam III (Primary beam)

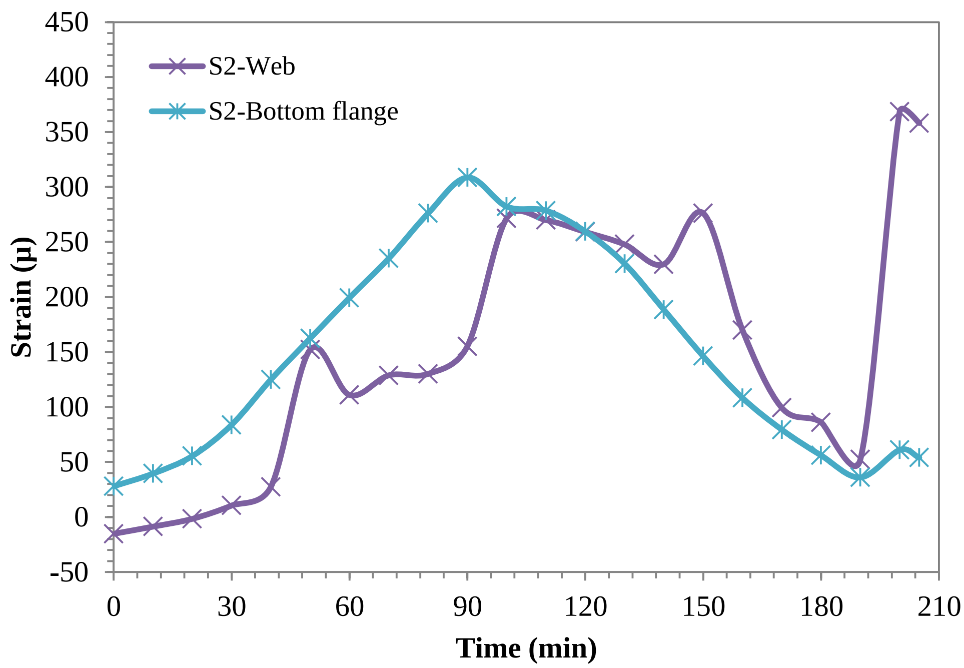

(d) Beam IV (Primary beam)

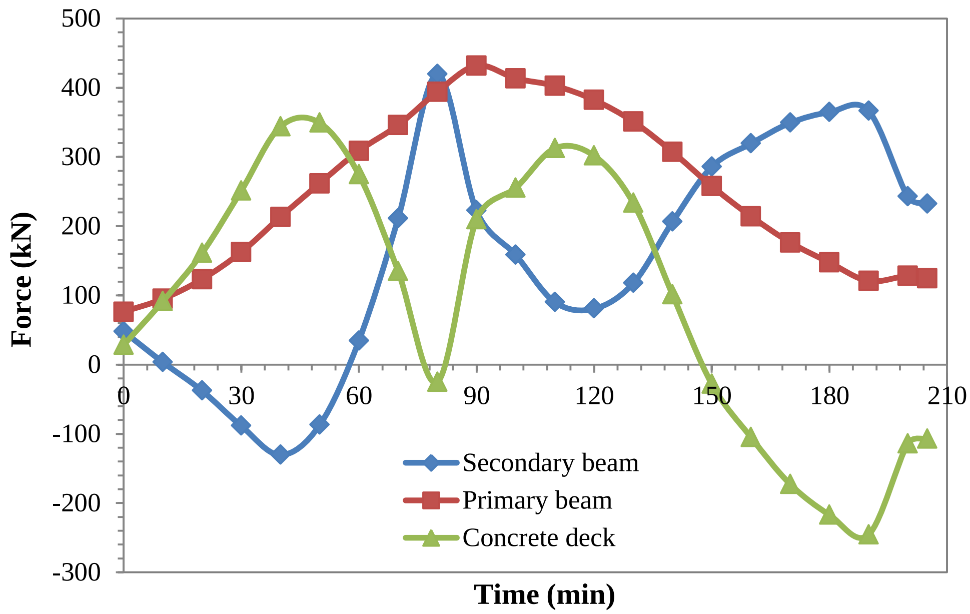

Figure 3.14: Variation of axial forces in secondary, primary beams and concrete deck as a function of fire exposure time

(a) Insulation fall off

(b) Local buckling of top flange and web

(c) Rotation of the beam end (top view)

(d) Rotation of the beam end (elevation)

Figure 3.15: (a) Local and (b) global buckling experienced by the secondary beam (Beam II-North) in assembly S1

(a) Beginning of cracking in the slab

(b) Concrete fragment spalled-off from slab

(c) Warping of the deck

(d) Insulation fall-off from deck and beams

Figure 3.16: Visual observations in the test assembly S2 during and after fire test

Chapter 4 figures

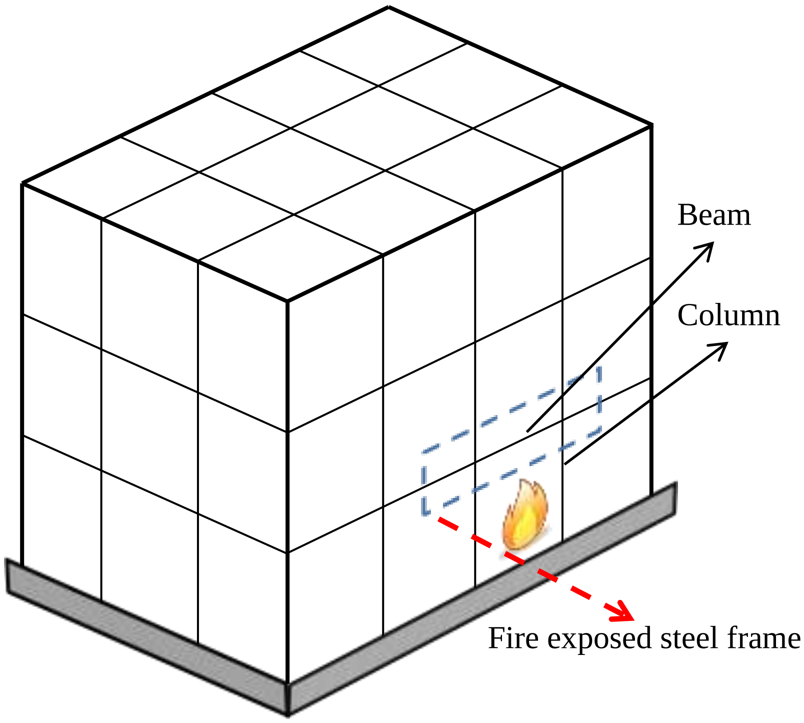

(a) Three dimensional perspective view of steel framed building

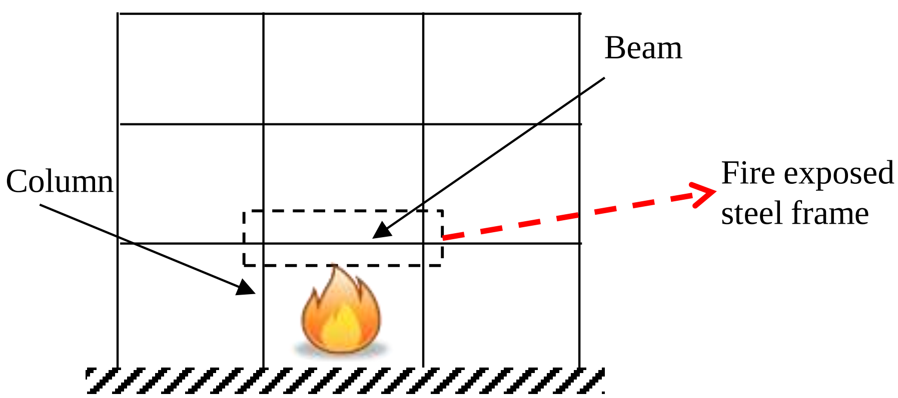

(b) Two dimensional view of steel framed building

Figure 4.1: Typical connection in a steel framed building along with different structural components present in connection region

Figure 4.1 (cont'd)

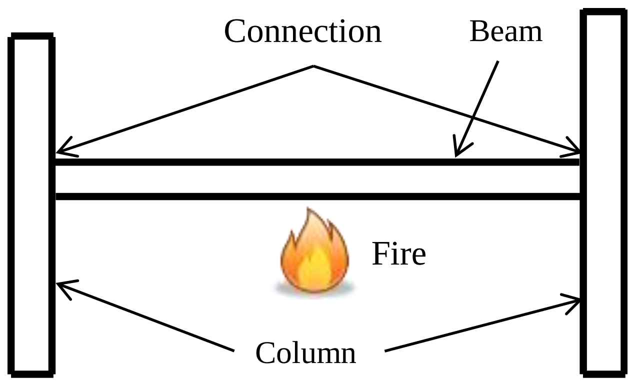

(c) Fire exposed steel frame

Figure 4.1 (cont'd)

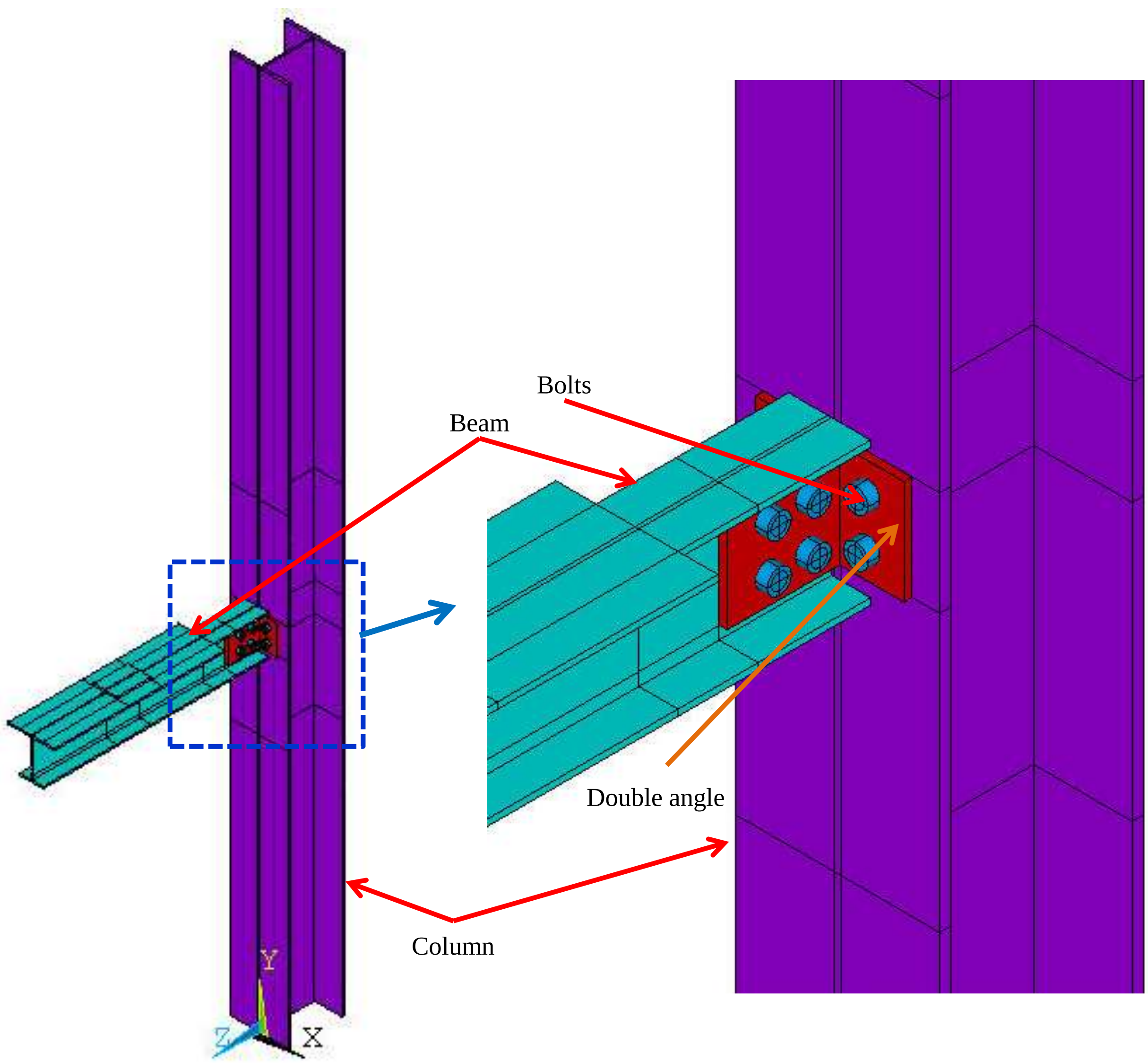

(d) Geometry of fire exposed steel frame

(e) Close up of connection region

Figure 4.1 (cont'd)

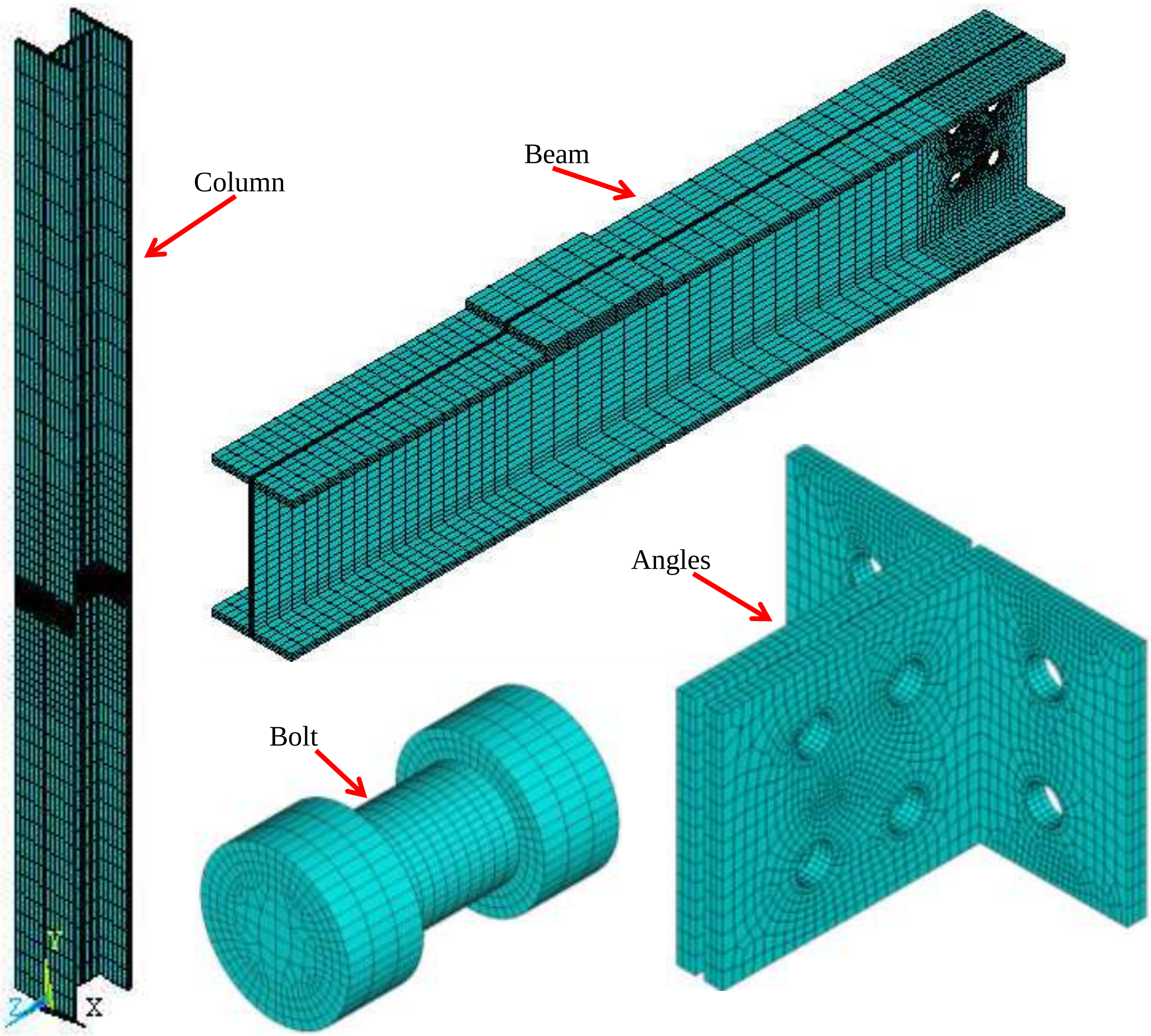

(f) Different structural components present in connection region

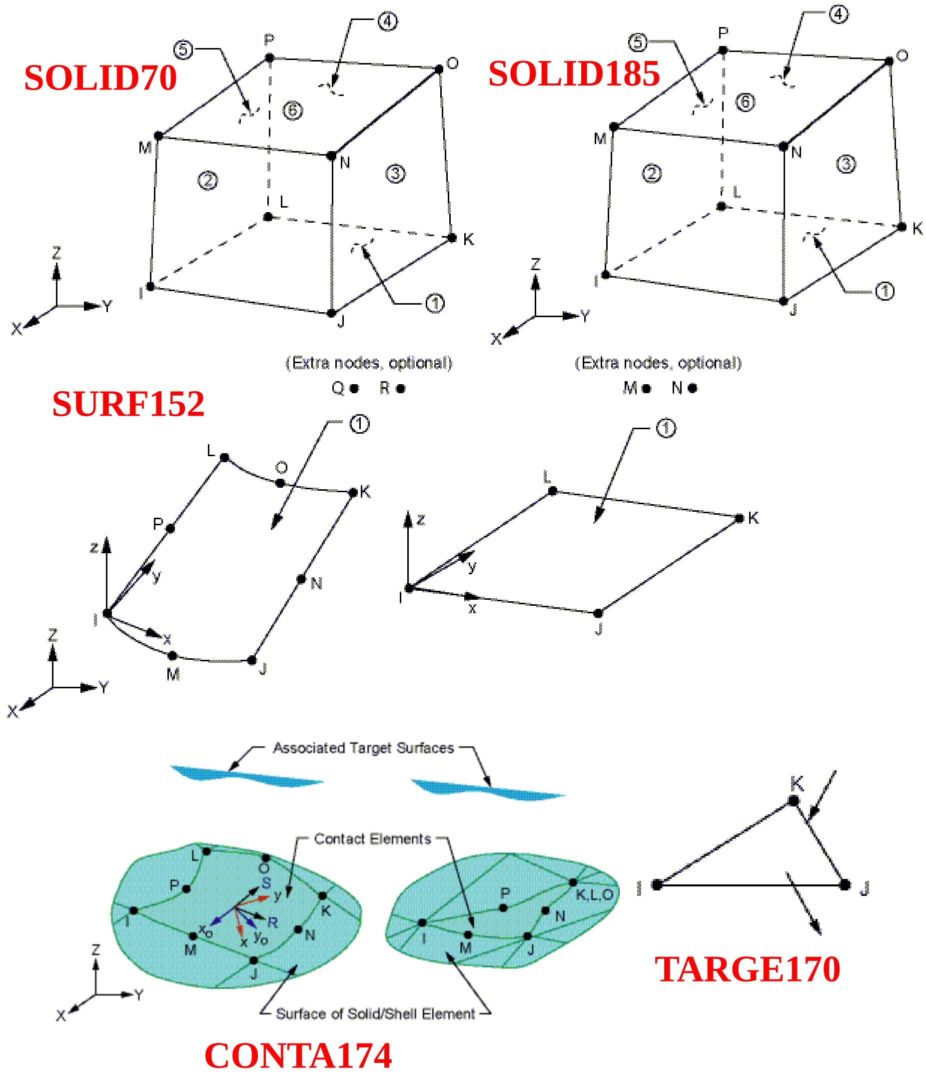

Figure 4.2: Different types of finite elements used for thermal and structural analysis in the model

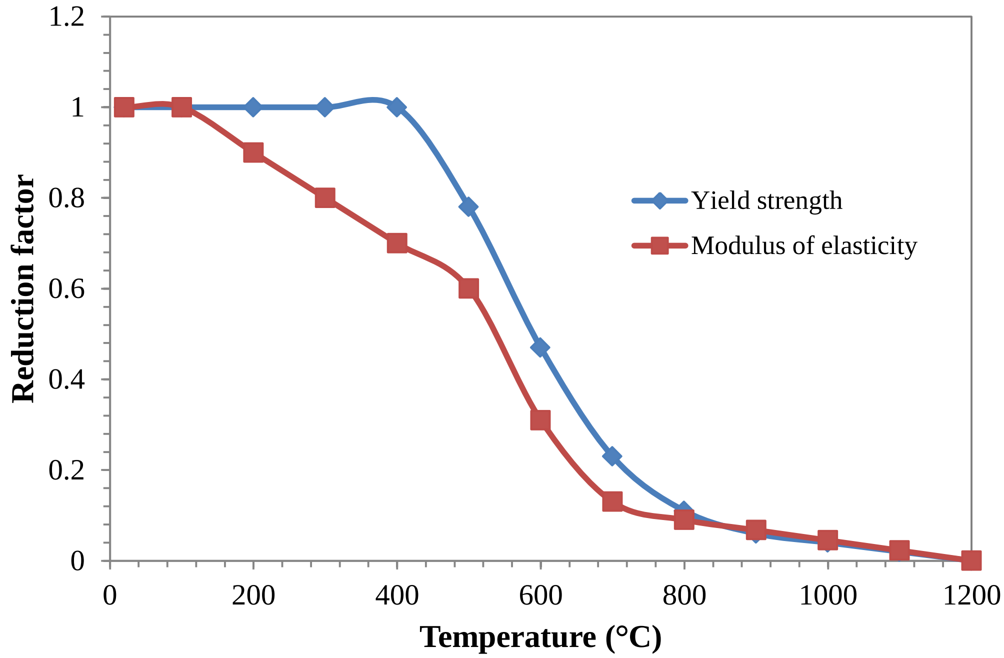

Figure 4.3: Strength reduction factors for steel specified in Eurocode 3

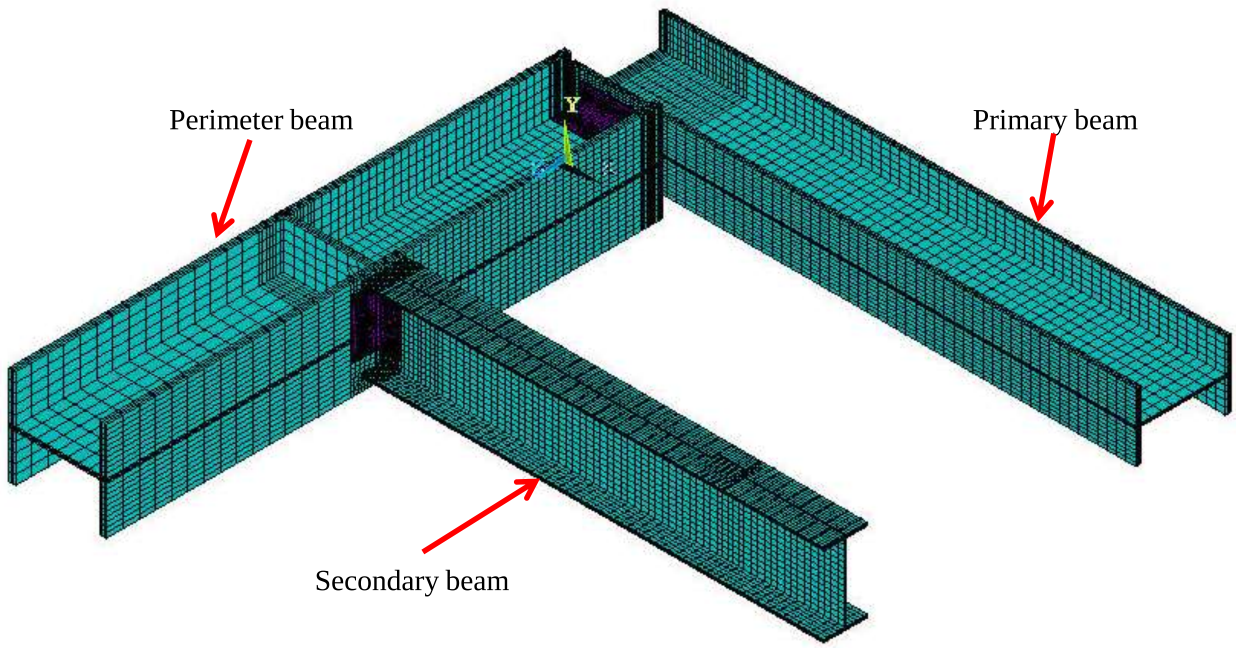

(a) S1

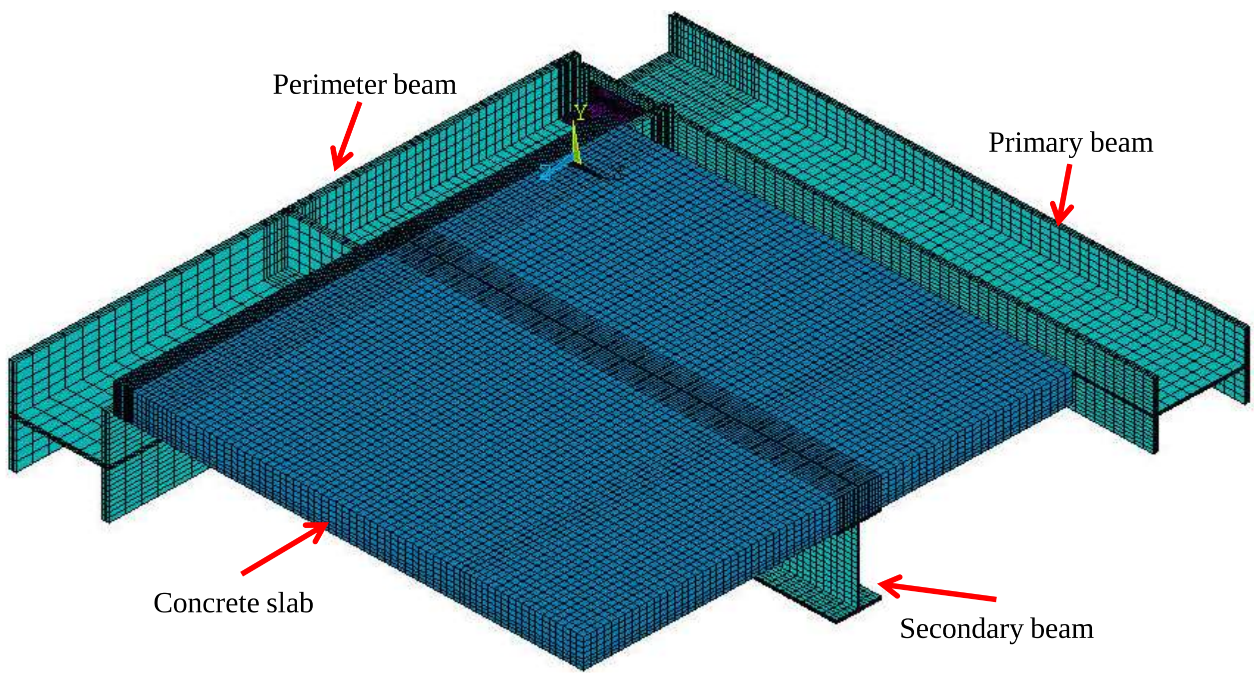

(b) S2

Figure 4.4: Discretized geometry (quarter) of the connection assembly (FEM1) modeled in ANSYS

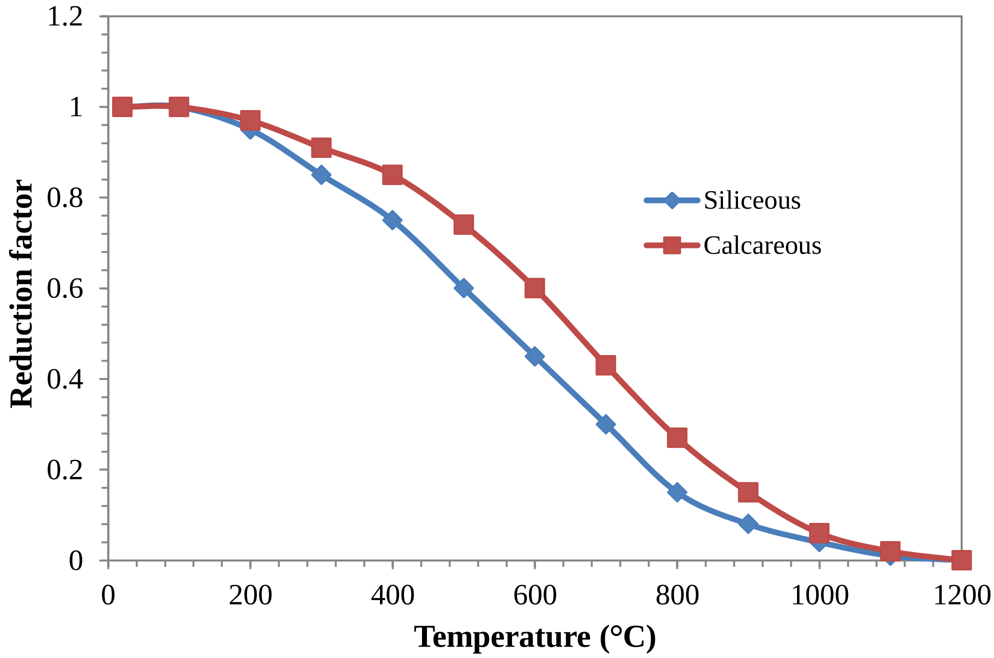

Figure 4.5: Strength reduction factors for different aggregate concrete specified in Eurocode 2

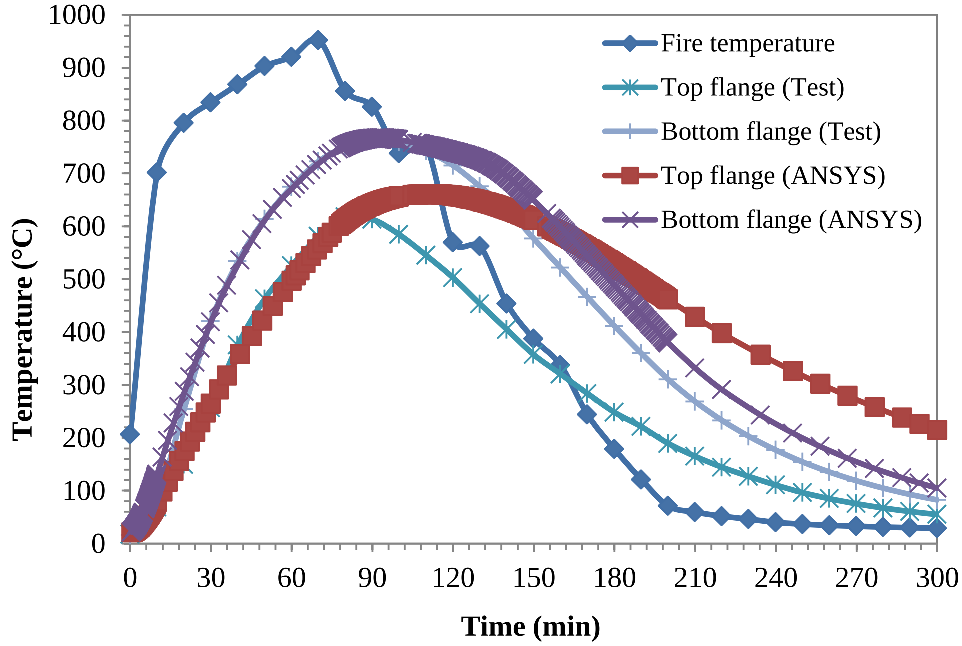

(a) S1

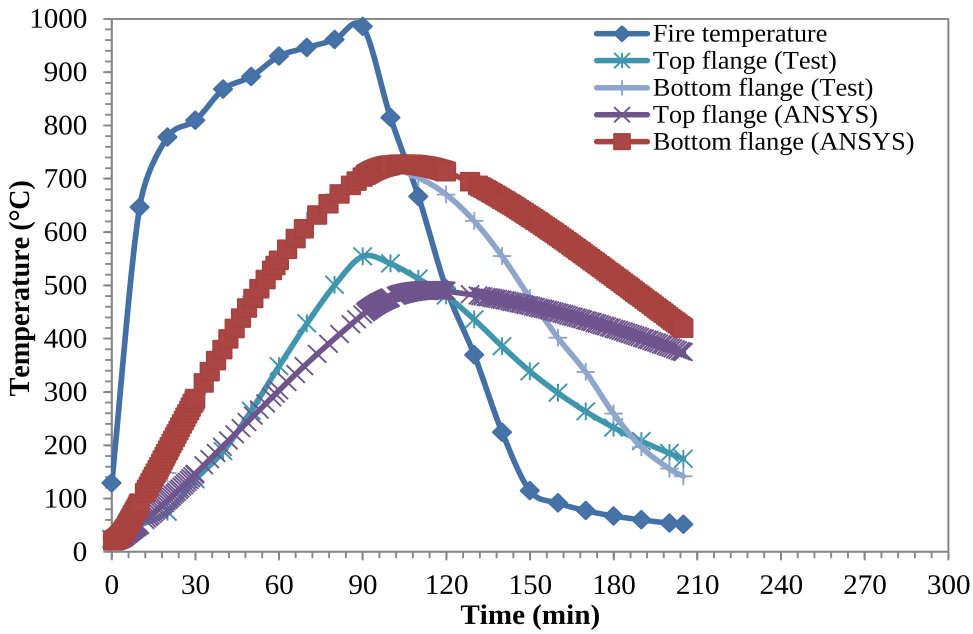

(b) S2

Figure 4.6: Comparison of measured and predicted secondary beam temperatures (top and bottom flanges) in tested assemblies (a) S1 and (b) S2

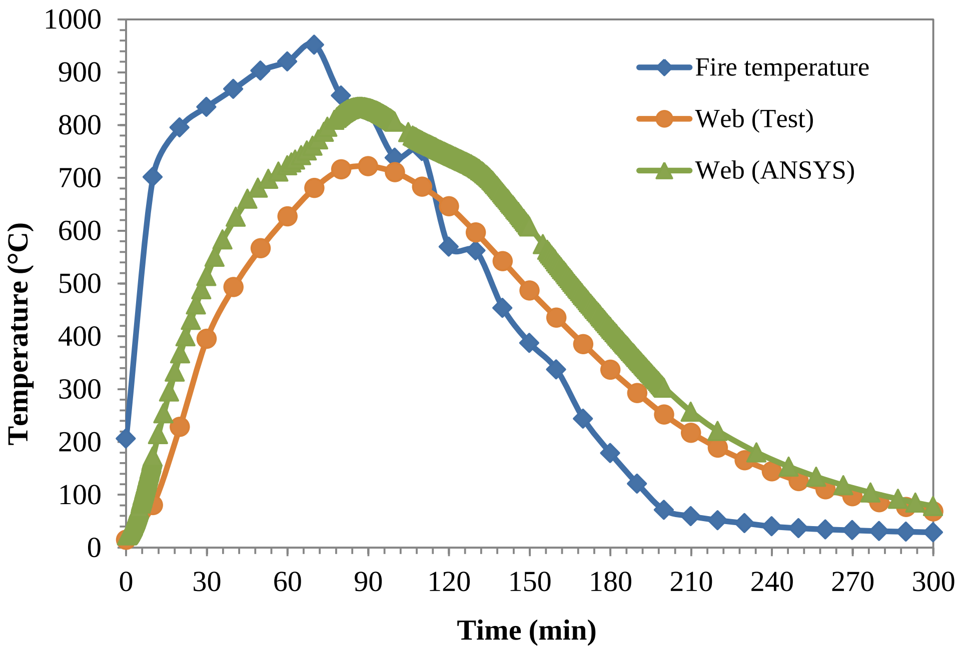

(a) S1

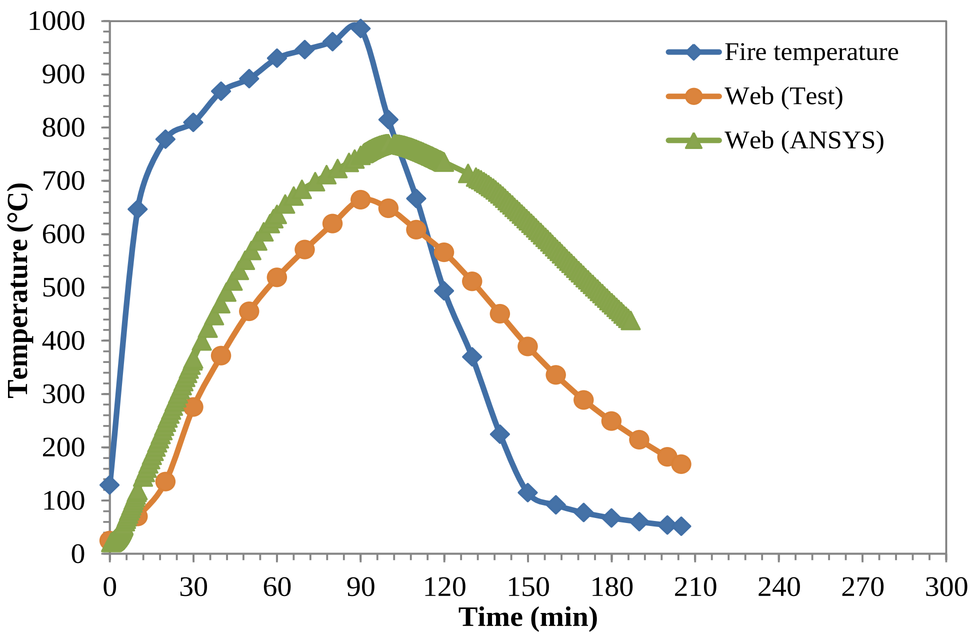

(b) S2

Figure 4.7: Comparison of measured and predicted secondary beam temperatures (web) in tested assemblies (a) S1 and (b) S2

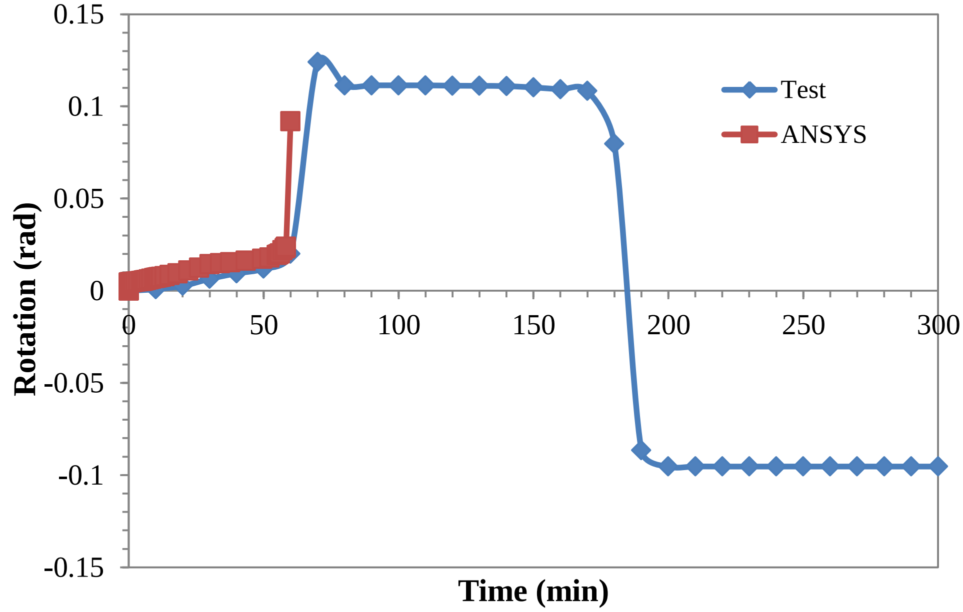

(a) S1

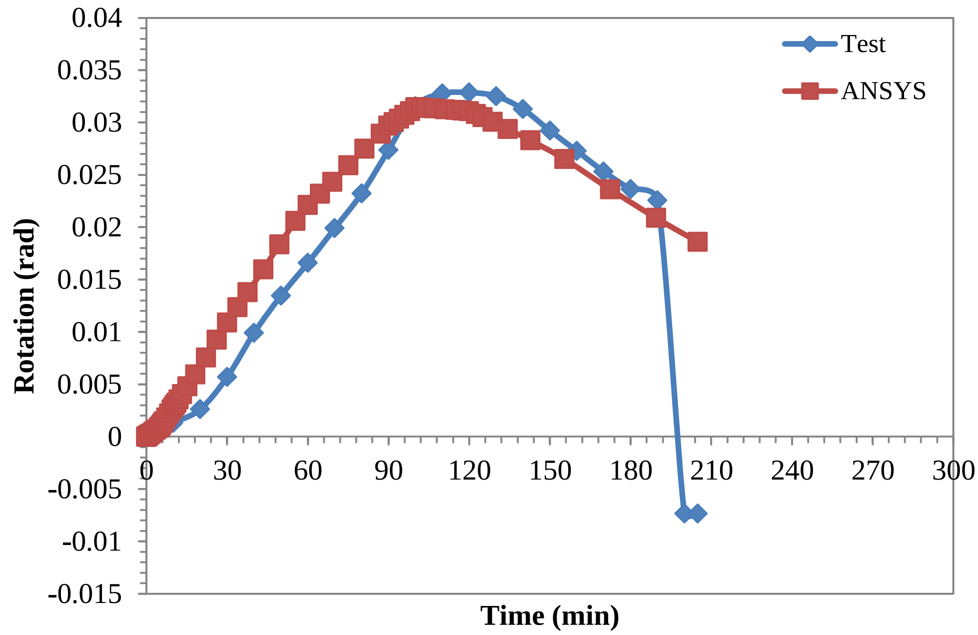

(b) S2

Figure 4.8: Comparison of predicted and measured connections rotation as a function of fire exposure time in test assemblies (a) S1 and (b) S2

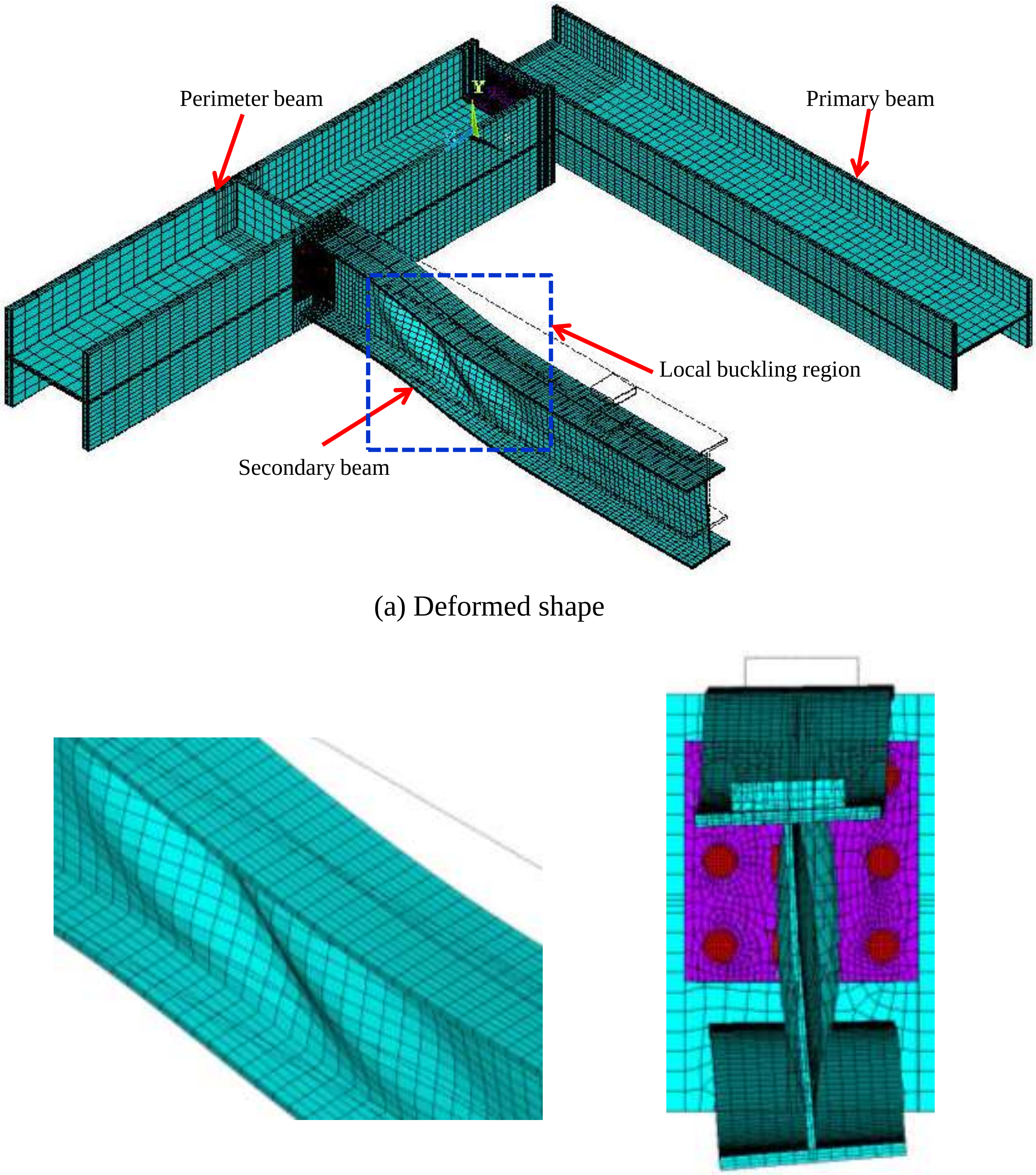

(a) Deformed shape

(b) Local buckling

(c) Lateral torsional buckling

Figure 4.9: Illustration of (a) deformed shape (b) local buckling of secondary beam and (c) lateral torsional buckling of secondary beam in assembly S1 predicted by the numerical model

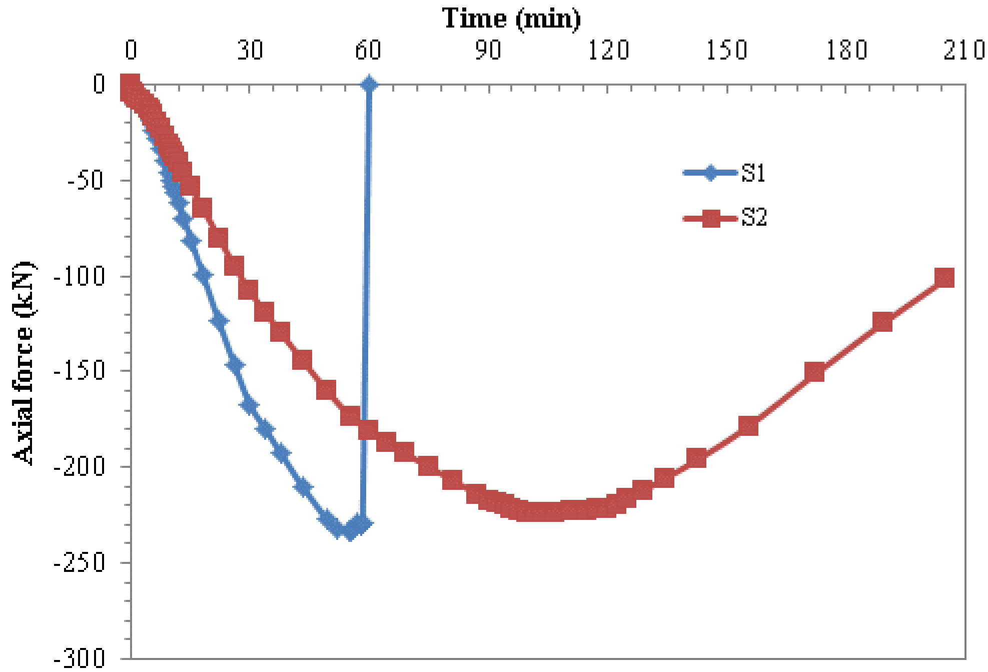

Figure 4.10: Fire induced axial forces on connections predicted as a function of fire exposure time (from model FEM1) in test assemblies (a) S1 and (b) S2

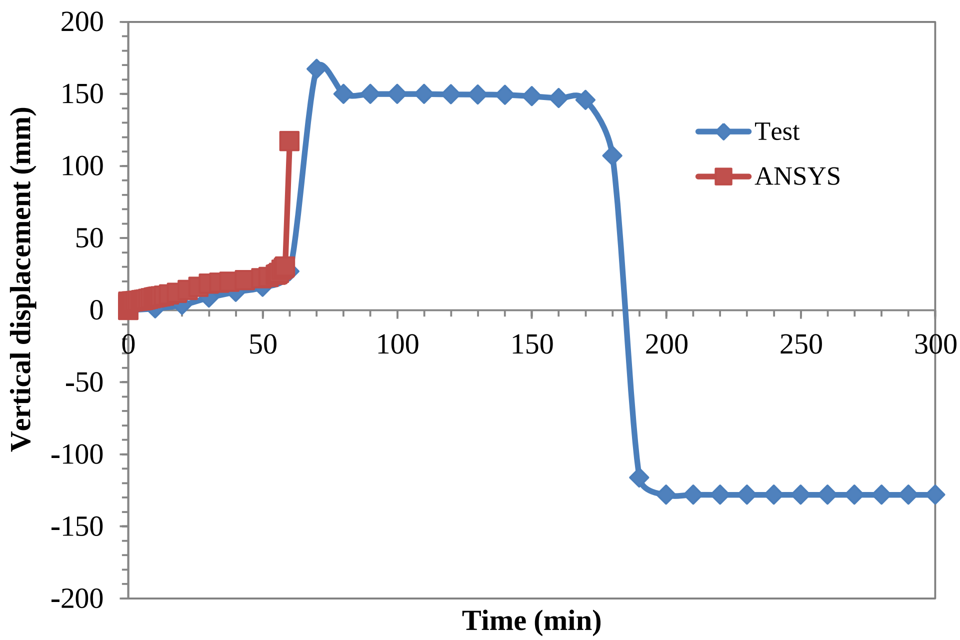

(a) S1

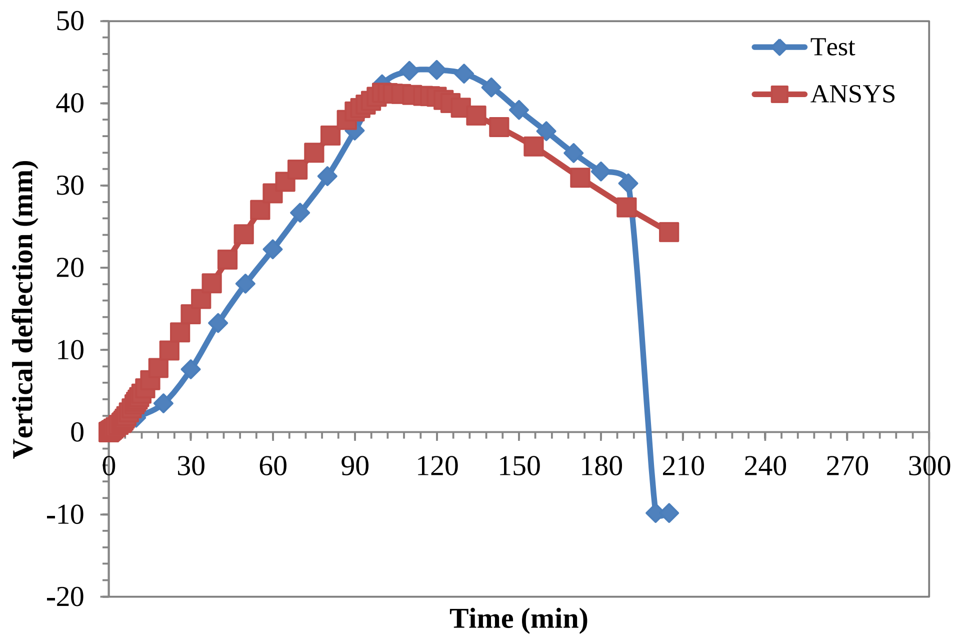

(b) S2

Figure 4.11: Vertical deflection of secondary beams (at loading actuator) predicted as a function of fire exposure time (from model FEM1) in test assemblies (a) S1 and (b) S2

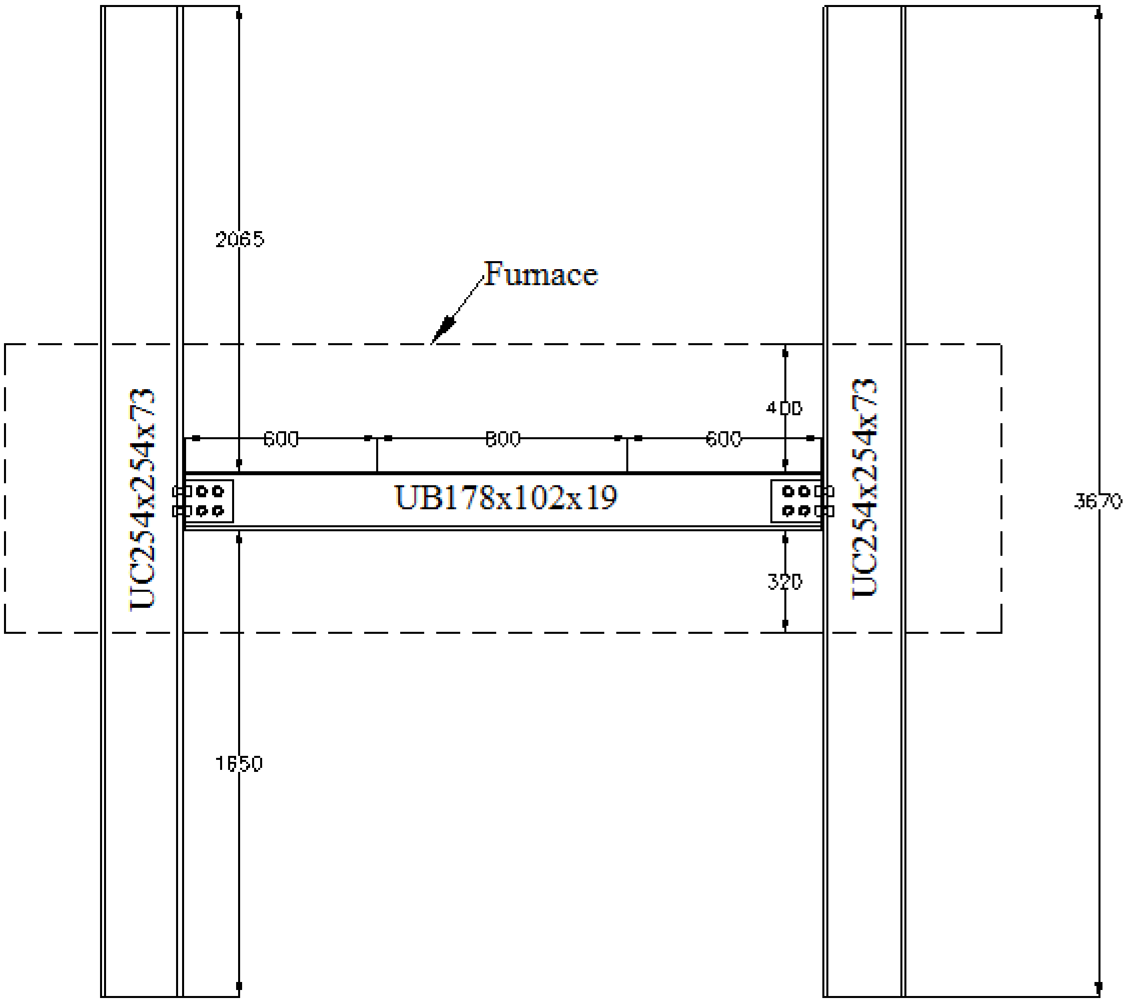

(a) Layout of the connection assembly

Figure 4.12: Geometrical details of the connection assembly used in the second finite element model FEM2 (all dimensions in mm)

Figure 4.12 (cont'd)

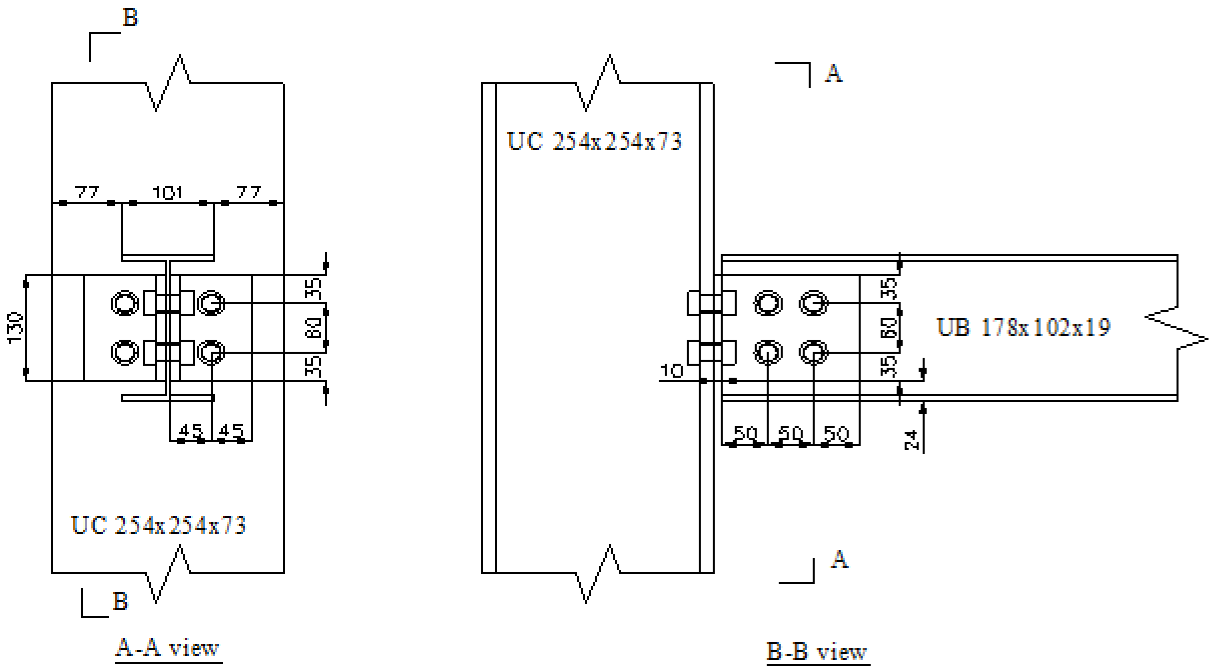

(b) Dimensions of the double angle connection

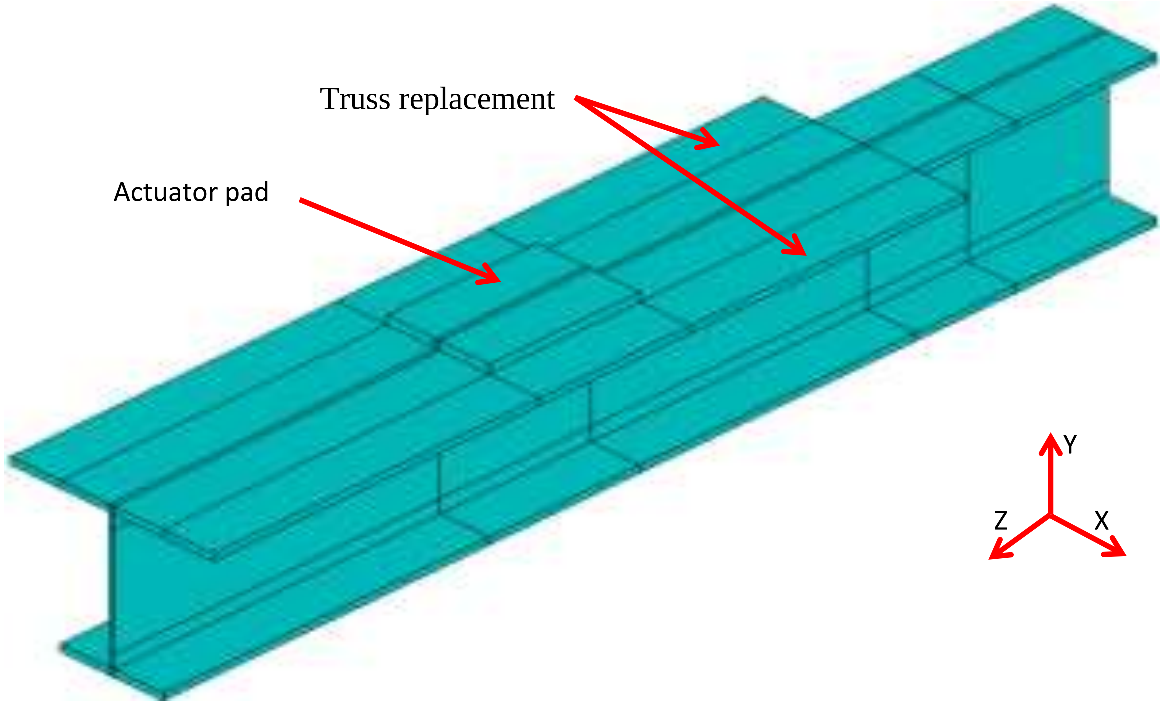

Figure 4.13: Modeling of truss replacement and actuator pad

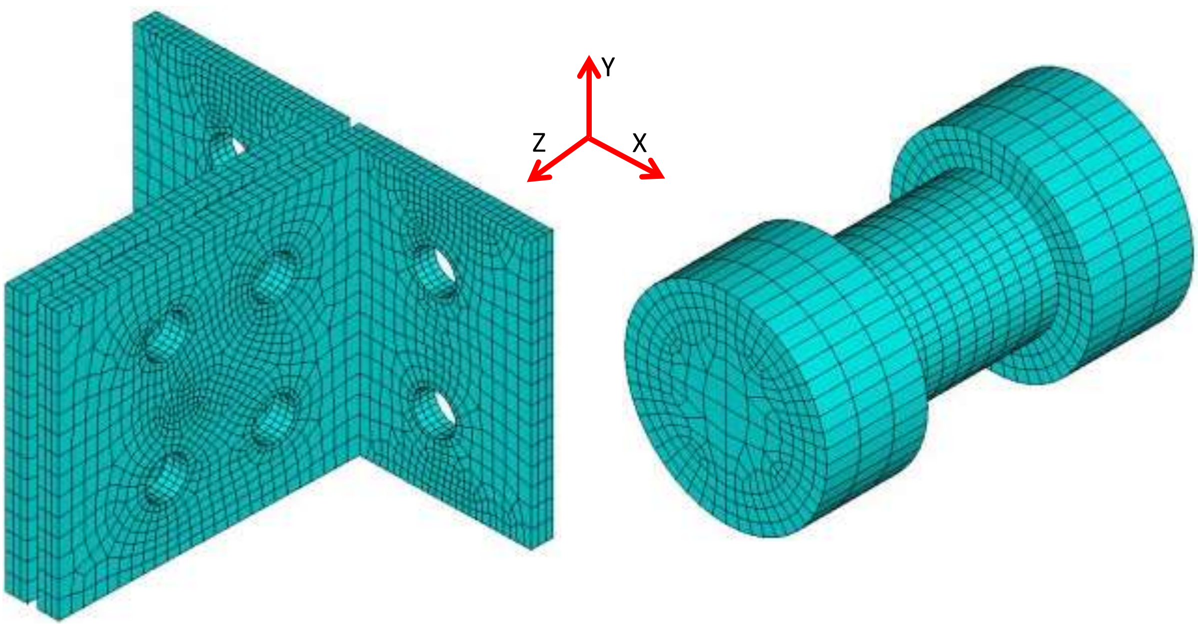

(a) Angles

(b) Bolt

Figure 4.14: Discretization of connection components (a) angles and (b) bolt

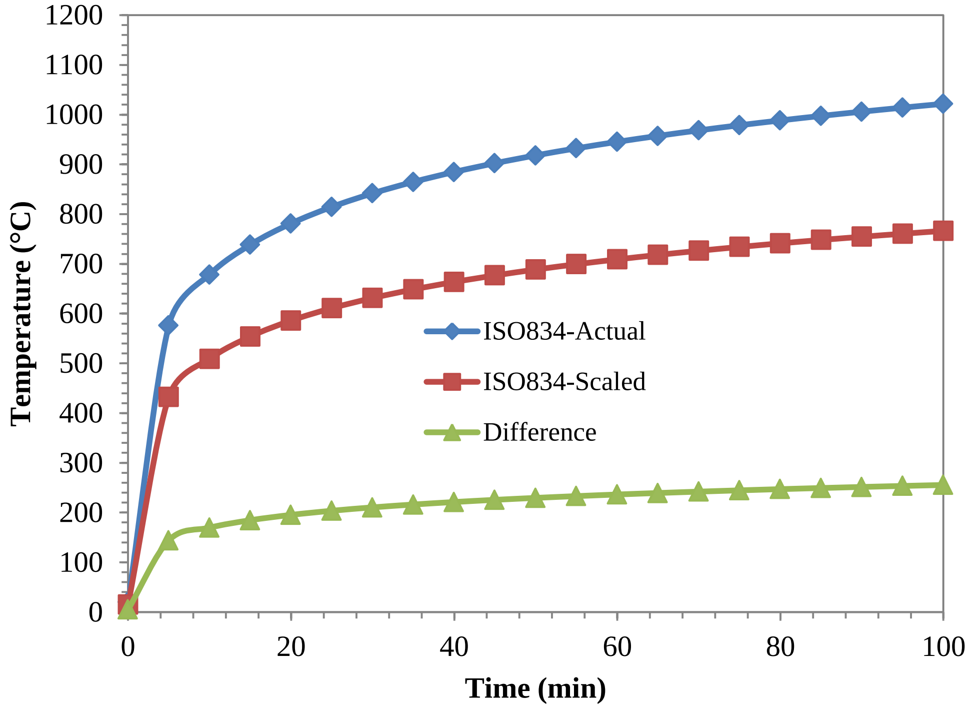

Figure 4.15: Standard and adjusted ISO834 standard fire time-temperature curves

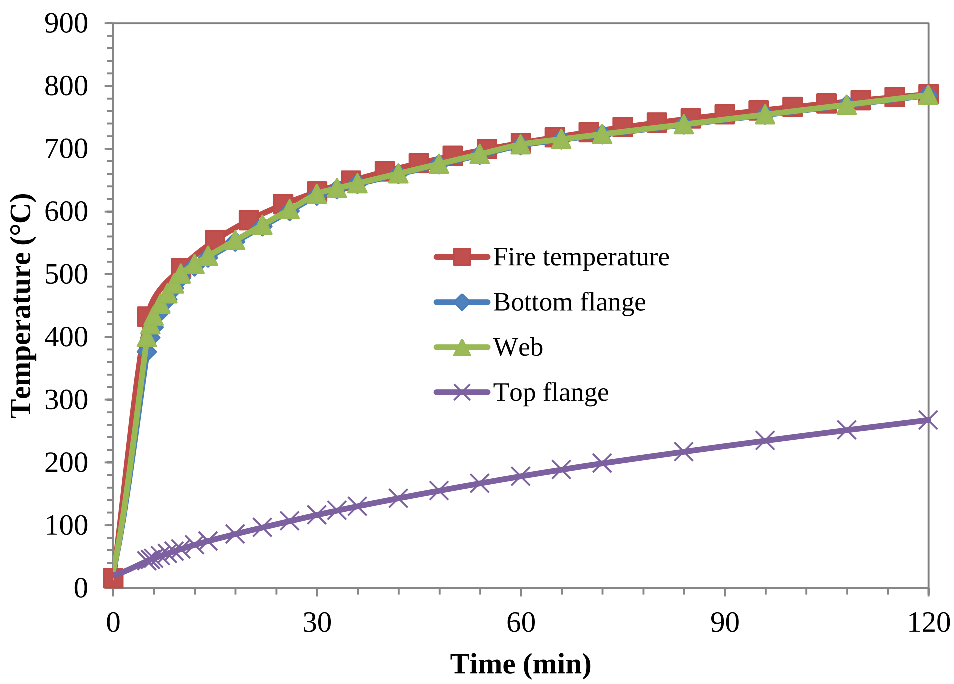

Figure 4.16: Predicted temperature distribution in the beam as a function of fire exposure time

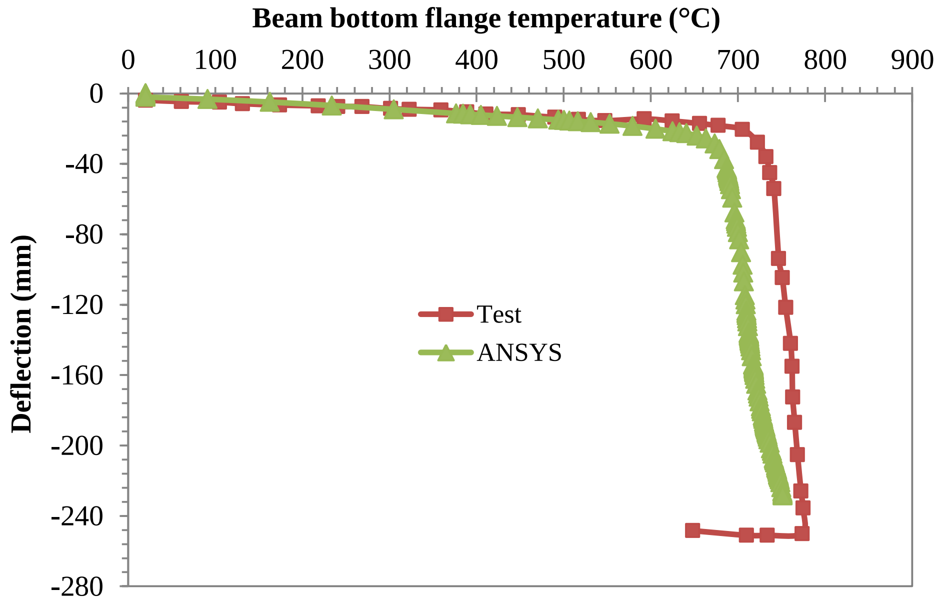

(a) Beam mid-span deflection

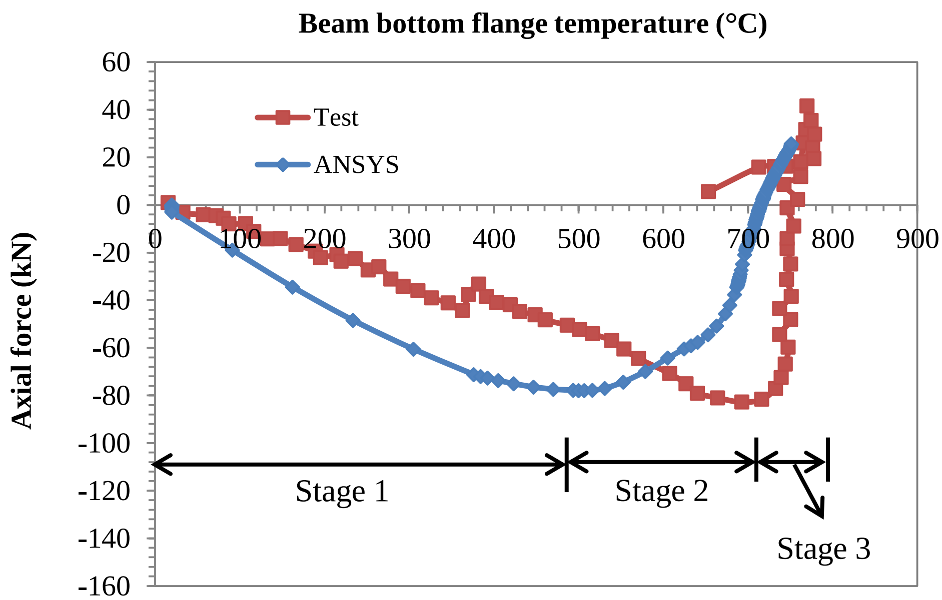

(b) Connection axial force

Figure 4.17: Comparison of predicted and measured (a) beam mid-span deflection (b) axial force in connection as a function of beam bottom flange temperature and (c) connection's rotation as a function of fire exposure time

Figure 4.17 (cont'd)

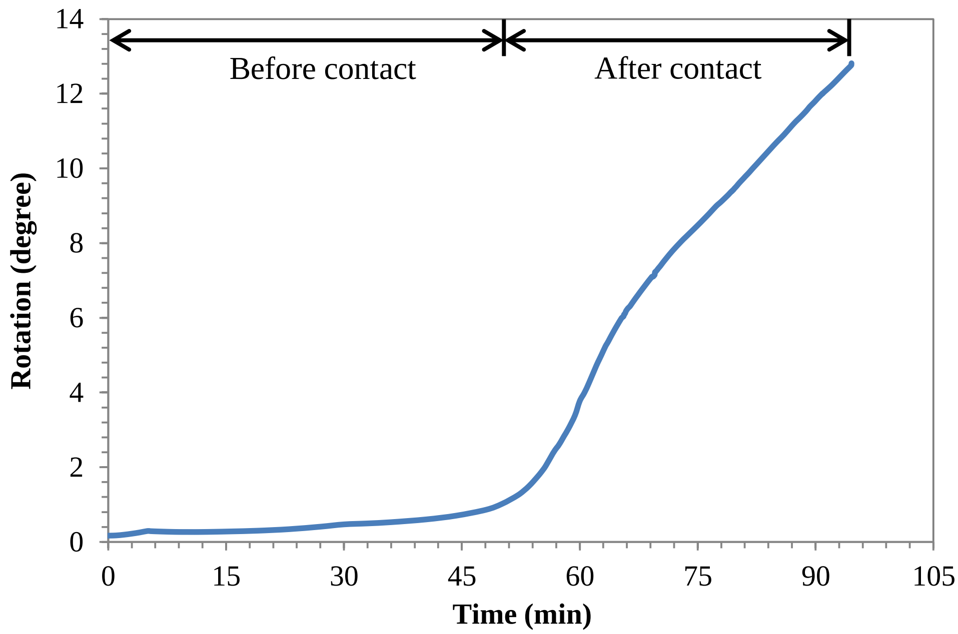

(c) Connection rotation

Chapter 5 figures

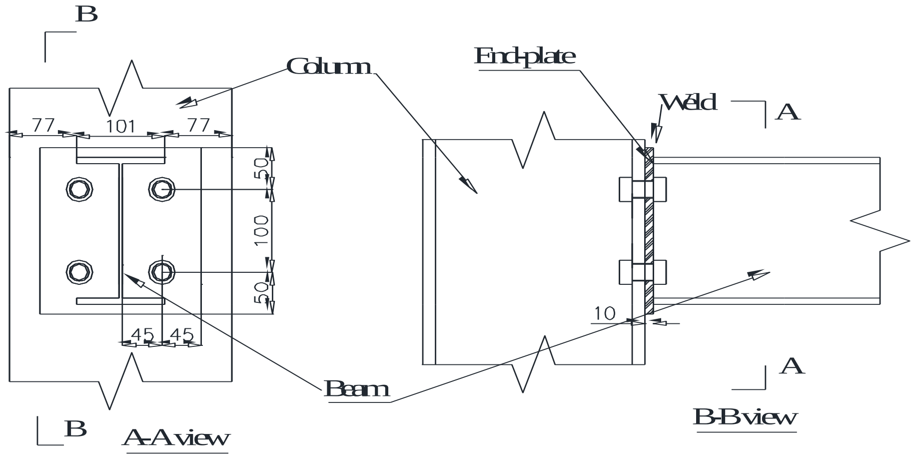

(a) Flush end-plate connection

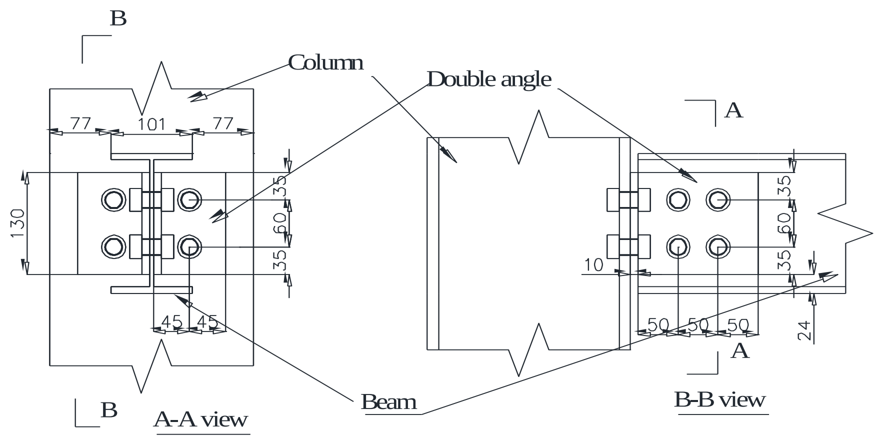

(b) Double angle connection

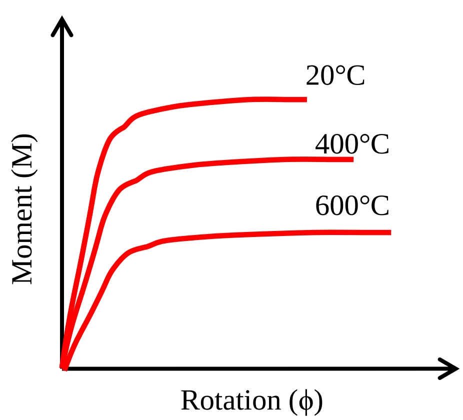

(c) Flush end-plate M-ϕ curves

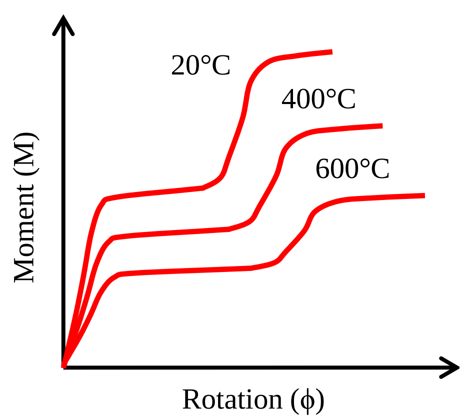

(d) Double angle M-ϕ curves

Figure 5.1: Connection details and moment-rotation curves for flush end-plate and double angle connections

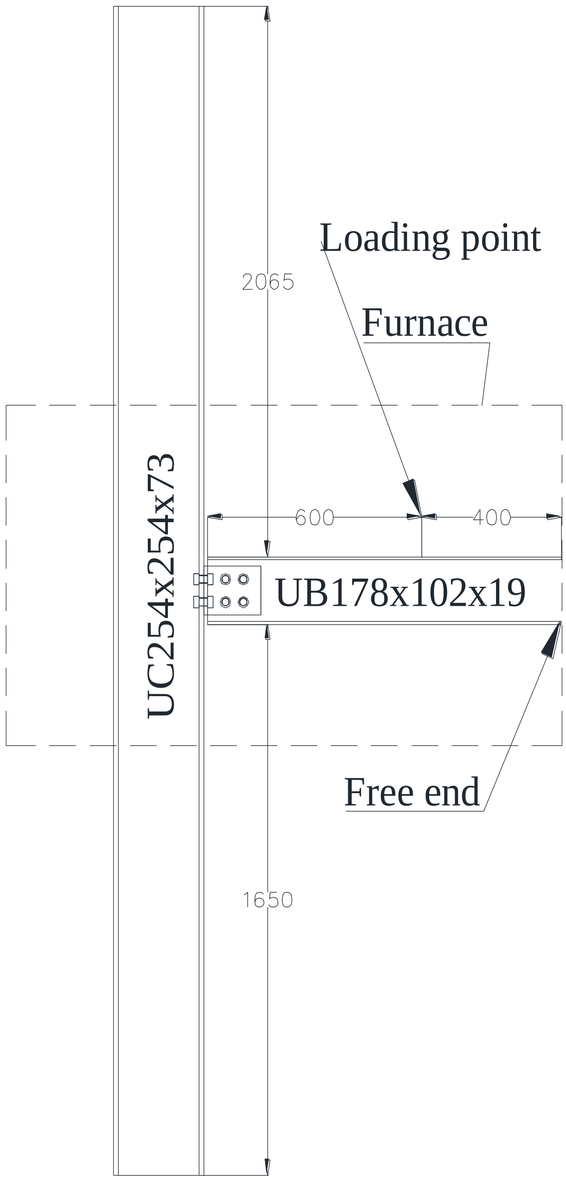

Figure 5.2: Illustration of the isolated connection assembly used in the finite element model (all dimensions in mm)

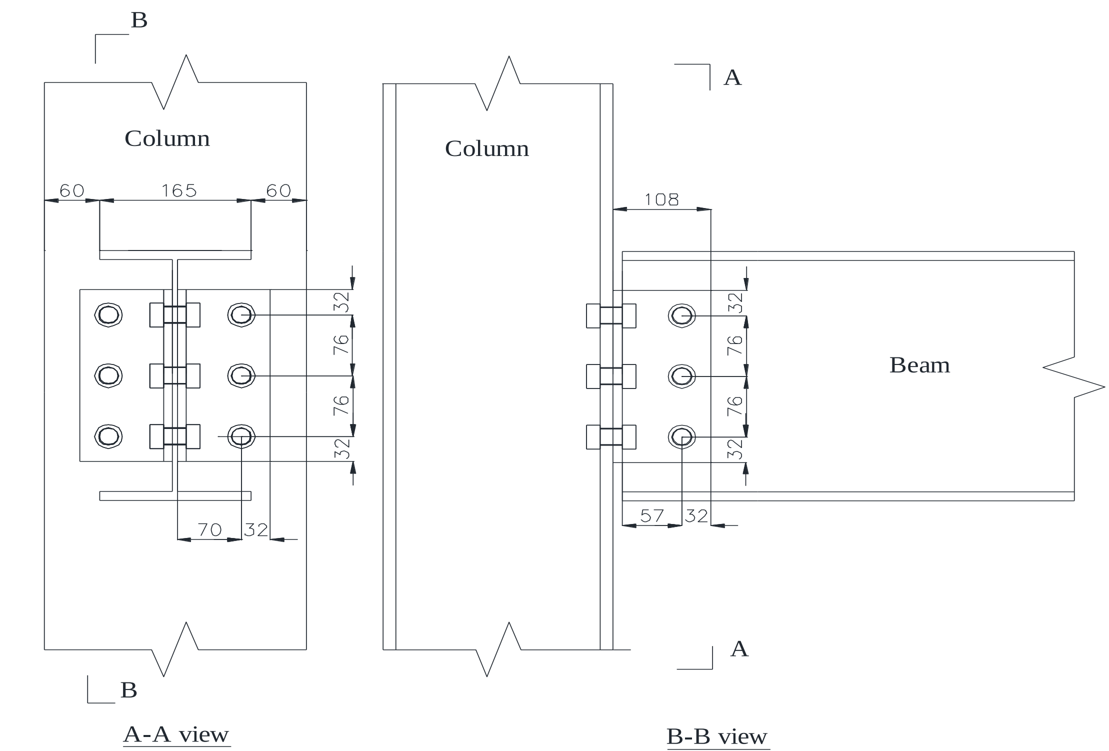

(a) Double angle connection

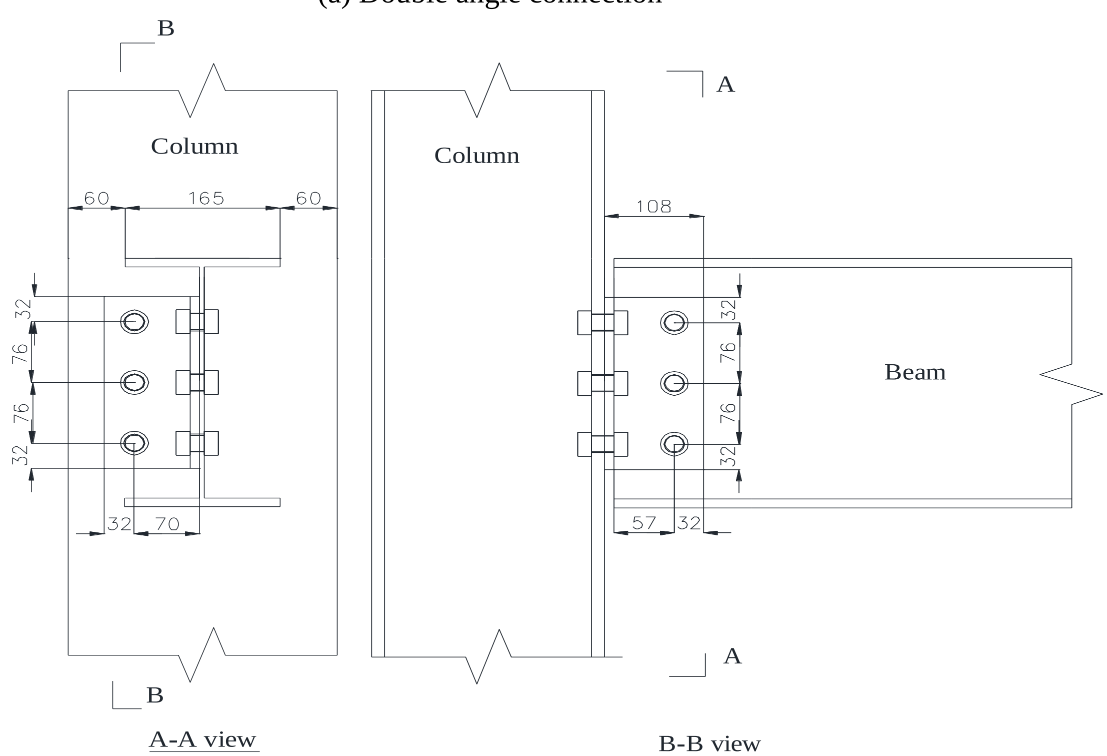

(b) Single angle connection

Figure 5.3: Geometrical details of different connection types (a) double angle (b) single angle and (c) shear tab connection

Figure 5.3 (cont'd)

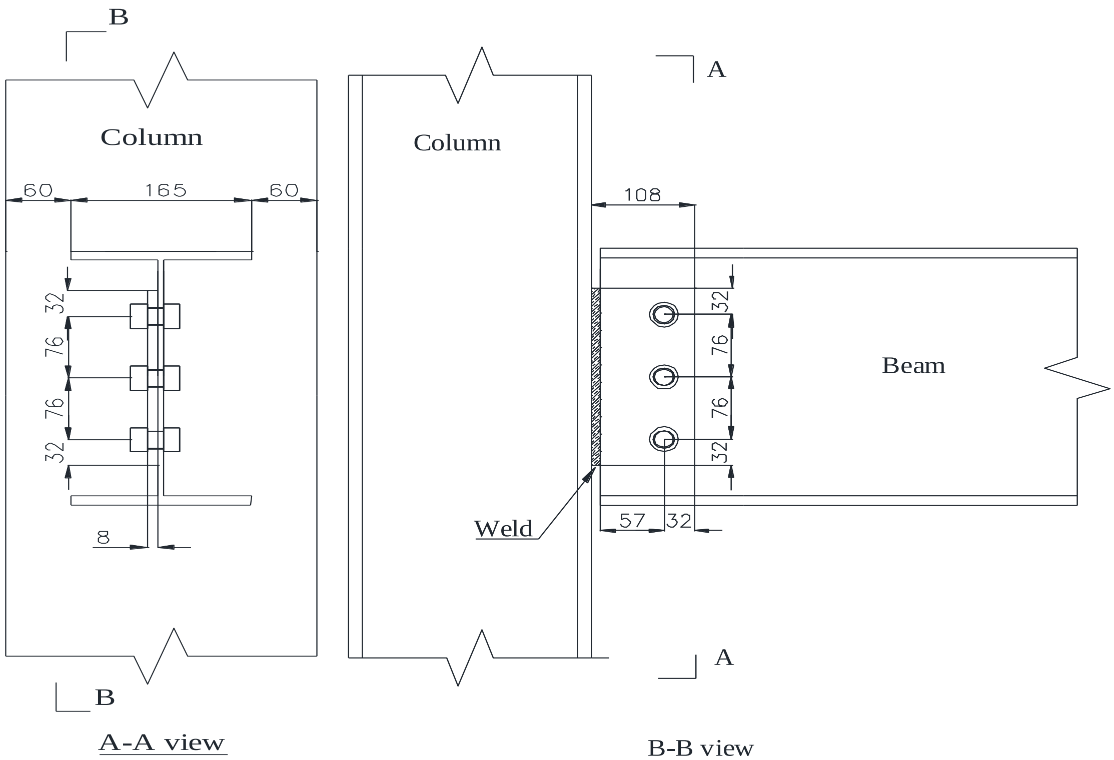

(c) Shear tab connection

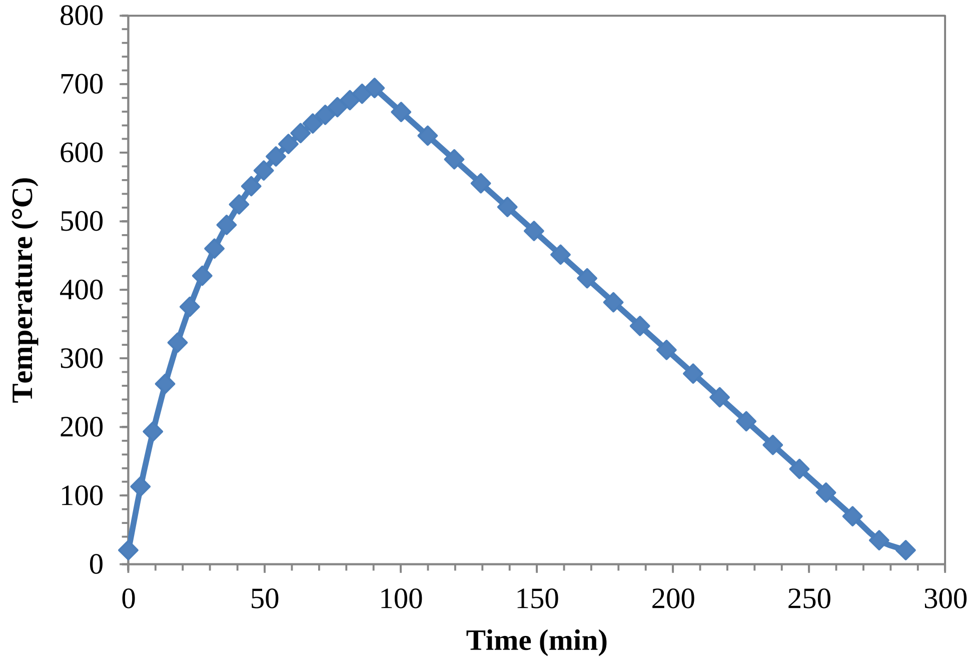

Figure 5.4: Parametric fire scenario (FS) used in the parametric studies

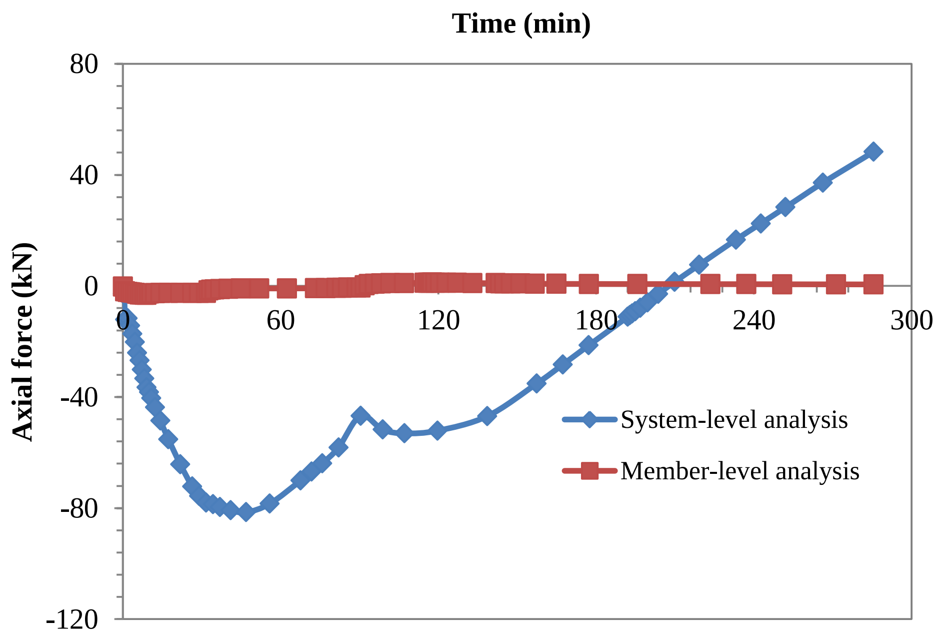

(a) Axial force

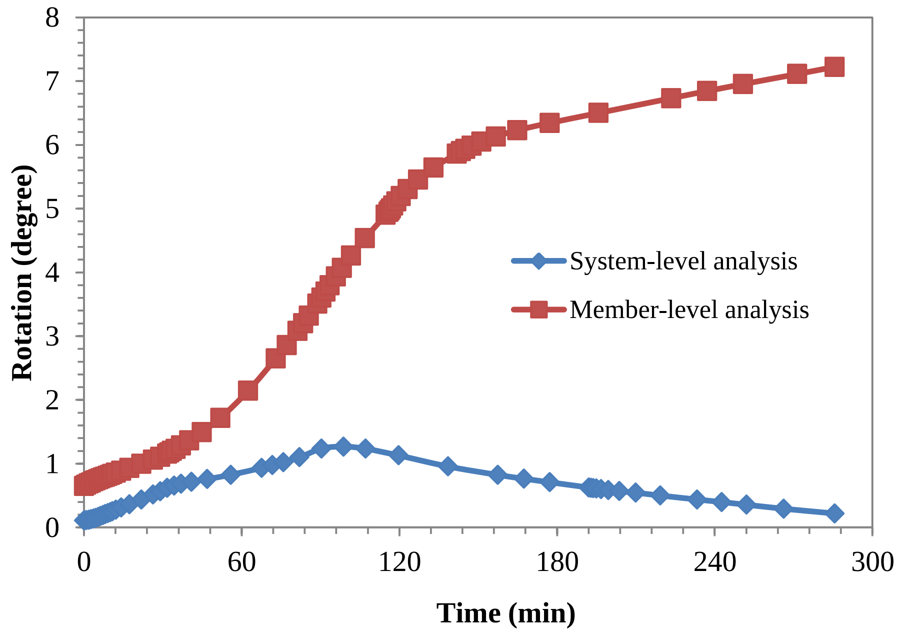

(b) Rotation

Figure 5.5: Variation of connections (a) axial force and (b) rotation as a function of fire exposure time obtained from system-level and isolated connection analysis

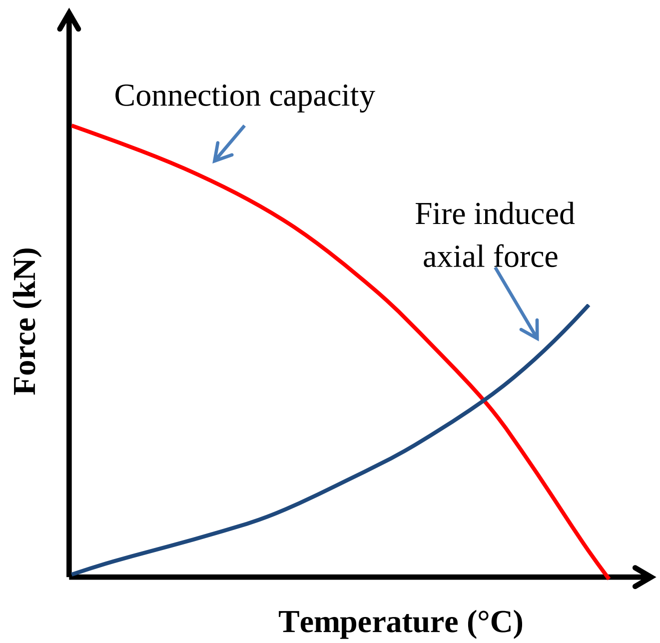

Figure 5.6: Illustration of connection capacity and fire induced axial force with temperature

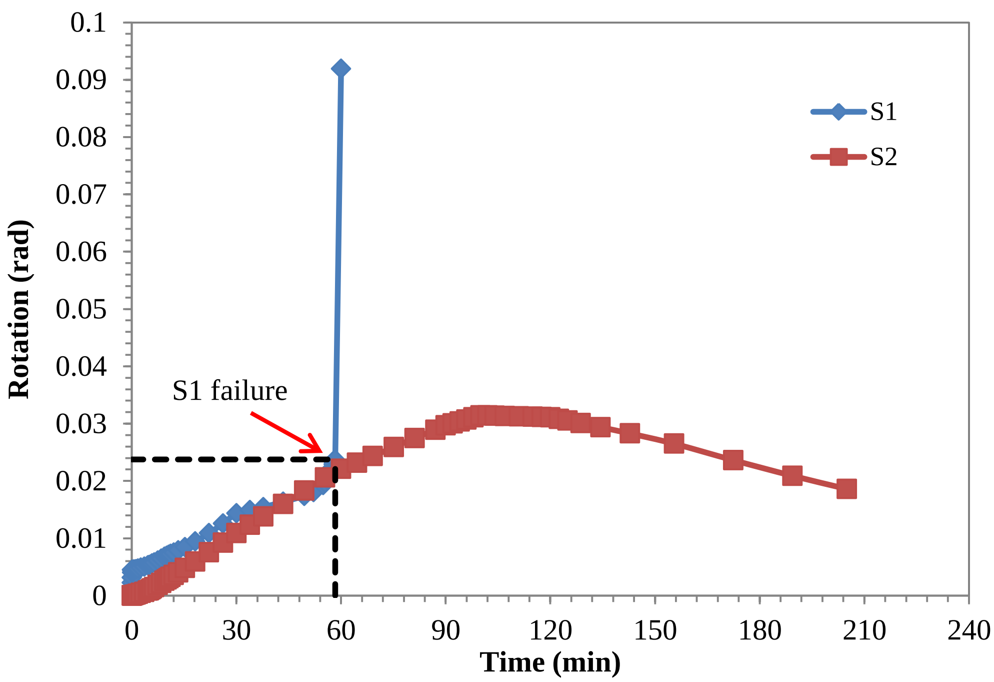

Figure 5.7: Comparison of rotation in connection as a function of fire exposure time in assemblies S1 and S2

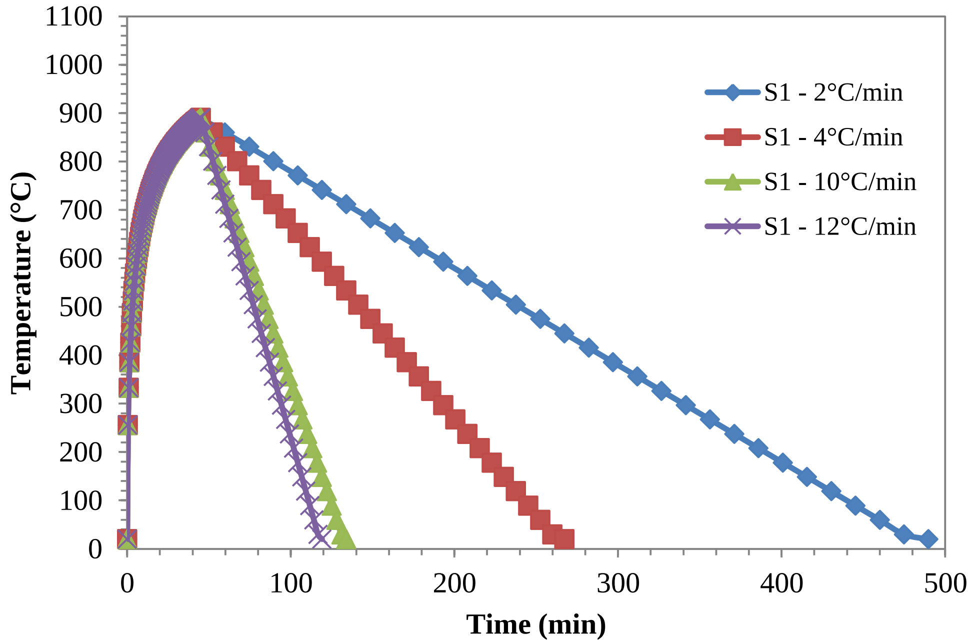

(a) S1

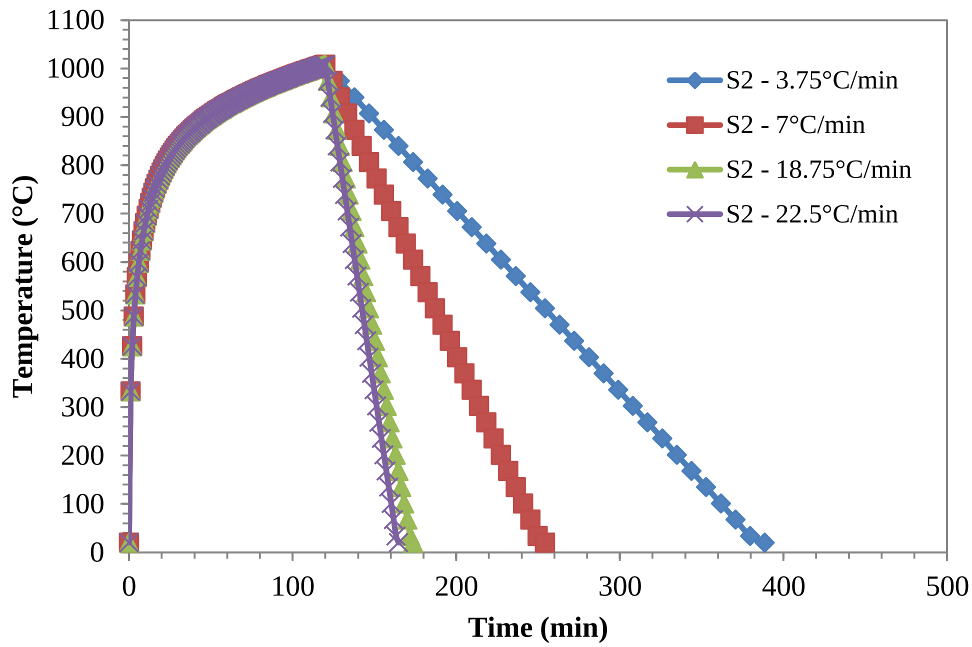

(b) S2

Figure 5.8: Time-temperature curves for design fire scenarios used to study the effect of decay rate

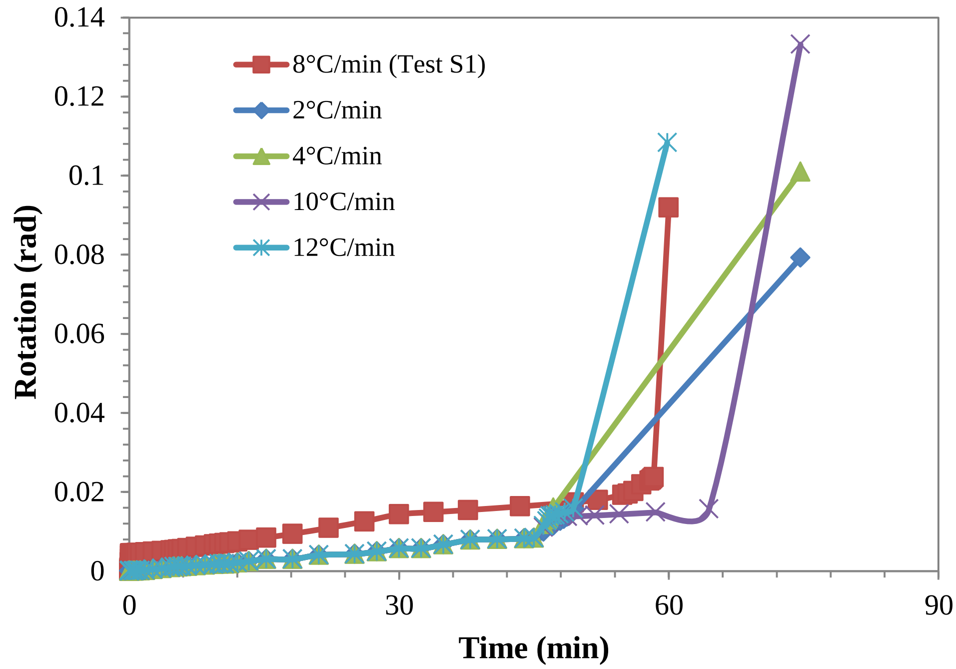

(a) S1

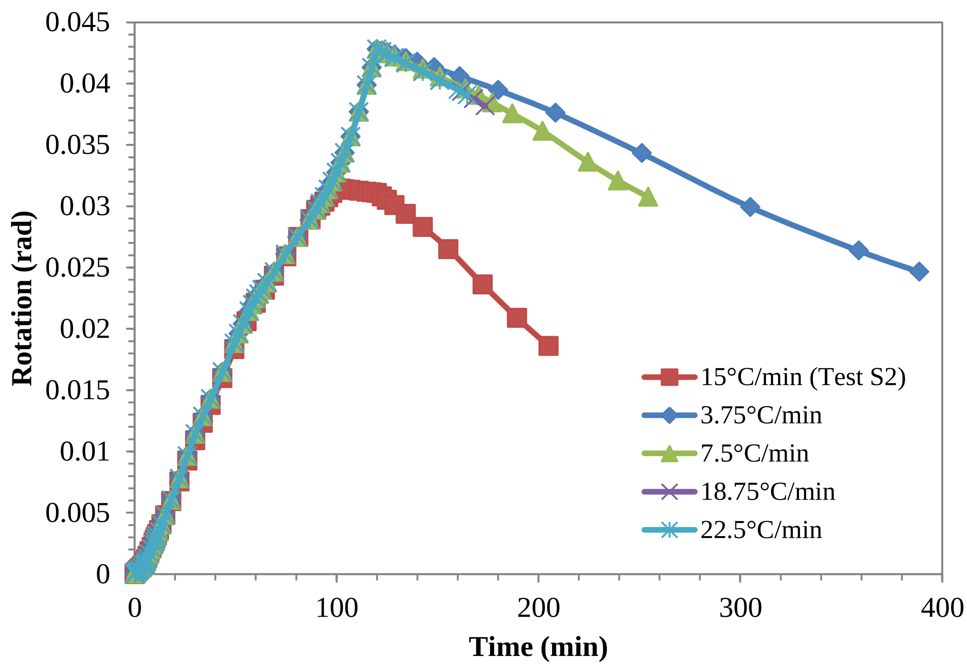

(b) S2

Figure 5.9: Variation of connections rotation as a function of fire exposure time for different decay rates in assembly (a) S1 and (b) S2

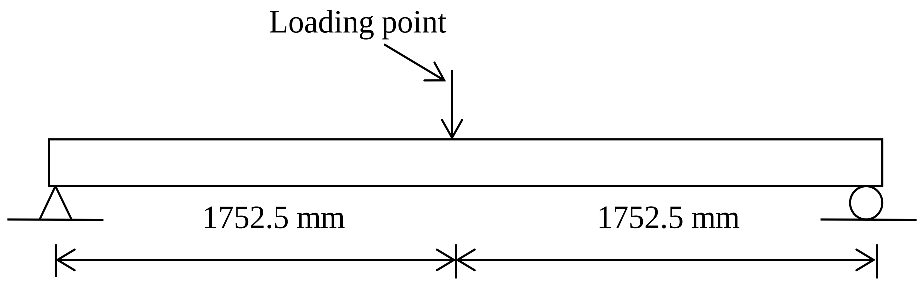

(a) Mid-point loading

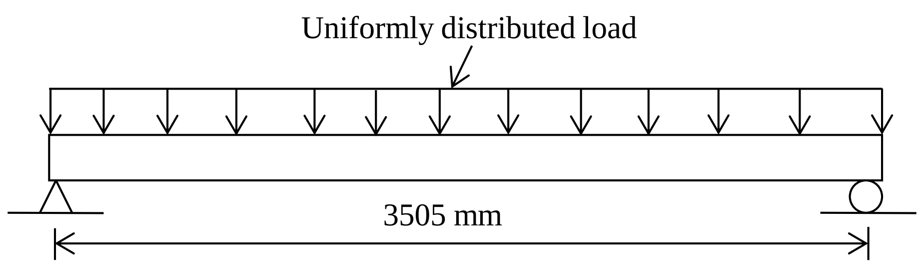

(b) Distributed loading

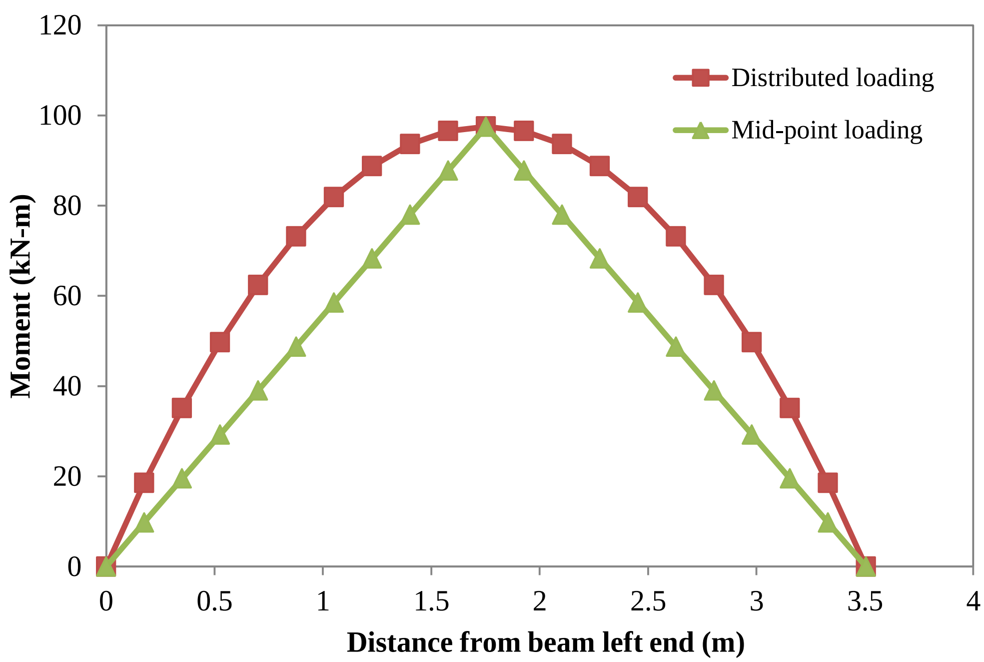

(c) Bending moment for different loading conditions

Figure 5.10: Illustration of different loading scenarios used in the analysis along with the corresponding bending moments

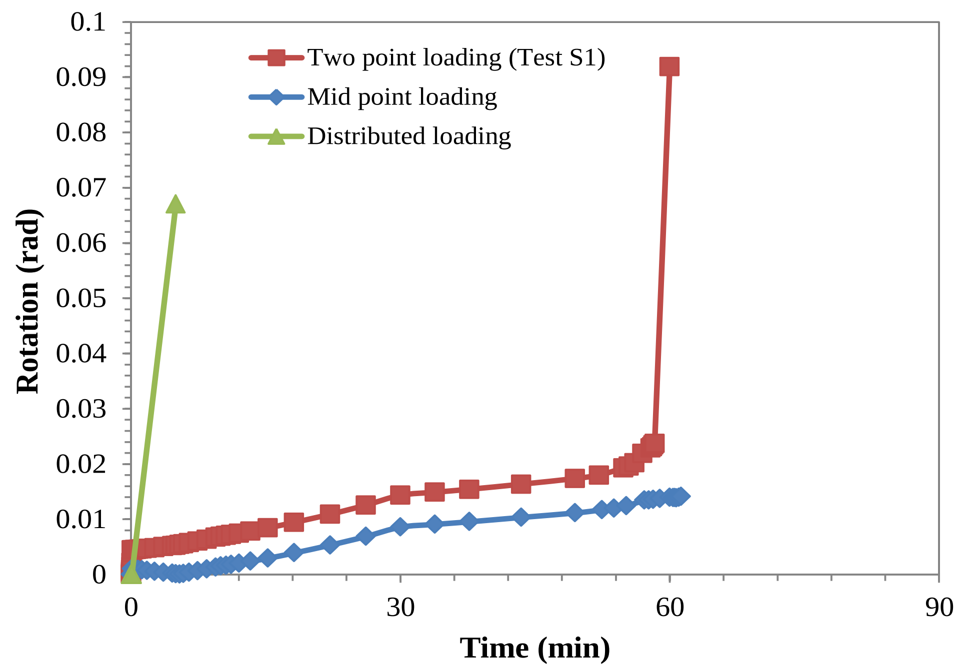

(a) S1

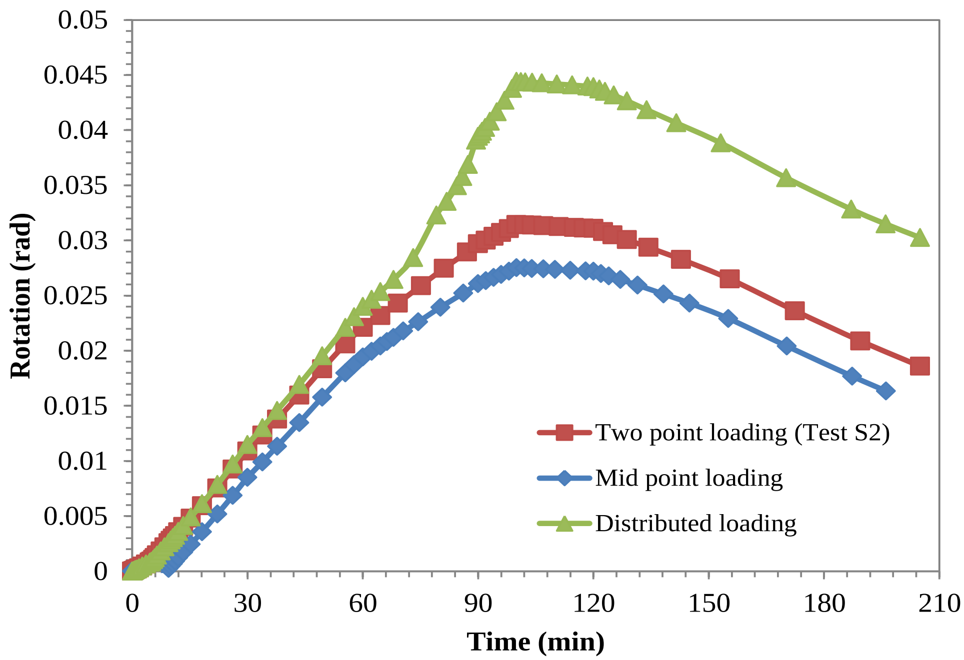

(b) S2

Figure 5.11: Progression of connections rotation as a function of fire exposure time for connection assemblies (a) S1 and (b) S2 with different loading types

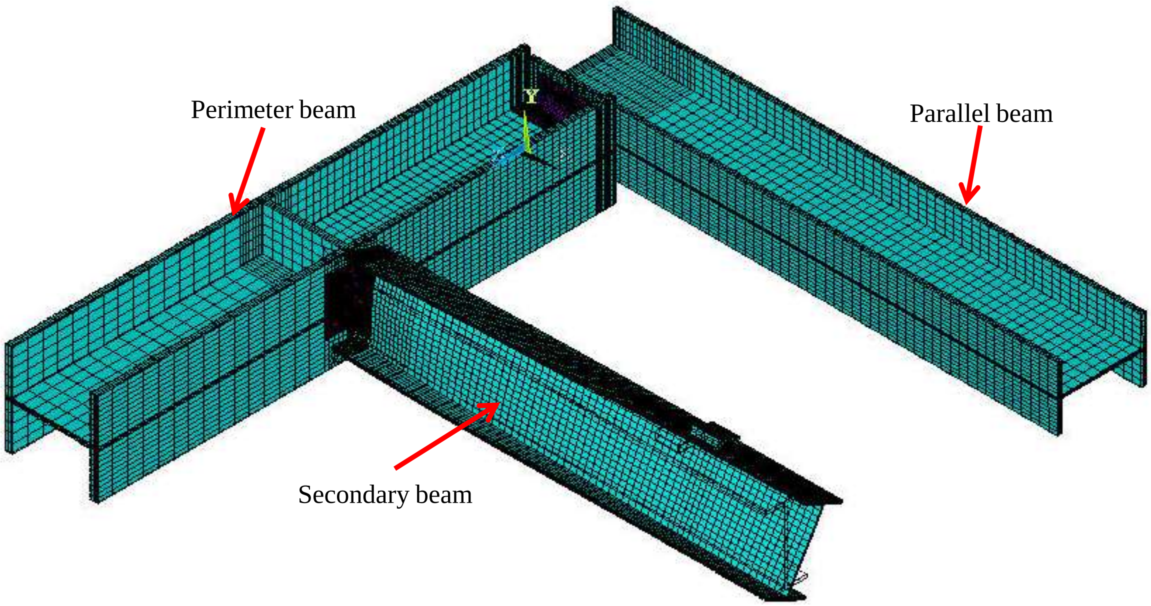

(a) Deformed shape

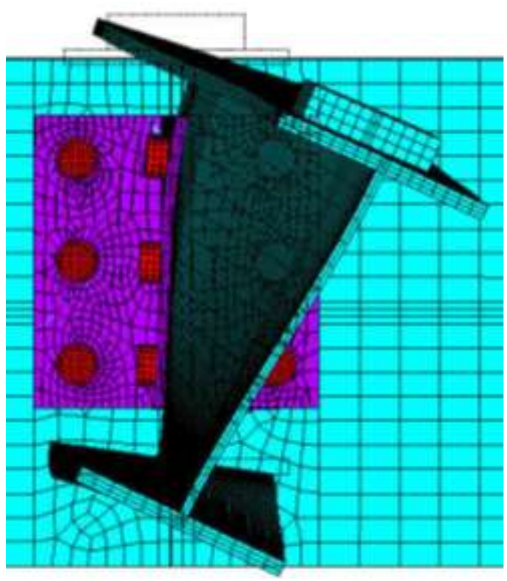

(b) Lateral torsional buckling

Figure 5.12: Illustration of (a) deformed shape and (c) lateral torsional buckling of secondary beam in assembly S1 analyzed with uniformly distributed loading

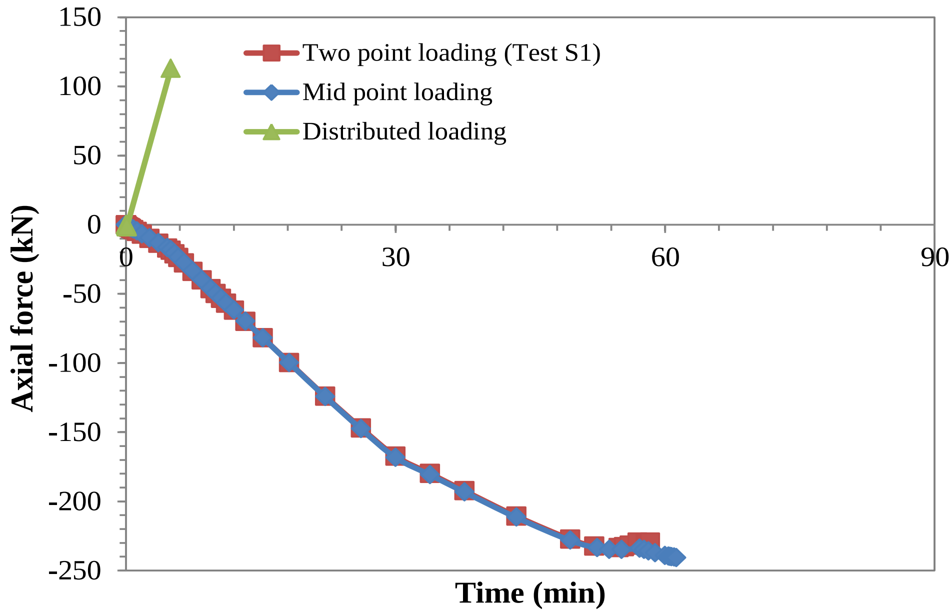

(a) S1

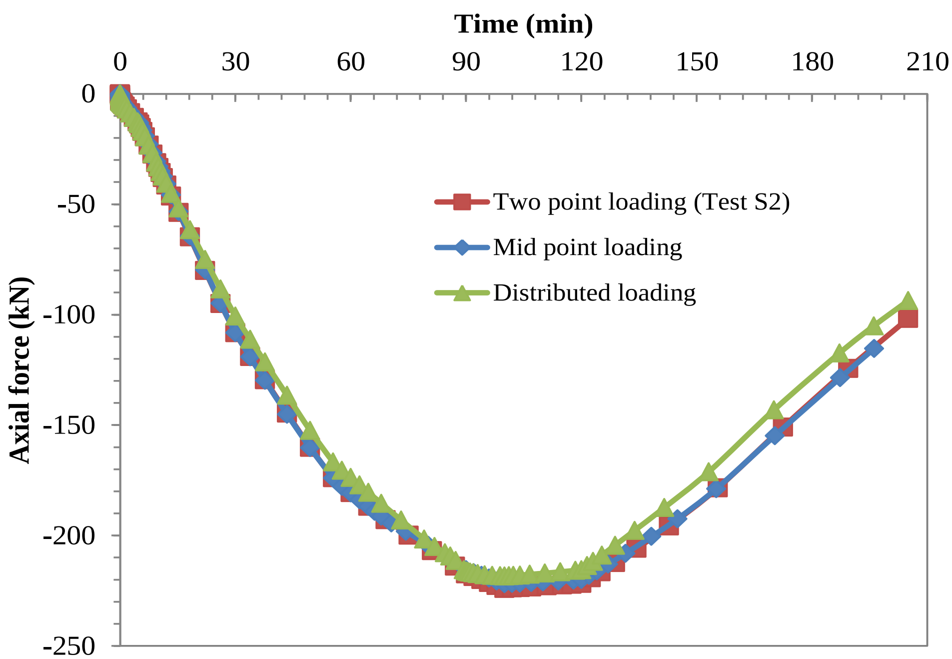

(b) S2

Figure 5.13: Variation of fire induced axial force in connections as a function of fire exposure time for connection assemblies (a) S1 and (b) S2 with different loading types

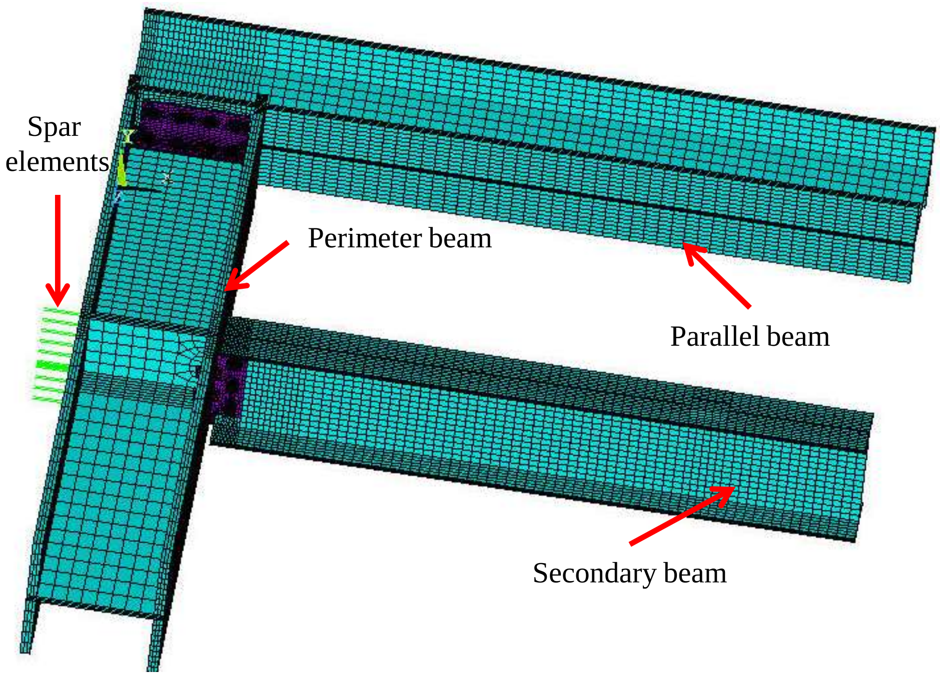

Figure 5.14: Schematic of the spar elements used in the analysis

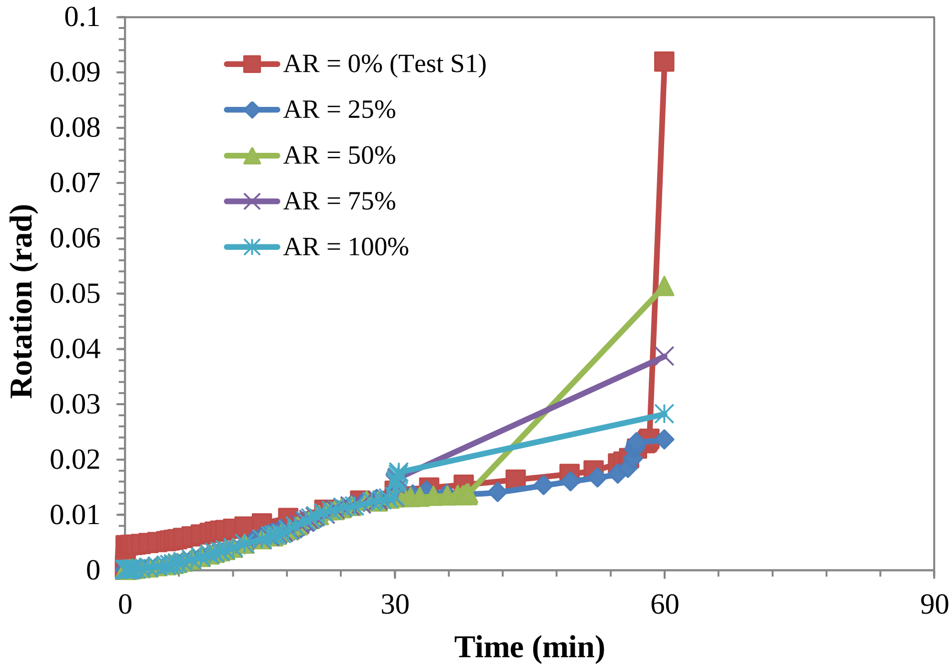

(a) S1

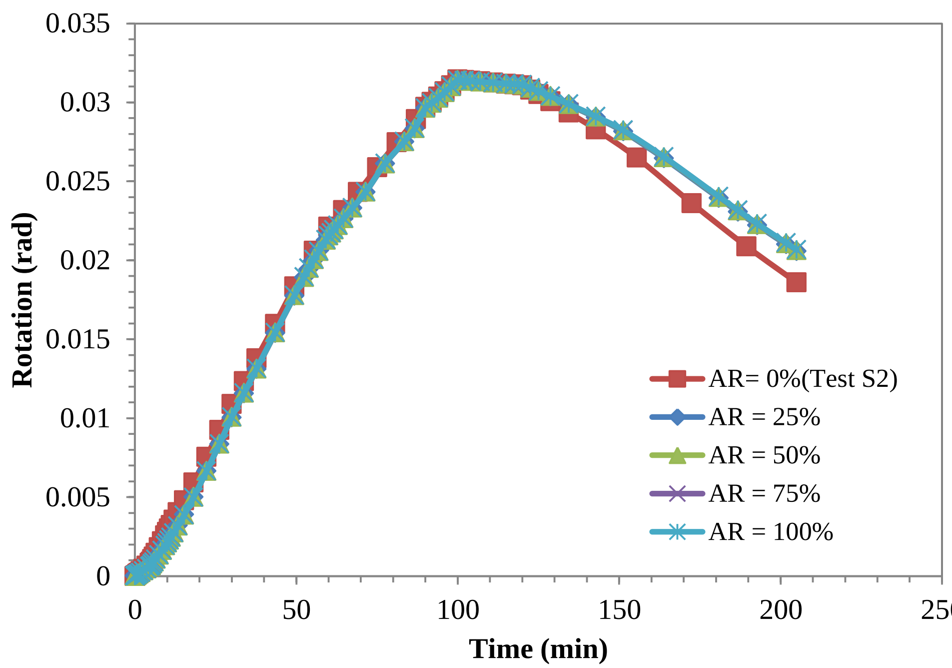

(b) S2

Figure 5.15: Effect of restraining axial stiffness on the fire response of double angle connection assemblies (a) S1 and (b) S2

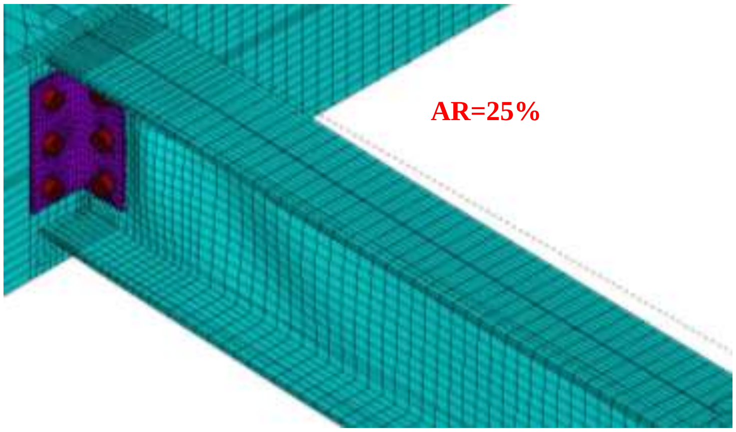

(a) Local buckling

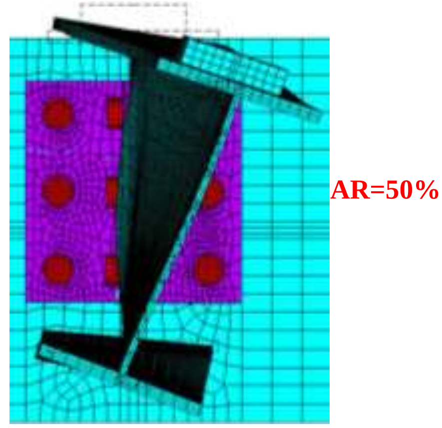

(b) Lateral torsional buckling

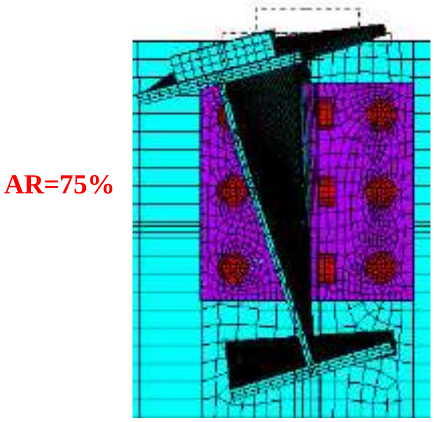

(c) Lateral torsional buckling

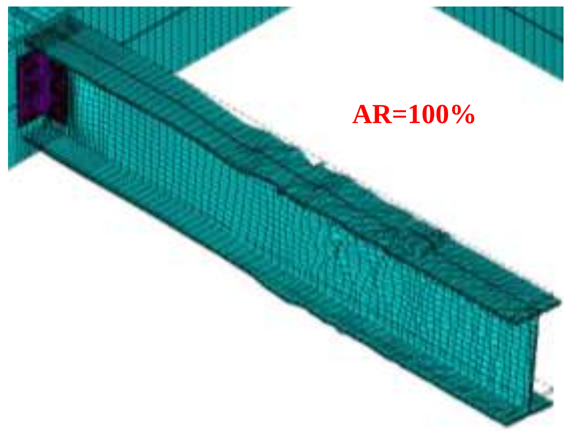

(d) Web and flanges crippling

Figure 5.16: Failure modes of connection assembly S1 for different values of axial restraint stiffness

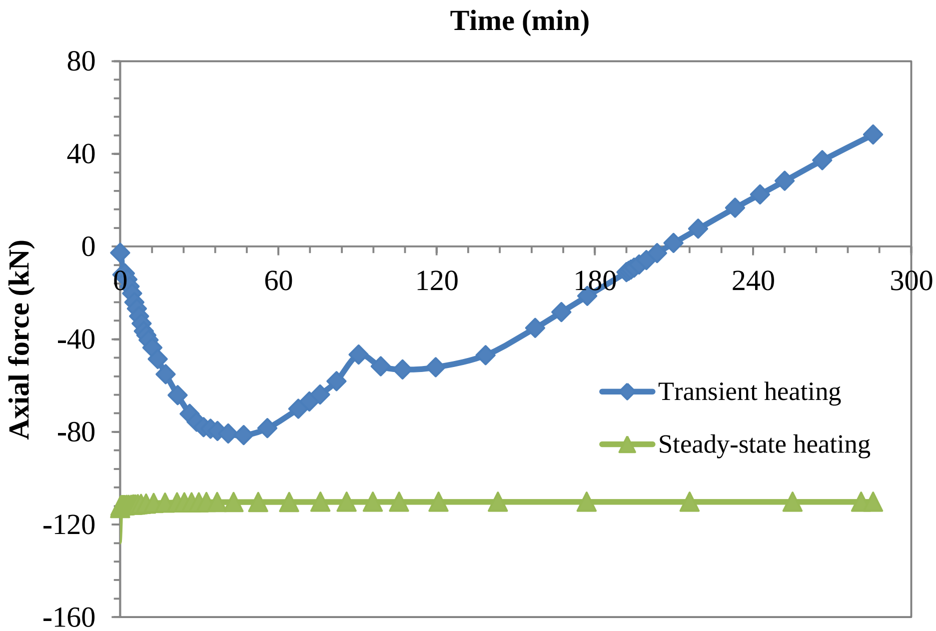

(a) Axial force

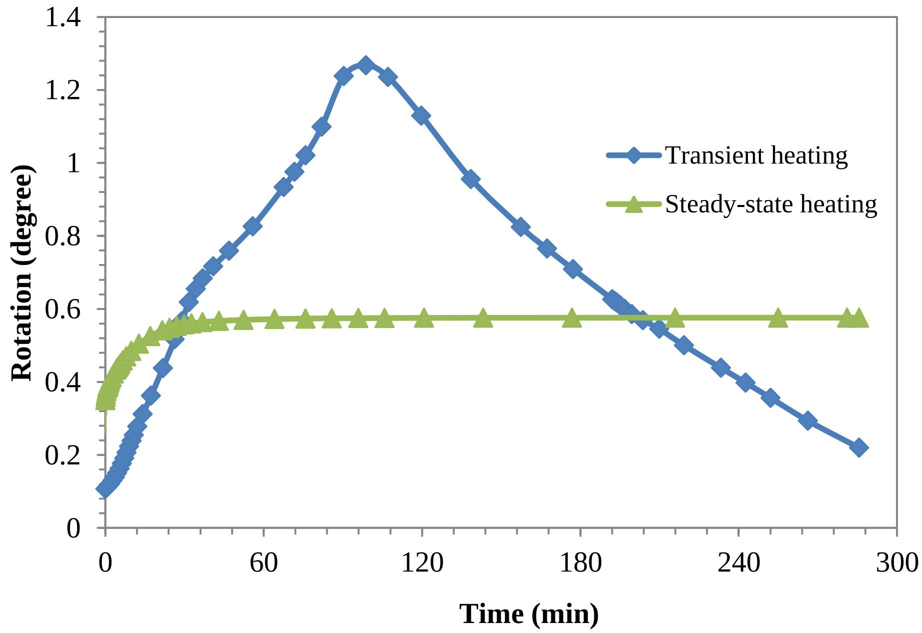

(b) Rotation

Figure 5.17: Variation of (a) axial force and (b) rotation in connection as a function of fire exposure time for transient and steady-state heating conditions

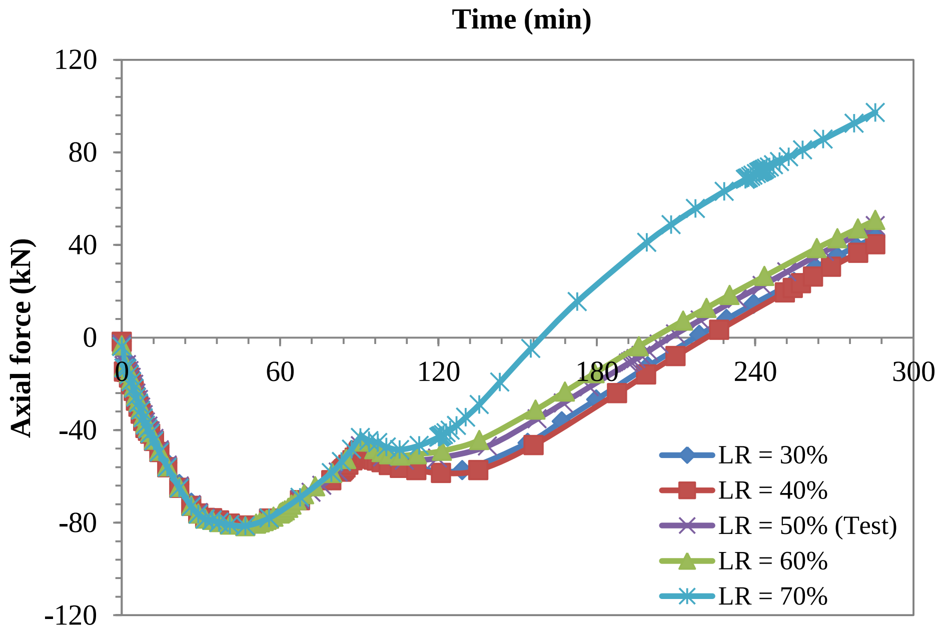

(a) Axial force

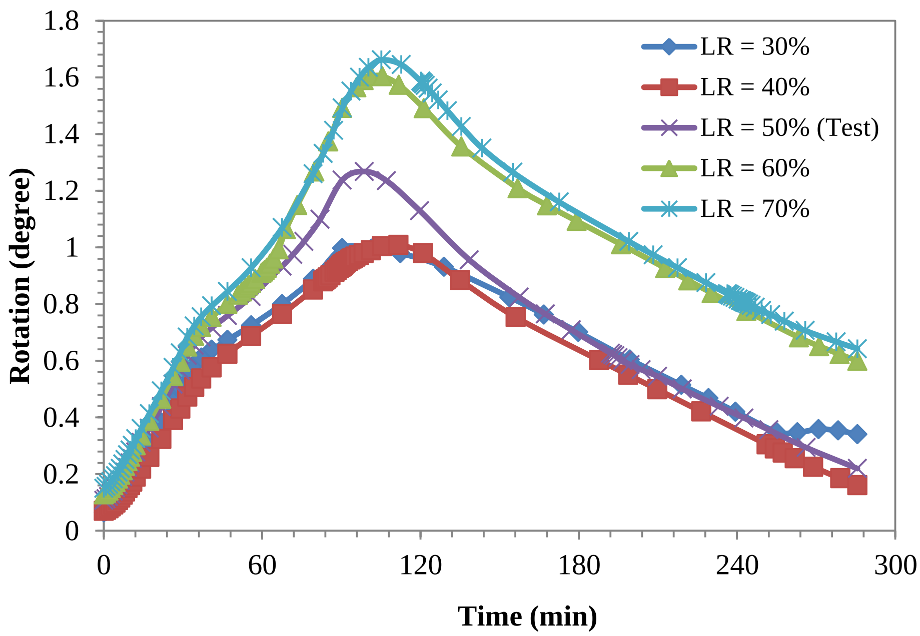

(b) Rotation

Figure 5.18: Variation of (a) axial force and (b) rotation in connection as a function of fire exposure time for different load ratios

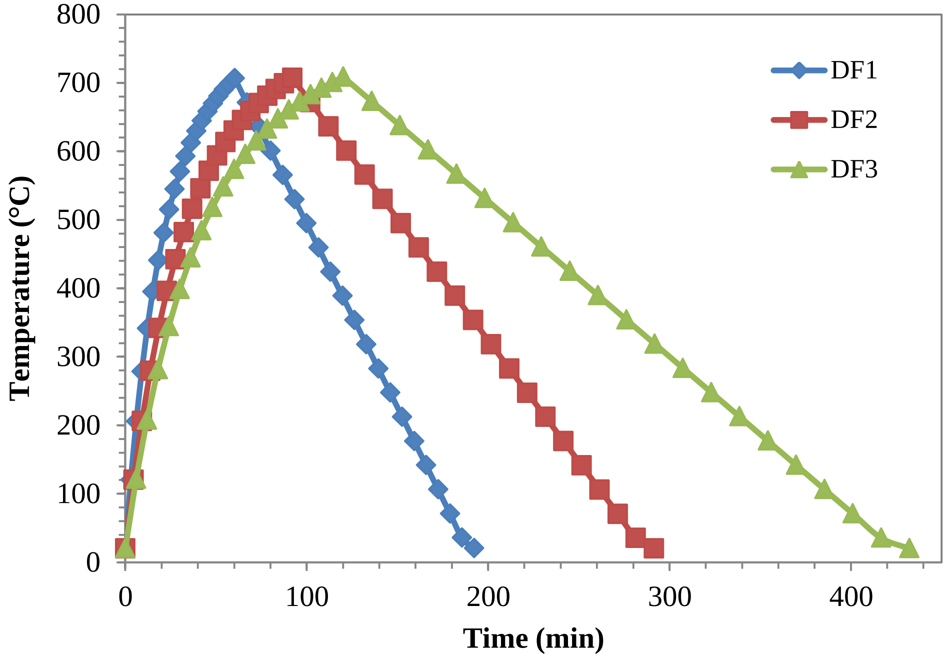

Figure 5.19: Time-temperature curves for design fire scenarios used in the analysis

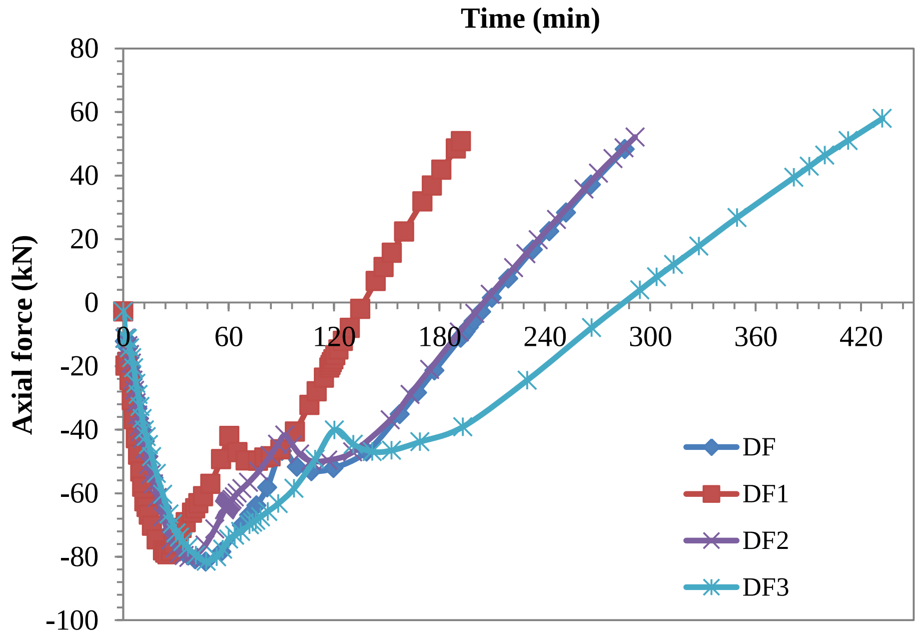

(a) Axial force

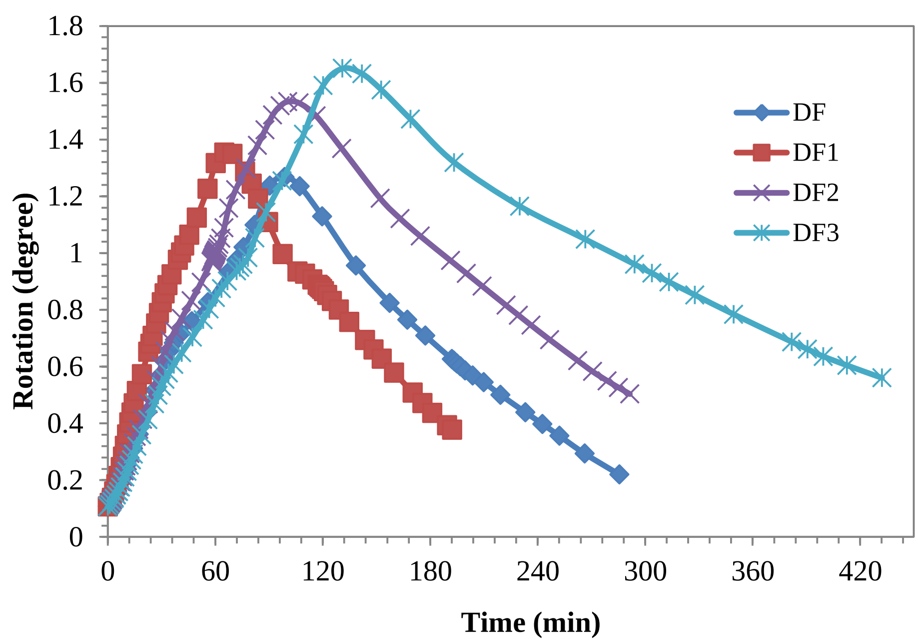

(b) Rotation

Figure 5.20: Fire induced (a) axial force and (b) rotation in connection under different design fire scenarios (see Fig. 5.14)

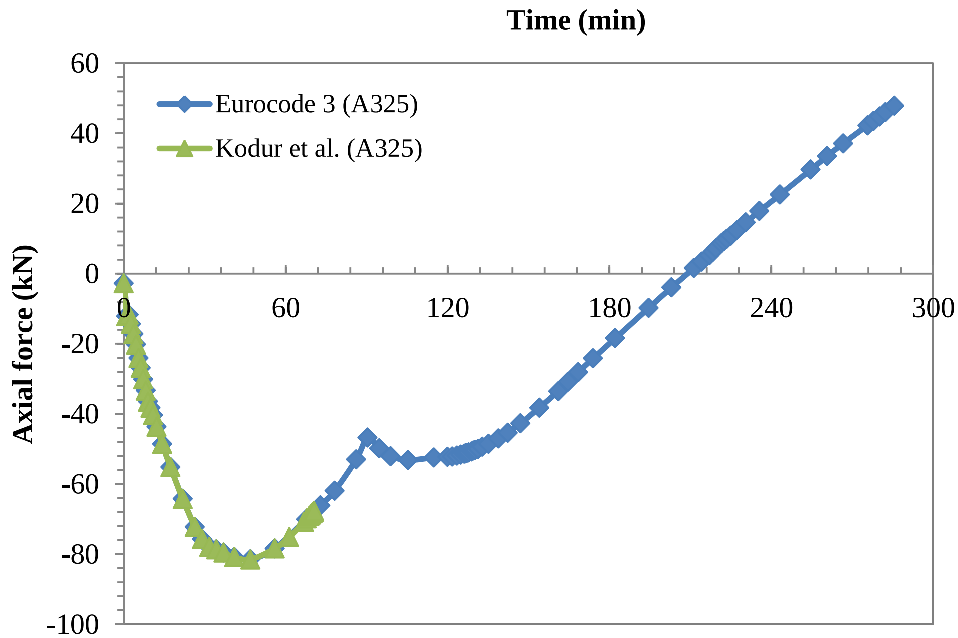

(a) A325 bolts

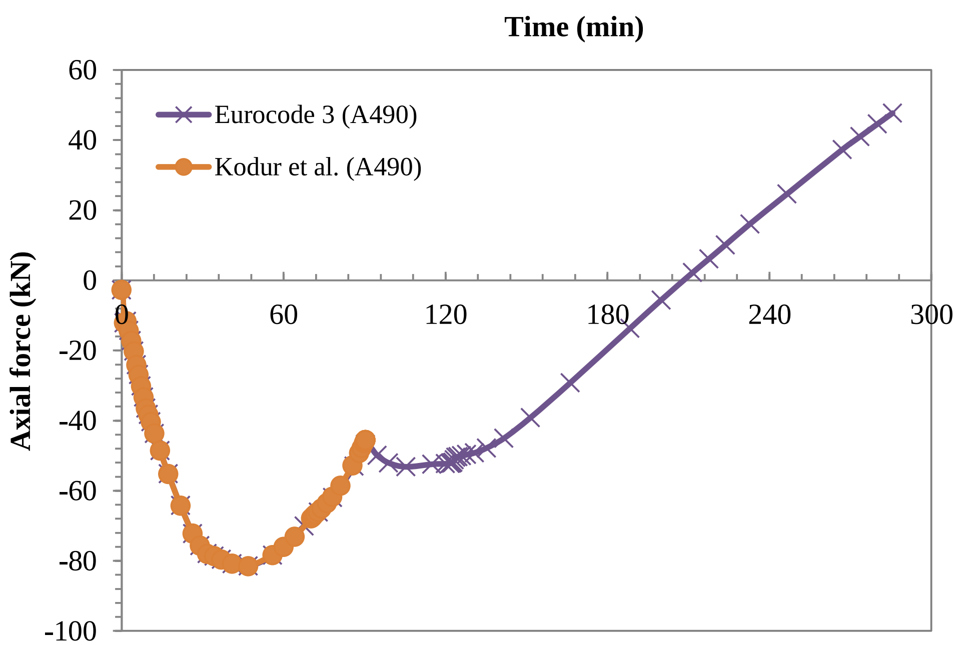

(b) A490 bolts

Figure 5.21: Progression of axial force in connection as a function of fire exposure time for (a) A325 and (b) A490 bolt types

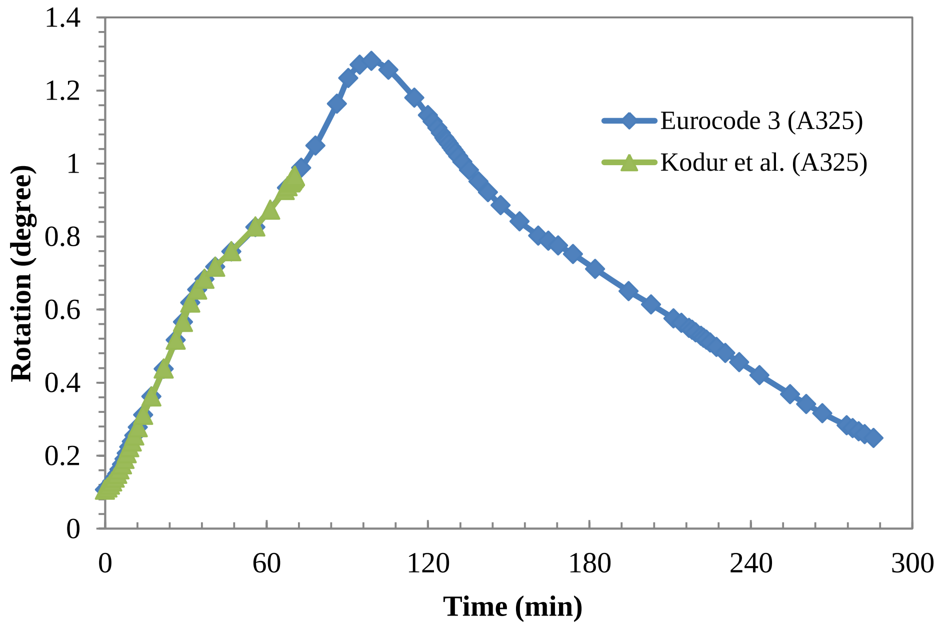

(a) A325 bolts

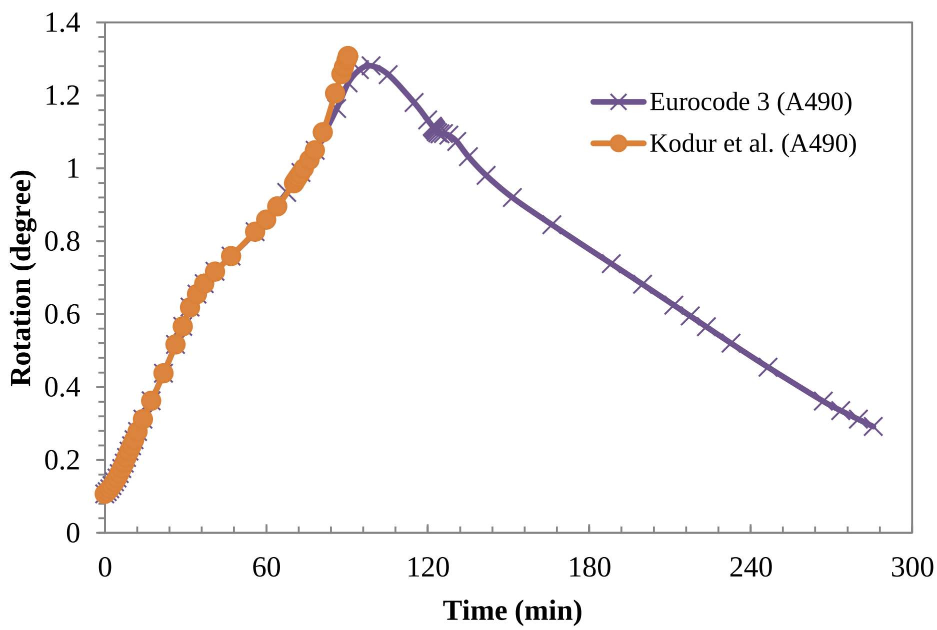

(b) A490 bolts

Figure 5.22: Comparison of connections rotations as a function of fire exposure time for (a) A325 and (b) A490 bolt types with different high-temperature material properties

Chapter 6 figures

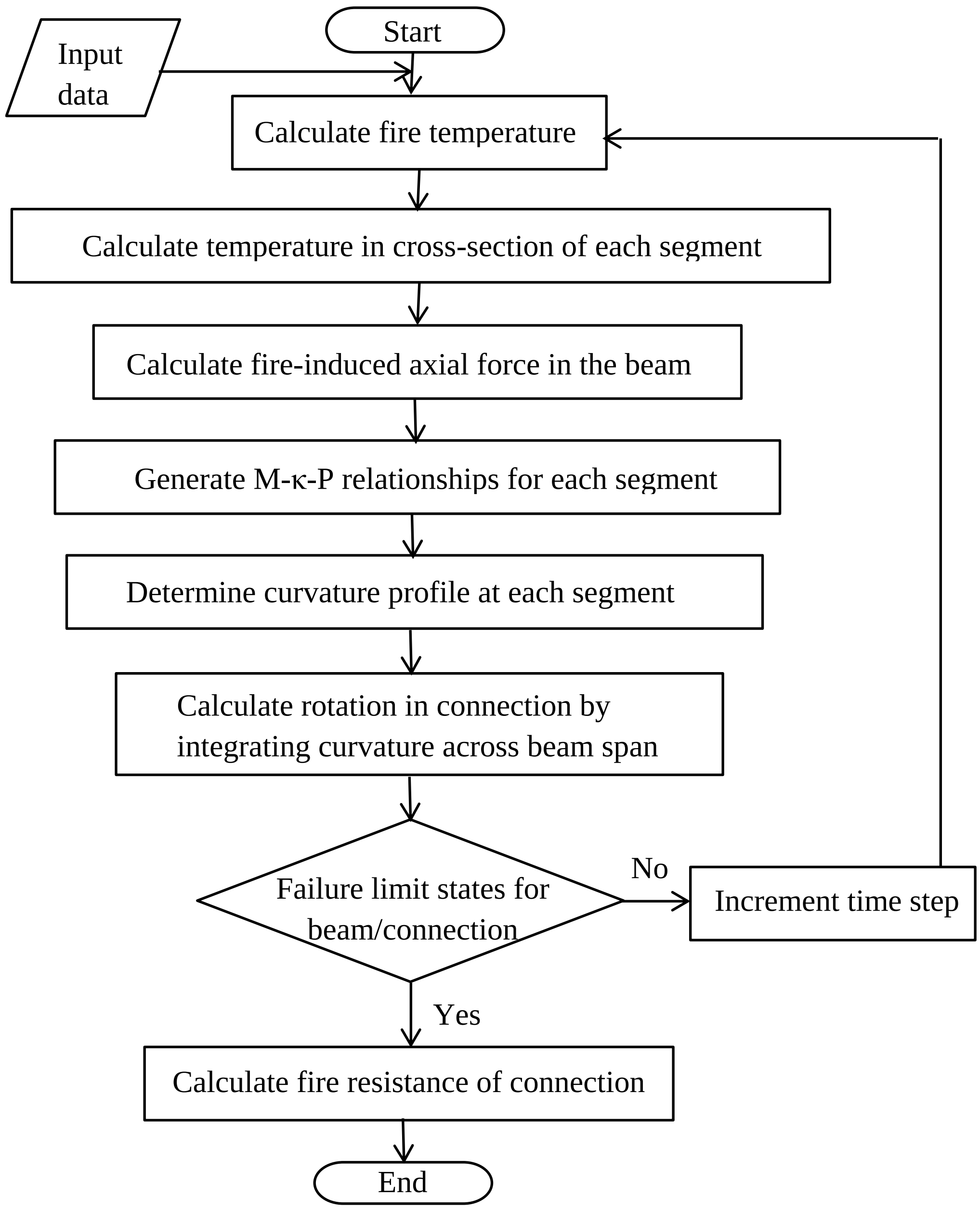

Figure 6.1: Flowchart summarizing the procedure to evaluate fire resistance of connection

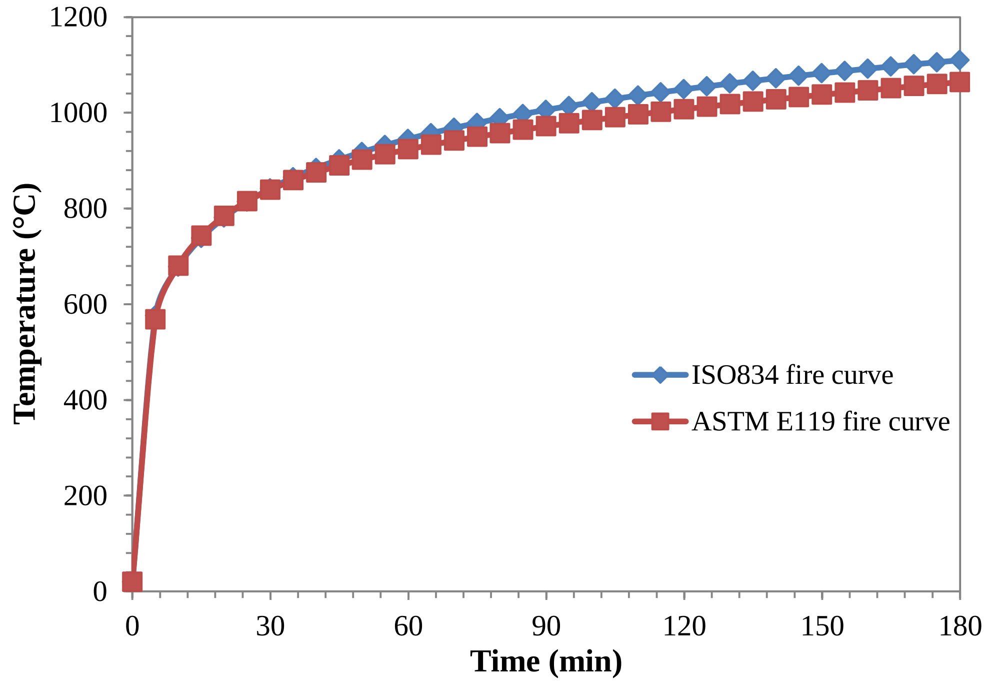

Figure 6.2: Comparison of ISO834 and ASTM E119 standard fire curves

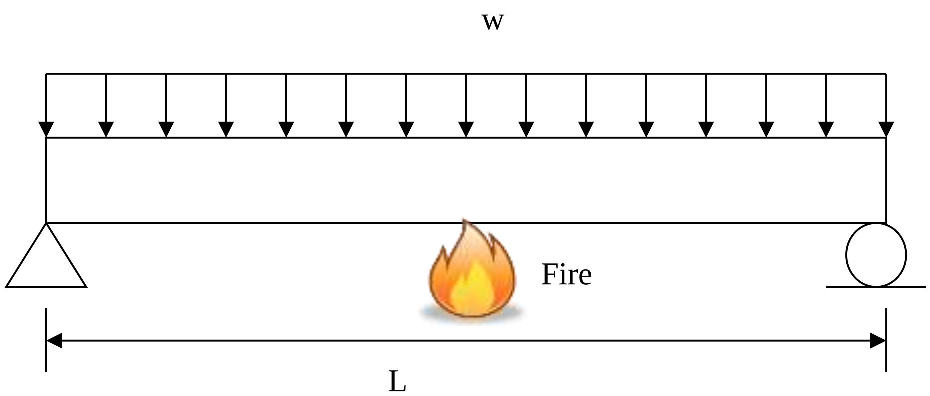

(a) Elevation of fire exposed beam

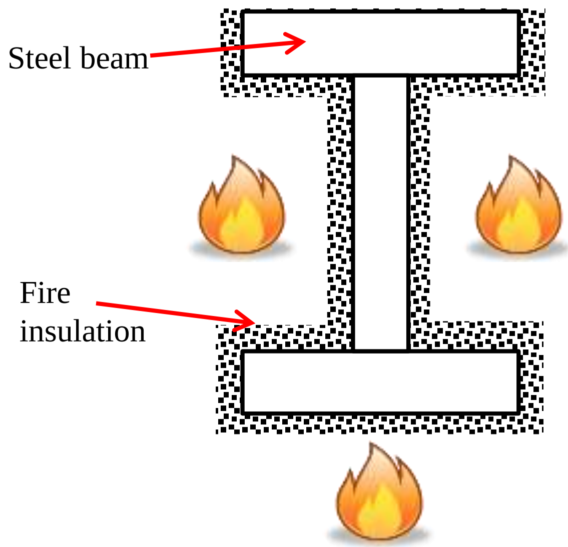

(b) Beam cross-section

Figure 6.3: Schematic of (a) beam elevation and (b) cross-section used for computing temperatures in fire protected steel sections

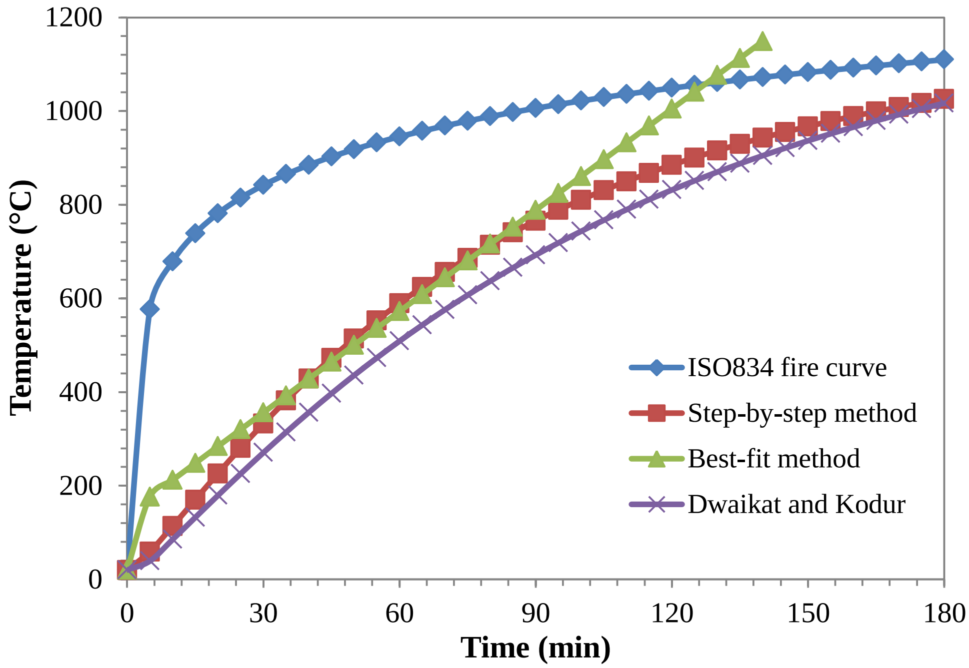

(a) W12x30

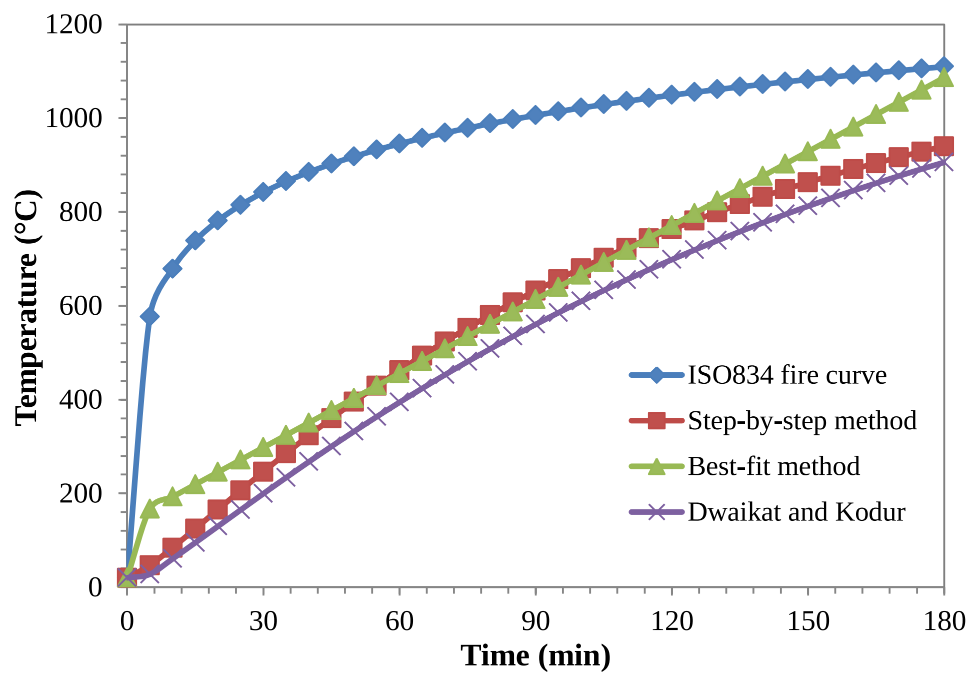

(b) W24x76

Figure 6.4: Comparison of steel temperatures obtained using different methods for (a) W12x30 and (b) W24x76 beam sections with 15mm fire protection

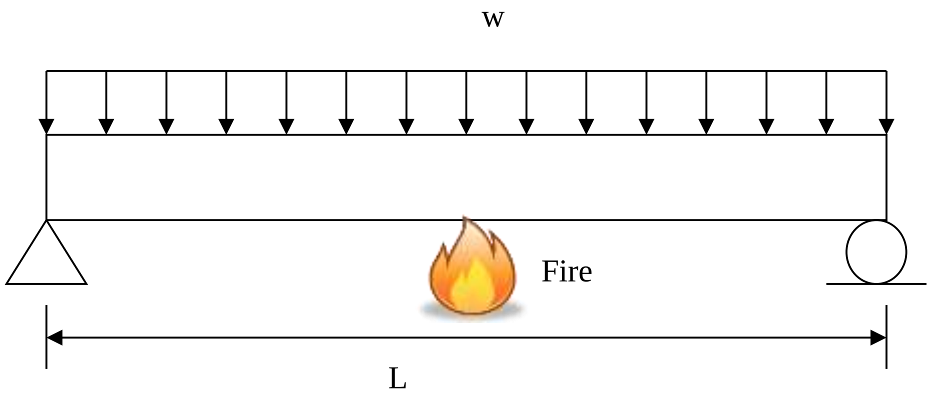

(a) Elevation of fire exposed beam

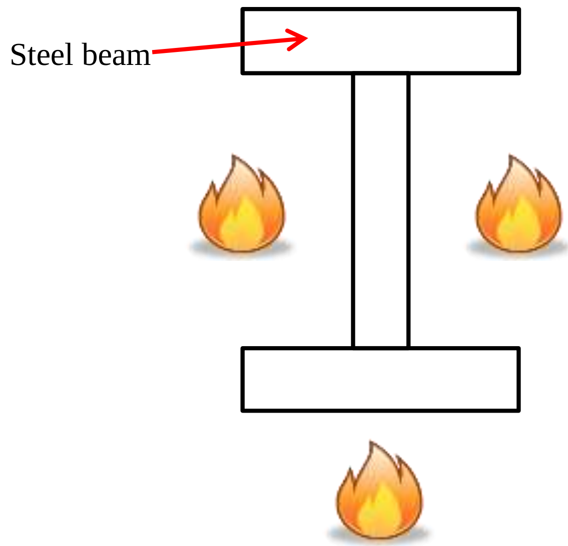

(b) Beam cross-section

Figure 6.5: Schematic of (a) beam elevation and (b) cross-section used for computing temperatures in unprotected steel sections

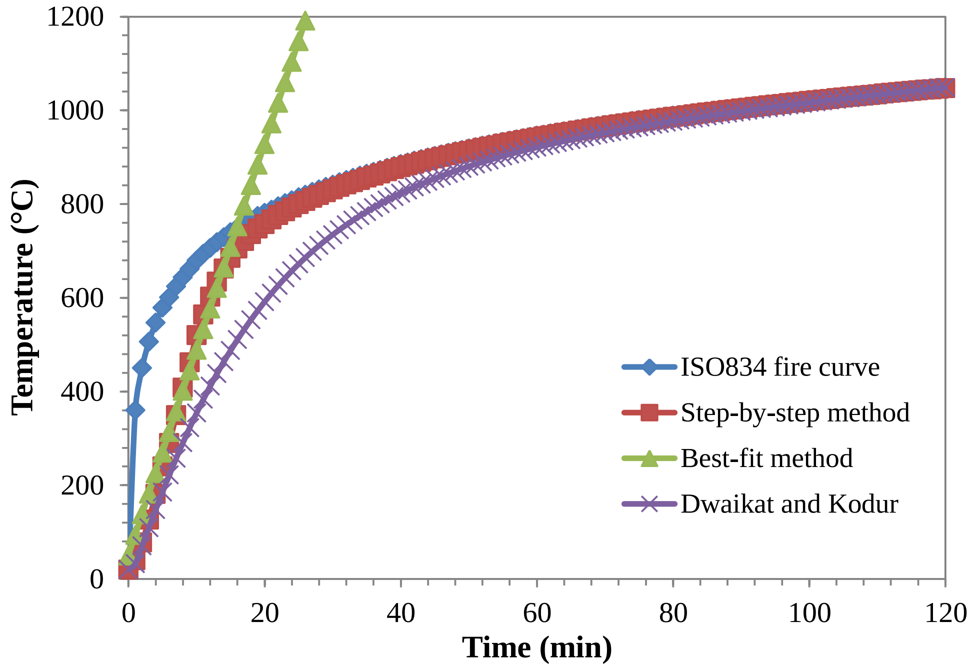

(a) W12x30

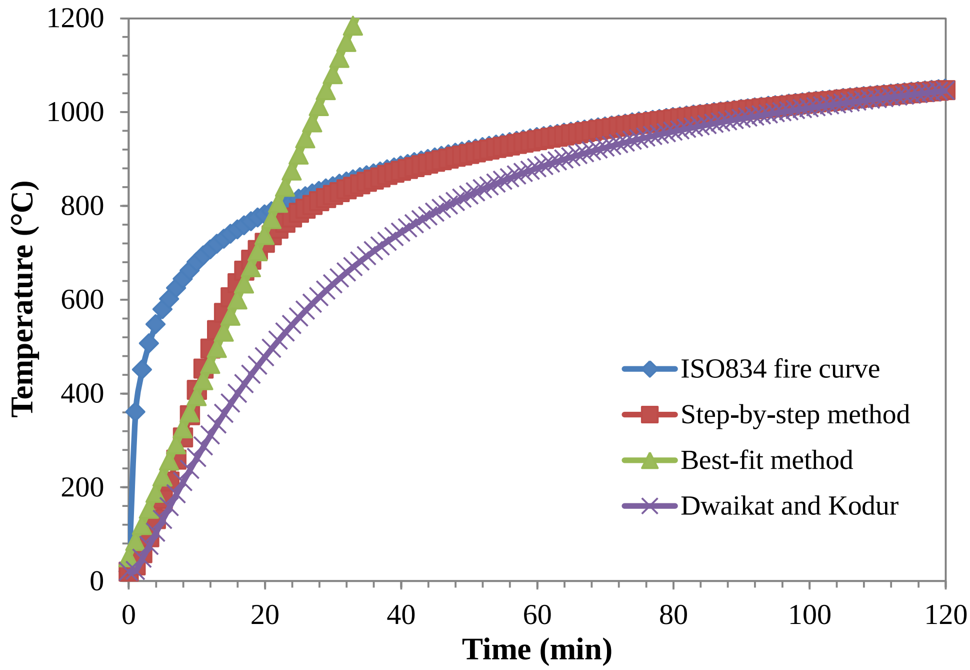

(b) W24x76

Figure 6.6: Comparison of steel temperatures obtained using different methods for (a) W12x30 and (b) W24x76 beam sections without fire protection

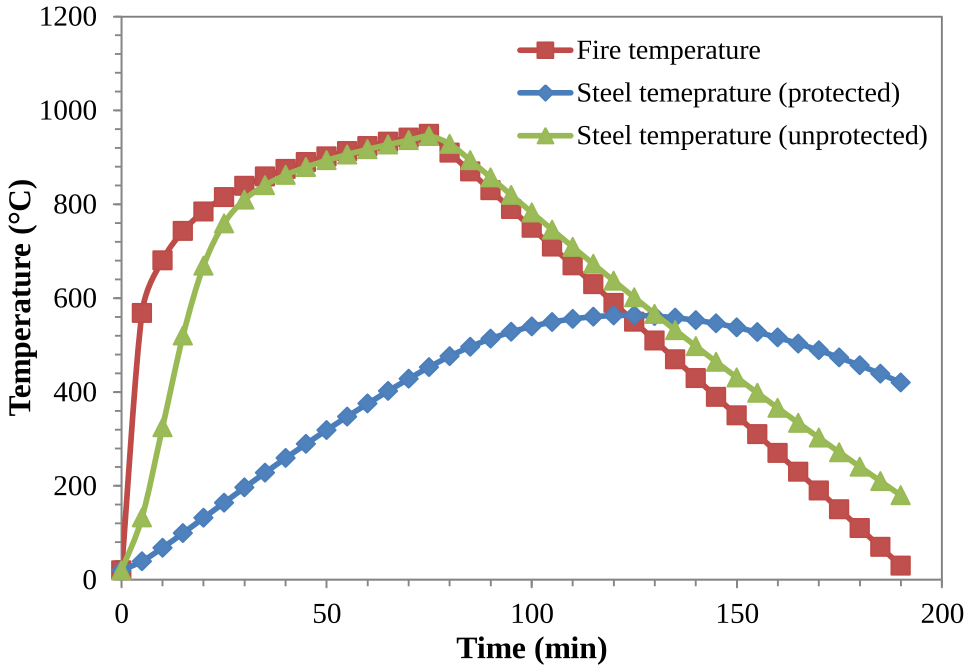

(a) W12x30

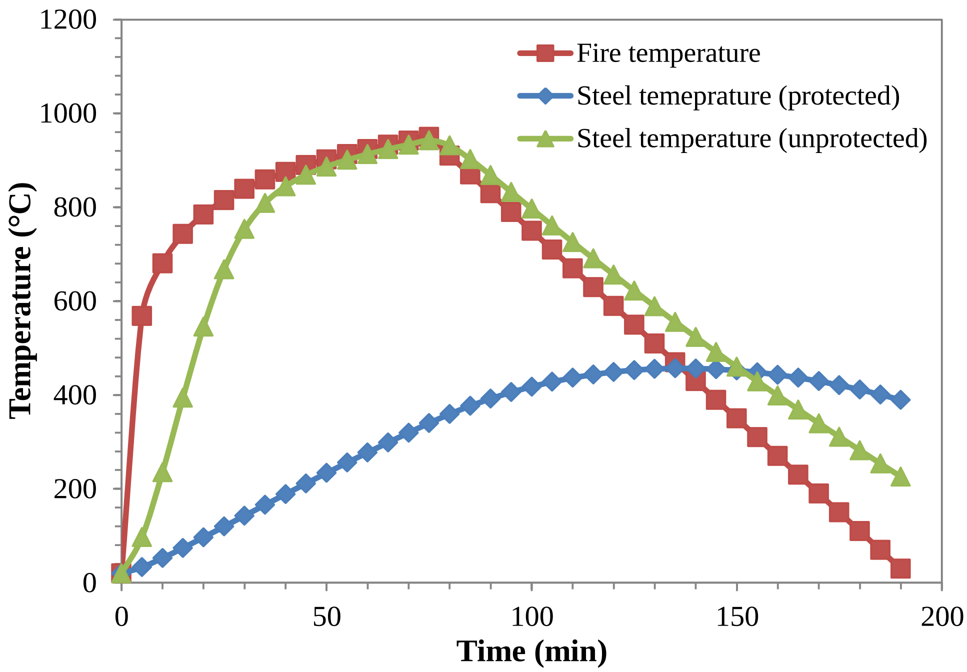

(b) W24x76

Figure 6.7: Comparison of steel temperatures obtained using step-by-step method for (a) W12x30 and (b) W24x76 beam sections subjected to design fire exposure

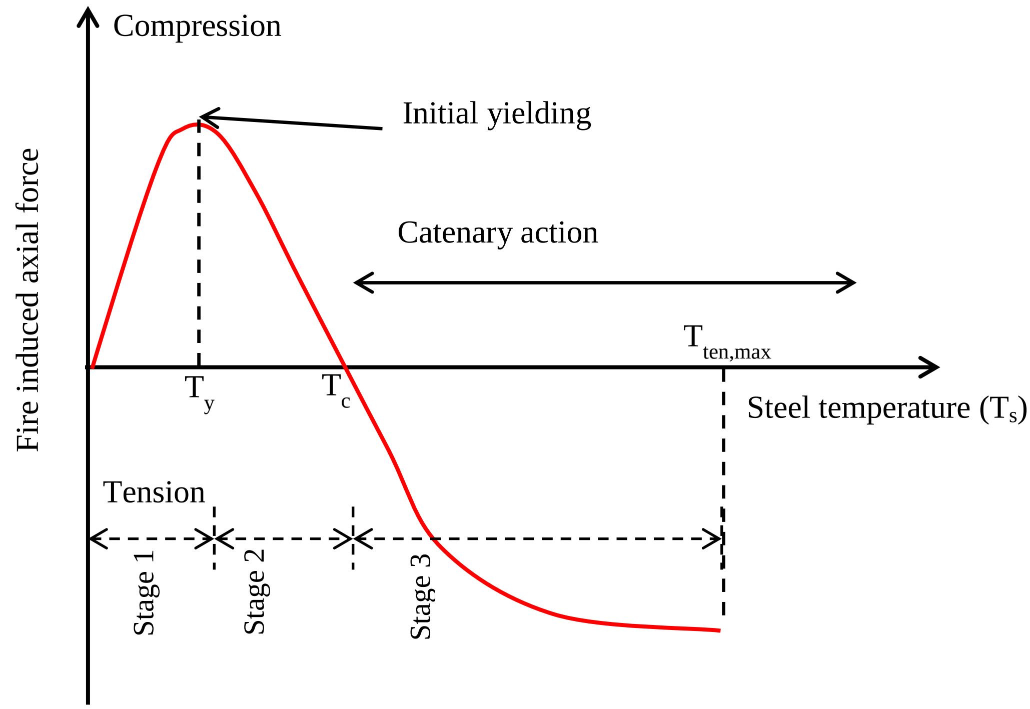

Figure 6.8: Fire induced axial force development in connection

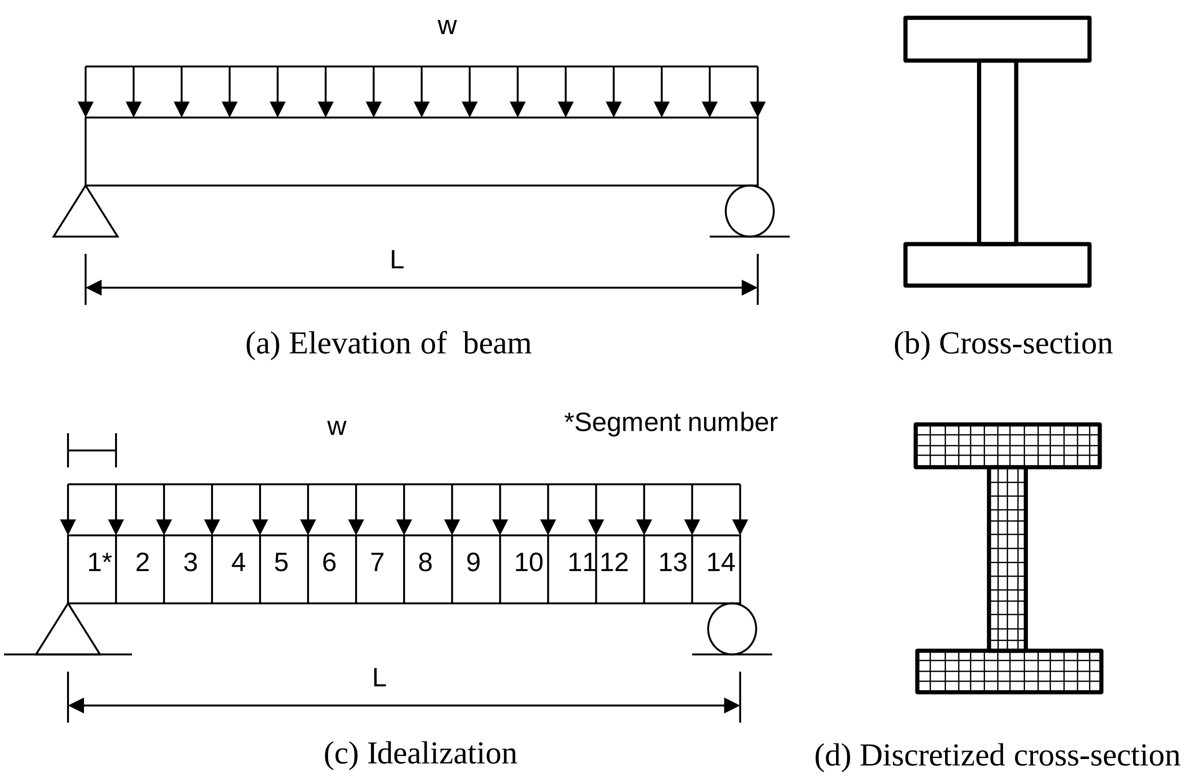

Figure 6.9: A schematic of beam idealization into segments and discretized cross-section

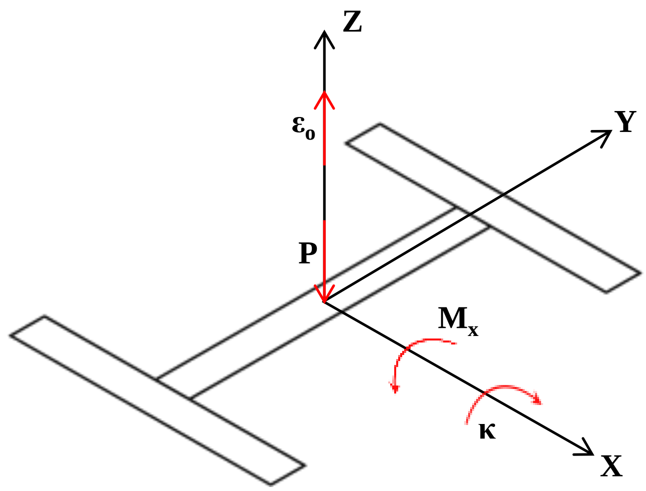

Figure 6.10: Illustration of generalized stress and generalized strains oriented in the direction corresponding to their positive values

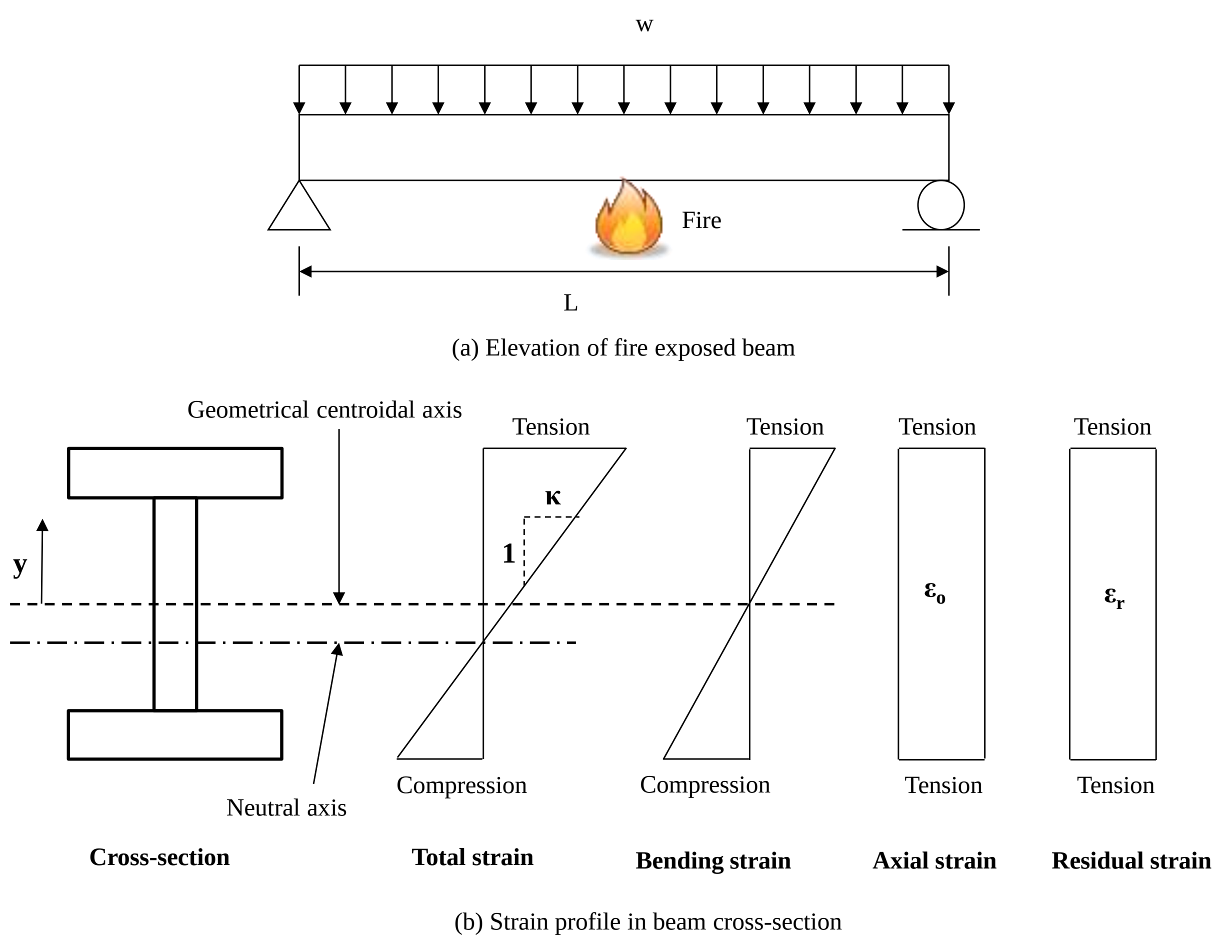

Figure 6.11: Total strain along the beam cross-section along with different strain components

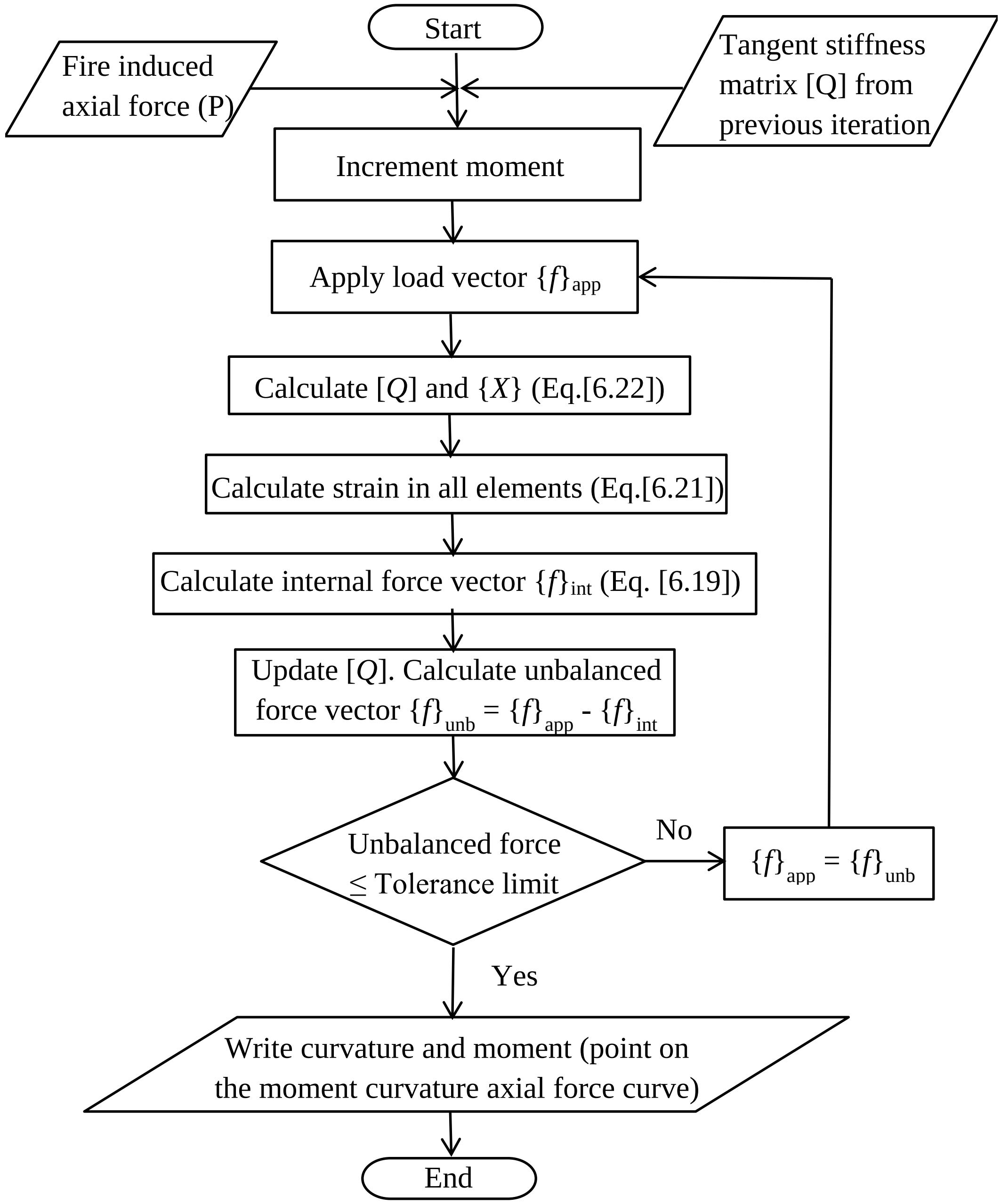

Figure 6.12: Flow chart illustrating the steps associated in the generation of moment-curvature-axial force curve

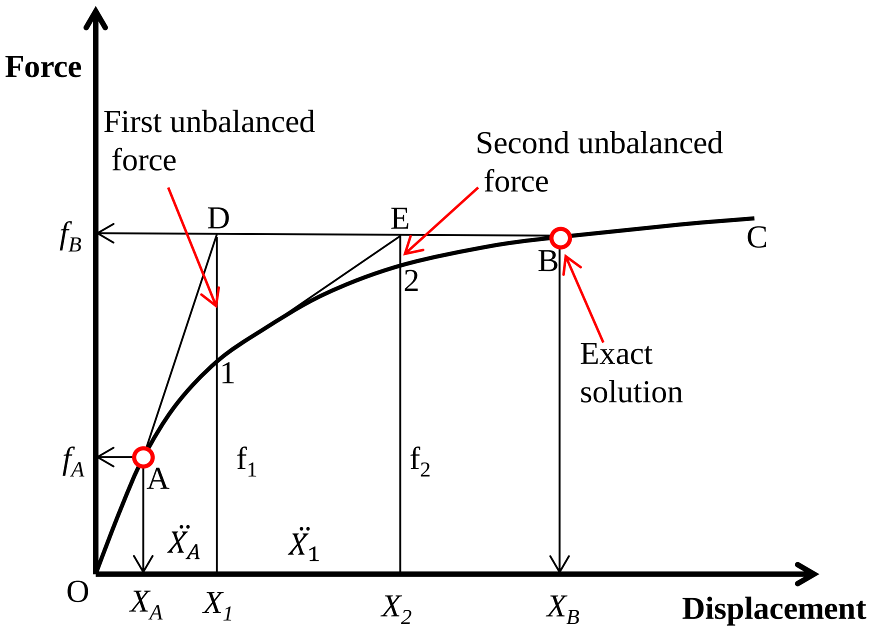

Figure 6.13: Iterative solution technique for generating force-deformation curves

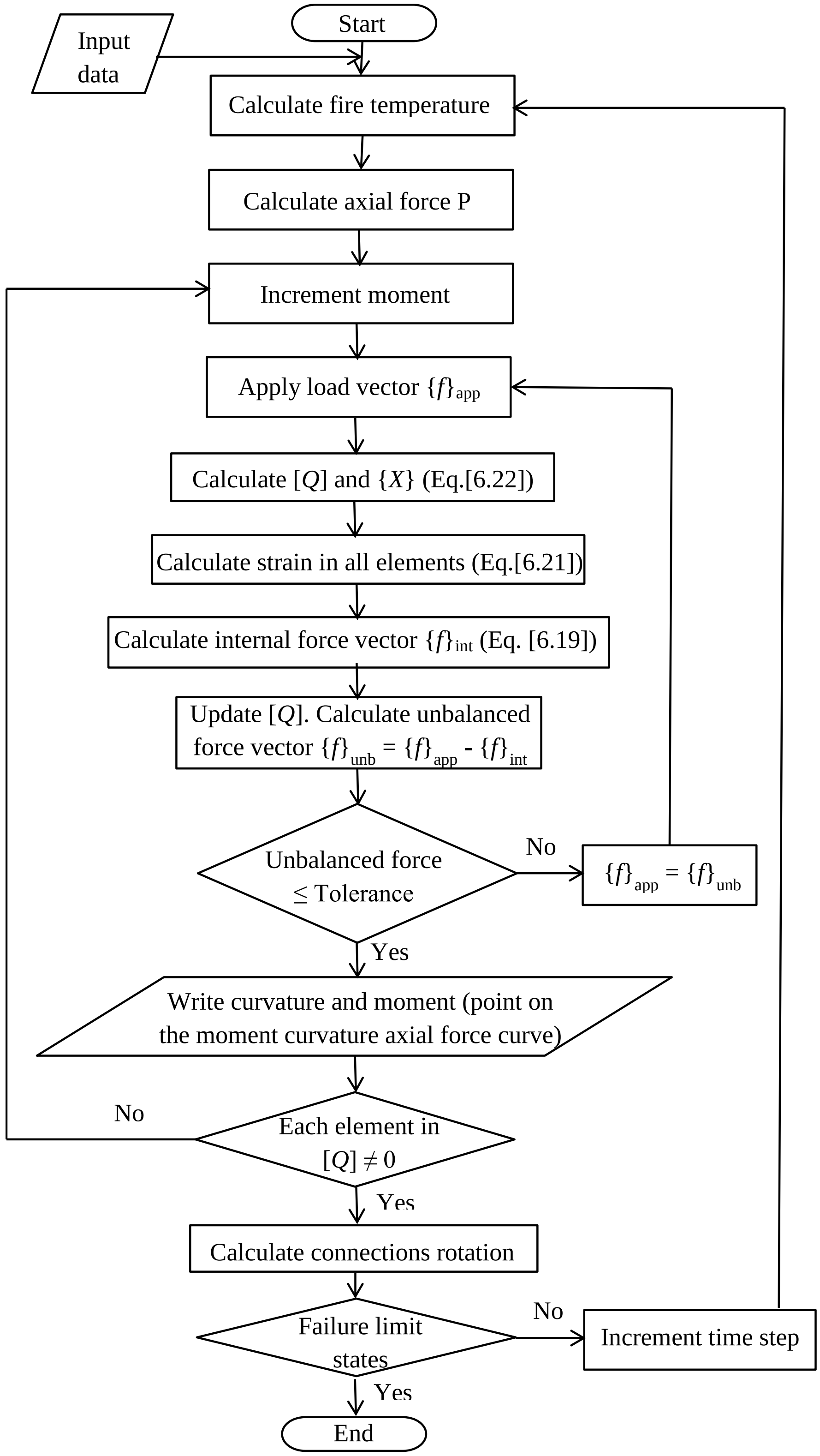

Figure 6.14: Flowchart showing the steps associated with the analysis of double angle connection

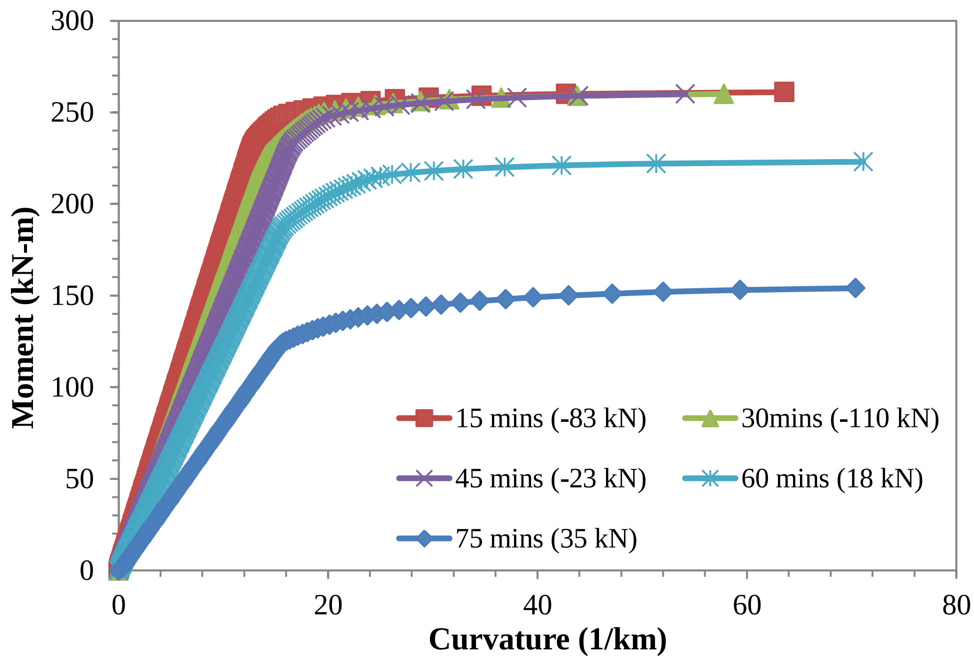

(a) W12x30

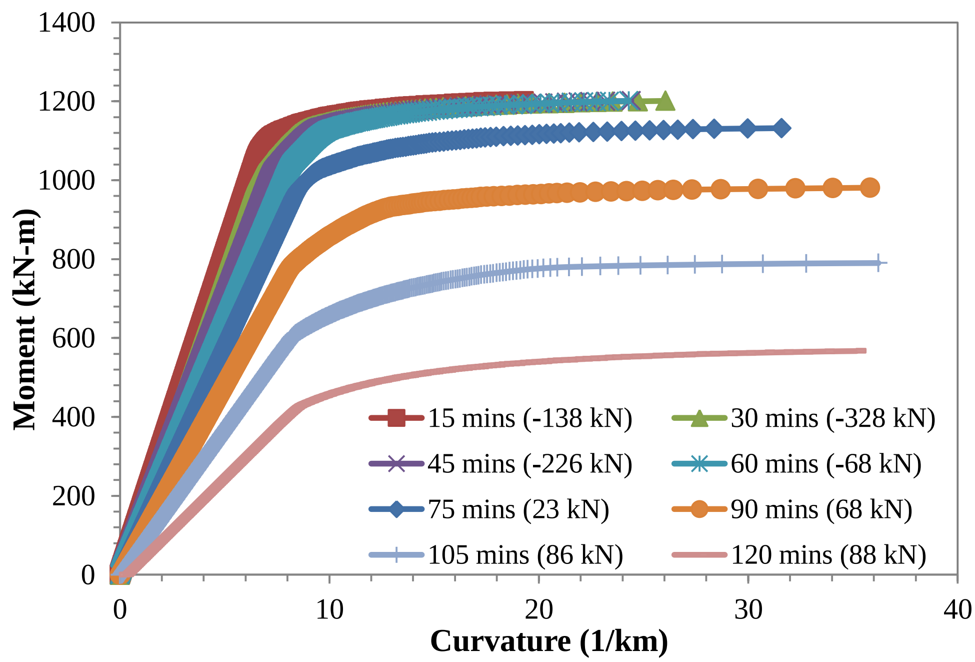

(b) W24x76

Figure 6.15: Moment-curvature curves as a function of fire exposure time for (a) W12x30 and (b) W24x76 steel section with 15mm of fire insulation (Note: The fire induced axial forces are shown in the parenthesis)

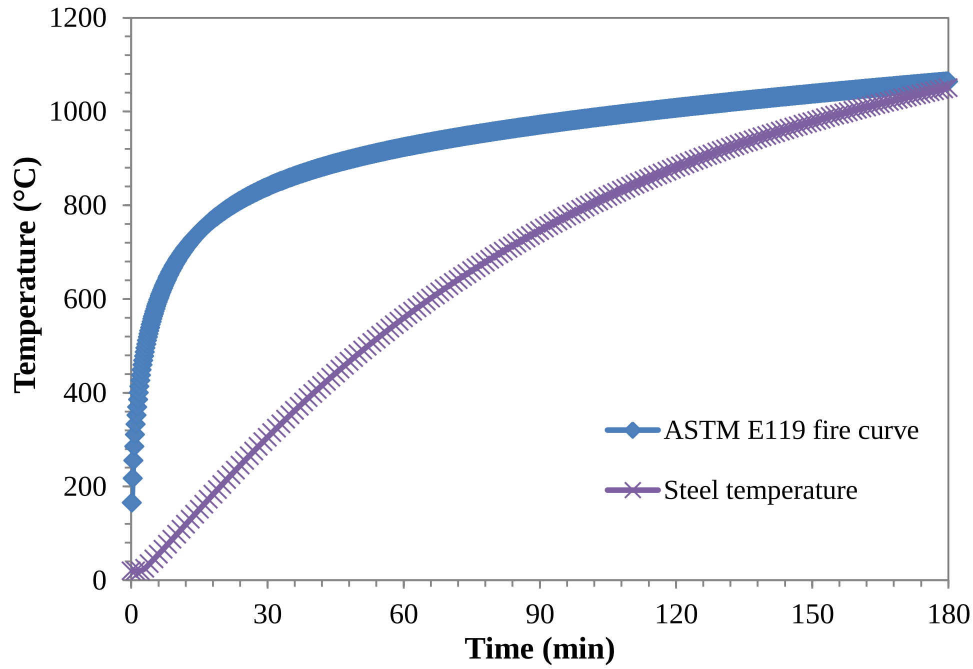

(a) Temperature

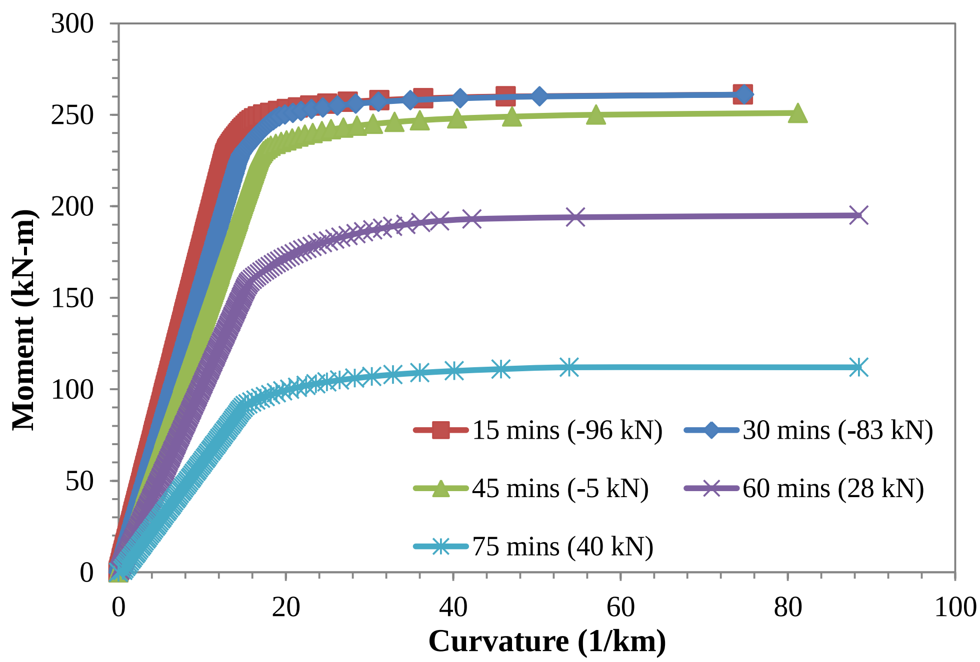

(b) Moment-curvature

Figure 6.16: Progression of (a) temperature in beam (b) moment-curvature-axial force in the beam, and (c) rotation at connection for double angle connection

Figure 6.16 (cont'd)

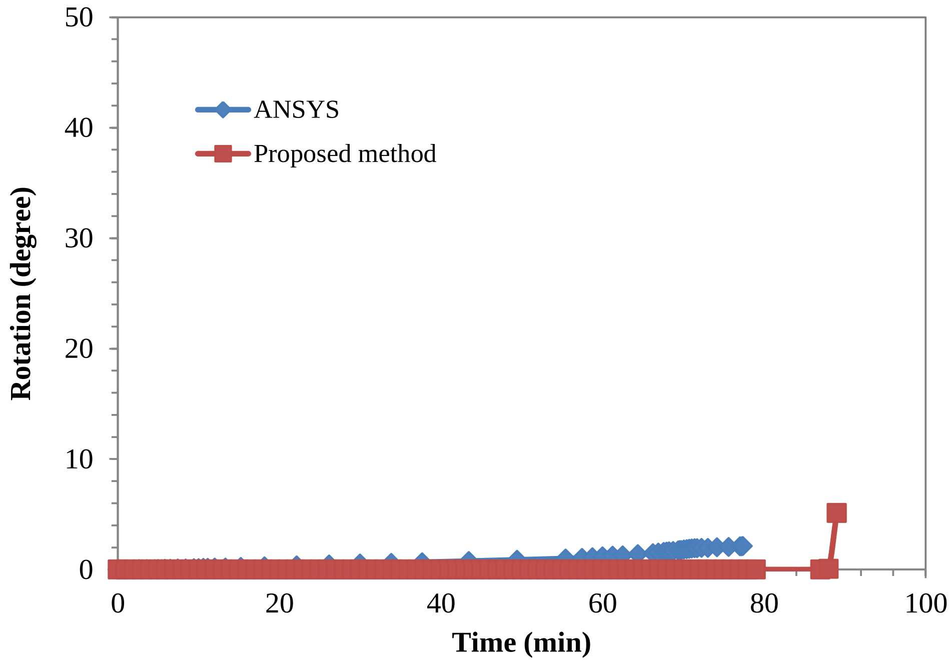

(c) Rotation

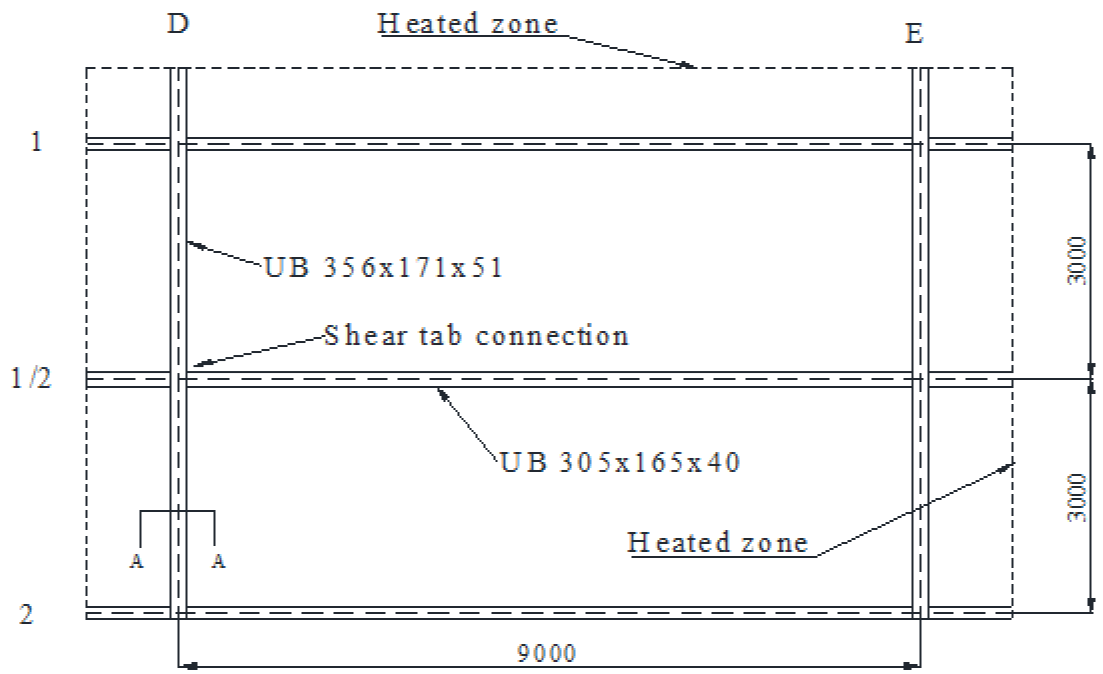

(a) Building plan

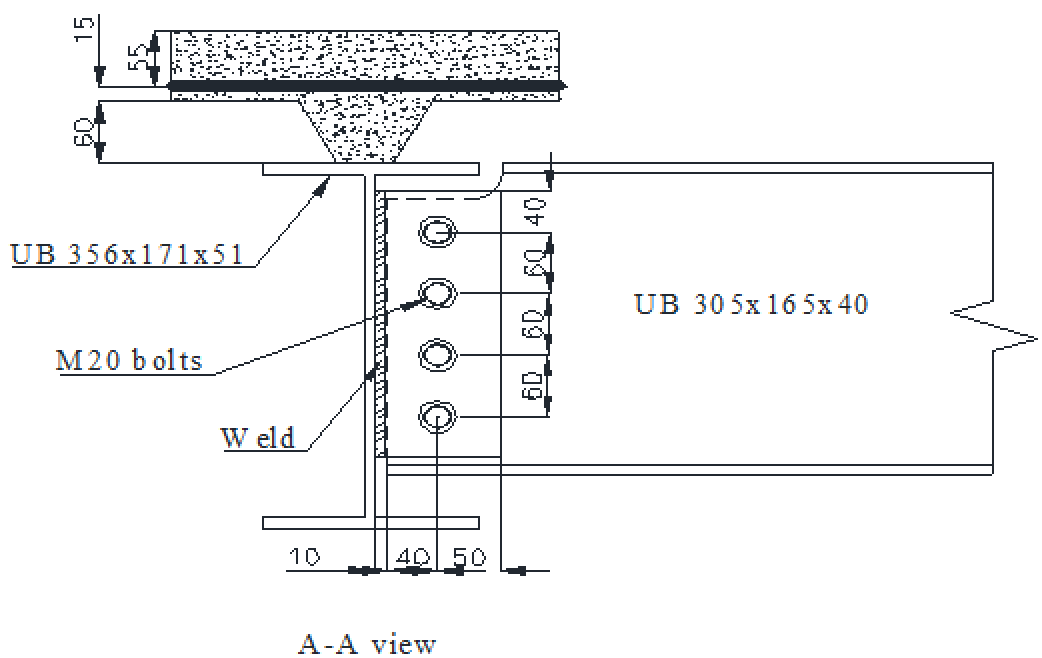

(b) Shear tab connection details

Figure 6.17: Illustration of the Cardington test (a) building plan and (b) shear tab connection geometry (Note: all dimensions are in mm)

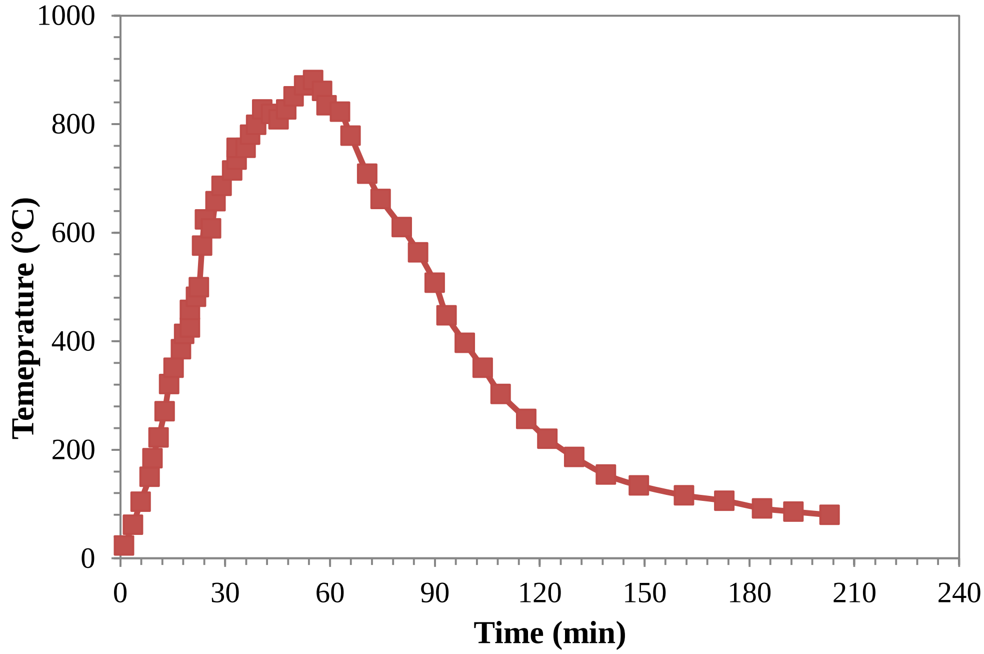

Figure 6.18: Measured fire (gas) temperatures during Cardington test

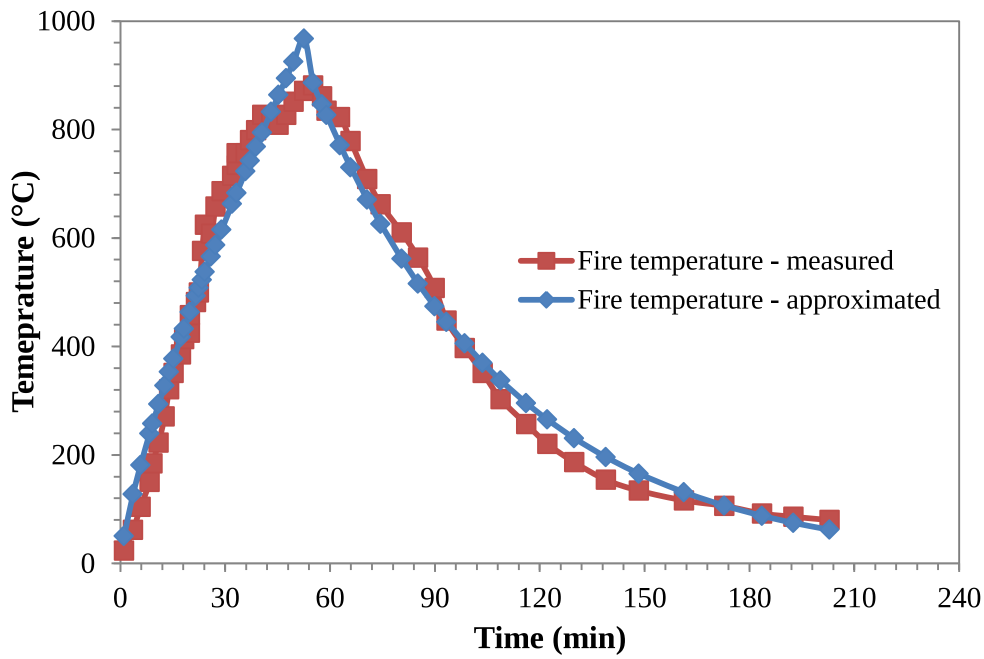

Figure 6.19: Comparison of measured and approximated fire temperature used for analyzing shear tab connection

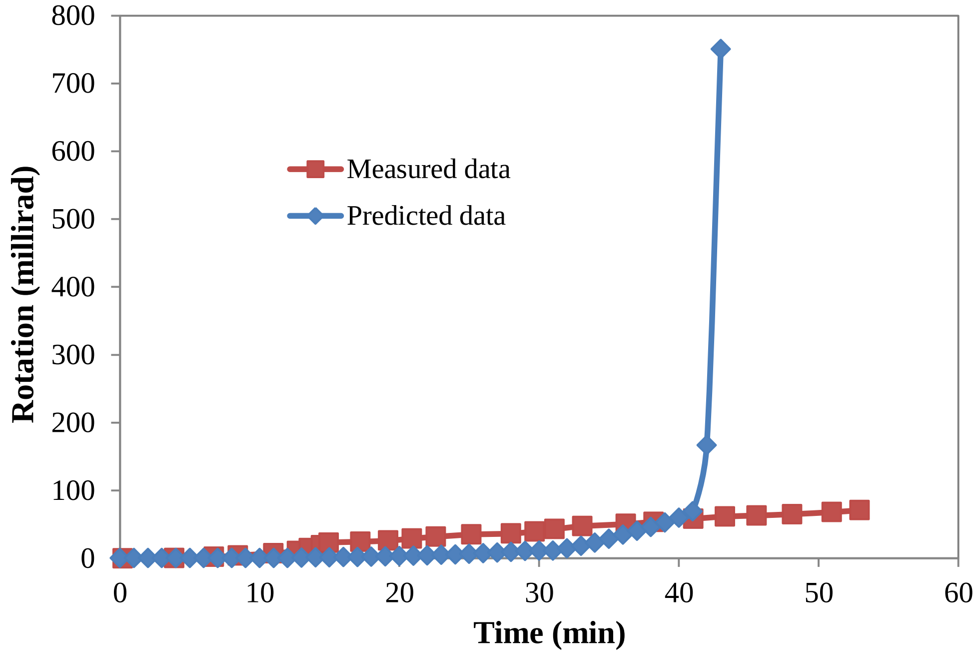

Figure 6.20: Comparison of predicted and measured rotation for shear tab connection

Appendix E figures

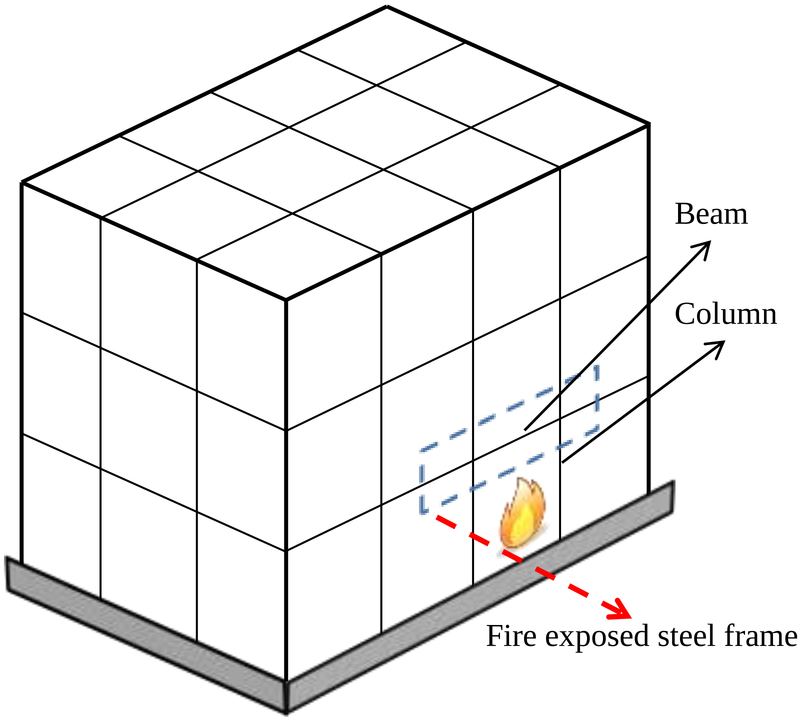

(a) Three dimensional perspective view of steel framed building

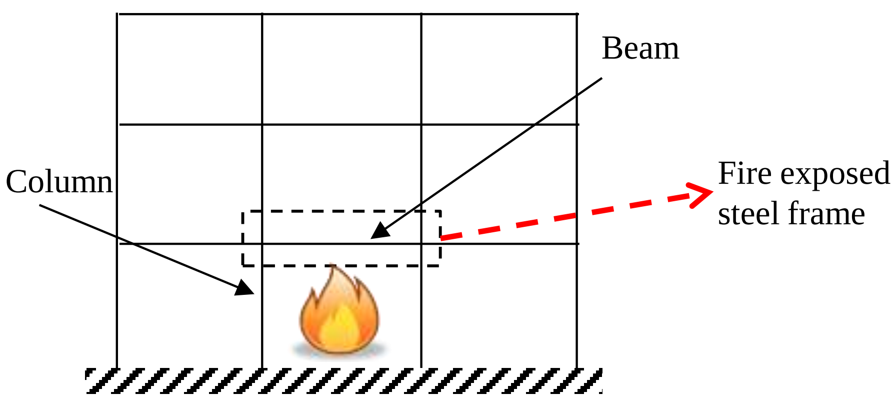

(b) Two dimensional view of steel framed building

Figure E.1: Illustration of the steel framed building used in the analysis

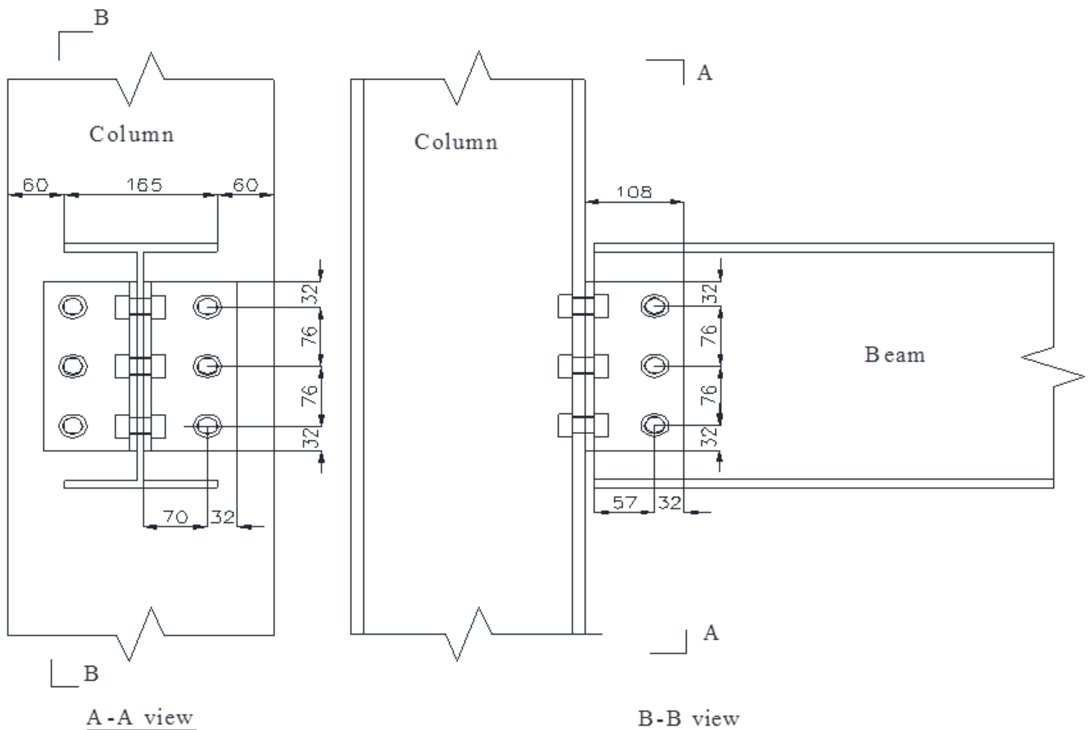

Figure E.2: Geometrical details of double angle connection

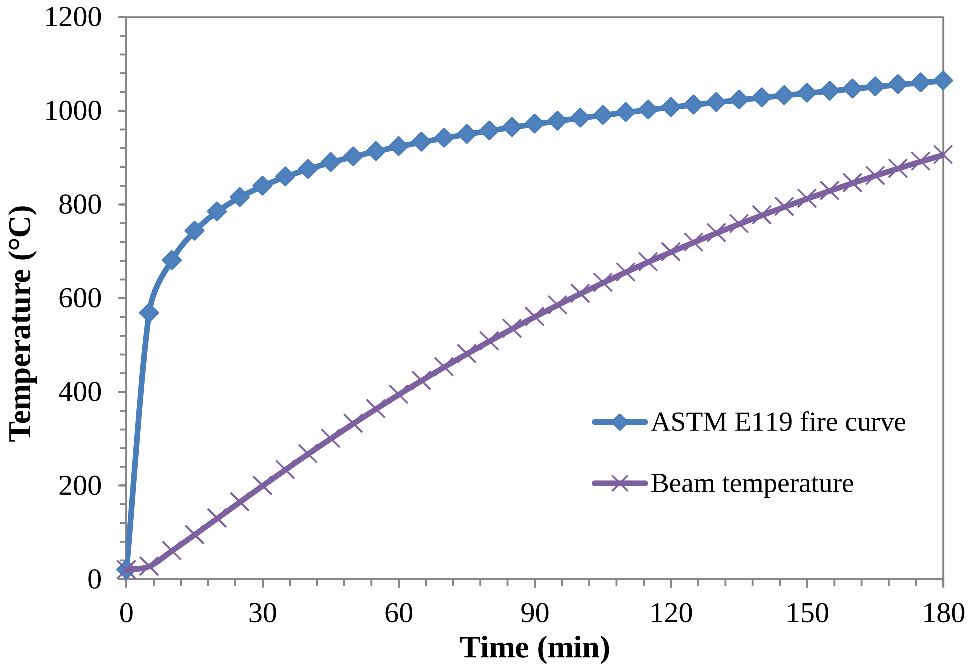

(a) Temperature

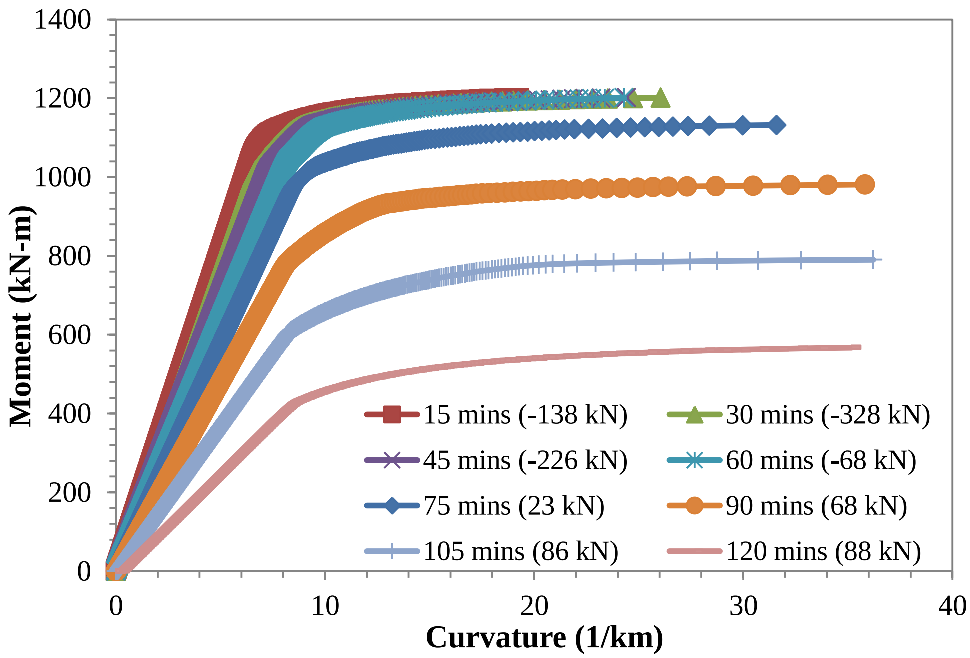

(b) Moment-curvature

Figure E.3: Progression of (a) temperature in beam (b) moment-curvature-axial force in the beam, and (c) fire-induced axial force in connection for the analyzed connection

Figure E.3 (cont'd)

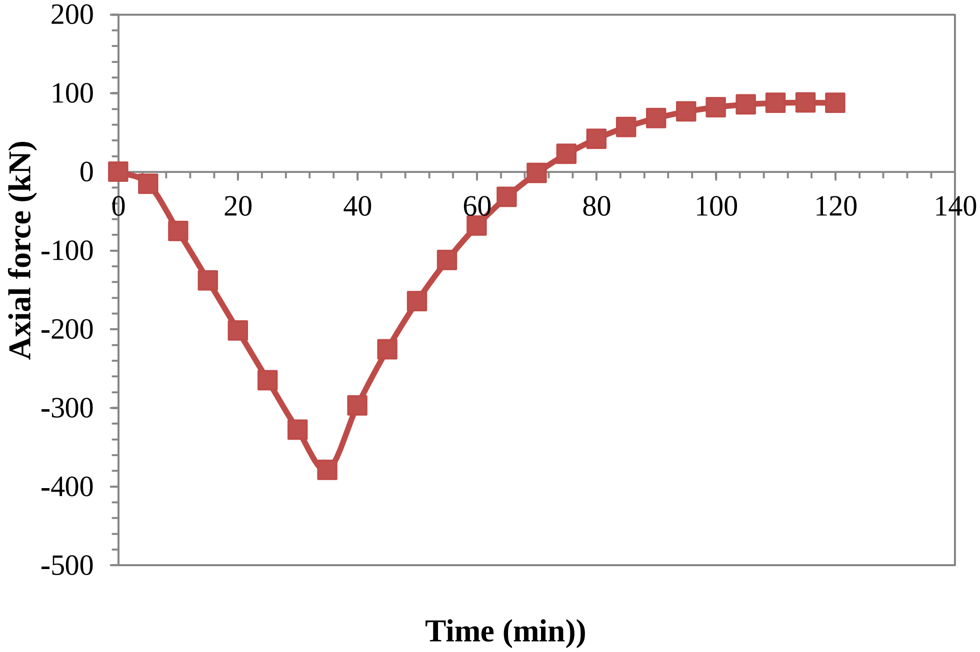

(c) Axial force

REFERENCES

RERERENCES

AISC (2005). Manual of Steel Construction, Load and resistance factor design, 13th Edition, American Institute of Steel Construction Inc., Chicago.

AISC (2011). Manual of Steel Construction, Load and resistance factor design, 14th Edition, American Institute of Steel Construction Inc., Chicago.

Al-Jabri, K.S., Burgess, I.W., Lennon, T., and Plank, R.J. (2005). Moment-rotation-temperature curves for semi-rigid joints. Journal of Constructional Steel Research *61*, 281-303.

Al-Jabri, K.S., Lennon, T., Burgess, I.W., and Plank, R.J. (1998). Behaviour of steel and composite beam-column connections in fire. Journal of Constructional Steel Research *46*, 308-309.

ANSYS Inc (2009a). ANSYS Command Reference.

ANSYS Inc (2009b). ANSYS Contact Technology Guide.

ANSYS Inc (2009c). ANSYS element reference.

ASTM (2011a). Designation E119 – 11a - Standard Test Methods for Fire Tests of Building Construction and Materials. (West Conshohocken, PA).

ASTM (2011b). Designation: A370-11 Standard Test Methods and Definitions for Mechanical Testing of Steel Products. (West Conshohocken, PA).

ASTM (2012). Designation A490 – 12 - Standard Specification for High-Strength Steel Bolts. (West Conshohocken, PA).

Bailey, C.G., Burgess, I.W., and Plank, R.J. (1996). Analyses of the effects of cooling and fire spread on steel-framed buildings. Fire Safety Journal *26*, 273-293.

Buchanan, A.H. (2002). Structural Design for Fire Safety (Chichester, England: John Wiley & Sons Ltd.,).

Bursi, O.S., and Jaspart, J.P. (1997a). Benchmarks for finite element modelling of bolted steel connections. Journal of Constructional Steel Research *43*, 17-42.

Bursi, O.S., and Jaspart, J.P. (1997b). Calibration of a finite element model for isolated bolted end-plate steel connections. Journal of Constructional Steel Research *44*, 225-262.

Bursi, O.S., and Jaspart, J.P. (1998). Basic issues in the finite element simulation of extended end plate connections. Computers & Structures *69*, 361-382.

Cook, R.D., Malkus, D.S., Plesha, M.E., and Witt, R.J. (2002). Concepts and Application of Finite Element Analysis, 4th Edition edn (John Wiley & Sons, Inc.).

Dai, X.H., Wang, Y.C., and Bailey, C.G. (2010). Numerical modelling of structural fire behaviour of restrained steel beam-column assemblies using typical joint types. Engineering Structures *32*, 2337-2351.

Daryan, A.S., and Yahyai, M. (2009). Behavior of bolted top-seat angle connections in fire. Journal of Constructional Steel Research *65*, 531-541.

Dwaikat, M.M.S., and Kodur, V.K.R. (2011). A performance based methodology for fire design of restrained steel beams. Journal of Constructional Steel Research *67*, 510-524.

Dwaikat, M.M.S., and Kodur, V.K.R. (2013). A simplified approach for predicting temperatures in fire exposed steel members. Fire Safety Journal *55*, 87-96.

Dwaikat, M.M.S., Kodur, V.K.R., Quiel, S.E., and Garlock, M.E.M. (2011). Experimental behavior of steel beam-columns subjected to fire-induced thermal gradients. Journal of Constructional Steel Research *67*, 30-38.

El-Rimawi, J.A., Burgess, I.W., and Plank, R.J. (1997). The influence of connection stiffness on the behaviour of steel beams in fire. Journal of Constructional Steel Research *43*, 1-15.

Eurocode1 (2002). Actions on structures, Part 1-2: General actions-Actions on structures exposed to fire, Document CEN, European Committee for Standardization, UK.

Eurocode2 (2004). Design of concrete structures, Part1-2: General rules-structural fire deisgn, ENV 1992-1-2, Document CEN, European Committee for Standardization, UK.

Eurocode3 (2005a). Design of steel structures, Part 1-8: Design of joints, Document CEN, European Committee for Standardization, UK.

Eurocode3 (2005b). Design of steel structures, Part 1.2: General rules-structural fire design, Document CEN, European Committee for Standardization, UK.

Feasey, R., and Buchanan, A. (2002). Post-flashover fires for structural design. Fire Safety Journal *37*, 83-105.

Garlock, M.E., and Selamet, S. (2010). Modeling and Behavior of Steel Plate Connections Subject to Various Fire Scenarios. Journal of Structural Engineering-Asce *136*, 897-906.

Ho, M.C., Chiou, Y.J., and Chen, S.J. (2007). Study on structural behavior of steel beam-column moment connections under fire load. In The research report of Architecture and Building Research Institute (Taipei, Taiwan).

ISO (1975). Designation 834 – Fire Resistance Tests- Elements of Building Construction.

Kirby, B.R. (1995). The behaviour of high-strength grade 8.8 bolts in fire. Journal of Constructional Steel Research *33*, 3-38.

Kodur, V., Dwaikat, M., and Fike, R. (2010). High-Temperature Properties of Steel for Fire Resistance Modeling of Structures. Journal of Materials in Civil Engineering *22*, 423-434.

Kodur, V., Kand, S., and Khaliq, W. (2011). Effect of Temperature on Thermal and Mechanical Properties of Steel Bolts. Journal of Materials in Civil Engineering *1*, 384-384.

Kodur, V., Kand, S., and Khaliq, W. (2012). Effect of Temperature on Thermal and Mechanical Properties of Steel Bolts. Journal of Materials in Civil Engineering *24*, 765-774.

Kodur, V.K.R., and Shakya, A.M. (2013). Effect of temperature on thermal properties of spray applied fire resistive materials. Fire Safety Journal *61*, 314-323.

Landesmann, A., de M. Batista, E., and Drummond Alves, J.L. (2005). Implementation of advanced analysis method for steel-framed structures under fire conditions. Fire Safety Journal *40*, 339-366.

Lange, J., and Gonzalez, F. (2012). Behavior of High-Strength Grade 10.9 Bolts under Fire Conditions. Structural Engineering International *22*, 470-475.

Lawson, R.M. (1990). Behaviour of steel beam-to-column connections in fire. Structural engineer *68*, 263-271.

Lennon, T., and Moore, D. (2003). The natural fire safety concept - full-scale tests at Cardington. Fire Safety Journal *38*, 623-643.

Leston-Jones, L.C., Lennon, T., Plank, R.J., and Burgess, I.W. (1997). Elevated temperature moment-rotation tests on steelwork connections. In Proceedings of the ICE - Structures and Buildings, pp. 410 –419.

Liu, T.C.H. (1996). Finite element modelling of behaviours of steel beams and connections in fire. Journal of Constructional Steel Research *36*, 181-199.

Liu, T.C.H. (1998). Effect of connection flexibility on fire resistance of steel beams. Journal of Constructional Steel Research *45*, 99-118.

Liu, T.C.H. (1999). Fire resistance of unprotected steel beams with moment connections. Journal of Constructional Steel Research *51*, 61-77.

Liu, T.C.H., Fahad, M.K., and Davies, J.M. (2002). Experimental investigation of behaviour of axially restrained steel beams in fire. Journal of Constructional Steel Research *58*, 1211-1230.

Mao, C.J., Chiou, Y.J., Hsiao, P.A., and Ho, M.C. (2009). Fire response of steel semi-rigid beam-column moment connections. Journal of Constructional Steel Research *65*, 1290-1303.

Pakala, P., and Kodur, V. (2013). System-level approach to predict the transient fire response of double angle connections. Journal of Constructional Steel Research *89*, 132-144.

Pakala, P., Kodur, V., and Dwaikat, M. (2012a). Critical factors influencing the fire performance of bolted double angle connections. Engineering Structures *42*, 106-114.

Pakala, P., Kodur, V., Selamet, S., and Garlock, M. (2012b). Fire behavior of shear angle connections in a restrained steel frame. Journal of Constructional Steel Research *77*, 119-130.

Reddy, J.N. (2005). An Introduction to the Finite Element Method, 3rd Edition edn (McGraw-Hill).

Santathadaporn, S., and Chen, W.-F. (1972). Tangent Stiffness Method for Biaxial Bending. Journal of the Structural Division *98*, 153-163.

Selamet, S., and Garlock, M. (2010a). Guidelines for modeling three dimensional structural connection models using finite element methods. In International Symposium "Steel Structures: Culture & Sustainability" (Istanbul, Turkey).

Selamet, S., and Garlock, M.E. (2010b). Robust fire design of single plate shear connections. Engineering Structures *32*, 2367-2378.

Van der Vegte, G.J., and Makino, Y. (2004). Numerical Simulation of Bolted Connections: The Implicit versus the Explicit Approach. In AISC-ECCS (Amsterdam, Netherlands).

Wald, F., da Silva, L.S., Moore, D.B., Lennon, T., Chladna, M., Santiago, A., Benes, M., and Borges, L. (2006). Experimental behaviour of a steel structure under natural fire. Fire Safety Journal *41*, 509-522.

Wang, W.Y., Li, G.Q., and Dong, Y.L. (2007). Experimental study and spring-component modelling of extended end-plate joints in fire. Journal of Constructional Steel Research *63*, 1127-1137.

Wang, Y.C., Dai, X.H., and Bailey, C.G. (2011). An experimental study of relative structural fire behaviour and robustness of different types of steel joint in restrained steel frames. Journal of Constructional Steel Research *67*, 1149-1163.

Yang, K.C., Chen, S.J., and Ho, M.C. (2009). Behavior of beam-to-column moment connections under fire load. Journal of Constructional Steel Research *65*, 1520-1527.

Yu, H., Burgess, I.W., Davison, J.B., and Plank, R.J. (2009a). Experimental investigation of the behaviour of fin plate connections in fire. Journal of Constructional Steel Research *65*, 723-736.

Yu, H., Burgess, I.W., Davison, J.B., and Plank, R.J. (2009b). Tying capacity of web cleat connections in fire, Part 1: Test and finite element simulation. Engineering Structures *31*, 651-663.

Yu, H., Burgess, I.W., Davison, J.B., and Plank, R.J. (2009c). Tying capacity of web cleat connections in fire, Part 2: Development of component-based model. Engineering Structures *31*, 697-708.

Yu, L. (2006). Behavior of bolted connections during and after a fire. (Austin, TX, University of Texas at Austin).

Yu, L.A., and Frank, K.H. (2009). Shear Behavior of A325 and A490 High-Strength Bolts in Fire and Post-Fire. Engineering Journal-American Institute of Steel Construction Inc *46*, 99-106.